

N°:



PhD Thesis

Flame retardancy of polybutylene succinate by multiple approaches

PhD defended at

UNIVERSITE DE LILLE

École doctorale Sciences de la Matière, du Rayonnement et de l'Environnement, UFR de Chimie

To obtain the grade of

DOCTEUR

Specialty: Materials Sciences

By

Chi HU

PhD thesis supervised by

Prof. Gaëlle Fontaine and Prof. Serge Bourbigot

Defended on November, 15th 2018 in front of the following dissertation committee:

Dr. LEFEBVRE Jean-Marc, Université de Lille	Président de jury
Prof. Gan Sabyasachi, EMPA Material science and technology	Rapporteur
Prof. FUCHS Sabine, Hamm-Lippstadt University of Applied Sciences	Rapporteur
Dr. MARCILLE Sophie, Roquette Frère	Examineur
Prof. Fontaine Gaëlle, Université de Lille	Directrice de thèse
Prof. Bourbigot Serge, Université de Lille	Co-directeur de thèse

Acknowledgements

First, I would like to thank Prof. Patrice Woisel, director of the UMET laboratory, and Prof. Serge Bourbigot, director of the group ISP and the team R2F (Reaction and Resistance to Fire). I would like to thank them for giving me the opportunity to join this laboratory, work on this project and achieve this PhD in excellent job conditions.

Obviously I would like to thank my supervisors, Gaëlle and Serge (aka the man who play with fire), who gave me the possibility to work with them and to pass my PhD thesis in the R2Fire lab. During these three years, they helped me a lot with my study with their broad and profound knowledge, but more than that, they always showed their patience and their kind even though I am a foreigner who speaks not very good French. I must underline that the time spend with them let me feel the real 'égalité', I was always welcome to discuss with them freely on any subject without any burden, this kind of relationship between the professors and the students is quite different from that in china, and I will benefit from it during my life time.

I am very grateful to Dr. Lefebvre Jean-Marc who agreed to chair the jury, and to Prof. Fuchs Sabine, to Prof. Gaan Sabyasachi as well as to Dr. Marcille Sophie who accepted to take their time, to bring their expertise as reviewers of this work and to be part of the jury.

I would like to acknowledge also the former director of IFMAS Antonio Molina, the CEO/COO of IFMAS François Ténégal, the other members of the former leader team Anne-Valentine, Dominique, Thierry, Marion and the industrial partner from Roquette Sophie Marcille for giving me the opportunity to work in a good experiment condition in IFMAS and also their kind guidance during these time.

I would like to thank specially Dr. Fanny Bonnet who was one of my supervisors (with Gaëlle) during my internship of the end of Master in the lab UMET and UCCS. She led me entered into the field of research (before this internship I didn't have many opportunities to work in the lab), and it was her who recommended this PhD thesis to me and who told me 'Gaëlle and Serge are super cool'. Particularly I felt very warm with the kind care of Fanny and Gaëlle when I had the accident in the lab. Thanks a thousand times!!!

Of course, I also want to thank all the current and former member of group R2Fire and IFMAS for their help and all the great moments that we had together. First thanks to the permanent members of the team: Gaëlle, Sophie, Serge, Fabienne, Mathilde, Michel, Maude, Charaf', Catherine, Séverine, Brigitte. Thanks also to the other members of the group R2Fire who create an easy-going atmosphere in the lab: Nico, Pierre, Pauline, Agnès, Audrey, Sawsen, Ninit, HiraK, JoJo, Ben (the two), Caroline, Mathieu, Bertrand, Renaud, Sarah, Johnathan, Katja, Laurie, Maryem, Tatenda, Adi, Sophie, Kai, Adrien, Laura, Charlotte, RoRo, Manon, Anne-Lise, Elodie, Morgane, Simone, Kata. I would like to thanks as well the members of IFMAS: Andy, Florian, Sarah, Khaled, Corentin, Julie, Adrien, Valentin, Théo, Imen, Pierre, David, Nazim, Aymeric, Nico, Axel, Charlotte, Chloé, Marion.

Finally I must thanks to all my friends who supported me during the three years and of course my parents who supported me to study in France.

Table of contents

Acknowledgements	5
Table of contents	7
Abbreviations	11
General introduction	15
I State of the art	21
I.1 Polybutylene succinate.....	21
I.1.1 Synthesis of polybutylene succinate	21
I.1.2 Physico-chemical properties of polybutylene succinate	23
I.1.3 Conclusion	26
I.2 Flame retardancy of the polymers	26
I.2.1 Combustion of polymers	27
I.2.2 Mode of action of flame retardancy	27
I.2.3 Flame retardant additives	28
I.2.4 Conclusion	43
I.3 Flame retardancy of polybutylene succinate	44
I.3.1 Flame retardancy of neat polybutylene succinate	44
I.3.2 Flame retardancy of composites of PBS reinforced by natural fibers.....	48
I.3.3 Conclusion	50
I.4 Conclusion	50
II Materials and Methods	53
II.1 Materials.....	53
II.1.1 Polymers and flame retardant additives	53
II.1.2 Modification of isosorbide	54
II.1.3 Compounding of materials	60
II.2 Methods	61
II.2.1 Fire testing.....	61
II.2.2 Physico-chemical analysis.....	66
II.2.3 Thermal analysis.....	68
II.2.4 Gas phase analysis.....	69
II.2.5 Condensed phase analysis.....	72
II.3 Conclusion	74
III Material screening	77

III.1	Formulation of PBS with isosorbide-modified FRs	77
III.1.1	Sulfur based modification of isosorbide.....	78
III.1.2	Silicon based modification of isosorbide.....	80
III.1.3	Phosphorus based modification of isosorbide	84
III.1.4	Conclusion	89
III.2	Isosorbide and isosorbide based polymer used as carbonization agent	89
III.2.1	Isosorbide as carbonization agent.....	89
III.2.2	Isosorbide based polymer as carbonization agent.....	91
III.2.3	Conclusion	93
III.3	Formulation based on DOPO or DOPO with conventional FRs for PBS.....	93
III.3.1	Formulation of neat DOPO with PBS.....	93
III.3.2	Formulation of DOPO derivatives with PBS.....	95
III.3.3	Formulation of DOPO and intumescent FRs with PBS	97
III.3.4	Formulation of DOPO and metal hydroxides and metal carbonate salts with PBS	98
III.3.5	Formulation of DOPO with carbon nanotubes with PBS.....	102
III.3.6	Conclusion	103
III.4	Conclusion	103
IV	Investigation of the mode of action of DOPO in PBS.....	107
IV.1	Investigation of the mechanism of PBS/DOPO in MLC test	107
IV.1.1	Investigation of the fire behavior of PBS/DOPO under different heat fluxes	107
IV.1.2	Comprehension of the thermal decomposition of PBS/DOPO	111
IV.1.3	Surface temperature evolution measured by thermocouples.....	116
IV.1.4	Investigation of released gases of PBS/DOPO upon heating	117
IV.1.5	Proposed mechanism of PBS/DOPO during MLC test.....	124
IV.1.6	Conclusion	125
IV.2	Investigation of dripping parameters of PBS/DOPO by UL-94 instrumentation.....	126
IV.2.1	Emissivity measurement of the drops.....	127
IV.2.2	Temperature evolution of the drops.....	131
IV.2.3	Influence of DOPO on physico-mechanical properties	135
IV.2.4	Conclusion	136
IV.3	Conclusion	136
V	Investigation of the mechanism of the flame retardancy of PBS/PIC/APP	141
V.1	Investigation of the mass and temperature evolution during MLC test.....	141
V.2	Investigation of the chemical composition of the forming char by solid state NMR.....	145
V.2.1	Characterization of ³¹ P NMR	145
V.2.2	Characterization of ¹³ C NMR	148

Contents

V.3	Thermal stability analysis	150
V.4	Analyses of the released gases by TGA-FTIR	153
V.5	Investigation of char morphology	154
V.5.1	Char morphology investigated by optical microscope	154
V.5.2	Char morphology investigated by SEM and EPMA.....	156
V.6	Mechanical analysis of the char	158
V.6.1	Measurement of viscosity	158
V.6.2	Measurement of the char resistance	159
V.7	Proposed mechanism of PBS/PIC/APP during MLC test.....	160
V.8	Conclusion	161
List of Figures and Tables.....		167
Appendix		172
References		173

Abbreviations

AP	ammonium phosphate
APP	ammonium polyphosphate
ABS	acrylonitrile-butadiene-styrene
ATH	aluminum trihydroxide
BDP	bisphenol A bis(diphenyl phosphate)
BPA	bisphenol A
CNTs	carbon nanotubes
CP	cross-polarization
DAP	dihydrogen ammonium phosphate
DOPO	9,10-dihydro-9-oxa-10-phosphaphenanthrene-10-oxide
DDi	di-DOPO-isosorbide
DMAP	4-Dimethylaminopyridine
DNA	deoxyribonucleic acid
DOPO-ACA	DOPO-3-propanamide
DOPO-PEPA	DOPO-1-oxypolysphosphazene-4-hydroxymethyl-2,6,7-trioxabicyclo[2,2,2]octane
DOPO-EDA	DOPO-ethane-1,2-diylbis(azanediy)l
DPPI	diphenylphosphate isosorbide
DPPII	diphenylphosphinate isosorbide
DSC	differential scanning calorimetry
Dti	di-tosyl-isosorbide
dTG	derivative of the TG curve
E&E	electric and electronic
EPMA	electron probe microanalysis
EVA	ethylene vinyl acetate
FR	flame retardant
FTIR	fourier transform infrared spectroscopy
HDPE	high density polyethylene
HRR	heat release rate
HX	hydrogen halide
LDHs	layered double hydroxides
LDPE	low density polyethylene

IR	infrared
L.O.I.	limiting oxygen index
MA	melamine
MAS	magic angle spinning
MCAPP	microencapsulated ammonium polyphosphate
MDH	magnesium dihydroxide
MHP	melamine hypophosphite
MFR	melt flow rate
MMT	montmorillonite
MP	melamine phosphate
MPi	melamine phosphite
MLC	mass loss calorimetry
MLC-FTIR	mass loss calorimeter coupled with Fourier transform infrared
Mn	molar mass in number
Mw	molar mass in weight
MWCNTs	multi-walled nanotubes
NC	no classified
NMR	nuclear magnetic resonance
PA	polyamide
PA-6	polyamide-6
PBS	polybutylene succinate
PBIT	poly(butylene-co-isosorbide terephthalate)
PBSA	poly(butylene succinate-co-adipate)
PC	polycarbonate
PCBs	polychlorobiphenyls
PCFC	pyrolysis Combustion Flow Calorimeter
PDMS	polydimethylsiloxane
PDMSi	polydimethylsiloxane isosorbide
PE	polyethylene
PEIT	poly(ethylene-co-isosorbide terephthalate)
PET	poly(ethylene terephthalate)
pHRR	peak of heat release rate
PIC	poly(isosorbide carbonate)

PLA	polylactide
PMMA	poly(methyl methacrylate)
PMPSi	polymethylphenylsiloxane isosorbide
POSS	polyhedral oligomeric silsesquioxane
PP	polypropylene
PPPAI	polyphenylphosphate isosorbide
PPPI	polyphenylphosphonate isosorbide
PU	polyurethane
py-GC/MS	pyrolysis-gas chromatography-mass spectrometry
RDP	resorcinal bis(diphenyl phosphate)
SEM	scanning electron microscopy
STA	simultaneous thermal analysis device
SWNTs	single-wall nanotubes
TEO	tetraethoxysilane
Tg	glass transition temperature
TGA or TG	thermogravimetric analysis
TGA-FTIR	thermogravimetric analysis coupled with Fourier transform infrared
TPP	triphenyl phosphate
THR	total heat release
Tm	melting temperature
TMS	tetramethylsilane
TTI	time to ignition

General introduction

Synthetic polymers have become one of the most important industrial products since the 20th century. Due to their low cost, good mechanical properties and ease of manufacture, polymers are widely used in packaging, medicine, construction and textile etc. The production of polymers has grown continuously since the 1950s. Up to 2016, the worldwide production of polymers is over 335 million tons/year. The production in Europe shares 19 % of it, which is around 60 million tons/year (**Figure 1**).¹

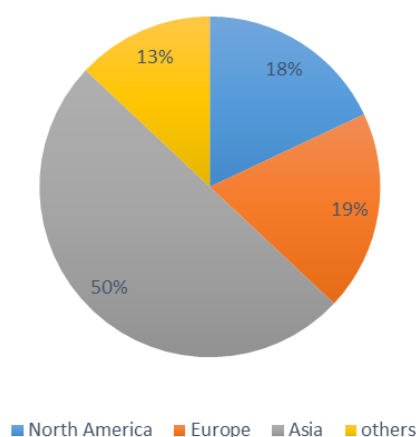


Figure 1: Global polymer market share in %

A major drawback of organic polymers is their high flammability. In many applications, such as construction, transportation, electric and electronic field, flame retarded polymers are required. By using fire retarded materials, the loss caused by the fire significantly decreased during the last ten years. From 2006 to 2015, in United States, the casualties (death and injured) caused by fire accident decreased from 19 645 to 18 980, and the loss of properties decreased by 20 % which is around 2.8 billion dollar.² Nevertheless, with a large number of casualties and a great loss of properties, there are still lot of work to do on fire retarded polymers.

Synthetic polymers bring convenience to our daily life, but at the same time, they bring us also serious environmental crisis. Its low degradability in the environment causes severe pollution in soil and water which affect wild life and human, thus leads to the development of bio-based polymers. Polybutylene succinate (PBS) is one of the most common bio-based polymers. It has good mechanical properties close to polypropylene (PP) and polyethylene (PE).³ It can be 100%

bio-based and it has good biodegradability. In addition to this, its good processability permits to adapt different application demands.⁴ Thanks to these properties, PBS is a polymer which can be used in a large domain of applications like packaging, medical articles and agriculture etc. Furthermore, it can be possibly applied in the field of electric and electronic (E&E) and transportations which can open new market for PBS.

However, PBS is highly flammable, and the forming drops during a fire scenario can spread the fire. Thus, its applications on the domains where the fire retardancy is needed are limited. This shortcoming of PBS draw much attention of the researchers. Papers concerning the PBS and its flame retardancy were increasing during the last twenty years (**Figure 2**). Despite more and more studies have been carried out to develop the new formulations to flame retard PBS, some of the studies has still some disadvantages: i) the content of loading is relatively high, ii) formulation of FR PBS is lack of bio-based content. Therefore, our study on FR PBS focused on these points. In order to solve the above mentioned problems, our study deals with the flame retardancy of PBS via three different approaches: i) synthesis of new bio-based flame retardants, ii) bio-based polymer as carbonization agent, iii) application of conventional fire retardants. Besides the investigation of new FR formulations for PBS, new methodologies to investigate the mode of action of the flame retardant system were also developed and are detailed in this work.

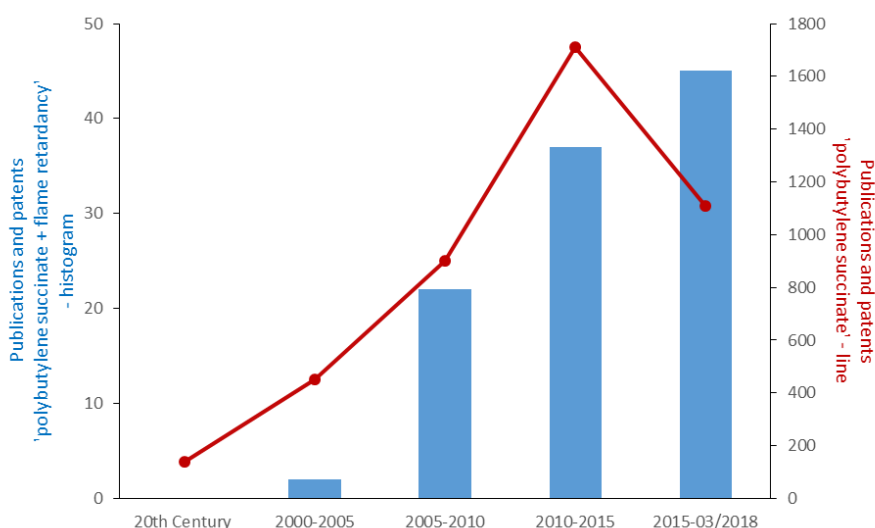


Figure 2: Number of publications and patents containing 'polybutylene succinate' and 'polybutylene succinate + flame retardancy' (scifinder march 2018).

Particularly, the synthesis of bio-based fire retardants and the bio-based polymers are based on a saccharide: Isosorbide, also named after 1,4:3,6-dianhydro-D-sorbitol or 1,4:3,6-dianhydro-D-glucitol. The global market of isosorbide share a value of 250 million dollar in 2014, and it has an estimation of 400 million dollar in 2020.⁵ The production capacities has also a growth from 31.5 kiloton/year in 2014 to an estimated 52.8 kiloton/year in 2020. A French plant-based chemicals firm Roquette, has launched the largest isosorbide production unit world widely in 2015 with a capacity of 20 kiloton/year.⁶ Isosorbide is mainly used in the medication domain and as a building block for polymers for the moment. Thus, the application of isosorbide for fire retarding polymers can enlarge its own market. For this work, study on mode of action of isosorbide in a FR system can extend our knowledge of the behavior of bio-based components in a fire situation.

This PhD thesis is organized in five chapters. The first chapter is a general overview of the background on PBS, flame retardancy of polymers and specifically flame retardancy of PBS. Particularly, isosorbide and its modifications acting as flame retardants are discussed.

The second chapter introduces the materials and the methodologies of the study. Identification of the synthesized of the isosorbide based FRs is described.

The third chapter presents the screening of different FR formulations of PBS with various additives. Characterization of isosorbide based FRs and the results of the fire tests are presented. Then the use of isosorbide and isosorbide-based polymers as carbonization agent and its fire tests are investigated. Formulation of PBS with a series of conventional FRs as well as their performance in the fire tests are also presented.

The fourth chapter investigates how 9,10-dihydro-9-oxa-10-phosphaphenanthrene-10-oxide (DOPO) works in PBS during a fire scenario. Its mode of action in MLC and UL-94 tests are deeply investigated using various techniques.

The fifth chapter focuses on the mechanism of the formulation where poly(isosorbide)carbonate (PIC) acts as a carbonization agent in an intumescent FR system.

The final part is a general conclusion of this study, and outlook on this subject is commented.

Chapter I - State of the art

I State of the art

This chapter is dedicated to an overview of the knowledge about polybutylene succinate (PBS) and its flame retardancy that have been described in the literature. In the first section of this chapter, synthesis and physico-chemical properties of PBS is presented. The second section gives the fundamental knowledge of the combustion of polymers, and a brief summarize of the existing flame retardants is introduced. The third section focus on the current methods of the flame retardancy of PBS and it composites enhanced by natural fibers. A conclusion is given in the final section.

I.1 Polybutylene succinate

PBS is an aliphatic thermoplastic polymer which is based on succinic acid and 1,4-butanediol. The studies on succinic acid based polymers began from the middle age of 19th century. Only since 1993 did a semi-industrialized plant of PBS was built by a Japanese company Showa High Polymer. Compared to some other bio-based polymers, an advantage of PBS is its good processability. As results, PBS can be easily manufactured and adapt to different processing methods such as extrusion, compress molding and injection etc. Nowadays, PBS is mainly used in applications like packaging, medical articles and agriculture etc.⁷

I.1.1 Synthesis of polybutylene succinate

The most common synthesis process of PBS is the direct esterification between 1,4-butanediol and succinic acid. This process consists in two steps (**Figure 3**), the first step involves a polycondensation between the diacid and the diol in excess leading to a formation of PBS oligomer, the second step is a trans-esterification among these PBS oligomers in presence of certain catalysts (mainly based on titanium (IV)) to form the high molar mass PBS.^{8,9}

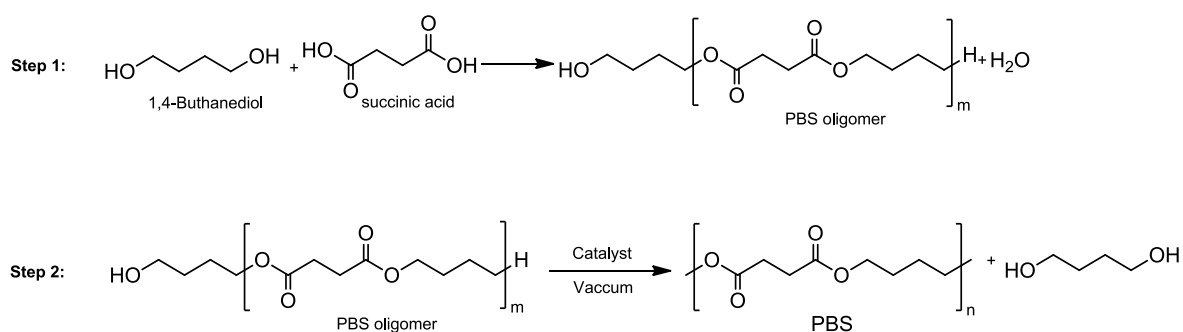


Figure 3: Two steps synthesis route of PBS

1,4-butanediol is an important intermediate in chemistry industry, which is used in wide variety of applications such as solvent or building block for several plastics, elastic fibers and polyurethanes. It can be obtained by several reactions starting from different components like acetylene, propylene oxide, maleic anhydride and butadiene etc. Nowadays, most of the productions of 1,4-butanediol are still petroleum-based. Recently, Novamont opened in 2016 the first industrial scale plant to produce bio-based 1,4-butanediol via microorganism. This process need only the fermentation of sugar by bacteria.¹⁰ It has a production capacity of 30 kilotons/year, which has 50 % reduction of CO₂ emission. This success provides a route for the synthesis of a bio-based PBS at commercial scale.

The other monomer for the synthesis of PBS, succinic acid, which is a component usually used as a precursor for polymer, resin and solvent. It has also been used as food additive and dietary supplement. Succinic acid market shares a value of 157 million dollar in 2015 and is estimated to reach a value of 900 million dollar by 2026 world widely.^{11,12} The production of fossil-sourced succinic acid is mainly from n-butane through maleic anhydride (**Figure 4**). However, succinic acid obtained starting from glucose (**Figure 4**) offers a lower price compared to the traditional fossil-sourced succinate acid (e.g. in 2006, 0.977\$/kg petroleum-based vs. 0.428\$/kg bio-based).¹³ It can be foreseen that the bio-based succinic acid will replace its fossil-based alternative for both economic and environmental reasons.

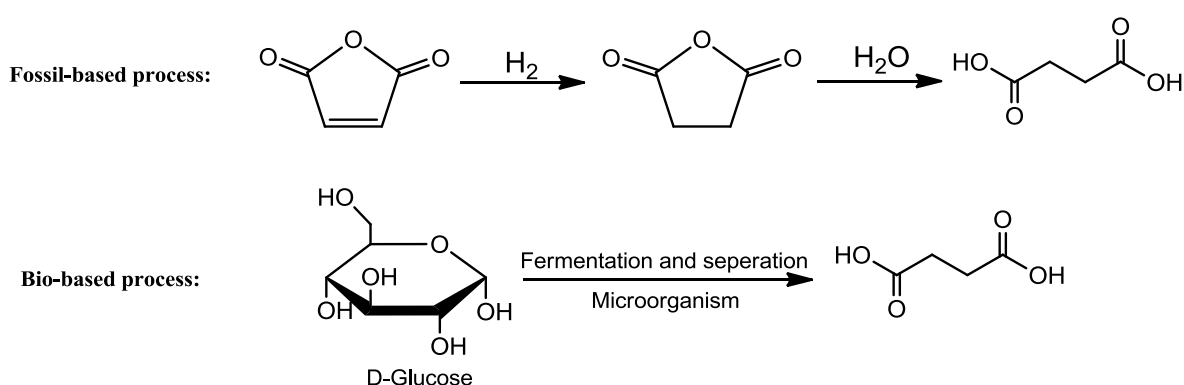


Figure 4: Two synthesis routes of succinic acid

The main production of PBS is currently still petroleum-based with a relatively small quantity. Nevertheless, the production capacity is rapidly increasing owing to the development of its bio-based precursors, knowing that bio-based succinic acid has a lower cost than its petroleum-based alternative. If the precursors (diacid and diol) can be all produced via a renewable source, it is suitable to produce bio-based PBS without changing the current

production equipment. It is estimated that the production of bio-based PBS could reach 80 % of all the production of PBS by 2020.¹⁴

I.1.2 Physico-chemical properties of polybutylene succinate

The applications of PBS is firmly related to its physico-chemical properties. Thus in this section the mechanical properties and the processability of PBS was firstly presented. Then its biodegradability and the thermal degradation are presented as well.

I.1.2.1 Mechanical properties and processability of PBS

The comparison of the mechanical properties of PBS with low density polyethylene (LDPE), high density polyethylene (HDPE) and polypropylene (PP) is presented in **Table 1**. The tensile strength of PBS is between PE and PP and the stiffness is between LDPE and HDPE.⁴

Table 1: Mechanical properties of PBS, LDPE, HDPE and PP

	PBS	LDPE	HDPE	PP
Yield strength (Kg/cm ²)	336	100	285	330
Elongation (%)	560	700	300	415
Stiffness 10 ³ (Kg/cm ²)	5.6	1.8	12.0	13.5

Compared to other bio-based polyesters, the big advantage of PBS is the processability. The processing methods for PBS or its copolymer poly(butylene succinate-co-adipate) (PBSA) depend on a relation between melt flow rate (MFR) and the molar mass (Mn and Mw) as showed in **Figure 5**.⁴ Thus according to different molar mass and MFR, PBS can be processed by different methods such as inject molding,^{15,16} film extrusion,¹⁷ flat and split yarn,¹⁸ filament¹⁹ etc.

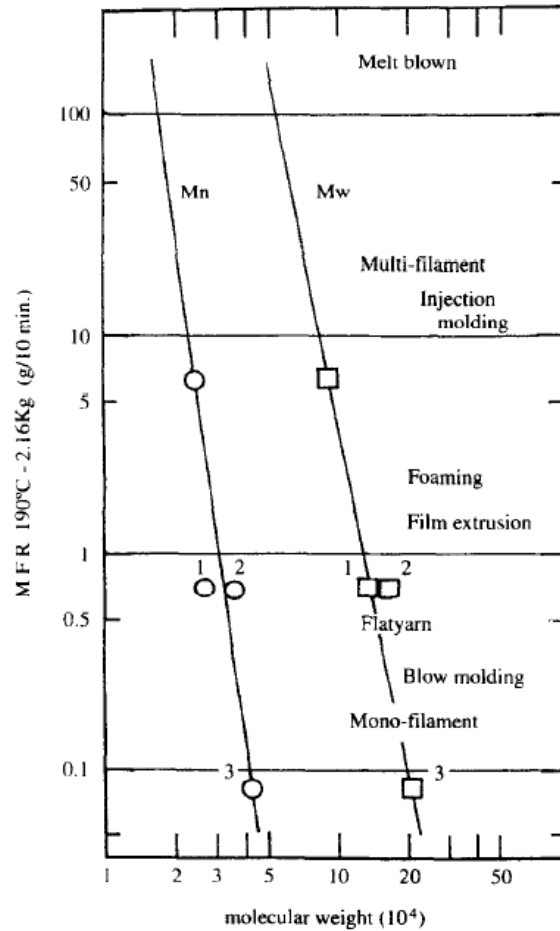


Figure 5: Relationship with molecular weight, melt flow rate (MFR) and processing methods of PBS and PBSA.

I.1.2.2 Bio-degradability of polybutylene succinate

PBS can completely decompose into CO₂ and H₂O in certain conditions: in compost, in moist soil (**Figure 6**), in fresh water with activated sludge, in sea water and under the presence of microorganisms etc.^{20, 21, 22} Biodegradation speed of the PBS depends on degradation conditions, form and size of the samples, and different type of microorganisms.^{20,23,24}



Figure 6: Degradation of PBS in moisture soil

I.1.2.3 Thermal degradation of polybutylene succinate

The onset degradation temperature (2% of mass loss, $T_{2\%}$) of PBS described in the literature is 329°C.^{25,26} TGA curve showed a one-step decomposition process from 396°C to 460°C under inert atmosphere. Whereas the dTG curve showed a very small divergences that can be observed before the major peak (**Figure 7**).²⁶ This kind of small pre-major weight loss can be also observed in poly (propylene terephthalate), it can be attributed to some small molecules: residual catalysts, 1,3-propanediol and carbon dioxide that devaluated from chain ends.²⁷ While in the case of PBS, it can be attributed to the oligomer degradation.

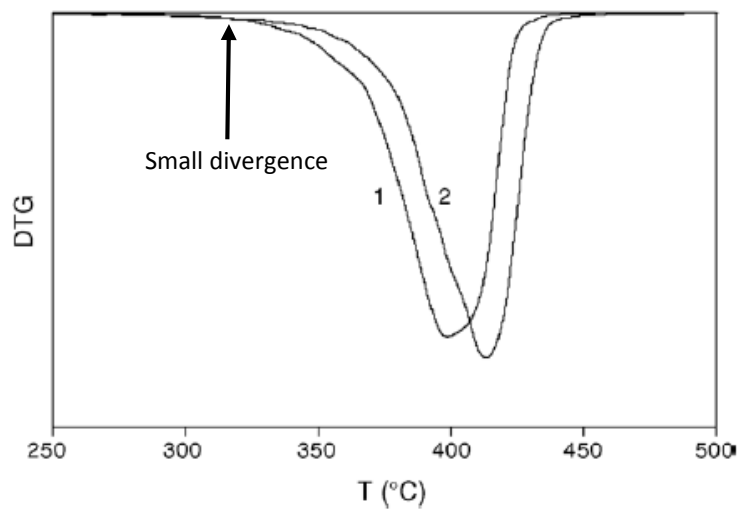


Figure 7: Derivative mass loss (DTG) of 1) polybutylene succinate 2) polyethylene succinate (10°C/min N₂)

According to the literature,^{28,29} the pyrolysis products of biodegradable polyesters are majorly various ester compounds containing monomers and hybrid dimers. These compounds were produced mainly through the reaction of random chain cleavage via cis-elimination. On the other hand, some cyclic compounds were found, which were likely formed through intramolecular transesterification.^{30,31} The pyrolysis products of PBS-co-adipate (PBSA) was firstly studied by Sato et al.³² Then Shih et al. studied the pyrolysis products of PBS.³³ Tetrahydrofuran, 1,4-butanediol, succinic anhydride, diallyl succinate, and dibutenyl succinate are the major products released at lower pyrolysis temperatures (50-300°C), and 1,3-butadiene, diallyl succinate, dibutenyl succinate, and other cyclic succinates are the major products at higher temperature. Promising mechanism of the formation of some pyrolysis products are presented: i) the formation of alkene and carboxylic groups at the end of the chain (**Figure 8**), ii) then a decarboxylation occurs at the end of chains containing carboxylic

acid group and along with a releasing of CO₂ (**Figure 9**) at the same time, iii) cyclic compounds are formed through intra-transesterification of the chain (**Figure 10**).

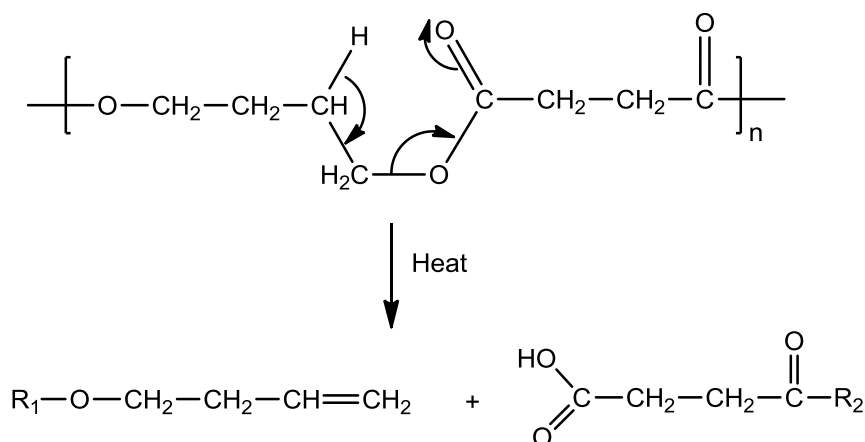


Figure 8: Formation of alkene and carboxylic groups at the chain end

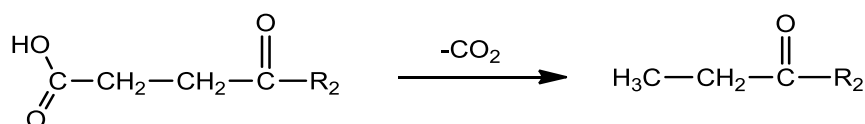


Figure 9: Decarboxylation at the end of chains

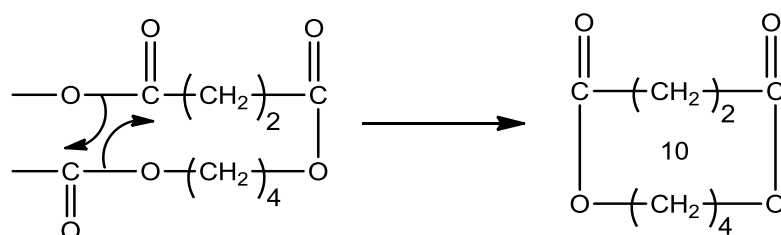


Figure 10: Formation of cyclic compounds

I.1.3 Conclusion

This section described the synthesis, and physico-chemical properties of PBS. It shows that good mechanical property and good processability of PBS permit various applications. However, until now there is no industrial use of PBS in the domain such as transportation, electric and electronic field caused by its high flammability. In this case, improvement of flame retardancy of PBS is necessary for these applications.

I.2 Flame retardancy of the polymers

To flame retard PBS, it is necessary to know the nature of the combustion and the methods to flame retard polymers. Therefore, this section described firstly the combustion of polymers

and the strategy to flame retard polymers. Then different types of flame retardants and their mode of actions are presented.

1.2.1 Combustion of polymers

Organic polymers are often highly flammable because of their own nature.³⁴ Three general elements of fire show on the 'fire triangle' (**Figure 11**): fuel, heat source and oxidation agent which is often oxygen. When a thermoplastic is exposed to heat, it become soft and start to melt. When energy reached on the surface of a polymer pass the critical energy to break the bonds in molecule, the polymer starts to decompose. Then gases are released and they mix with oxygen. When combustible gases reach a critical concentration, they start to burn. The burning fuel can reproduce heat to decompose more un-burning polymer, and the newly decomposed polymer feedback more fuels.

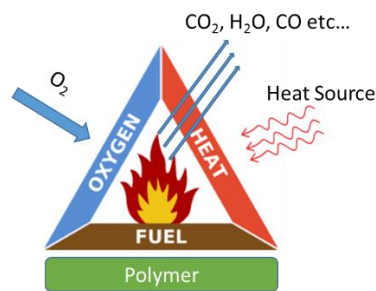


Figure 11: General aspects of fire showed on 'Fire Triangle'

1.2.2 Mode of action of flame retardancy

Methods to stop or inhibit the flame have been proposed in the literature.³⁵ The principle of flame retardancy is to stop any one of these elements of the fire triangle. Modification on the polymer or addition of flame retardants provides a pathway to achieve this goal without changing the outer condition such as the heat source and the oxygen source.

First of all, some flame retardants or modification of polymer lead to less combustible gases released upon decomposition which cut or decrease the supply of the fuel. This process often has a formation of char or release of nonflammable gases.

Secondly, several compounds are endothermic when they decompose, so the heat feedback of the fuel can be reduced. Especially when intumescent fire retardants are used, the creation

of a protective barrier can also give a similar effect to reduce the heat feedback on the polymers.

Thirdly, regarding the presence of oxygen, the protective barrier can isolate the inner side of polymer from the oxygen. Additionally, additives that produce nonflammable gases such as H_2O and CO_2 can reduce the concentration of oxygen. Finally, introduction of 'flame poisoner' can act in the gaseous phase to inhibit the active radicals.

I.2.3 Flame retardant additives

The major method to flame retard polymers is by addition of flame retardants. The history of fire retardants begins from a very early age. Ancient Egyptians and ancient Romans used asbestos to produce flame retarded textiles. The dangerous negative health effects of asbestos limits its applications. Modern FRs have large development after the 1950s. Dramatically increasing of use of synthetic polymers in applications such as vehicles, foams, textiles and E&E leads the further study of FRs. The FRs market was valued about 6 billion dollar in 2014 and it will have still a large growth in the following years.³⁶

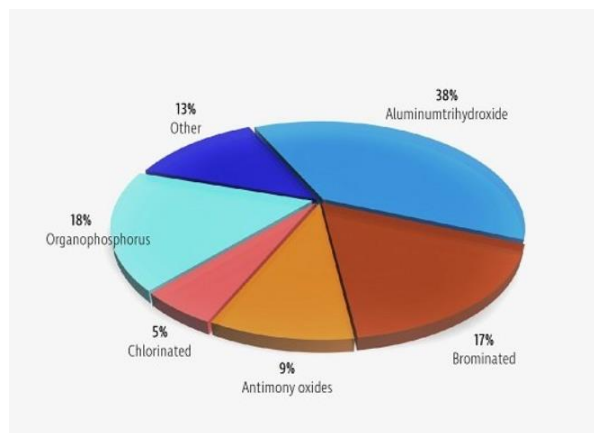


Figure 12: Global FRs share by type in 2016

I.2.3.1 Halogen-containing flame retardants

During a very long period, halogen-containing FRs possess the major position on the market due to its good efficiency of fireproofing and its commercial ability. Even today, they still share 22 % of all the commercialized FRs (**Figure 12**), which is the second largest among them.³⁷ The session of carbon-halogen bond creates halogen radicals (**Figure 13**). Then the halogen radicals react with polymer chain which can generate hydrogen halide (HX). The hydrogen

halide can trap the active free radicals which leads to an effective inhibition of the flame.³⁸ Day et al.³⁹ showed also that as a flame poisoner, HX can be regenerated by a reaction in **Figure 13**, which means the HX would not be consumed in the reaction and can always support the anti-fire system.

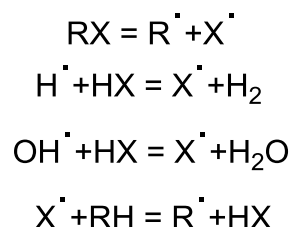


Figure 13: Mechanism of radical quenching by halogenated FRs, X = F, Cl, Br and I, R = organic group

The stability of carbon-halogen bond can be classified by this order: F>Cl>Br>I. In reality, the carbon-iodine bonds are too weak to resist the polymer processing, however the fluorine-carbon bonds are too stable to generate the anti-fire reaction. So, chlorinated and brominated compounds are usually used in the fire retardant domain.

Environmental concerns related to halogenated fire retardant have been evidenced by several environmental and consumers agencies. Halogenated fire retardant can probably produce toxic and corrosive products, and increase the production of smoke when the fire retardant action is performed or when a fire is fully developed. Furthermore, the entire life cycle of halogenated FR has been considered as a great environmental concern since the synthetic halogenated compounds such as polychlorobiphenyls (PCBs), 1,3,7,8-tetrachlorodibenzodioxine (Dioxine) and benzofuranes have been proved to have a contamination effect by bioaccumulation.³⁸ For these reasons, halogenated flame retardants are not taken into account in our works.

1.2.3.2 Phosphorus-based flame retardants

Phosphorus-based fire retardants are the most used alternative to halogenated fire retardants. In the last decades, elemental phosphorus and phosphorus-based compounds have been already used as fire retardants and it can be foreseen that they will possess the largest growing parts in the future flame retardant market. Phosphorus-based fire retardants are very effective and usually considered non-toxic due to the formation of protective char in which

the phosphorus are locked.⁴⁰ Nevertheless, they are not effective for some important class of polymer like polyolefin and styrenic resin, and they also possibly increase the production of smoke in a fire scenario.

Phosphorus based fire retardant can act in gaseous phase and/or in condense phase. In the gaseous phase,⁴¹ some of them act as flame inhibitor by trapping the radicals (e.g. **Figure 14**). This action is similar to halogenated FRs, radicals like PO· and P· are formed and they are capable to react with high energy free radicals to poison the flame. In the condensed phase, they can react with carbon rich components and promote the formation of char (often called intumescent char) which protects the inner polymer matrix^{42,43}.

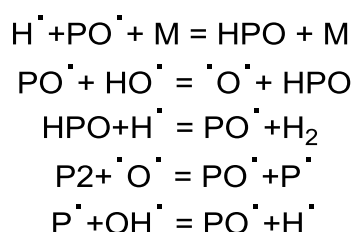


Figure 14: Fire retardant action of triphenylphosphine oxide and triphenyl phosphate in gaseous phase (M is a third body species)

Phosphorus containing flame retardants are majorly organophosphorus compounds and inorganic phosphorus compounds. In the organophosphorus compounds, metal salts (zinc, aluminum and calcium) of dialkyl phosphinates have been developed and commercialized since the 1970s.^{44,45,46} Especially, the aluminum salts of diethyl phosphinate (**Figure 15**) was proven to be effective in novolac, epoxy resin, glass-fiber reinforced polyamide (PA) and polyester.^{47,48} It was also found that the efficiency of metal phosphinate can be significantly improved when blending with nitrogen containing components.⁴⁹ Aromatic phosphates (**Figure 16**) are also a series of organophosphorus flame retardants such as triphenyl phosphate (TPP), resorcinol bis(diphenyl phosphate) (RDP) and Bisphenol A bis(diphenyl phosphate) (BDP) etc., which are often effective to flame retard polycarbonate (PC).^{50,51} Another important series of organophosphorus flame retardants are 9,10-dihydro-9-oxa-10-phosphaphenanthrene-10-oxide (DOPO) (**Figure 17**) and DOPO-based flame retardants. DOPO was firstly patented by Sanko Chemical Co. Ltd.⁵² The phosphorus atom in DOPO can be reactive toward nucleophiles and electrophiles.⁵³ Thus, a large number of DOPO derivatives

were synthesized.⁵⁴ This phosphorus containing compound and its derivatives have been largely applied mainly for flame retarding epoxy resin.^{55,56,57}

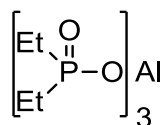
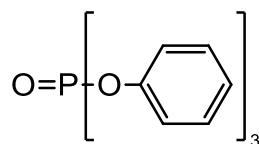
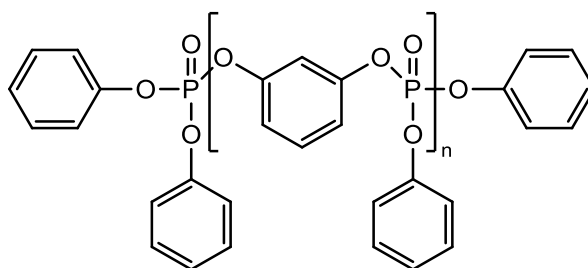


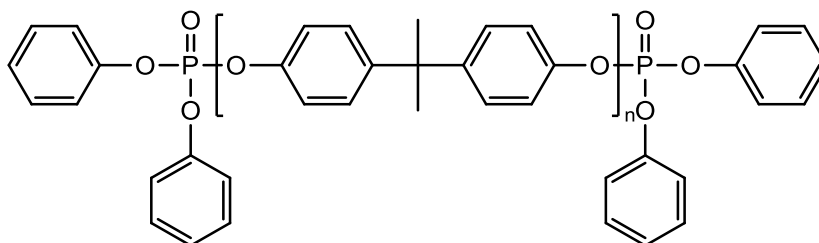
Figure 15: Commercially available aluminium phosphinates (Exolit OP 930/935)



Triphenyl phosphate (TPP)



bis(diphenyl phosphate) (RDP)



Bisphenol A bis(diphenyl phosphate) (BDP)

Figure 16: Aromatic phosphates

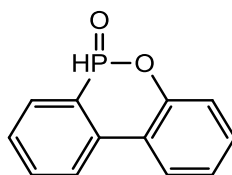


Figure 17: 9,10-dihydro-9-oxa-10-phosphaphenanthrene-10-oxide (DOPO)

In the inorganic phosphorus flame retardants, red phosphorus has been known for long time as a very effective fire retardant. It's mainly used in polyamides, polycarbonates and polyesters.^{58,59} In a flame, red phosphorus decomposes to form P_2 which can act in gaseous phase. It has also some obvious disadvantages: toxic phosphine (PH_3) can be released when it

reacts with moisture, thus the storage needs to be in suitable stabilization and encapsulated in an appropriate polymer matrix.

There are some other organophosphorus and inorganic phosphorus flame retardants can create a special intumescent phenomenon in a fire scenario. Thus, these phosphorus based flame retardants and the fundamentals of intumescence are presented in the next part.

1.2.3.3 Intumescent-based flame retardants

Intumescent-based flame retardants are widely used to flame retard polymers. Even though the concept of intumescent was proposed since the 1970s, it plays still an important role today in the field of the flame retardancy of polymeric materials.^{60, 61} The fundamentals of intumescence are investigated by Camino et al.,⁶² which include three components:

- An acid source: inorganic acid, acid salts or organophosphorus compounds that promotes the dehydration of carbonization agent. The inorganic acid can often be phosphoric, sulfuric and boric acid. Ammonium salts such as ammonium phosphate (AP) or ammonium polyphosphate (APP) can be used as acid source as well. Besides, some alkyl phosphates and tricresyl phosphate can also be used as acid source.
- A carbonization agent: carbohydrates that can be dehydrate by the acid to promote a protective char. The efficiency of the formation of char does not rely on the number of carbon atom, but the rate of dehydration depends on the number of the reactive hydroxyl sites which is highly related to the rate of formation of char.⁶³ For this reason the carbonization agent can often be the components that contains reactive hydroxyl groups such as pentaerythritol and starch. It was also found that some of the polymers that promotes the char forming such as polyamide-6 (PA-6), Polyurethane (PU) can also act as carbonization agent.
- A blowing agent: components that release gases upon decomposition which leads to the expansion of the formed char. Nitrogen containing components such as Urea and melamine are often used as the blowing agent.

With these three components, the processing of the intumescent flame retardant system can be summarized: the acid is released during the decomposition of the acid source leading to the dehydration of the carbonization agent. With an expansion effect brought by the blowing

agent, a protective shield can be formed. It is noteworthy that the temperature of release of the acid must be lower than the decomposition temperature of the carbonization agent. It is also important that the dehydration must occur at a temperature lower than the decomposition temperature of the polymer matrix.

I.2.3.4 Metallic hydroxides

Another alternative to halogenated fire retardants is metallic hydroxide such as aluminum trihydroxide (ATH) and magnesium dihydroxide (MDH). Fire retardant effect of metallic hydroxide acts both in the condensed phase and in the gaseous phase. The decomposition of metallic hydroxides results in water and metal oxides. This reaction is highly endothermic that reduces the energy transferred to the polymer matrix (**Figure 18**). Evaporation of the water formed in the reaction cools down the substrate and dilute the concentration of the flammable gases⁶⁴. Metal oxides released during the reaction can form on the surface which prevents the heat and gases release.

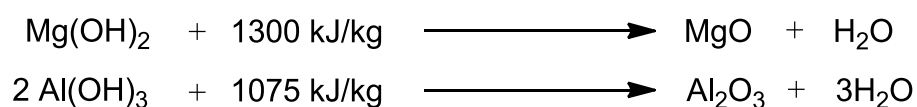


Figure 18: Degradation of Magnesium hydroxide and aluminum hydroxide

This category of fire retardant isn't expensive, relatively abundant and non-toxic.⁶⁵ ATH was widely applied for the polymers that possess a relatively low processing temperature such as ethylene vinyl acetate (EVA), polyethylene (PE), epoxy and phenolic resin.^{66,67,68} MDH have a higher decomposition temperature, thus the polymers such PP, PA, acrylonitrile-butadiene-styrene (ABS) which possess higher processing temperature can be flame retarded by MDH.^{69,70,71}

Despite these advantage and the wide application of ATH and MDH, relatively high charge of these additives is often needed (30 % - 60 %), which modify physical and chemical properties of the polymer matrix.

I.2.3.5 Silicon-based flame retardants

Silicon is an element existing almost everywhere around us. In the domain of fire retardancy, lots of researches have shown that silicon containing compounds has a good improvement of

fire resistance for several polymers. Silicon based fire retardants have less environmental impact compared to halogen containing fire retardants. So they are considered as eco-friendly fire retardants for polymeric materials.

Silicon based flame retardants includes silicones and silica. Silicones are a class of polymers containing repeating unit of siloxane. Siloxane is a functional group which has a Si-O-Si linkage such as Polydimethylsiloxane (PDMS) (**Figure 19**). It was often incorporated in polymer chains to form co-polymer. It provides relatively low rates of heat release. This phenomenon was previously reported by Kashiwagi et al., which used the silicone as an additive or a copolymer to incorporate into PC.⁷² In addition to this, silicone is also effective for PU, epoxy resin, ethylene-acrylate copolymer, polystyrene and Poly(methyl methacrylate) (PMMA) when incorporated in the polymer chains.^{73,74,75,76}

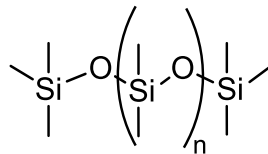


Figure 19: structure of polydimethylsiloxane (PDMS)

Another type of silicon containing fire retardant is silica. The direct use or acting as synergist of Silica showed good performance when incorporated in PP, PMMA, EVA.^{77,78,79} It showed that in these formulations, silicate can accumulated at the surface which can generate a protective layer during the combustion.

1.2.3.6 Nanoparticles

The formation of nanocomposite has huge influence on polymers in mechanical, solvent-resistance and barrier properties etc.⁸⁰ In the field of fire retardancy of polymers, the addition of nano additives has become an effective and popular solution to improve the fire resistance of polymers in the last few decades. Particularly, they enable a significant reduction of the loading rate as the interfacial area between the polymer and the nanoparticles is largely increased.

The properties and efficiency of the nanoparticles in a flame retarded formulation depend a lot on their chemical structure and geometry. The layered nanoparticles such as nanoclay (e.g. montmorillonite: MMT) (**Figure 20**) consist in stacking of multilayer sheets where each sheet

is composed of two outer layers of silica tetrahedra and one central layer containing monovalent, bivalent or trivalent atoms (Al^{3+} , Mg^{2+} , Fe^{3+} , Fe^{2+} , Na^+ , K^+ , etc.) that negatively charge the sheet. The negative charge is compensated by the presence of cations between the stacked sheets. Moreover, nanoclay was often modified with organic cations (alkylammonium, alkyl phosphonium and alkyl imidazol(idin)ium cations) to improve their dispersion in the polymer.⁸¹ Layered double hydroxide is another layered nanoparticle which possess a similar structure as nanoclay, these layered nanoparticles are often used for the fire retardancy of PP, EVA, PA-6 etc.^{82,83,84}

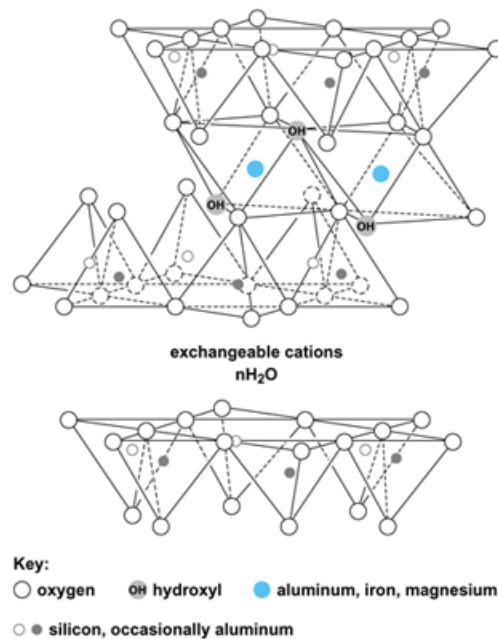


Figure 20: Structure of montmorillonite⁸⁵

Carbon based nanoparticles such as carbon nanotubes and graphene, are also used for the flame retardancy of polymers. Carbon nanotubes (CNTs) are cylindrical shells made, in concept, by rolling graphene sheets into a seamless cylinder. CNTs exist as either single-wall nanotubes (SWNTs) or multi-walled nanotubes (MWCNTs).⁸⁶ Graphene was first reported in 2004,⁸⁷ with which the inventors won the Nobel Prize in 2010. Since then, lot of work and the application researches have been carried out due to its special two-dimensional atomic carbon sheet structure (**Figure 21**).⁸⁸ These carbon based nanoparticles can be used for fire retardancy of epoxy resin, PLA, PA-6 etc.^{89,90,91,92}

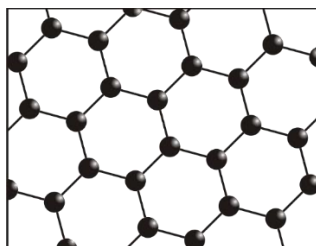


Figure 21: Structure of graphene

Particulate nanoparticle such as polyhedral oligomeric silsesquioxane (POSS) is also proved to be efficient for flame retardancy of polymers. It is a molecule containing a polyhedral silicon-oxygen nanostructured skeleton which was first found in 1946.⁹³ It has a special structure: stable framework of silicon-oxygen and each silicon atom on the corner can be attached with different organic functional substituents (**Figure 22**). As a nano additive for the fire retardancy of polymer, POSS was proved to be an effective fire retardant synergist with phosphorus compounds for poly(ethylene terephthalate) (PET) and epoxy resin etc.^{94,95}

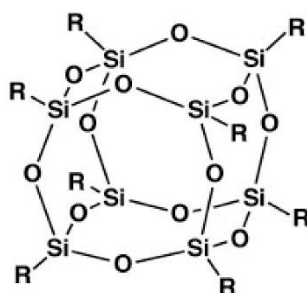


Figure 22: Structure of POSS

In general, the nanoparticles incorporated in polymer matrix can often improve the thermal stability of the composite, reduce the heat release rate and improve the char yield. An additional phenomenon that should be noted is that these polymer nanocomposite can usually had no dripping and retain the shape of the original sample during the course of combustion. These properties make it possible to apply for the improvement of flame retardancy of PBS.

1.2.3.7 Isosorbide-based flame retardants

Besides the conventional flame retardants as presented in the previous parts, development of flame retardants derived from bio-mass such as lignin, deoxyribonucleic acid (DNA) and protein showed interesting features.⁹⁶ Among these bio-based components, isosorbide drew

our attention for its easy access of the modification by flame retardant functional groups. Thus the physico-chemical properties of isosorbide and the modification of isosorbide are described in this part.

I.2.3.7.1 Generality of isosorbide

Environmental problem caused by petroleum-based products may be solved by the utilization of products from biomass. Especially, cellulose is one of the most abundant products of the biomass (35 – 50 %).⁹⁷ Cellulose has a barely competition with food production, which is an advantage compared to some other types of saccharide (e.g. starch). The conversion (depolymerization) from cellulose to glucose by hydrolysis has been well researched. Glucose is an important immediate for producing other biomass-based products, and isosorbide is one of them.

Isosorbide, also named after 1,4:3,6-dianhydro-D-sorbitol or 1,4:3,6-dianhydro-D-glucitol, is a heterocyclic compound obtained by dehydration of sorbitol which derived from D-glucose (**Figure 23**). It is a stable white solid in room temperature, and it can be dissolved in water. Isosorbide has two isomers, isomannide and isoidide (**Figure 24**).

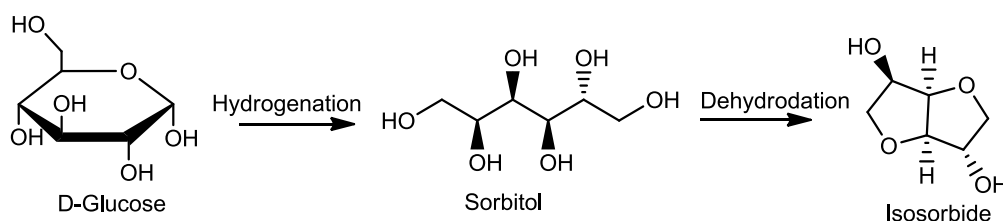


Figure 23: Synthesis route of isosorbide

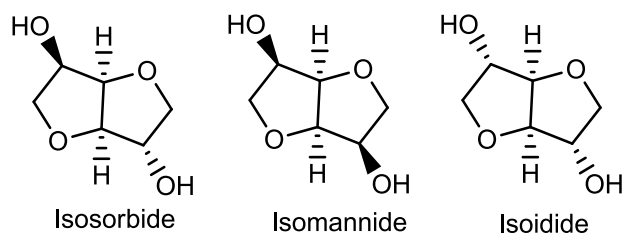


Figure 24: Isosorbide and its isomers

Isosorbide has two cis-connected tetrahydrofuran rings structure. These two rings are not in the same flat surface, in fact, they are in a V-shape with an angle of 120°. Two hydroxyl groups are in the 5- and 2- positions with exo and endo positions respectively.^{98,99} The endo hydroxyl

group can form an intra-molecule hydrogen bond. However, the exo hydroxyl group cannot form the hydrogen bond. Influence of the different configuration of the hydroxyl groups can be seen from the comparison of isosorbide with its isomers. Isoidide possess a totally exo configurations, on the contrary isomannide possess a totally endo configuration. This difference leads to different physical properties between isosorbide and its isomers e.g. the different melting temperature⁹⁸. The chemical reactivity of the hydroxyl groups depends also on their configuration. It was proved that the endo hydroxyl group is more nucleophile than the exo hydroxyl group because of the presence of hydrogen bond.¹⁰⁰ Whereas steric hindrance of 2-position can inert the reaction when steric substituent is demanded, and in this case 5- position substitution is more preferable.

These two different configurations show different performance when characterized by Fourier Transform Infra-Red spectroscopy (FTIR): (i) band at 3624 cm^{-1} corresponding to the O-H vibration of which do not have a hydrogen bond in exo position, and (ii) band at 3540 cm^{-1} corresponding to the O-H vibration of which has a hydrogen bond in endo position.¹⁰¹ This provides us a simple method to characterize the isomers and the reactions on only one hydroxyl groups.¹⁰²

Isosorbide is more widely used than its isomers. The reasons are compared to isomannide, isosorbide is more reactive and lower in price because mannitol, the precursor of isomannide, is harder to obtain than sorbitol; and considering isoidide, even though it is more reactive, the precursor L-idose cannot be obtained directly from biomass.

One of the major applications of isosorbide is on the medication domain. Isosorbide and isosorbide-based medicine are usually used to treat some diseases like hydrocephalus, glaucoma, angina pectoris etc. Di/mono-Nitrate isosorbide has been used for the ischemic heart disease.¹⁰³

Another application of isosorbide is for the construction of polymer as a monomer (**Figure 25**): i) isosorbide can replace bisphenol A (BPA) to form isosorbide based polycarbonate which can be less toxic and which possesses still a good optical property;^{104,105,106,107,108} ii) isosorbide can react with epichlorhydrin to form polyglycidyl ether;^{109,110,111} iii) isosorbide can be building block to form poly(ethylene-co-isosorbide terephthalate) (PEIT) and poly(butylene-co-isosorbide terephthalate) (PBIT) which have higher Tg than petroleum based PET and

poly(butylene terephthalate) (PBT);^{112,113,114,115} iv) isosorbide can react with diisocyanate to form polyurethane. Furthermore, the amine^{116,117,118} and diisocyanated^{119,120} modification of isosorbide (**Figure 25**) may act as new types of monomer to synthesize bio-based polyamide and polyurethane.

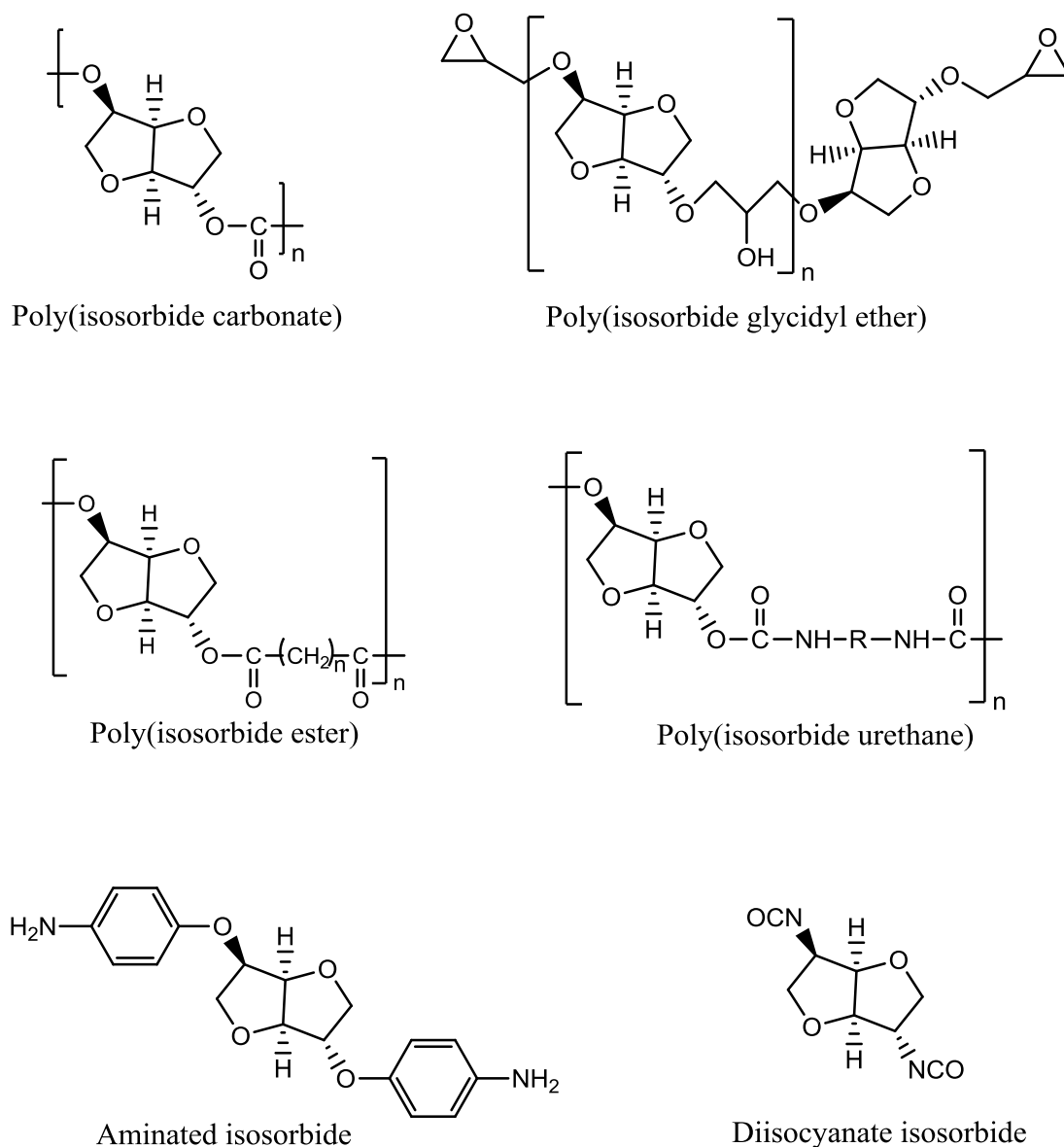


Figure 25: Isosorbide based polymers and aminated, diisocyanated isosorbide

I.2.3.7.2 Chemical modification of isosorbide as flame retardants

Isosorbide is a heavily researched molecule, most of the researches focused on functionalization or substitution of the two hydroxyl groups. Along with these modifications of isosorbide, the molecules derived from isosorbide can carry different chemical and physical properties, which give us plenty of ideas to synthesize the fire retardants based on isosorbide.

Phosphorus and sulfur containing derivatives of isosorbide have been synthesized since several decades.^{121,122,123,124} In the field of fire retardancy of polymers, some of these derivatives of isosorbide have been studied for designing novel non-halogen flame retardants.

Howell et al. synthesized a series of bio-based phosphorus ester starting from a combination of isosorbide and 10-undecenoic acid (from castor oil) (**Figure 26**).¹²⁵ Except DPPE, the other components showed good thermal stability, their degradation temperatures are over 262°C. Particularly, the residue of these components after 10 hours' treatment under 200°C in nitrogen still remain as high as 73 wt% (from 38 % to 73 %). However, the synthesis of these components are quite complicated with several different steps. Other researches proposed simpler synthesis path.

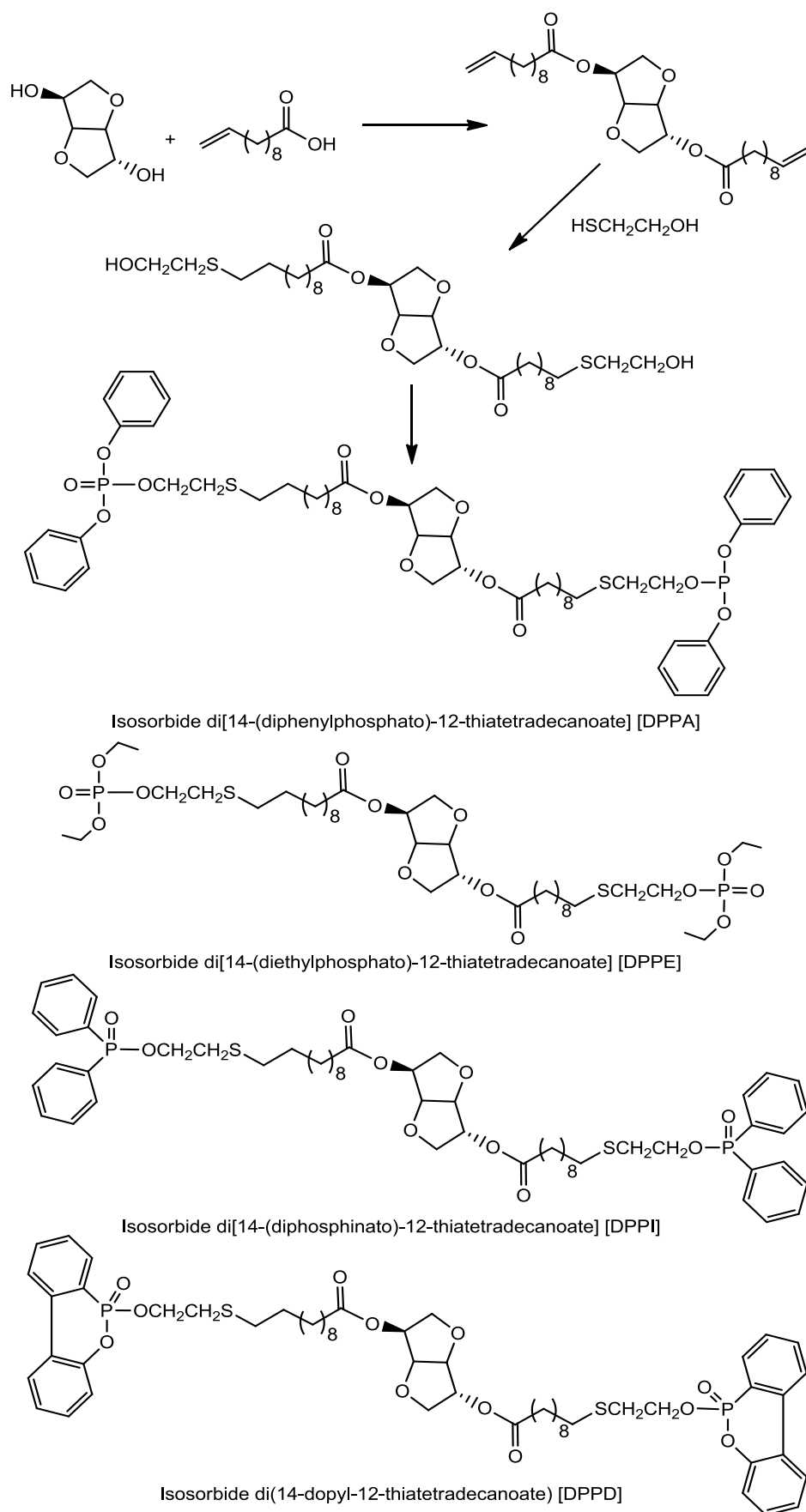


Figure 26: Phosphorus ester starting from a combination of isosorbide and 10-undecenoic acid

In the patent of BASF SE Company, isosorbide bis(diphenylphosphate), isosorbide bis(diphenylphosphinic ester), isosorbide bis(diphenylthiophosphinic ester) and isosorbide bis(diphenylphosphinite) were synthesized (**Figure 27**).¹²⁶ These synthesis were realized in toluene as solvent and triethylamine as catalyst. Then these flame retardants were incorporated into foam sheets of polystyrene, the fire performance was determined by DIN 4102 (fire test B2). According to the results, all these flame retardants showed a significant effect on the fire resistance performance. In another patent¹²⁷, they developed a new synthesis route to obtain the isosorbide bis(diphenylphosphate) by using carbonate of potassium as catalyst and without the presence of organic solvent which is a green chemistry concept.

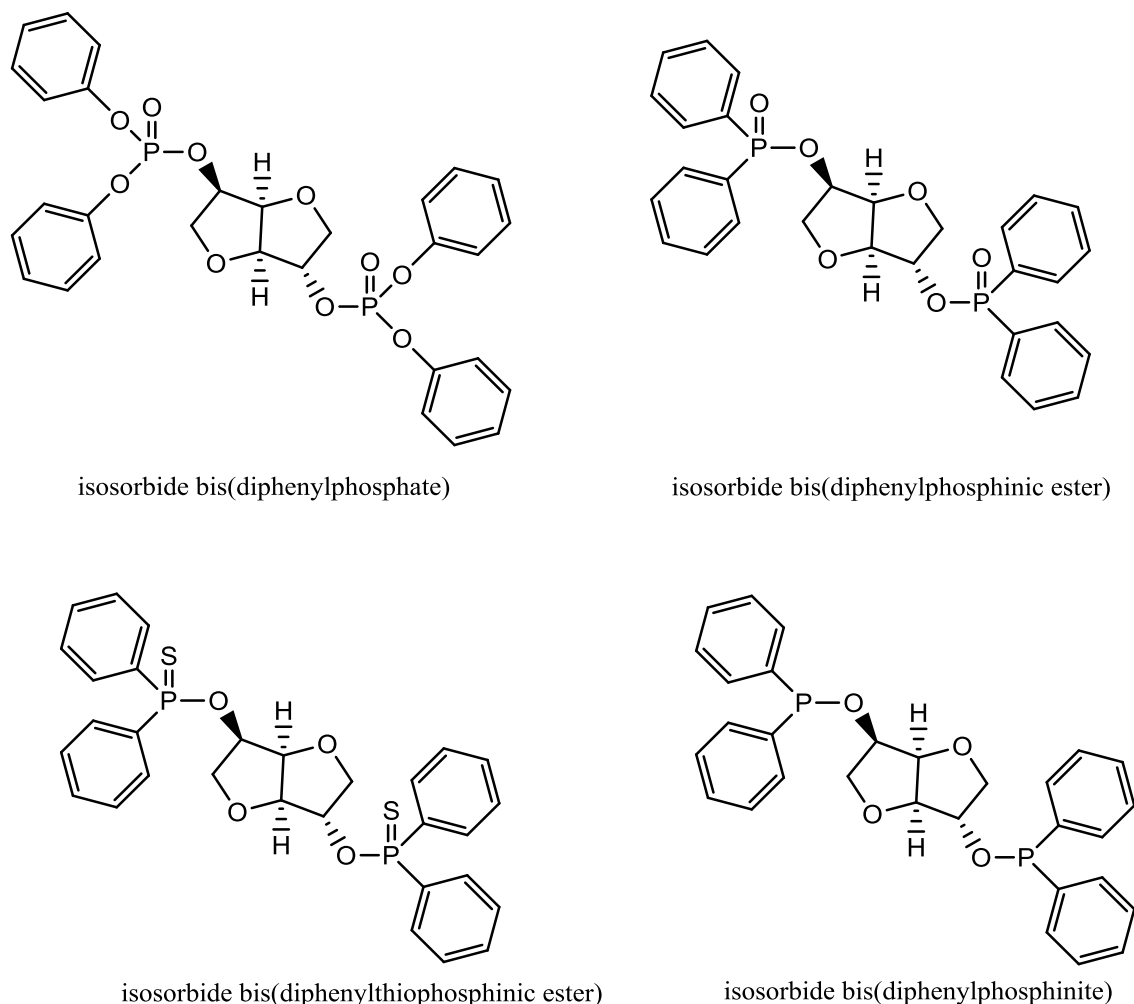


Figure 27: Chemical structure of isosorbide based fire retardants proposed by BASF Company

Daniel et al. did a similar modification of isosorbide by phosphorus compounds to incorporate into epoxy resin.¹²⁸ Apart from the isosorbide bis(diphenylphosphate) and isosorbide bis(diphenylphosphinic ester) which has been mentioned in **Figure 27**, they synthesized also

two other phosphorus esters showed in **Figure 28**. Except Isosorbide bis-(diethylphosphate), others showed good thermal stability with degradation temperature over than 270°C. In PCFC, with 2 % of phosphorus content, all of them showed at least 40 % of decreasing of peak of heat release rate (pHRR).

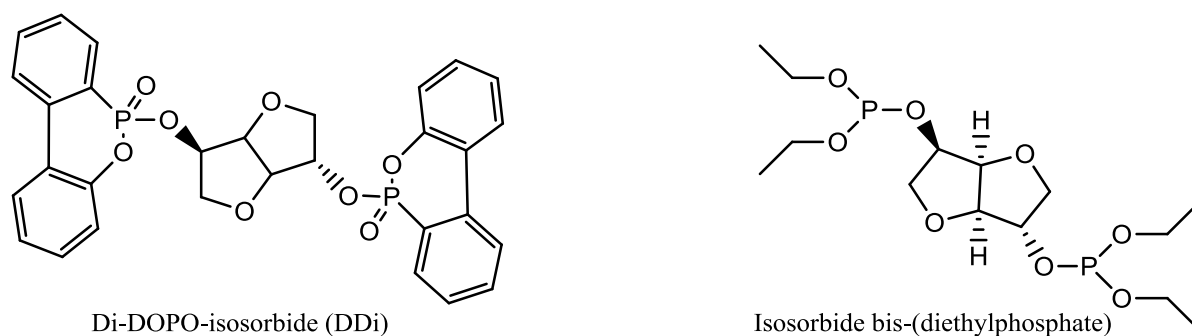


Figure 28: Isosorbide based bis-phosphorus ester

Mauldin et al.¹²⁹ have successfully achieved a polymerization between isosorbide and phenylphosphonic dichloride in presence of 4-Dimethylaminopyridine (DMAP) as catalyst (**Figure 29**) to improve the fire resistance of polylactide (PLA). A V-0 rating was obtained in UL-94 test with a 15 % charge of this FR polymer. However, no improvement in the MLC test was obtained. As PLA and PBS are both biodegradable aliphatic polyester derived from agricultural products, their work could be interesting for our study of fire resistance of PBS.

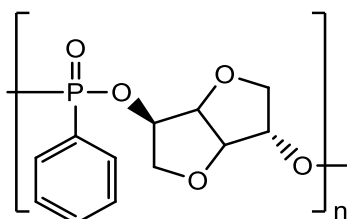


Figure 29: polymer based on isosorbide and phosphorus compound

1.2.4 Conclusion

This section was dedicated to the basic information of combustion of polymers and the mode of action of flame retardancy. Different types of additives were presented more precisely. The brief introduction of these additives provide the sources to flame retard PBS, and the flame retardancy of PBS is discussed in detail in the next section.

I.3 Flame retardancy of polybutylene succinate

In the previous section, different types of flame retardant additives and their mode of action were described. In this section, it is more precisely focused on the flame retardancy of polybutylene succinate and its composite reinforced by natural fibers

I.3.1 Flame retardancy of neat polybutylene succinate

I.3.1.1 Phosphorus based flame retardant

Phosphorus-based flame retardants are the most described to flame retard PBS in the literature. Ammonium polyphosphate (APP) (**Figure 30**) was used to flame retard PBS. APP is an effective fire retardant which has a high phosphorus content (up to 30 %) in many polymers. Kuan et al.¹³⁰ applied APP to flame retard PBS, with 30 % of APP incorporated into PBS, in UL-94 test (1.6 mm and 3.2 mm), V-0 rating and no dripping were observed. However, lack of carbon source makes this system not very efficient. In their study, when only 15% of APP added into PBS, V-2 rating and dripping were observed. To enhance this system, in combination of melamine, two different studies^{131,132} showed when 20% additive added into PBS with APP/melamine (MA) = 5/1, V-1 rating and no dripping was observed, which is still not efficient enough.

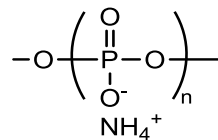


Figure 30: Chemical structure of APP

Different oxidation degree of phosphorus has been proved to have different effect on flame retarded polymer.¹³³ Low oxidation degree of phosphorus can often have an action in the gaseous phase whereas high oxidation degree of phosphorus prefer to act in the condensed phase. Recently, Yang et al.¹³⁴ prepared Intumescent FR PBS composites to test the FR efficiency of different melamine phosphorus-based fire retardant on PBS. Melamine phosphate (MP), melamine phosphite (MPi) and melamine hypophosphite (MHP) were used as FR (**Figure 31**).

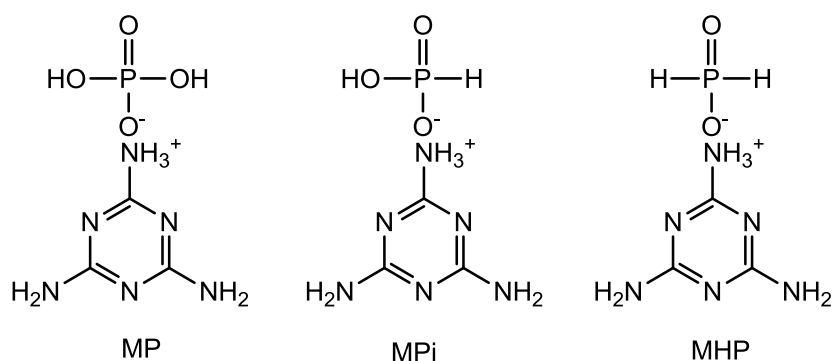


Figure 31: Chemical structure of MP, MPi, MHP

Limiting oxygen index (L.O.I.) test demonstrate that the values follow a sequence of $\text{MP} < \text{MHP} < \text{MPi}$ with the same loading of additives. In UL-94 test (1.6 mm), all three composites can only exhibit V-2 rating when the loading was 10 % and 20 %, however, V-0 rating was observed when the loading was 30 %. TGA results showed the onset temperature of degradation of PBS composite decreases with the decrease of phosphorus valence state, and all these three FRs can promote the formation of char. In cone calorimeter test, the addition of these FRs can obviously decrease the pHRR, but total heat release (THR) was not significantly decreased. According to the analysis, the possible mechanisms of these three FRs behave differently in PBS matrix. The mechanism of MP in the composite is similar to traditional intumescent FR mechanism. MP acts as a source of acid and a source of blowing agent, so that it can promote the formation of char which can inhibit the propagation of heat and oxygen into interior substance. Furthermore, some gaseous products (CO_2 , NH_3) are capable to dilute the concentration of oxygen and flammable gas in the gaseous phase. It was found that MPi and MHP act almost in the same way as MP, however the release of PH_3 during the combustion process enhances the performance of resistance of fire of MPi and MHP. The PH_3 can be quickly oxidized to form H_3PO_4 , then this acid can generate polyphosphoric acid to cover the surface of substrate and catalyze the formation of char to protect the substrate from the flame.

Besides the addition of flame retardants in PBS, phosphorus compounds were also incorporated in the polymer chain as reactive flame retardant. Pospiech et al.¹³⁵ have succeed a copolymerization of a series of bio-based aliphatic polyester with DOPO containing monomer (**Figure 32**). It is noteworthy that PBS was one of these polyesters. PCFC and L.O.I.

was performed as fire tests. Copolymers based on PBS showed no significant reduction of pHRR in PCFC, whereas the L.O.I. increased from 28 to 47.

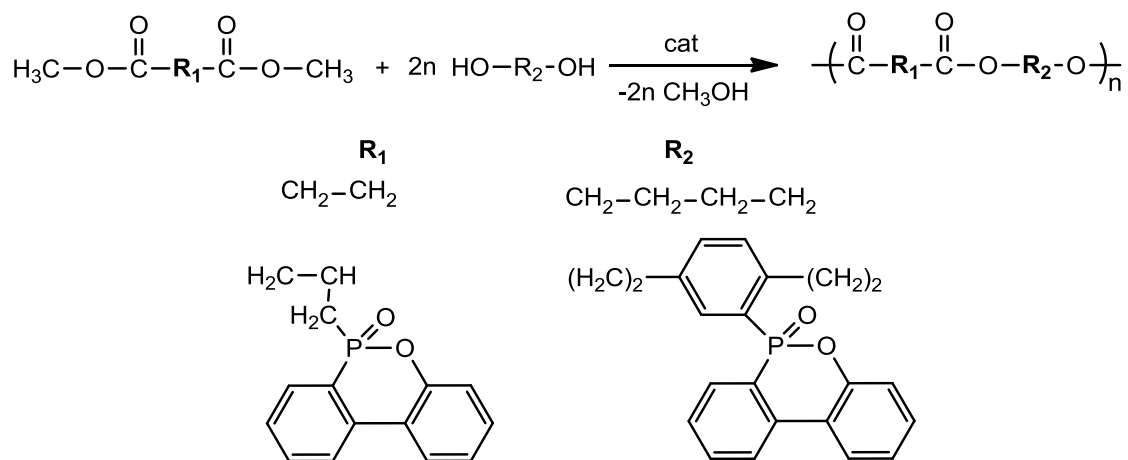


Figure 32: Synthesis of copolyester based on monomers modified by DOPO

I.3.1.2 Metallic hydroxide

It is less discussed using metallic hydroxide to flame retard PBS than the phosphorus based flame retardants in the literature. Chen et al. incorporated MDH with different particle size into PBS.¹³⁶ They showed that the particles size displayed different results on efficiency to flame retard PBS. In order to get a significant improvement of the fire retardancy (V-0 rating in UL-94), 60 % filler having an average particles size of 20 μm diameter is needed, and 40 % filler having particles size of 5 μm and 500 nm diameter is needed. Furthermore, with the same percentage of filler, MDH of 5 μm and 20 μm showed better results than MDH of 500 nm in MLC test. They found that smaller particle size has faster degradation rate, which showed faster release of H₂O during a fire scenario with the decomposition of MDH. So the char layer could be broken by water vapor. Even though they get a good performance of the flame retarded PBS by using MDH of a right particle size, the drawback is still obvious, at least 40 % MDH is needed to get the desired performance.

I.3.1.3 Silicon-based flame retardants

Silica was found capable to act as synergists when combined with other fire retardants. Chen et al.¹³¹ used fumed silica to combine with APP and melamine as an intumescent system to incorporate into PBS. Compared to neat PBS, this PBS fire retardant composite showed an increase of L.O.I. value from 24 to 36 with 18 % APP+MA and only 2 % fumed silica in weight.

Still, with 2% fumed silica, in order to reach V-0 rating and no dripping, only 17 % APP+MA are needed. It was claimed that the presence of silica increased the quantity of char and the viscosity of the matrix during a fire. Meanwhile, as fumed silica has a large surface area, low density, and low superficial free energy in heating, it is possible accumulate on the surface of sample, which leads to form a physically strong char on the surface of sample. That prevent both the melt from dripping and the propagation of oxygen and heat into the interior substrate. In addition, the trapped inert atmosphere can dilute the density of oxygen and combustible gas in the gas phase. Shortcoming of this formulation is that it has only 18 % of decrease of pHRR and 8 % of decrease of THR in a microscale combustion calorimetry test.

Instead of incorporation of the silicon-based flame retardant in PBS, Kuan et al. proposed a method by grafting Tetraethoxysilane (TEO) in the polymer chain.¹³⁰ The thermal stability of the PBS was significantly improved after the grafting of TEO. In the UL-94 test, PBS/APP 85/15 without TEO had only V-2 rating with dripping, whereas for PBS/APP/TEO 84/15/1, V-0 without dripping was observed.

I.3.1.4 Nanoparticles

To enhance the intumescent flame retardant system for PBS, study was achieved by addition of the nanoparticles. Liu et al.¹³² studied the fire retardancy by preparing a composite with MgAlZnFe-CO₃ layered double hydroxides (LDHs) as synergetic agent and APP/MA as intumescent FR. It was reported that a suitable quantity of LDHs could have a significant synergistic effect on the fire resistance performance. With a presence of 1 % LDHs (20 % intumescent FR in total), V-0 rating for UL-94 test and a 35 for L.O.I. can be obtained. Additionally, in cone calorimetry test, pHRR is decreased by 30 % and THR is decreased by 19 %. It indicated that the LDHs and PBS have strong hydrogen bond interactions. Meanwhile, the addition of LDHs involved a crosslinking reaction with PBS and intumescent FR. These factors results in an increase of viscosity of the composite. The solid structure promoted formation of stable char layer, which can contribute to better thermal stability and flame resistance.

Wang et al.^{137,138} investigated the fire retardancy of PBS by preparing a composite with ammonium phosphate and melamine as intumescent FR and graphene used as synergist. The composite showed good fire resistance. A V-0 rating in UL-94 test was obtained with 18 %

APP/MA and 2 % graphene in weight, and it possesses an excellent anti-dripping property. Especially when 18 % MP and 2 % graphene incorporated into PBS, in MLC test, pHRR was decreased by 63 % and THR was decreased by 22%. The presence of graphene increases noticeably the melt viscosity and restrained the melt dripping. It can also improve the char yield and thermal stability of the char at high temperature compared with neat PBS.

Wang et al.¹³⁸ achieved as well a comparative study of graphene and POSS for an intumescent FR PBS composite. The different influence of graphene and POSS on thermal properties and flammability of this flame retarded PBS composite was investigated. The addition of graphene and POSS can both improve the L.O.I. value of the composite. However, in the UL-94 test, with 18 % MP and 2 % graphene or POSS, V-0 rating and V-1 rating was observed respectively. These two synergists are both proved to improve the char yield which results in decreasing the pHRR (40 % for 2 % loading of POSS, 60 % for 2 % loading of graphene) and THR (3 % for 2 % loading of POSS, 22 % for 2 % of graphene), but the composite incorporated with graphene exhibits a better thermal oxidative resistance of the char layer. In general, compared to POSS, graphene displayed better thermal and fire retardant properties.

1.3.2 Flame retardancy of composites of PBS reinforced by natural fibers

PBS is a polymer which can be processed at a relatively low temperature (120°C to 130°C), bio-composite based on PBS can thus avoid the thermal degradation of natural fibers. Bio-composites produced by blending PBS and no-expensive natural additives such as flax,¹³⁹ bamboo fiber,¹⁴⁰ starch^{141, 142} and lignin¹⁴³ showed good improvement of mechanical properties and a relatively low price. However, the high flammability can still be a shortcoming in many applications (e.g. transportation, electric and electronic applications). Solutions to improve their flame retardancy have been proposed in the literature.

1.3.2.1 PBS/flax

Flax is a type of natural fiber known for thousands of years mainly for producing textiles. Flax is mainly formed by cellulose, Dorez et al.¹³⁹ studied the fire retardancy of PBS/flax by using three phosphorus compounds which are commonly used for cellulose fibers: APP, dihydrogen ammonium phosphate (DAP), and phosphoric acid. No presence of phosphorus-based flame retardant in the PBS/flax showed poor resistance of fire. In order to have a considerable

improvement, 30 % of flax fiber and 15 % APP were added into PBS. The pHRR is decreased by 60 % and the THR is decreased by 50 % in MLC test.

I.3.2.2 PBS/lignin

Lignin is a class of complex organic polymers which can often be found in wood. Literature described the use of lignin for flame retarding polymers.^{144,145,146}

Ferry et al.¹⁴⁷ investigated the flame retardancy of composite of PBS with alkali and organosolv lignin, and the alkali lignin was furtherly modified by phosphorus compounds. It shows that alkali lignin was more efficient than organosolv lignin due to the release of sulfur dioxide during the decomposition. It was also found that when 20 wt% phosphorus modified lignin was incorporated, there was a decrease of ignition time and THR had no significant change, whereas pHRR was decreased by 45 % compare to neat PBS.

Jiang et al.¹⁴⁸ used the wood from *Pinus massoniana* which contains cellulose and lignin to incorporate in PBS. Mechanical properties was increased with the presence of wood. Then CaCO_3 and phosphorus flame retardant were incorporated in this composite. With 10 wt% of additives added in the composite, pHRR was decreased by 24 % and THR was decreased by 14 %.

I.3.2.3 PBS/bamboo fiber

Bamboo fiber is an abundant material with low price and high toughness. Compared to some other natural additives: unlike starch, bamboo fiber has no competition with food industry; and unlike lignin, the wood which provide lignin need a much longer period to grow (10-20 years) than bamboo (2-3 years).¹⁴⁹

Like the flax fiber, the main component of bamboo is also the cellulose which gives the opportunity to create residual char in the fire retardancy of bio-composite PBS/Bamboo fiber. Nie et al. studied the fire retardancy of bio-composite PBS/Bamboo fiber.¹⁴⁰ Microencapsulated ammonium polyphosphate (MCAPP) were added into the bio-composite to form an intumescent system. $\text{Al}(\text{OH})_3$ and $\text{Mg}(\text{OH})_2$ have also been used as fire retardant to compare the efficiency with MCAPP.

It was shown that more bamboo fiber added in the composite, better resistance of flame could be obtained. In order to get a V-0 rate in UL-94 test, with 20 % MCAPP in weight, the quantity of bamboo fiber needs to reach at least 40 % in weight. The cone calorimeter tests indicate that the addition of MCAPP decrease noticeably pHRR and THR. With 20 % MCAPP and 50 % bamboo fiber in weight, the HRR and THR were decreased by 47 % and 42 % respectively compared with the bio-composite without MCAPP. It was also observed that with 20 % addition of $\text{Al}(\text{OH})_3$ and $\text{Mg}(\text{OH})_2$, no classified and dripping was observed in UL-94 test. The enhancement of fire resistance of this bio-composite by increasing the quantity of bamboo fiber can be explained by the fact that bamboo fiber acts as a carbon source in the intumescent FR system, the addition of bamboo fiber supports the formation of char.

I.3.3 Conclusion

Different approaches to flame retard PBS has been reported. Most of the studies focused on the intumescent flame retardant system with the presence of phosphorus, nitrogen, silicon and nanoparticle containing flame retardants. Some of these formulations showed significant improvement of the flame retardancy of PBS and its composites enhanced by natural fibers. However, disadvantages such as high content of loading still need to be improved.

I.4 Conclusion

The state of art showed firstly the synthesis and physico-chemical properties of PBS. Especially its thermal degradation behavior is important for understanding the mode of action of flame retarded PBS. Secondly, fundamental information of combustion and the mode of action of flame retardancy were described. Furthermore, an overview of the current flame retardant additives were summarized which provide solutions to flame retard PBS. Particularly, isosorbide based flame retardants which are derived from the bio-mass draw a lot the interests. Finally, the existing methods for the improvement of flame retardancy of PBS were discussed. It is showed in the literature that some of the phosphorus and nitrogen based flame retardants have good flame retardant property in PBS when blended with synergists. With the information provided in this chapter, we should be capable to design our flame retardant formulations for PBS. After the presentation of material and research methods in the next chapter, a screening of different approaches to flame retard PBS is presented in Chapter III.

Chapter II - Materials and Methods

II Materials and Methods

This second chapter is dedicated to the description of materials used in this study including the synthesis and analyses of the isosorbide based flame retardants. Then, the characterization techniques as well as the formulation methods used are shown. Meanwhile, fire tests chosen to evaluate the flame retardant formulations are presented. To investigate the mode of action of fire retarded PBS, special techniques and instrumentations which permit to gain more information of the materials in the gaseous and the condensed phases are specifically introduced in detail.

II.1 Materials

This part describes the materials used in our work, which include the PBS to be flame retarded, polymers as carbonization agent, flame retardant additives and isosorbide-based FRs. The synthesis methods and identification of the isosorbide based FRs are detailed. Compounding of PBS with the additives are also specified in this part.

II.1.1 Polymers and flame retardant additives

The polymer to be fire retarded in this work is PBS bionolle™ 1001MD, which was supplied by Showa Denko (Japan). Some of its mechanical properties and thermal properties provided by the supplier are presented in **Appendix 1**. It shows that bionolle™ 1001MD has similar mechanical properties to PP and PE. Meanwhile, a relatively low melting point of PBS (112 to 115 °C) permits to process PBS at a relatively low temperature, especially when it is blended with the additives which has low degradation temperature.

The polymers choosing as carbonization agent are bio-based polycarbonate. Bio-based polycarbonate i.e. poly (isosorbide carbonate) (PIC), DURABIO™ D7340 is based on isosorbide which is supplied by Mitsubishi Chemical (Japan). It has good transparency, which can be better than conventional petroleum-based PC. PIC is mainly applied for touch screen, optical film and some automobile devices.

The flame retardant additives are supplied by Sigma-Aldrich and Thermo Fisher Scientific. Special acknowledgements to the group EMPA for supplying the DOPO-based derivatives.

II.1.2 Modification of isosorbide

Synthesis of the isosorbide-based flame retardants is presented in this part. These molecules includes sulfur based modification of the isosorbide, polymers of isosorbide with silicon based compounds, the phosphorus modifications which have the components of different oxidation rate of the phosphorus and the polymers or small molecules based on phosphorus (**Figure 33**). Isosorbide used in this study was supplied by Roquette.⁶ The synthesized FRs are all identified by liquid state nuclear magnetic resonance (NMR), ^1H , ^{13}C , ^{31}P (for phosphorus based compounds). Distribution of the peaks presented in NMR are all in δ ppm. Multiplicity is presented by s for singlet, d for doublet, t for triplet and m for multiplet.

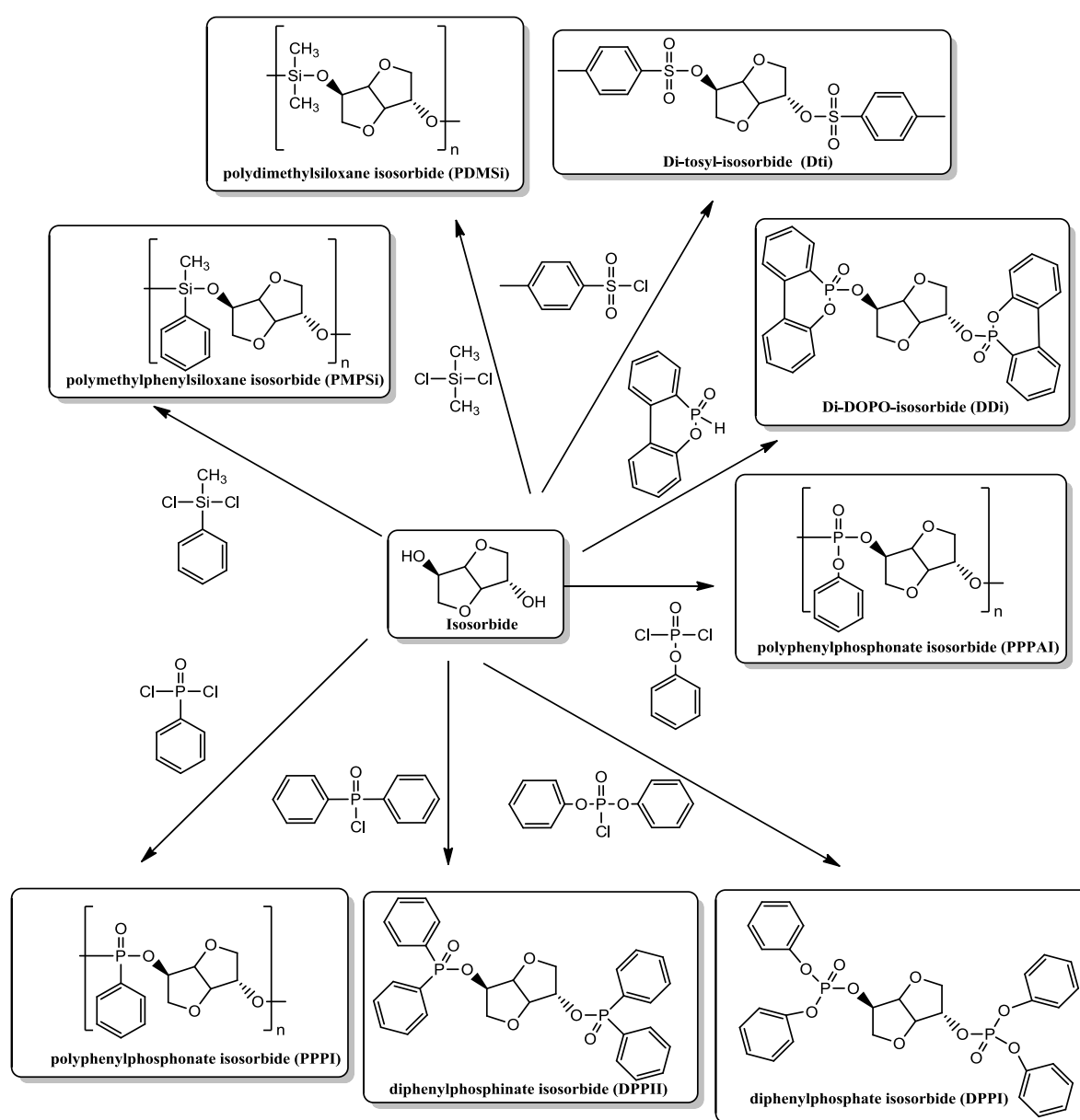


Figure 33: modification of isosorbide with sulfur, silicon and phosphorus compounds

II.1.2.1 Sulfur based modified isosorbide

Di-tosyl-isosorbide (Dti) (Figure 34):

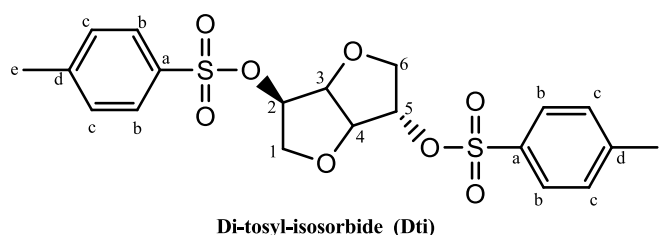


Figure 34: chemical structure of Di-tosyl-isosorbide (Dti)

To a round bottom flask at 0°C, 3.5092 g (24 mmol) of isosorbide was added in 10 mL of pyridine under N₂ flow. Then, a solution of 9.0984 g (48 mmol) of 4-toluenesulfonyl chloride in 25 mL of pyridine was added dropwise, over a period of 15 min then the mixture was stirred for 3 hours. Afterward, the reactor was placed in a refrigerator overnight. The mixture was poured in 200 mL of icy water and stirred for 1 h. The obtained white solid was filtered and washed successively with water, 0.2 M of HCl and water again. The white solid was recrystallized in ethanol affording Di-tosyle-isosorbide as a white powder with a yield of 92.6 %.

Dti: ¹H NMR (CDCl₃, stand. TMS): δ (ppm) 2.45 (6H, s, H-e), 3.67-3.71 (1H, m, H-6), 3.82-3.95 (3H, m, H-1 and 2H-6), 4.48 (1H, t, H-4), 4.59 (1H, t, H-3), 4.83-4.86 (2H, m, H-2 and H-5), 7.43 (4H, d, J_{HcHb}=8 Hz, H-c), 7.78 (4H, d, J_{HbHc}=8 Hz, H-b). ¹³C NMR dec-¹H (CDCl₃, stand. TMS): δ (ppm) 21.7 (s, C-e), 69.7 (s, C-6), 73.3 (s, C-1), 78.2 (s, C-5), 80.3 (s, C-3), 83.2 (s, C-2), 85.6 (s, C-4), 127.9 (d, J=7.74 Hz, C-b), 130.1 (d, J= 12.09 Hz, C-c), 132.9 (s, C-d), 145.5 (s, C-a).

II.1.2.2 Silicon based modified isosorbide

Polydimethylsiloxane isosorbide (PDMSi) (Figure 35):

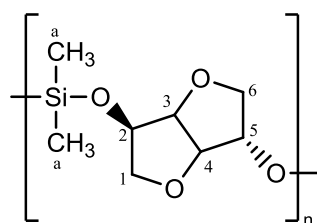


Figure 35: Chemical structure of Polydimethylsiloxane isosorbide (PDMSi)

To a round bottom flask equipped with a condenser, 16.56 g (113.4 mmol) of isosorbide was added in 100 mL of toluene and 50 mL of triethylamine under N₂. The temperature was

allowed to rise up to 89°C. Then, 13.80 mL (113.4 mmol) of dichlorodimethylsilane was added, dropwise to the mixture. The mixture was maintained at 89°C and stirred for 1 h. The white formed solid during the reaction was removed by filtration and the filtrate was evaporated in order to remove toluene. The residue was dissolved in 100 mL of dichloromethane. Extraction of the organic layer was achieved five times with 200 mL of water. The organic layer was dried over MgSO₄ and the solvent was removed under reduced pressure. A semi-transparent yellowish solid was obtained with a yield of 95.4 %.

PDMSi: ¹H NMR (CDCl₃, stand. TMS): δ (ppm) 0.06 to 0.22, (6H, m, H-a), 3.49 and 3.79-3.97 (4H, m, 2H-1 and 2H-6), 4.27 to 4.62 (4H, m, H-2, H-3, H-4 and H-5). ¹³C NMR dec⁻¹H (CDCl₃, stand. TMS): δ (ppm) -2.4, -0.6, 1.1 (m, C-a), 71.2 (m, C-6), 72.2 (m, C-5), 73.1 (m, C-1), 73.7 (m, C-3), 81.4 (m, C-2), 88.2 (m, C-4).

Polymethylphenylsiloxane isosorbide (PMPSi) (Figure 36):

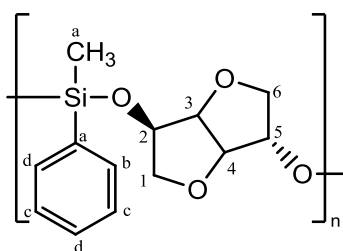


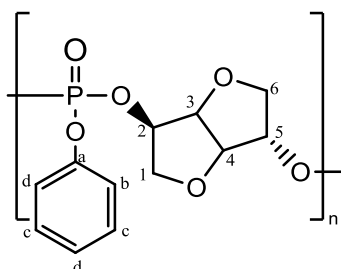
Figure 36: Chemical structure of Polymethylphenylsiloxane isosorbide (PMPSi)

The synthesis of PMPSi share the same protocol as PDMSi: with 18.4 mL (113.4 mmol) of dichloromethylphenylsilane, a semi-transparent yellowish solid was obtained with a yield of 92.3 %

PMPSi: ¹H NMR (CDCl₃, stand. TMS): δ (ppm) 0.39-0.46 (3H, m, H-a), 3.48-3.96 (4H, m, 2H-1 and 2H-6), 4.32- 4.59 (4H, m, H-2, H-3, H-4 and H-5), 7.35-7.41 (3H, m, 2H-d and H-e), 7.54-7.65 (2H, m, 2H-c). ¹³C NMR dec⁻¹H (CDCl₃, stand. TMS): δ (ppm) -3.5 (m, C-a), 71.2 (m, C-6), 73.5 (m, C-5), 75.7 (m, C-1), 77.5 (m, C-3), 81.5 (m, C-2), 88.2 (m, C-4), 128.2 (m, C-d), 130.6 (m, C-c), 133.3 (m, C-e), 134.1 (m, C-b).

II.1.2.3 Phosphorus based modified isosorbide

Polyphenylphosphate isosorbide (PPPAI) (Figure 37):

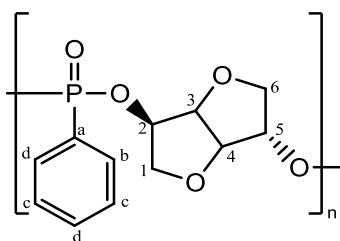


polyphenylphosphonate isosorbide (PPPAI)

Figure 37: Chemical structure of Polyphenylphosphate isosorbide (PPPAI)

To a round bottom flask equipped with a condenser, 8.3 g (56 mmol) of isosorbide and 338 mg (2.5 mmol) of 4-Dimethylaminopyridine (DMAP) were added under N_2 . The temperature was then brought to $90^\circ C$ until the DMAP was totally dissolved. Afterward, 7.927 mL (56 mmol) of dichlorophenylphosphate were added dropwise over a period of 20 min. Upon the completion of the addition, the temperature was allowed to slowly rise to $120^\circ C$ and the mixture was stirred for 4 h. A solution of NaOH (0.1 M) in water was set to react with HCl released during the reaction. The product was then dissolved in 100 mL of dichloromethane, followed by five times extraction with water. Organic layer was dried over $MgSO_4$, after the filtration, the solvent of the mixture was removed under reduced pressure. A brown solid was obtained with a yield of 72.1%.

PPPAI: 1H NMR ($CDCl_3$, stand. TMS): δ (ppm) 3.52 to 4.95 (8H, m, H of isosorbide), 7.14-7.25 (3H, m, 2H-c, H-d), 7.29-7.40 (2H, m, 2H-b). ^{13}C NMR dec- 1H ($CDCl_3$, stand. TMS): δ (ppm) 70.7 (m, C-1), 73.9 (m, C-6), 77.6 (m, C-2), 80.9 (m, C-5), 81.9 (m, C-3), 86.2 (m, C-4), 120.1 (m, C-c), 125.7 (m, C-b), 129.9 (m, C-d), 148.2 (m, C-a). ^{31}P NMR (dec- 1H , $CDCl_3$): δ (ppm) -8.1 (m), -7.7 (m)

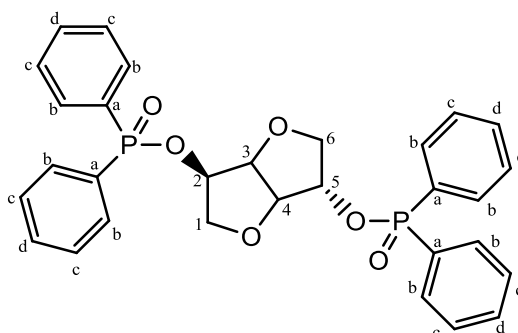
Polyphenylphosphonate isosorbide (PPPI) (Figure 38):

polyphenylphosphonate isosorbide (PPPI)

Figure 38: Chemical structure of polyphenylphosphonate isosorbide (PPPI)

The synthesis of PPPI share the same protocol as PPPAI: with 7.941 mL (56 mmol) of phenylphosphoric dichloride, a dark brown solid was obtained with a yield of 85.4 %.

PPPI: $^1\text{H NMR}$ (CDCl_3 , stand. TMS): δ (ppm) 3.64 to 4.88 (8H, m, H of isosorbide), 7.48-7.79 (5H, m, aromatic protons). $^{13}\text{C NMR}$ dec- ^1H (CDCl_3 , stand. TMS): δ (ppm) 70.4 (m, C-1), 74.3 (m, C-6), 75.5 (m, C-2), 79.8 (m, C-5), 80.9 (m, C-3), 86.4 (m, C-4), 125.7 (m, C-a), 128.7 (m, C-c), 131.8 (m, C-b), 133.1 (m, C-d). $^{31}\text{P NMR}$ (dec- ^1H , CDCl_3): δ (ppm) 18.9 (s), 19.7 (s)

Diphenylphosphinate isosorbide (DPPII) (Figure 39):

diphenylphosphinate isosorbide (DPPII)

Figure 39: Chemical structure of Diphenylphosphinate isosorbide (DPPII)

The synthesis of DPPII share the same protocol as PPPAI: with 23.81 mL (112 mmol) of diphenylphosphoric chloride, a brown solid was obtained with a yield of 74.4 %.

DPPII: $^1\text{H NMR}$ (CDCl_3 , stand. TMS): δ (ppm) 3.72-4.89 (8H, m, isosorbide protons), 7.34-7.91 (20H, m, aromatic protons). $^{13}\text{C NMR}$ dec- ^1H (CDCl_3 , stand. TMS): δ (ppm) 70.6 (d, $J_{\text{C1P}}=3.7\text{Hz}$, C-1), 74.3 (d, $J_{\text{C2P}}=5.90\text{ Hz}$, C-2), 74.8 (d, $J_{\text{C6P}}=4.38\text{ Hz}$, C-6), 78.9 (d, $J_{\text{C5P}}=5.88\text{Hz}$, C-5), 81.2 (d, $J_{\text{C3P}}=4.27\text{ Hz}$, C-3), 86.4 (d, $J_{\text{C4P}}=3.92\text{ Hz}$, C-4), 128.6, 131.4, 131.9 (m, C-b, C-c and C-d), 129.7 (m, C-a). $^{31}\text{P NMR}$ (dec- ^1H , CDCl_3): δ (ppm) 32.6 (m), 33.4 (m).

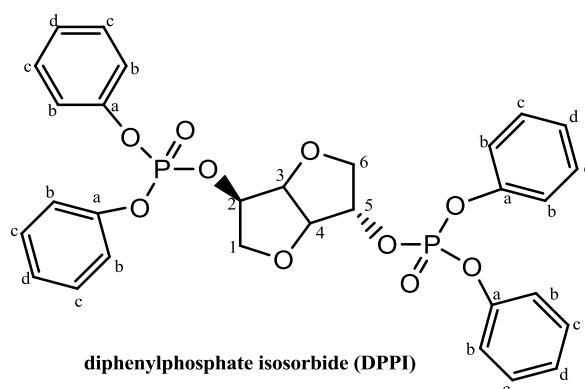
Diphenylphosphate isosorbide (DPPI) (Figure 40):

Figure 40: Chemical structure of Diphenylphosphate isosorbide (DPPI)

The synthesis of PPPI share the same protocol as PPPAI: with 23.21 mL (112 mmol) of diphenylphosphate chloride, a brown solid was obtained with a yield of 65.3 %.

DPPI: $^1\text{H NMR}$ (CDCl_3 , stand. TMS): δ (ppm) 3.72-3.89 (4H, m, 2H-1 and 2H-6), 4.56, 5.04 (2H, m, H-3 and H-4), 5.08 (2H, m, H-2 and H-5), 7.21 to 7.39 (m, aromatic protons). $^{13}\text{C NMR}$ dec- ^1H (CDCl_3 , stand. TMS): δ (ppm) 70.1 (d, $J_{\text{C1P}}=3.96$ Hz, C-1), 73.7 (d, $J_{\text{C2P}}=5.98$ Hz, C-2), 74.3 (d, $J_{\text{C6P}}=4.39$ Hz, C-6), 78.4 (d, $J_{\text{C5P}}=5.86$ Hz, C-5), 80.7 (d, $J_{\text{C3P}}=3.95$ Hz, C-3), 85.9 (d, $J_{\text{C4P}}=3.87$ Hz, C-4), 120.1-129.7 (m, C-b, C-c, C-d), 150.3 (m, C-a). $^{31}\text{P NMR}$ (dec- ^1H , CDCl_3): δ (ppm) -11.2 (s) -12.1 (m), -13.1 (d).

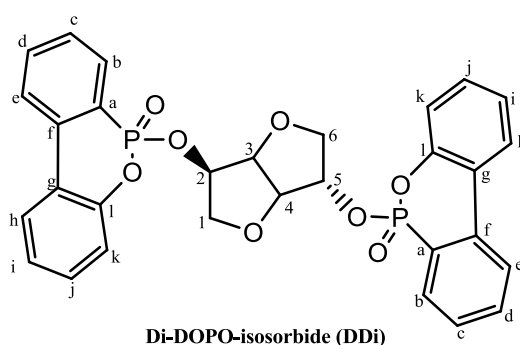
Di-DOPO-isosorbide (DDi) (Figure 41):

Figure 41: Chemical structure of Di-DOPO-isosorbide (DDi)

Isosorbide (11.7238 g, 80.3 mmol) was added to a solution of 34.5723 g (160.6 mmol) 9,10-dihydro-9-oxa-10-phosphaphenanthrene-10-oxide (DOPO) in 100 mL of dichloromethane. Then 23 mL of triethylamine was added and the mixture was cooled down from 25°C to 0°C using an ice bath. Afterward, tetrachloromethane was added dropwise, in the mixture over a period

of 1 h. This reaction was then carried out overnight at room temperature. The mixture was filtrated, and the filtrate was extracted five times with 200 mL of water. Organic layer was dried with MgSO_4 , filtrated and concentrated under reduced pressure. Finally, the mixture was recrystallized in ethanol. White crystal was obtained with a yield of 43.2 %.

DDi: $^1\text{H NMR}$ (DMSO, stand. TMS): δ (ppm) 3.48 (2H, m, H-6), 3.73 (2H, m, H-1), 4.36 (1H, m, CH-4), 4.52 (1H, m, H-3), 4.80 (1H, m, H-5), 5.01 (1H, m, H-2), 7.23-7.41 (4H, m, 2H-i and 2H-k), 7.41-7.56 (2H, m, 2H-j), 7.56-7.69 (2H, m, 2H-c) 7.80-7.95 (4H, m, 2H-b and 2H-d), 8.15-8.29 (4H, m, 2H-e and 2H-h). $^{13}\text{C NMR}$ dec- ^1H (DMSO, stand. TMS): δ (ppm) 71.1 (m, C-1), 73.7 (m, C-6), 76.2 (m, C-2), 79.8 (m, C-5), 80.9 (m, C-3), 86.3 (m, C-4), 120.4 (m, C-i/C-k), 120.9 (m, C-f), 122.4 (m, C-g), 125.2 (m, C-i/C-k), 125.7 (m, C-e/C-h), 126.4 (m, C-e/C-h), 129.3 (m, C-c), 130.5 (m, C-b/C-d), 131.5 (m, C-j), 134.7 (m, C-b/C-d), 136.7 (m, C-a), 149.5 (m, C-l). $^{31}\text{P NMR}$ (dec- ^1H , DMSO): δ (ppm) 9.6 (m), 10.7 (m).

II.1.3 Compounding of materials

Raw materials were dried at least for one night at 80 °C before use. The loading of additives varied from 5 wt% to 30 wt% according to the different formulations.

The formulations were prepared using a DSM Xplore Micro15 twin-screw micro-extruder having a volume of 15 cm³ (Figure 42). PBS and additives were melt mixed for 10 minutes with a shear rate of 50 rpm at 140°C, the temperature is fixed at 160°C when poly(isosorbide)carbonate is blended with PBS.



Figure 42: DSM micro extruder

The plaque and bar shape materials for the different testing were prepared by a press. The temperature was set at the processing temperature of the polymeric matrix (140°C or 160°C

according to the formulations). The pressure was set at 20 kN for 2 min and then increased at 40 kN for 6 min. Materials were pressed to make bars of 127 x 12,7 x 3.2 mm³ (UL-94 samples), plates 50 x 50 x 3 mm³ (MLC samples), and 10 x 10 x 1 mm³ viscosity samples.

II.2 Methods

This section presents the methods and technologies used to characterize the formulations. The first part is the fire testing used to characterize the fire properties of the formulations. The second part describes the thermal analysis of the formulations. The third and fourth parts present the characterization technics in the gaseous and condensed phase.

II.2.1 Fire testing

II.2.1.1 UL-94

The set of UL-94 tests, “Test of Flammability of Plastic Materials for Parts in Devices and Appliances”, is an example for small heat-source ignition tests that is approved by the Underwriters Laboratories Inc. The most common and widely used test is the UL-94 V (IEC 60695-11-10) that describes the tendency of a material to extinguish or to spread the flame after ignition of the material. It classifies specimens from NC (not classified), V-2, V-1 to V-0, whereas V-0 is the best rating. The different criteria for the classifications are presented in **Table 2**. The experimental set-up for the UL-94 test can be seen in **Figure 43**.

A blue flame with a 20 mm high central cone is applied for 10 s to the bottom edge of the vertical specimen. After 10 s the flame is removed and the after flame time required to extinguish the flame is recorded. The flame is reapplied for another 10 s and removed again. After the second burning, the time to extinguish and the afterglow time are noted. It is possible that during the burning, the barrels begin to drop and the burning drops inflame the piece of cotton that is below the specimen. For each material, a set of 5 bars was tested. The specimens have a size of 127 x 13 x 1.5 mm³.

Table 2: The different criteria for the classifications of UL-94 test

Criteria	V-0	V-1	V-2
Afterflame time for each individual flaming	≤ 10 s	≤30 s	≤30 s
Afterflame and glow time for each individual specimen, after second flaming	≤30 s	≤60 s	≤60 s
Total afterflame time for any condition set (5 flamings)	≤50 s	≤250 s	≤250 s
Cotton indicator ignited by flaming drops	No	No	Yes
Afterflame or afterglow of any specimen up to the holding clamp	No	No	No

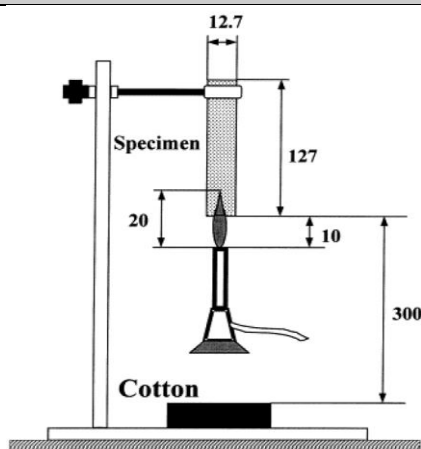


Figure 43: The experimental set-up for the UL-94 test

II.2.1.2 Optimized UL-94 instrumentation

In order to obtain more information, UL-94 test (ASTM D3801) is instrumented with thermocouples embedded in the polymer bars and equipped with a specific IR camera. Setups are designed as reported in **Figure 44**. The thermocouples embedded in the bar aim at measuring temperature gradients inside the bar during the test (**Figure 44 a**), whereas the IR camera aims at measuring the evolution of the surface temperature of melting drops and bar during the test (**Figure 44 a**) and visualizing the shape of the drop.

In the “thermocouples” configuration, a “brush” made of five thermocouples purchased from Omega (TJC100, K-type, 0.5 mm diameter) is connected to a Graphtek midi Logger GL220. The thermocouples are embedded every 5 mm in the bar after drilling in the material as shown in **Figure 44 b**. The first thermocouple (T1) is close to the bottom of the bar (2 mm). Repeatability of the measurement of temperature gradient is checked based on neat PBS. Three

experiments are carried out where T1 showed a good repeatability with an error margin within $\pm 10^{\circ}\text{C}$ when the thermocouple is embedded in the bar (from 0 s to 15 s) (**Figure 45**). Unlike the T1, the thermocouples from T2 to T5 is not totally surrounded by the flame at the beginning of the ignition. Thus the temperature evolution measured by the thermocouples from T2 to T5 depends largely on the flame propagation, which occurs often on the two sides of the bar. For this reason, the thermocouple from T2 to T5 can only show a trend of the temperature evolution in the bar, but with a larger error margin which is within $\pm 40^{\circ}\text{C}$. In the case of no propagation of the flame, the error margin of all five thermocouples is reduced and is within $\pm 15^{\circ}\text{C}$.

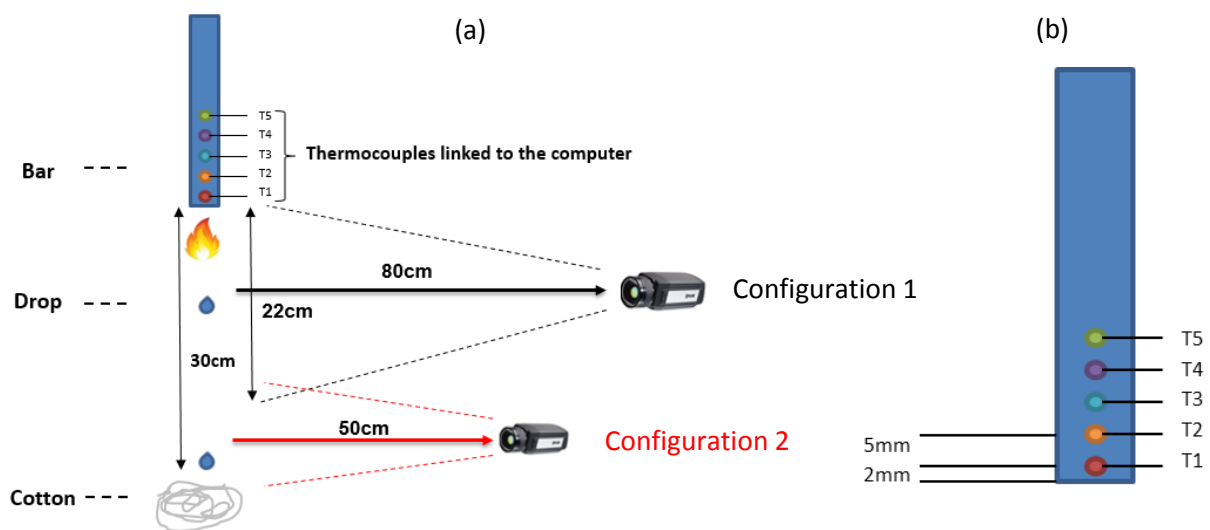


Figure 44: a) Instrumentation of UL-94 b) Position of thermocouple embedded in the bar

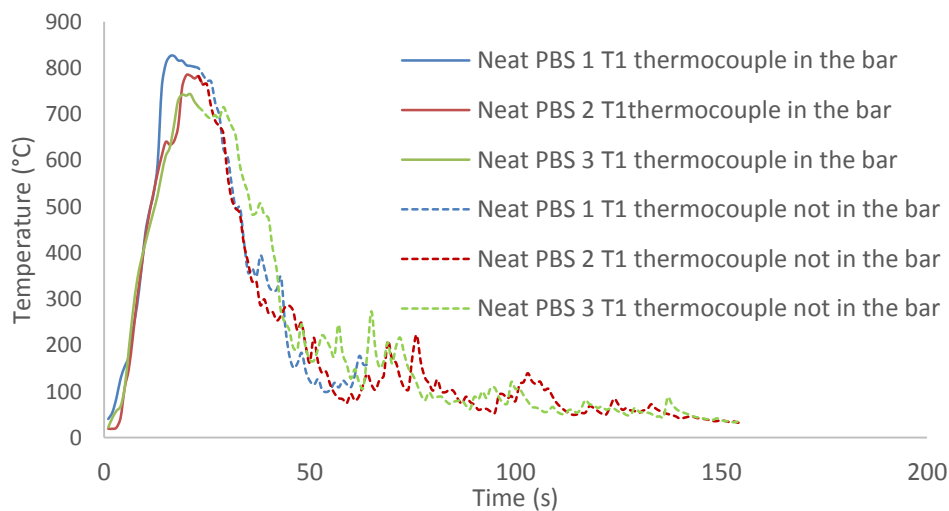


Figure 45: Repeatability study of temperature measured by Thermocouple (T1)

Besides the thermocouples, an IR camera (FLIR model X6540sc calibrated from 20 °C to 1500 °C) is used and equipped with a specific filter eliminating wavelength corresponding to H₂O and CO₂ (the main products of combustion are water and CO₂). It permits visualization of the surface of a material through the flame. In our test, this camera permits to measure the surface temperature of the bar and of the flaming (or non-flaming) drops during the UL-94 test. **Figure 46** makes comparison between the visualization of flaming drops during UL-94 test using IR camera with and without flame filter. Obvious differences can be seen: (i) without filter, it is not possible to visualize the surface of the drops (thus the surface measurement is impossible) (**Figure 46 a**) and (ii) with a filter (**Figure 46 b**) the surface of the burning drops as well as the flaming bar can be clearly observed. So, knowing the emissivity of the material, the surface temperature can be estimated.

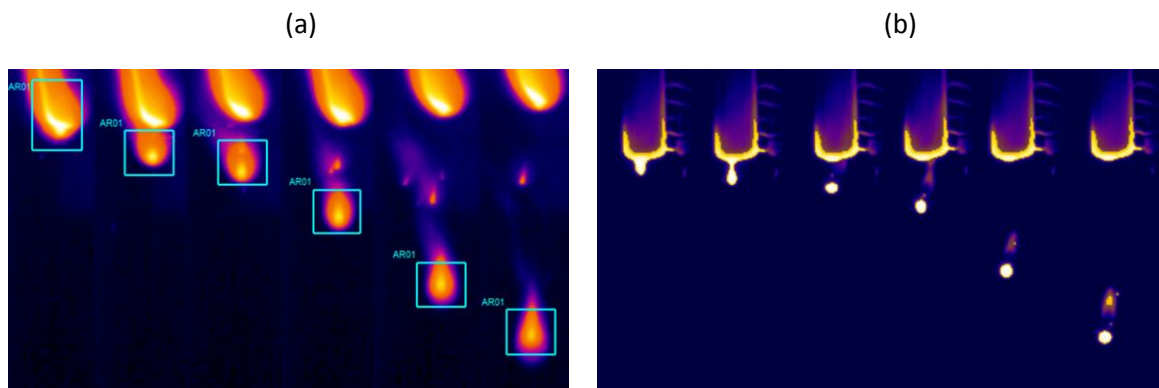


Figure 46: different results obtained with (a) conventional IR camera and (b) IR camera with a specific filter

The IR camera is placed at 80 cm from the plan of the bar and the drops (**Figure 44** configuration 1). The focus of the camera is calibrated based on the bar. At this distance from the bar, the camera is capable to capture images on 22 cm vertical side. Particularly, the moment when drops detach the bars, the maximum of temperature of the drops and the surface of bars are taken on the IR image. Five experiments are made and the measured temperature are repeatable in a reasonable error margin ($\pm 10^\circ\text{C}$), then the average value of the measured temperatures are calculated. To measure the temperature of the melting drops when they touch the cotton, the IR camera needs to be moved down (**Figure 44** configuration 2). In this case, the calibration of the focus can no longer be based on the bar. So, it is calibrated by focusing on a hot object (a finger or a hot metal) which is at the same distance from the bar to the IR camera. To get better resolution of the images, the camera is moved to

50 cm far from the bar. Four experiments are carried out, the average value of the measured temperatures are calculated. Particularly for this experiment, even the distance between the IR camera and the bar have changed, and with a new calibration of focus of the IR camera, the measurement of the temperature of drops when they hit the cotton provides still a good repeatability (error margin within $\pm 5^{\circ}\text{C}$ for neat PBS and within $\pm 10^{\circ}\text{C}$ for PBS/DOPO). Thus the reliability of this optimized UL-94 instrumentation is quite acceptable.

II.2.1.3 Mass loss calorimetry

A standard mass loss calorimetry (MLC) is a bench-scale reaction-to-fire test which provides a forced-flaming combustion scenario that is typical of developing or developed fires. The measurements were carried out on a Fire Testing Technology mass loss calorimeter device (ISO 13927, ASTM E906). The schematic representation of the device is shown in **Figure 47**. The sample ($50 \times 50 \times 3 \text{ mm}^3$) is covered by a grid ($100 \times 100 \text{ mm}^3$) to avoid contact between the material and the spark igniter due to bloating of the sample before ignition (grid not mentioned in ISO 13927). The distance between the sample holder and the heat source was 25 mm. An external heat flux (35 kW/m^2 or other heat flux) produced by a conical heater element is applied to the sample. The temperature of the gaseous combustion products is measured at the top of the chimney with a thermopile.

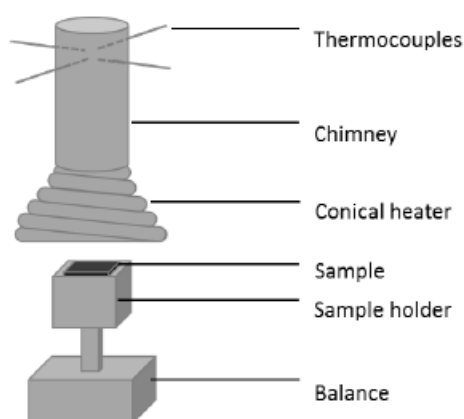


Figure 47: configuration of the mass loss cone

The values measured by mass loss calorimeter are: the heat release rate (HRR), the peak of heat release rate (pHRR), the total heat release (THR), the time to ignition (TTI) and the mass loss of the sample during combustion (ML). All measurements were performed at least twice.

The presented curves are the worst case of repeatable results. The acceptable error of measurement is estimated at 10 % for all values.

II.2.2 Physico-chemical analysis

II.2.2.1 Viscosity measurement and char resistance by Rheometer

The study of the rheology of during the thermal degradation of a charring material is consequently an important parameter to understand the charring process. All rheological measurements have been carried out on a parallel plate high temperature rheometer ARES 20A from Rheometric Scientific (**Figure 48**). Testing is carried out using a “Dynamic Temperature Ramp Test” with a heating rate of 10 °C/min in the range 25-500 °C, a strain of 1 % and a constant normal force of 100 N (200 Pa). This test leads to the apparent complex viscosity values (used as measurements about the abilities of the systems to expand). It is important to point out that only an apparent viscosity measurement is carried out (depending on the testing conditions) and that these results should be used only for comparison between the samples.

The char resistance can be also an important impact factor of the char, thus it can be measured by tracing the force in function of the distance between the gaps.

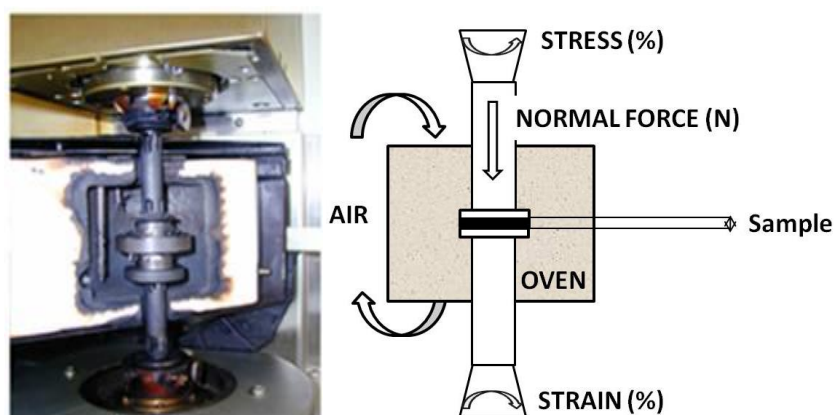


Figure 48: rheometer ARES 20A and the parameter recorded

II.2.2.2 Liquid state NMR

^{31}P , ^{13}C and ^1H NMR measurements were performed on a Bruker Advance 400 (magnetic field $B_0=7\text{ T}$). Tetramethylsilane was used as a reference. ^1H measurements were done with a pulse of 30° and 16 scans. ^{13}C measurements were done with a proton-decoupling method, a pulse

of 30° and 1024 scans. ³¹P measurements were done with a proton-decoupling method and 32 scans.

II.2.2.3 Emissivity measurement by integrating sphere

Hemispherical emissivity of PBS and PBS/DOPO are determined by a Vertex 70v with an integrating sphere accessory A 562-G supplied by Bruker. The samples used in the test have square shape (12.7 × 12.7 × 3.2 mm) which are also prepared by compression molding. According to the definition of hemispherical emissivity of a material, the measurement is carried out on the ratio of the emittance from a surface to the emittance from an ideal black surface at the same temperature, which can be defined by the following equation:

$$\epsilon = E1/E2$$

Where

E1 is the emittance of the surface of that material

E2 is the emittance of the surface of an ideal black body

The emittance cannot be measured directly. Whereas in an opaque material, it is considered no transmission when a beam of light hits the surface of a material. Thus in this case, the emittance and reflection have the following relation:

$$\epsilon + \delta = 1$$

Where

δ is the reflectance of the surface of the material

Thus by measuring the reflectance of a surface, the emittance can be estimated and the emissivity can be determined. A reference of a metal sample coated with a layer of diffuse reflecting gold which can reflect the incoming light is firstly measured. Then the collected drops of PBS and PBS/DOPO after the UL-94 test are measured at room temperature. Four experiments for each formulation are performed to evaluate the repeatability. The error margin is observed to be ± 0.005 . As the IR camera with a specific filter visualize the light in a specific wavelength range (from 3.5 μm to 4.5 μm), the experiment is performed in this range.

II.2.3 Thermal analysis

II.2.3.1 Thermogravimetric analysis

Thermogravimetric analysis (TGA or TG) measurements were carried out on a Setaram TG92-16. Argon was chosen as protective gas for the furnace. Samples were contained in silica crucibles robed with gold sheet to prevent reactions between phosphorus and silica. Samples were ground into powder using a cryo-grinder (500 μm filter). Fluid flow rate was set at 100 mL/min, nitrogen or air were chosen to examine the decomposition of the materials in pyrolysis or thermo-oxidative conditions. Samples of 8 ± 1 mg were submitted to an isotherm at 50 °C for 20 minutes for thermal homogeneity then followed by a heating ramp up to 800 °C. The heating ramps are detailed in the text depending on the experiment. Each sample was tested two times to ensure repeatability of the obtained results.

TG curves allow determining characteristic points. The derivative of the TG curve (DTG) permits finding the mass loss rate and so identify the main steps of the decomposition. DTG_{max} is the DTG value for each step (maximum), and the related temperature is noted T_{MAX}. Another characteristic point is the onset temperature of degradation (T_{2%}), which corresponds to the temperature when 2 wt% weight loss is observed. Finally, the amount of residue obtained at 800 °C is called residue.

Differential weight loss curves were calculated (**Equation 1**) in order to determine potential interactions which could occur between the polymeric matrix and the additives. These represent the difference between the experimental TGA curve for the mixture ($w_{exp}(T)$) and the linear combination of TGA curves ($w_{calc}(T)$) for the neat components (**Equation 2**) (e.g. PBS/DOPO 90/10).

$$\text{Equation 1: } \Delta w(T) = w_{exp}(T) - w_{calc}(T)$$

$$\text{Equation 2: } w_{calc}(T) = 0,9 \times w_{PBS}(T) + 0,1 \times w_{DOPO}(T)$$

Where $w_{PBS}(T)$ and $w_{DOPO}(T)$ are the experimental TGA curves of PBS and DOPO respectively. The main objective of this technique is to point out if the addition of the FR additives will stabilize or destabilize the system. When $\Delta w < 0$, the weight loss is higher than theoretical one, showing that the reactivity and/or interaction of the polymer with the additives leads to a

thermal destabilization of the material. On the opposite, when $\Delta w > 0$, the system is thermally stabilized.

II.2.3.2 Differential scanning calorimetry

Differential scanning calorimetry, performed on DSC Q100, from TA Instrument, was used to study the behavior of polymers (T_g , T_m etc.) when exposed to a temperature gradient (rise and / or decrease of the temperature at a controlled rate) under inert atmosphere. Especially in our study, the influence of incorporation of additives on the thermos-physical properties were investigated by DSC. The samples in sealed crucibles were put in the oven in which the nitrogen flow was set 50 mL/min. An isotherm of 3 minutes at 40 °C was performed to allow temperature homogeneity of the samples. The sample were heated at 10 °C/min up to 160 °C, followed by an isotherm of 3 minutes. Then, the samples were cooled to 40 °C at 10 °C/min. This cycle was repeated a second time to evaluate the possible impact of thermal history of the materials. Each sample was tested two times to ensure repeatability of the obtained results.

II.2.3.3 Simultaneous Thermal Analysis

A simultaneous measurement of TGA and DSC were conducted using a Netzsch 449 F1 Jupiter simultaneous thermal analysis device (STA). Samples were put in platinum/rhodium pans with lids. The lids had a small orifice (0.25 mm in diameter) for gas escape. This container configuration was used to maximize the thermal contact between a degrading sample and heat flow sensing thermocouples located underneath the pan. Before each experiments, a blank with empty crucibles was performed and subtracted to the experiments so both mass and heat flow signal were independent of the crucibles. Samples were tested at a heating rate of 10 K/min from 50 to 1000 °C.

II.2.4 Gas phase analysis

The nature of the evolved gases in a pyrolytic condition or in a real fire scenario are analyzed by various technics.

II.2.4.1 Thermogravimetric analysis - Fourier transform infrared

Thermogravimetric analysis coupled with Fourier transform infra-red (TGA-FTIR) is performed on a TA Instrument TGA Q5000IR coupled with a Thermo Scientific Nicolet iS10 spectrometer. Analyses are carried out in air in alumina crucibles. The balance flow is set to 15 mL/min whereas the nitrogen flow is fixed to 100 mL/min. Samples are heated up from 50 to 800 °C (10 °C/min) after an isothermal of 10 min at 50 °C. Gases evolved during the TGA experiment are detected continuously by the FTIR device. The spectra are recorded every 10 seconds with the OMNIC® software in a range from 400-4000 cm⁻¹. The number of scans is fixed at 8 and the resolution at 4. The temperature of the transfer line between the TGA and the FTIR instrument is set to 225 °C to avoid condensation of the evolved gases.

II.2.4.2 Mass loss calorimeter - Fourier transform infrared

Mass loss calorimeter coupled with Fourier transform infrared (MLC-FTIR) is performed on the mass loss calorimeter described above (**Figure 47**), whereas MLC experiment is performed as described above at 35 kW/m², with a distance between resistance and sample of 25 mm, using plates of 50 x 50 x 3 mm³ size covered by a grid.

Gas picking pistol and transfer line are provided by M&C Tech Group. FTIR, AntarisTM Industrial Gas System, is provided by ThermoFisher. The transfer line between MLC and FTIR is 2 m long and is heated up to 200 °C. To assure constant temperature of the transfer line, two temperature controllers are installed. Before analyzing the gases by FTIR, soot particles are filtered by two different filters (2 and 0.1 µm). Filters consist of glass fibers and ceramic respectively. The FTIR gas cell is set at 185 °C and 652 Torr. The optical pathway is 2 m long and the chamber of the spectrometer is filled with dry air. FTIR spectra obtained using MLC-FTIR are treated using OMNIC software. To quantify gases, spectra have to be recorded at different concentrations for targeted gases and a quantification method has to be created using TQ Analyst. Creating a method, representative regions in the spectra of the selected gas have to be chosen and interactions with other gases have to be taken into account. Using MLC-FTIR the following gases can be quantified: water, carbon monoxide, carbon dioxide, acetic acid, ammonia, methane, nitrogen monoxide, nitrogen dioxide, hydrogen cyanide. Quantification is reproducible within 10 %.

II.2.4.3 Pyrolysis-Gas chromatography-mass spectrometry

Pyrolysis-gas chromatography-mass spectrometry (py-GCMS) analyses are performed on a device provided by Shimadzu (**Figure 49**). The device consists of a micro-furnace pyrolyzer (Frontier Lab PY-2020iD) coupled with a GCMS (Shimadzu GCMS QP2010 SE). Experiments are performed under inert conditions using helium. Sample size is about 200 μg .

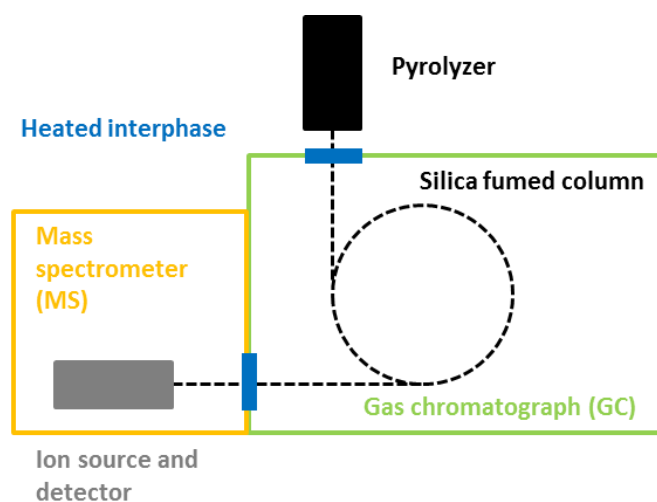


Figure 49: Schematic presentation of the Py-GCMS device

Samples (in a stainless steel cup) are heated up from 50 to 800°C with a heating ramp of 10 °C/min. After the decomposition process evolved gases are introduced into the GC/MS system whereas a part of the gases is split to avoid blockage in the column or saturation of the detector. Released decomposition gases are separated using a 30 m long fused silica capillary column. The temperature of the column is set at 35 °C during the desorption process. The column is then heated up to 300 °C with a heating rate of 10 °C/min followed by an isotherm at 300 °C for 30 min. The linear velocity of the carrier gas helium is set to 40 cm/s. The separated gases and fragments are then analyzed with the quadrupole mass spectrometer with an Electron-Impact (IE) ionization source. The IE spectra are recorded at 70 eV with a mass scan of 2 scans per second. The interface between the pyrolyzer and the GC is heated up to 320 °C; the interface GC-MS to 280 °C. The temperature of the ion source is set at 230 °C. After the experiments, data is analyzed using the GC/MS post-run analysis from Shimadzu and F-Search from Frontier lab, whereas products are identified using NIST database.

II.2.5 Condensed phase analysis

II.2.5.1 Solid state NMR

The solid-state nuclear magnetic resonance (NMR) is an effective tool to analyze the changes in the chemical environment of an atom inside a material. In the solid state (on the contrary to liquid state), the chemical shift anisotropy (anisotropy of magnetic moment, CSA), has a strong effect on the spectra, by broadening peaks. Through a tensorial analysis of the magnetic moments in a molecule, it is possible to demonstrate that there exists a “Magic Angle” with respect to the applied magnetic field at which the spinning of the sample leads to a minimization of absorption line broadening due to CSA. This method of analysis is so called “Magic Angle Spinning” (MAS).

In the case of carbon, the resonance of atoms is only possible in their isotopic form (^{13}C). However their low abundance leads to poor signal. This poor signal can be overcome by an excitation of protons in the sample and have them resonate at the same frequency than that of target atom (Hartman-Hahn condition). This process is called cross-polarization (CP), and the time of polarization is also called contact time. CP leads to a high enhancement of the excitation of studied nuclei. However there exists an interference of the large number of protons on the decay of isolated nuclei, due to weak spin interactions. In this case, the dampening of the signal can be removed with a strong radiofrequency signal which holds the protons in a high resonance state so that they do not absorb resonance from the nuclei. This is called ^1H decoupling.

^{13}C NMR measurements were done using a Bruker Avance spectrometer and a 4mm probe, operating at 100.6 MHz (9.4 T) with cross polarization (CP) ^1H - ^{13}C and dipolar decoupling (DD) with MAS (spinning frequency: 10kHz).

^{31}P NMR measurements were performed on a Bruker Avance II spectrometer, operating at 161.9 MHz (9.4 T) and at a spinning rate of 10 kHz. Bruker probe heads equipped with 4 mm MAS assembly were used. Experiments have been carried out using CP because of the long relaxation time of the phosphorus nuclei (10 to 500 s) with ^1H high power dipolar decoupling (HPDEC). A recycle delay of 30 s was optimized and was applied for all samples. H_3PO_4 in aqueous solution (85%) was used as reference for 0 ppm.

II.2.5.2 Elemental analysis

Elemental analyses for carbon, hydrogen and nitrogen were performed with an Elementar micro cube CHN analyzer. The sample is weighed in a tin capsule and burned with O₂ under Helium atmosphere. Different catalysts are used to convert the elements into specific compounds (C to CO₂, H to H₂O and N to various nitrogen oxides) which are detected by a thermal conductivity detector (TCD). The initial weight of the sample is 1 – 10 mg. The quantification limit is 0.5 g / 100 g and the measuring accuracy is ±0.1 g / 100 g.

Elemental analyses for phosphorus were performed with a Vista pro spectrometer system. The experiments are conducted as follows: 0.1 g of the sample is added to a solution of Cs₂SO₄ as well as to a mixture of concentrated sulfuric and nitric acids. After solubilizing the sample with the oxidizing acids, the mixture is vaporized and the residue is dissolved in hypochloric acid. The relative percentages of Al and P of this solution are determined by means of atomic emission spectroscopy with inductive coupled plasma (ICP-AES). The standard deviation of the method is inferior to 2 %.

II.2.5.3 Scanning electron microscopy

Scanning electron microscopy (SEM) is a technique that uses the interactions occurring between electrons and matter. An electron beam is sent on the sample, leading among other things to the emission of secondary electrons and backscattered electrons, which are then used to obtain topographic and chemical information respectively. SEM analyses were carried out using a Hitachi S4700 at 6 kV. All the samples were microtomed with a diamond knife on a Leica UltraCut microtome at cryogenic temperature (-120 °C) to obtain smooth surfaces.

II.2.5.4 Electron-probe micro-analysis

Electron probe microanalysis (EPMA) is an analytical technique that is used to establish the composition of specimens. A beam of accelerated electrons is focused on the surface of a specimen using a series of electromagnetic lenses, and these energetic electrons produce characteristic X-rays within a small volume (typically 1 to 9 μm³) of the specimen. These X-rays are detected at particular wavelengths, and their intensities are measured to determine the concentrations of elements. All elements (except H, He, and Li) can be detected. This analytical technique has a high spatial resolution and sensitivity. Additionally, the electron

microprobe obtaining highly magnified secondary- and backscattered-electron images of a sample. In this work EPMA (Cameca – SX 100) was used to characterize the distribution of the phosphorus in the char.

II.2.5.5 Optical microscopy

Digital microscopes are a variation of traditional optical microscope that uses optics and a charge-coupled device (CCD) camera to output a digital image to a monitor. In this work, the microscope enables to get a clear view of the char thanks to the high depth of field. The diameter of the char was thus measured with this technique on a Keyence – VHX-1000 digital microscope. Measurements were repeated ten times on randomly chosen parts of the char, to ensure representative values.

II.3 Conclusion

The first part of this chapter has described the used polymer, the used flame retardants in the study and synthesized isosorbide FRs. The synthesis and the characterization of these FRs were detailed. The preparation and compounding techniques were also presented in this part. Then the second part of this chapter described the fire testing used in the study. Methods of physico-chemical and thermal analysis were presented as well. Furthermore, analytical techniques to investigate the flame retardancy mechanism in the gaseous phase and in the condensed phase were detailed.

In the next chapter, to flame retard PBS, a screening of the formulations to flame retard PBS is presented. The performances of these formulations according to different fire tests are described.

Chapter III - Material screening

III Material screening

This chapter deals with the screening of different types of FR additives to flame retard PBS. The first part of this chapter describes the thermal stability and the use of isosorbide-based FRs modified by silicon, sulfur and phosphorus compounds, their fire behaviors when incorporated in PBS are evaluated. Then the second part describes the formulations of flame retarded PBS with isosorbide and isosorbide based polymer acting as carbonization agent in intumescent FR system. The third part describes firstly the formulations of PBS with DOPO and some of its derivatives. Then various conventional FRs which act in the condensed phase such as phosphorus based non-intumescent FRs, carbon nanotube, metal hydroxides and metal carbonate salts were formulated with DOPO in PBS. In the last part of this chapter, promising formulations of flame retarded PBS are selected to be further studied in chapter IV and chapter V.

Mass loss cone and UL-94 tests were chosen to evaluate the fire behavior of the PBS formulations. Mass loss cone can provide specific data, such as heat release rate (pHRR), ignition time (TTI) and total heat release (THR). With additional devices, this equipment is also capable to measure the smoke and the gas production. Despite the advantages, MLC test has only thermal radiation heat source, which corresponds to a specific fire scenario and so, it limits the evaluation of a FR formulation. Thus, in order to evaluate FR properties in different fire scenarios, UL-94 test was chosen since the heat source is mainly heat convection. Limit of UL-94 compared to MLC is that it is mainly a pass/fail test. It provides only the classification of the materials and dripping behavior of the samples. Even if this test lacks scientific parameters, it will be used for the screening of the FR formulation. The instrumentation of the UL-94 will be used and presented in the next chapter in order to get new insights.

III.1 Formulation of PBS with isosorbide-modified FRs

Isosorbide is a bio-based diol which can be modified by different functional groups. Especially the modifications of isosorbide by silicon, sulfur, nitrogen and/or phosphorus containing compounds should be effective as FR additive for polymers. Several modifications of isosorbide by phosphorus functional groups have been presented in literatures, and some of these FRs have shown good flame retardancy when used in polystyrene, epoxy resin and PLA.^{125,126,128,129} Since more possible isosorbide-based FRs can be synthesized and used to

flame retard PBS, isosorbide-derivatives (modification of isosorbide by phosphorus, sulfur and silicon based groups) have been synthesized. These syntheses are based on a nucleophile substitution of the halogeno (phosphorus, silicon or sulfur) group by the isosorbide. Their efficiency as FRs when incorporated in PBS was evaluated. The amount of isosorbide derivatives was chosen from 10 % to 20 %.

III.1.1 Sulfur based modification of isosorbide

Sulfur based FRs are often considered as effective FRs with an action in the gaseous phase by quenching the free radicals or in the condensed phase promoting the charring of the material.^{150,151,152,153,154} However, as far as we know they have not been described to flame retard PBS. Isosorbide can be easily modified by a tosylate group which is a sulfur based compound.¹⁵⁵ Di-tosyl-isosorbide (Dti) was synthesized by reaction of 4-toluenesulfonyl chloride with isosorbide at 0°C in pyridine (**Figure 50**).

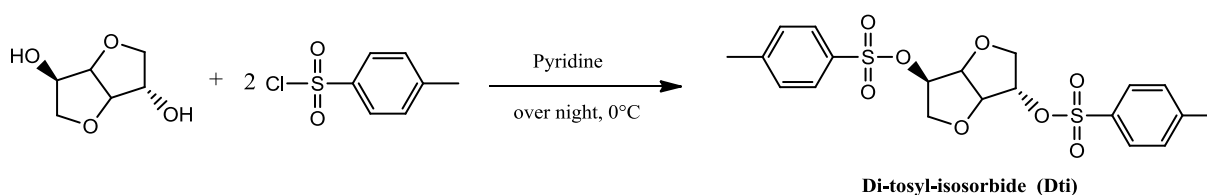


Figure 50: Synthesis of Di-tosyl-isosorbide (Dti)

Thermo-stability of the Dti under air shows that the degradation temperature is 250°C at 10°C/min when the degradation temperature is taken at 2 % mass loss (**Figure 51**) which is acceptable for the processing of PBS. The TG curve shows two mainly degradation steps for Dti, which occurred mainly from 250°C to 300°C and from 450°C to 600°C respectively. It can be observed that during the first step of decomposition, the mass loss from 100 % to 30 % occurred within only 50°C. During the second step of degradation, the mass loss from 30 % to 3 % within 150°C.

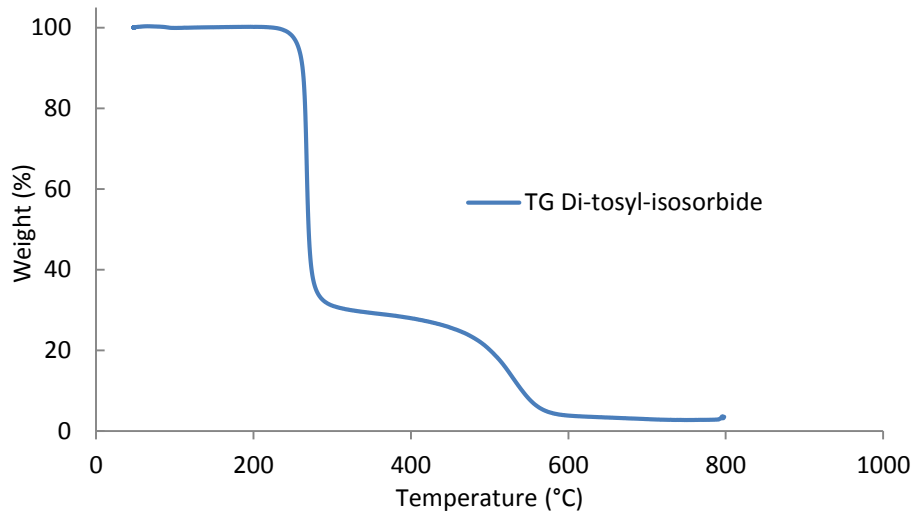


Figure 51: Thermal stability of Di-tosyl-isosorbide (Dti) (10°C/min under air)

Fire properties of PBS/Dti (80/20) formulation were evaluated by MLC (**Figure 52** and **Table 3**). It shows that Dti has negative effect on the fire properties of PBS, indeed, pHRR is increased by 41 %, TTI is decreased by 50 s and THR is decreased by 2 %. None of the major factors of the MLC test is improved with this FR. With no success of this sulfur-based compound, the modification of isosorbide was then focused on silicon or phosphorus based compounds.

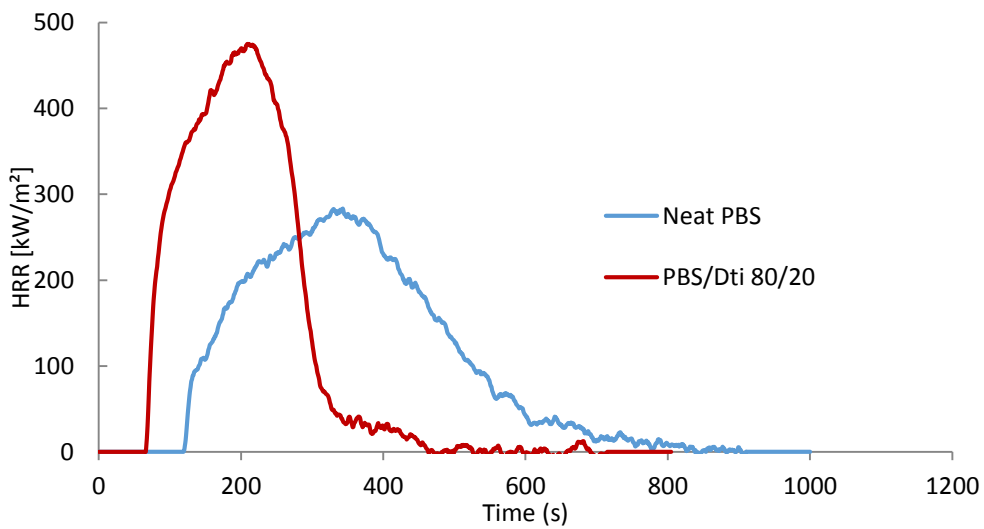


Figure 52: MLC test of PBS and PBS/Dti (50 x 50 x 3 mm³, 35 kW/m², 25 mm)

Table 3: Results of MLC tests for PBS and PBS/Dti

Ratio [wt.%]	pHRR [kW/m ²]	THR [MJ/m ²]	t _{ignition} [s]	t _{flameout} [s]	residue
Neat PBS	282	91	122	605	2%

PBS/Dti 80/20	475 (+41%)	90 (-2%)	69	310	1%
---------------	------------	----------	----	-----	----

III.1.2 Silicon based modification of isosorbide

The silicon based FRs are often considered to improve the yield and the quality of the forming char. Silicon based FRs has been proven to be efficient to flame retard polycarbonate.⁷² Moreover, it was reported in the literature that fumed silica could improve the flame retardancy of PBS especially when blended with APP and melamine.¹³² Thus, in our case, polydimethylsiloxane isosorbide (PDMSi) (**Figure 53, 1**) was synthesized by reaction of dichloride dimethylsilane with isosorbide at 89°C in toluene and triethylamine. Polymethylphenylsiloxane isosorbide (PMPSi) (**Figure 53, 2**) was synthesized by reaction of dichloride dimethylphenylsilane with isosorbide at 89°C in toluene and triethylamine.

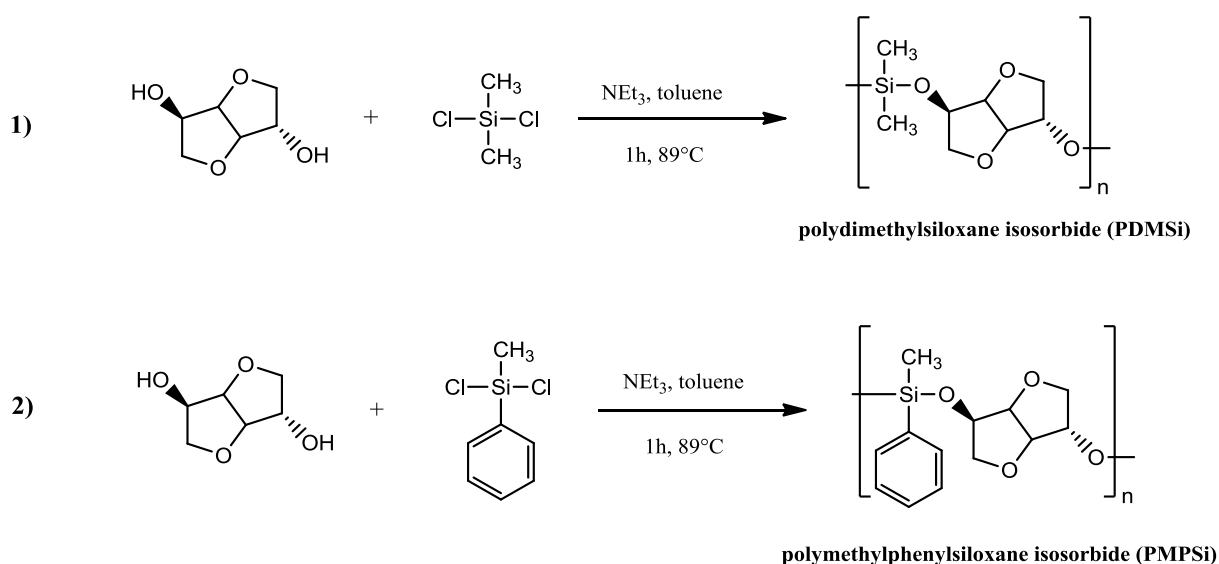


Figure 53: Synthesis of 1) polydimethylsiloxane isosorbide (PDMSi) and 2) polymethylphenylsiloxane isosorbide PMPSi

The thermal stability of PDMSi and PMPSi were evaluated under air (**Figure 54**). The degradation temperature of PDMSi starts at 172°C. Whereas the thermal stability changes a lot when methyl group is replaced by a phenyl group. The degradation temperature of PMPSi reached 273°C. Thus, these two molecules are suitable for the processing in PBS. Especially, PMPSi has a relatively high degradation temperature, therefore besides PBS, it can be also compounded with other polymers exhibiting higher processing temperature. Furthermore, PMPSi has a residue yield of 17 % which is higher than that of PDMSi (9 %).

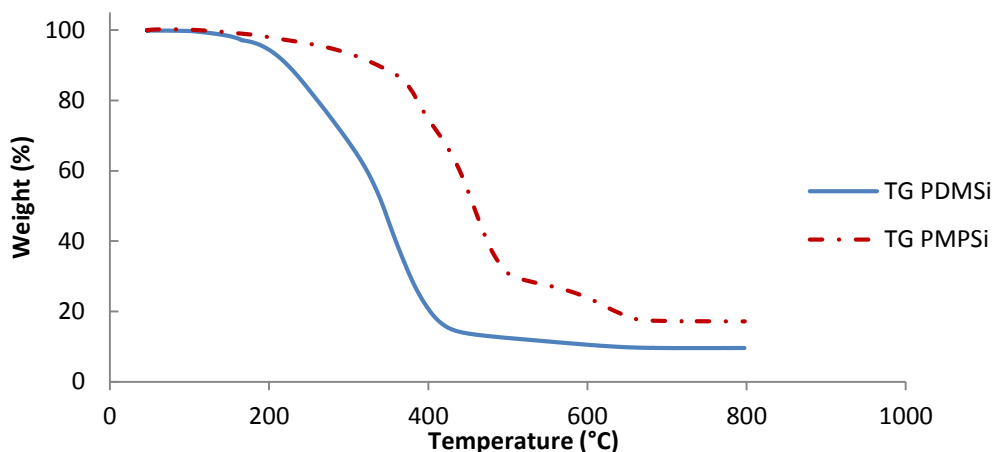


Figure 54: Thermal stability of polydimethylsiloxane isosorbide (PDMSi) and polymethylphenylsiloxane isosorbide (PMPSi) (10°C/min under air)

When 10 wt% of PDMSi and PMPSi were incorporated in PBS, results of MLC test are presented in **Figure 55** and **Table 4**. Negative effects were obtained: the pHRR is increased by 26 % and 28 % respectively, and the other parameters had no significant change. As mentioned in the literature, silicon based compounds can often be blended with phosphorus and nitrogen based FRs to enhance the performances. Thus, ammonium polyphosphate (APP) was added to our silicon based FR system (**Figure 56** and **Table 4**). It shows that for 10 wt% of PDMSi or PMPSi, with 20 wt% of APP, the pHRR is decreased by 34 % and 32 % respectively and the THR is decreased by 27 % and 26 % respectively. However, compared to PBS/APP 70/30, which had 19 % of decrease of pHRR and 25 % of decrease of THR, the addition of PDMSi and PMPSi does not bring any significant improvement. The photos of the residual char of PBS/PDMSi/APP 70/10/20 and PBS/PMPSi/APP 70/10/20 after the MLC test are presented on **Figure 57**. For both residues the char is white suggesting the formation of silica at the surface of the residues. However, the quantity of the char is too low to have protective function of the polymer. Results of UL-94 test (**Table 4**) shows also that the incorporation of PDMSi and PMPSi had no significant improvement of the fire retardancy of PBS: without APP, PBS/PDMSi and PBS/PMPSi have no classification in UL-94 test. No protective char is formed during the test and the drops formed ignite the cotton. Even with 20 wt% of APP added into the formulations, for PBS/PDMSi/APP and PBS/PMPSi/APP only V-1 can be achieved.

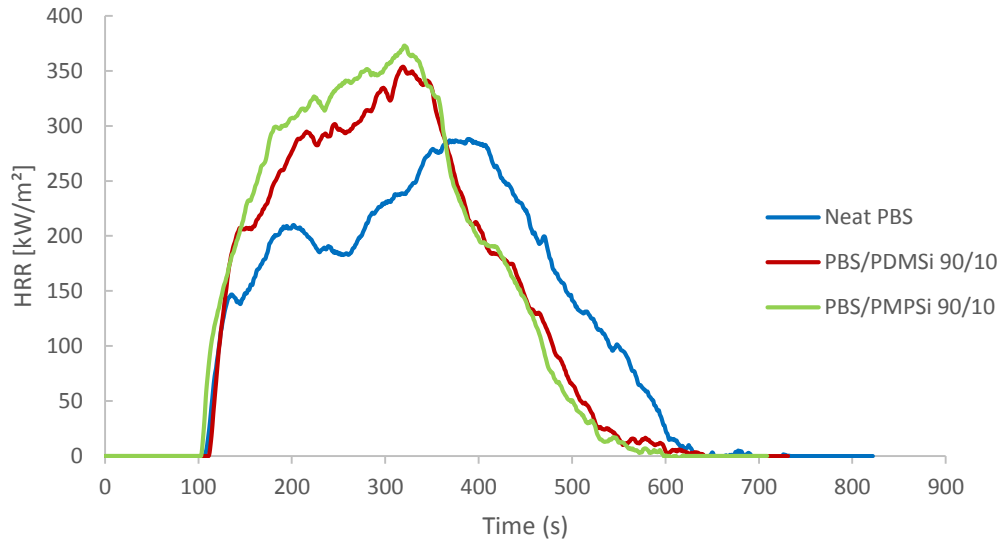


Figure 55: MLC tests of PBS with PDMSi, PMPSi (50 x 50 x 3 mm³, 35 kW/m², 25 mm)

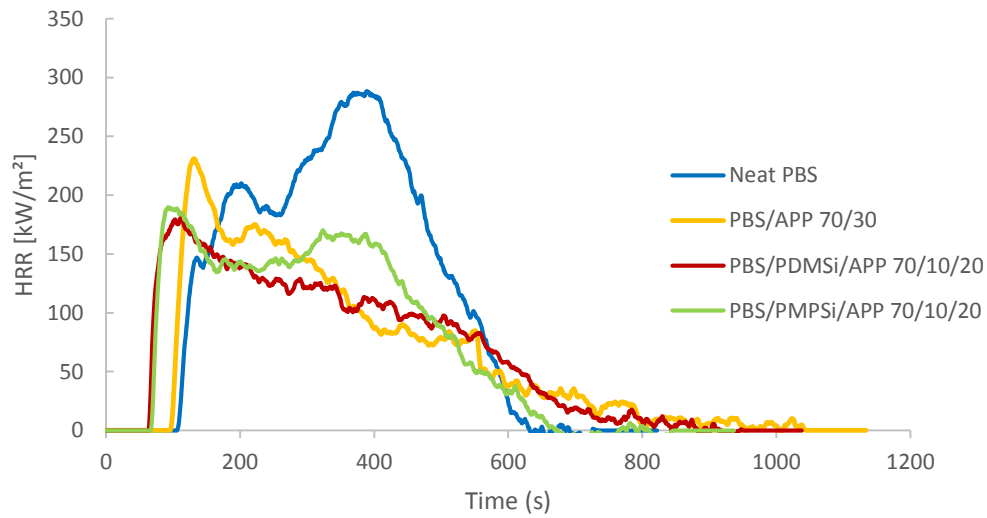


Figure 56: MLC tests of PBS with PDMSi, PMPSi and APP (50 x 50 x 3 mm³, 35 kW/m², 25 mm)

Table 4: Results of MLC tests of PBS with PDMSi, PMPSi and APP

Ratio [wt.%]	pHRR [kW/m ²]	THR [MJ/m ²]	t _{ignition} [s]	t _{flameout} [s]	residue	UL-94 (3.2 mm)	drippings
Neat PBS	283	91	110	605	2%	NC	yes
PBS/APP 70/30	231 (-19%)	67 (-25%)	99	712	31%	V-0	No
PBS/PDMSi 90/10	354 (+26%)	93 (+5%)	114	538	2%	NC	yes

PBS/PDMSi/APP 70/10/20	181 (-34%)	67 (-27%)	67	844	23%	V-1	No
PBS/PMPSi 90/10	371 (+28%)	95 (+5%)	116	520	1%	NC	yes
PBS/PMPSi/APP 70/10/20	192 (-32%)	66 (-26%)	69	678	24%	V-1	No

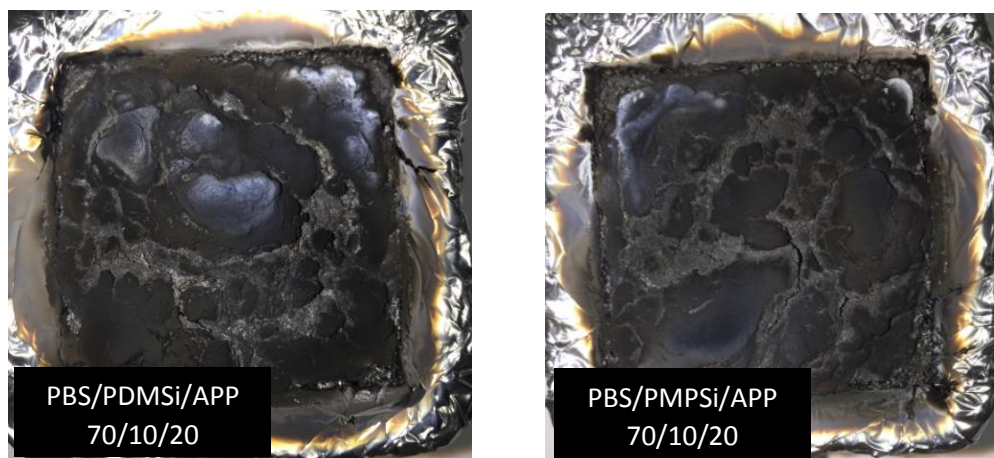


Figure 57: MLC residual char of PBS/PDMSi/APP 70/10/20 (left) and PBS/PMPSi/APP 70/10/20 (right)

Despite the unsuccessful MLC test when silicon based modification of isosorbide was blended with PBS, PMPSi has a relatively high degradation temperature. Polycarbonate (PC) has a slightly lower processing temperature than degradation temperature of PMPSi and this latter seems to be appropriate for PC. Thus, PMPSi was incorporated at 10 wt% in PC, MLC results shows that the incorporation of PMPSi decreased the pHRR by 29 % and the THR by 29 % but the ignition time had a significant decreasing from 221 s to 98 s (**Figure 58**) (**Table 5**). White residual char is also observed (**Figure 59**) after MLC. However, it is also like the forming char in the case of PBS, the char is porous and it separate into pieces which cannot protect the inner side of the plaques efficiently.

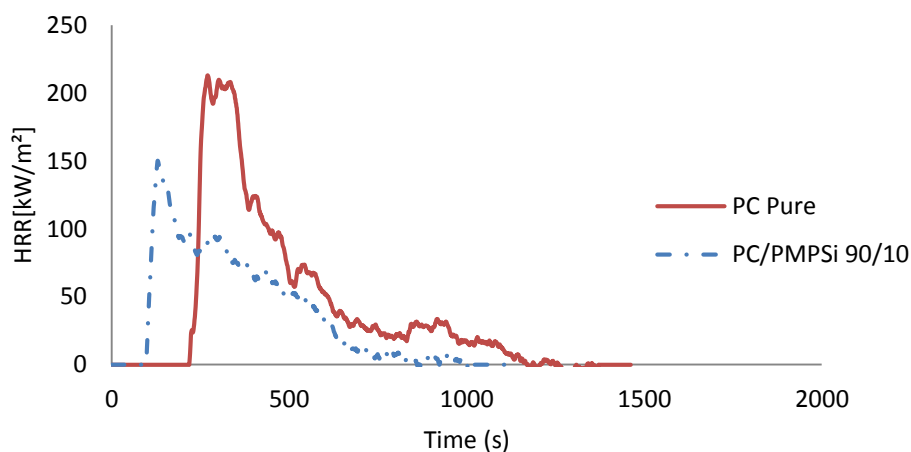


Figure 58: MLC results of PC and PC/PMPSi 90/10 (50 x 50 x 3 mm³, 50 kW/m², 25 mm)

Table 5: Results of MLC test of PC and PC/PMPSi

Ratio [wt.%]	pHRR [kW/m ²]	THR [MJ/m ²]	t _{ignition} [s]	t _{flameout} [s]	residue
Neat PC	212	58	221	1135	19%
PC/PMPSi 90/10	150 (-29%)	41 (-29%)	98	1204	18%

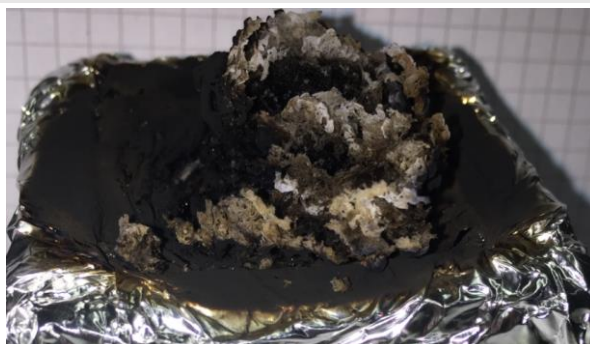


Figure 59: MLC Residual char of PC/PMPSi

III.1.3 Phosphorus based modification of isosorbide

Phosphorus based FRs are one of the most developed alternative to halogenated FRs. As mentioned in the literature, phosphorus based compounds are the most used FRs to improve the flame retardancy of PBS. Different synthesis of the phosphorus based modification of isosorbide were achieved: low molecular weight products and polymers; modification with different oxidation degree of the phosphorus. Polyphenylphosphate isosorbide (PPPAI) was synthesized by reaction of dichlorophenylphosphate with isosorbide at 120°C in presence of DMAP (**Figure 60, 1**). Polyphenylphosphonate isosorbide (PPPI) was synthesized by reaction of phenylphosphoric dichloride with isosorbide at 120°C in presence of DMAP (**Figure 60, 2**),

Di-DOPO-isosorbide (DDi) was synthesized by reaction of DOPO with isosorbide in dichloromethane at 0°C in presence of triethylamine and tetrachloromethane (**Figure 60, 3**). diphenylphosphinate isosorbide (DPPII) was synthesized by reaction of diphenylphosphoric chloride with isosorbide at 120°C in presence of DMAP (**Figure 60, 4**). Diphenylphosphate isosorbide (DPPI) was synthesized by reaction of diphenylphosphate chloride with isosorbide at 120°C in presence of DMAP (**Figure 60, 5**).^{126,127,128,129}

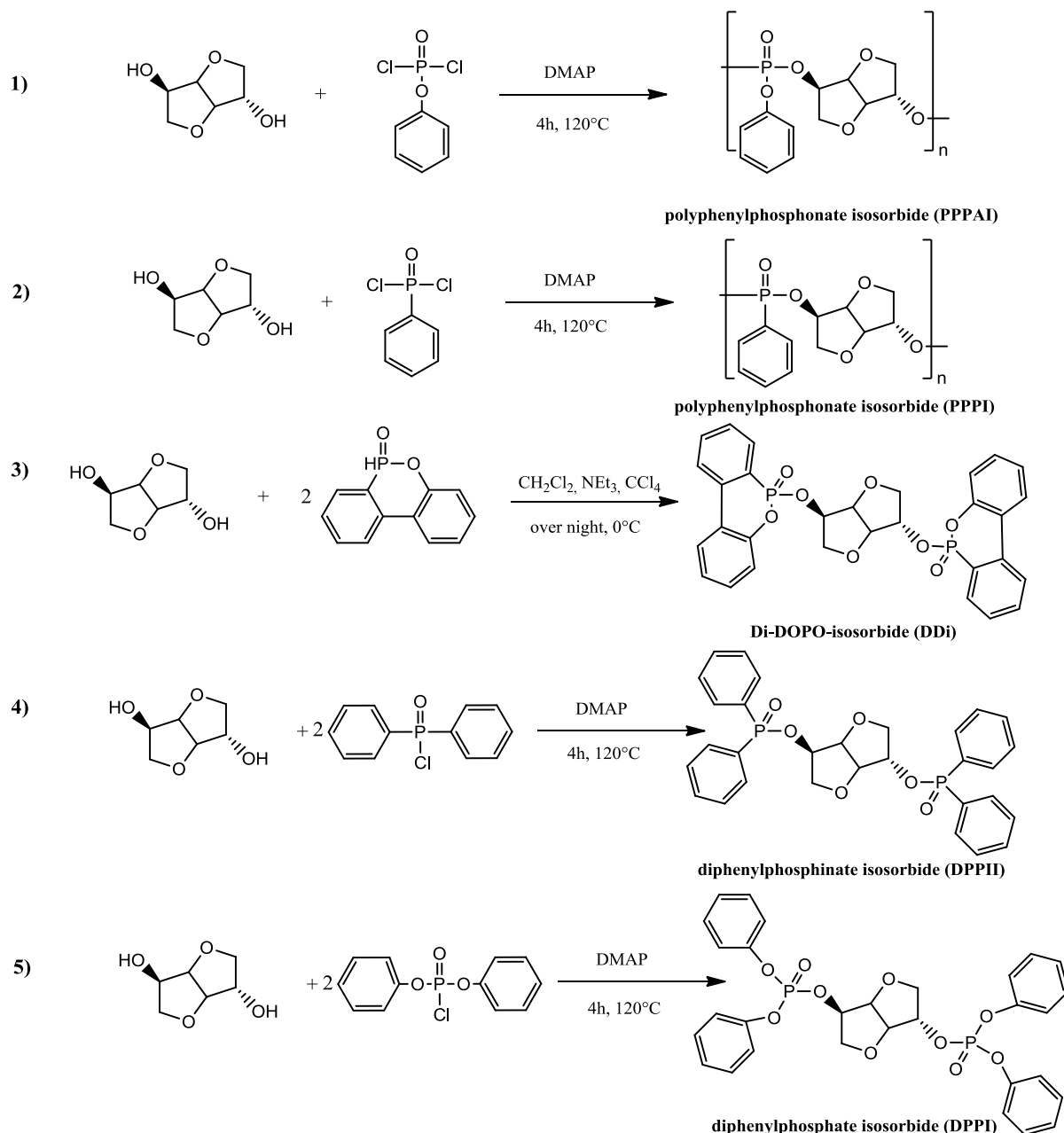


Figure 60: Synthesis of (1) polyphenylphosphate isosorbide (PPAI), (2) polyphenylphosphonate isosorbide (PPPI), (3) Di-DOPO-isosorbide (DDi), (4) diphenylphosphinate isosorbide (DPPII), (5) diphenylphosphate isosorbide (DPPI)

Thermal stability of these synthesized phosphorus based isosorbide are evaluated (**Figure 61**) (**Table 6**) It shows that all these molecules are acceptable for the processing of PBS. PPPAI has two degradation steps under air, the first step is from 280°C to 320°C which has 45 % mass loss; the second degradation step is above 400°C which has 26 % mass loss. Its degradation under N₂ has similar two degradation steps. PPPI has three degradation steps under air, the first degradation step is from 290°C to 330°C which has 36 % mass loss; the second step is from 330°C to 400°C which has 23 % mass loss; the third step is above 400°C which has 32 % mass loss. Its degradation under N₂ has also similar three degradation steps. DPPI has only one degradation step under N₂ which is from 300°C to 420°C, whereas it has two degradation steps under air: the first step is from 295°C to 430°C and the second step is above 450°C. DPPPII has also only one degradation step under N₂ from 297°C to 430°C, whereas under air an extra degradation step was observed above 450°C. The same phenomenon was observed for DDi, it has one degradation step under N₂ from 320°C to 460°C, and an extra degradation step is observed above 460°C. The oxidation degree of phosphorus influences also the quantity of residue, the highest residues yield were obtained with the phosphates. The residue of PPPAI reached 40 % and 29 % in N₂ and in air respectively which is more than that obtained in PPPI (21 % in N₂ and 7 % in air) which is a phosphonate. Same phenomenon was found for another phosphate DPPI, which has 21 % and 15 % residue in N₂ and in air respectively, whereas almost no residue was found in DPPPII (3 % in N₂ and 1% in air) which is a phosphinate. It was also found that the atmospheres used in the test influence a lot the degradation steps and the residue yield. With air it occurs additional decomposition steps in some cases (DPPPII and DDi), and the residue yield is always higher under N₂. It makes sense because oxidation creates a transient char which is further degraded by oxidation at higher temperature.

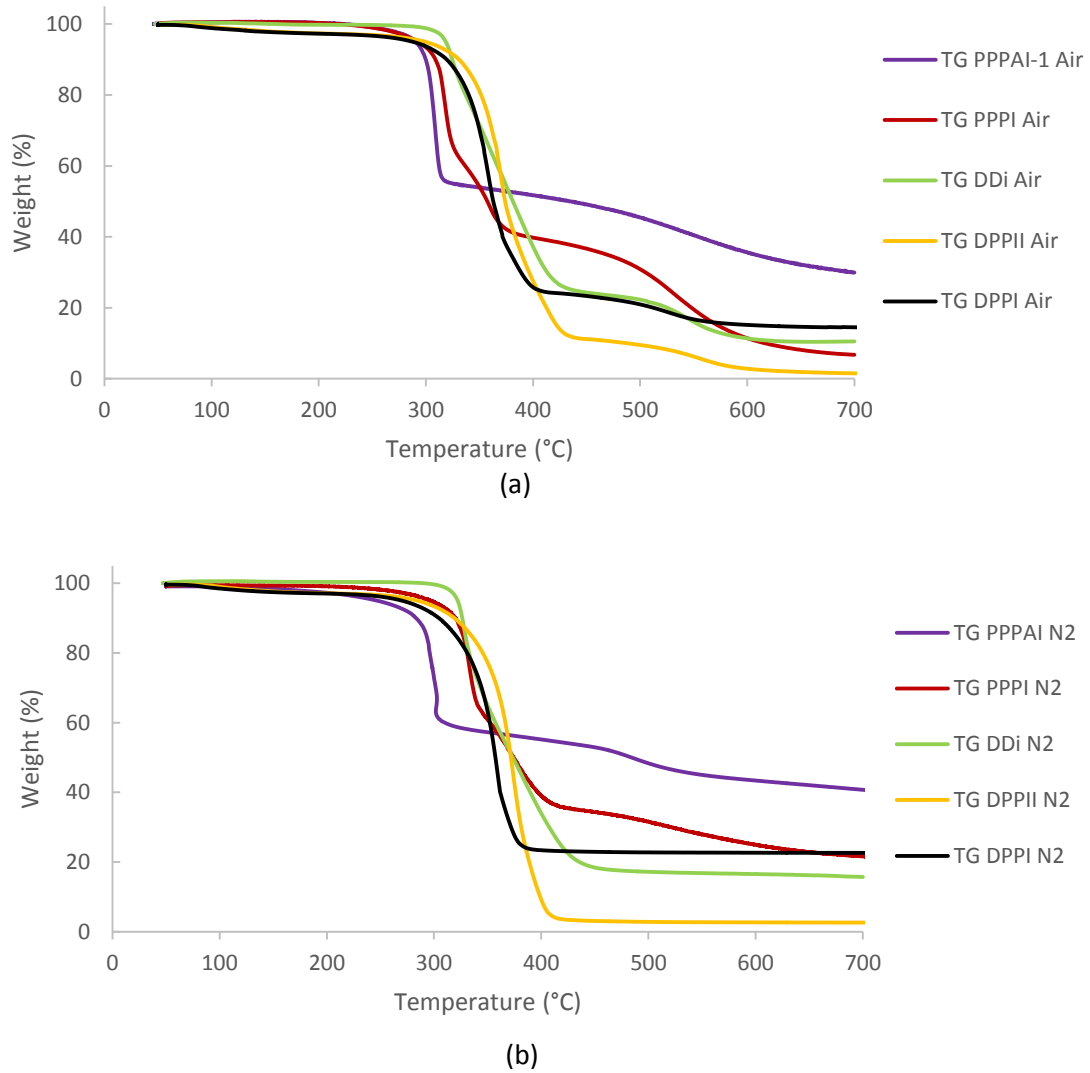


Figure 61: Thermal stability of PPPAI, PPPI, DPPI, DPPII and DDi under a) Air and b) N₂ (10°C/min)

Table 6: Thermal stability and residues of phosphorus modified isosorbide

	PPPAI	PPPI	DDi	DPPII	DPPI
Degradation temperature (°C) Air	279	295	305	297	295
Residue (%) Air	29	7	10	1	15
Degradation temperature (°C) N ₂	289	294	321	297	299
Residue (%) N ₂	40	22	15	3	21

The results of MLC test is presented in **Figure 62** and **Table 7**. The different oxidation degree of the phosphorus showed different performances. With low degree of oxidation, phosphinate (DPPII and DDi) showed improvement of the ignition time, flame extinguishing phenomenon was observed before the ignition suggesting the action of phosphorus species

in the gaseous phase. With higher degree of oxidation, phosphonate or phosphate showed higher char yield, however the yield is too low to be effective (7% for PPPAI and 4% for DPPI). All these phosphorus based FRs had no improvement on the pHRR when incorporated in PBS. In UL-94 test, the systems PBS/phosphorus modified FRs have good performance, V-0 rating is achieved with the presence of drops which do not ignite the cotton (**Table 7**). These drops take away materials and heats from the burning bar and the drops cannot ignite the cotton, thus a good classification can be achieved

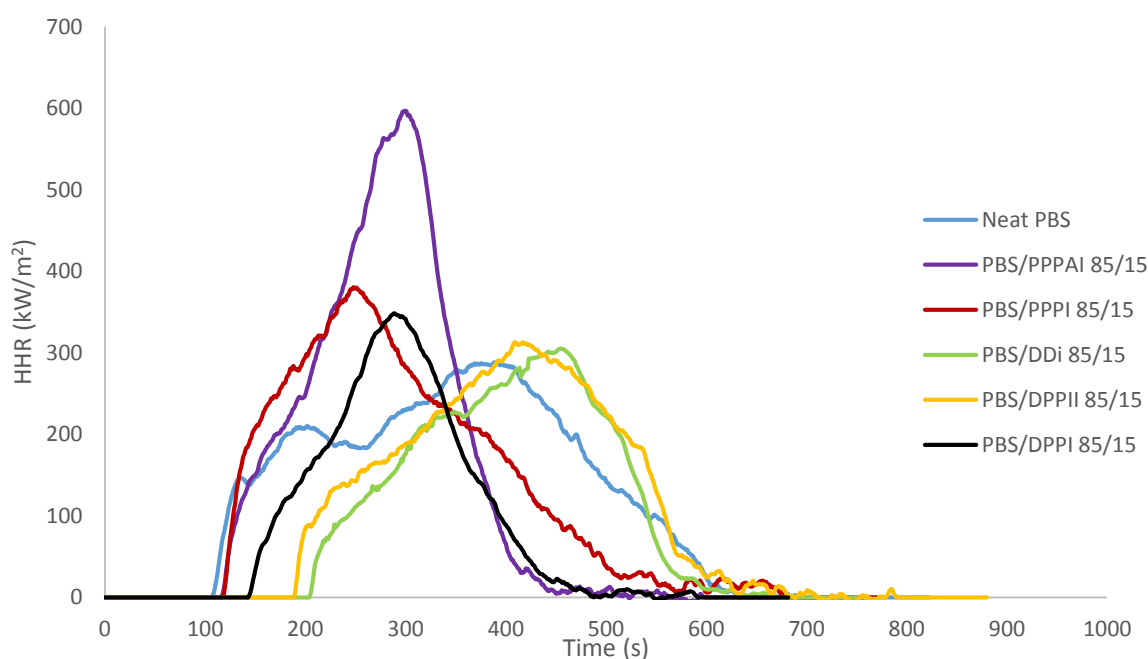


Figure 62: MLC test of PBS with PPPI, PPPAI, DPPII, DPPI and DDI ($50 \times 50 \times 3 \text{ mm}^3$, 35 kW/m^2 , 25 mm)

Table 7: Results of MLC test of PBS with PPPI, PPPAI, Di-DOPO-isosorbide, DPPII and DPPI

Ratio [wt.%]	pHRR [kW/m ²]	THR [MJ/m ²]	t _{ignition} [s]	t _{flameout} [s]	residue	UL-94 (3.2 mm)	dripping
Neat PBS	283	91	110	605	2%	NC	yes
PBS/PPPI 85/15	380 (+35%)	86 (-6%)	121	518	4%	V-0	yes
PBS/PPPAI 85/15	596 (+107%)	114 (+24%)	119	436	7%	V-0	yes
PBS/DPPII 85/15	325 (+15%)	83 (-9%)	194	628	1%	V-0	yes
PBS/DPPI 85/15	345 (+22%)	84 (-9%)	148	455	4%	V-0	yes
PBS/DDi 85/15	312 (+11%)	79 (-13%)	205	559	1%	V-0	yes

III.1.4 Conclusion

Isosorbide was modified by sulfur, phosphorus and silicon based functional groups. It shows that the thermal stability of isosorbide is significantly enhanced. Sulfur modification of isosorbide showed negative effect in MLC tests. The single use of silicon-based modification of isosorbide had no significant improvement of fire retardancy of PBS. Nevertheless, when combining with APP, these silicon based FRs can slightly improve the performance of PBS in a fire scenario. Phosphorus compounds showed different performance according to the different oxidation degree of the phosphorus. It shows that the lower oxidation degree of phosphorus leads to an action in the gaseous phase (phosphonate and phosphinate). Higher oxidation degree (phosphate) leads to an action in the condensed phase. In the MLC test, the performance of the phosphorus compounds showed no significant improvement on the THR and pHRR, only some of the FRs showed improvement of TTI due to the effect in the gaseous phase. Whereas in the UL-94 tests, no matter which oxidation of the phosphorus is used, these phosphorus compounds can often reach a good classification (V-0), which indicates that in our case, the oxidation degree of phosphorus does not influence the classification, but the drops formed during the test is the key point.

It has been proven that synthesis of isosorbide based FRs may be a good solution to flame retard PBS when UL-94 test is required. Meanwhile, another advantage of using isosorbide is that it improves the content of bio-based material in the formulation.

Isosorbide is a saccharide which can be potentially used as carbonization agent, hence the next part will be focused on the isosorbide and isosorbide based polymer acting as carbonization agent.

III.2 Isosorbide and isosorbide based polymer used as carbonization agent

APP was proven to be an efficient acid source which is one of the major factor in an intumescent FR system. Another major factor is the carbon source, thus isosorbide and isosorbide based polymer are potential carbonization agent for our intumescent FR system.

III.2.1 Isosorbide as carbonization agent

MLC tests of the intumescent FR system of PBS/APP containing isosorbide are presented in **Figure 63** and **Table 8**. In order to determine the best ratio between carbonization agent and

phosphorus acid, the incorporation of isosorbide was done at different levels i.e. APP/Isosorbide ratios tested were 3/1, 1/1 and 1/3. Within these ratios, isosorbide/APP 1/3 presented the best results: pHRR is slightly decreased and THR is decreased by 25 %. However, with this ratio, there is no improvement compared to the formulation PBS/APP 70/30, even the TTI is decreased from 110 s to 70 s. It shows that the residual char has visible cracks on the surface which cannot protect the polymer (**Figure 64**). Thus, isosorbide is not a good candidate as carbonization agent for these formulations.

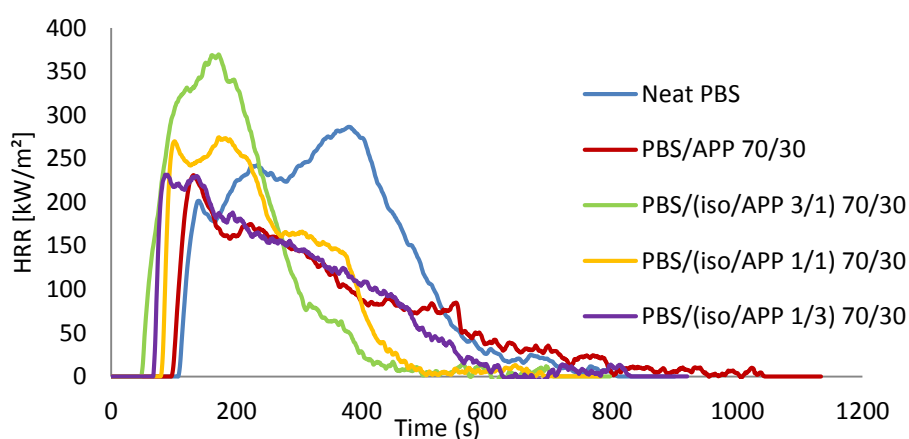


Figure 63: MLC tests of PBS with APP and isosorbide ($50 \times 50 \times 3 \text{ mm}^3$, 35 kW/m^2 , 25 mm)

Table 8: Results of MLC tests of PBS with APP and isosorbide

Ratio [wt.%]	pHRR [kW/m ²]	THR [MJ/m ²]	t _{ignition} [s]	t _{flameout} [s]	residue
Neat PBS	283	91	110	605	2%
PBS/APP 70/30	231 (-19%)	67 (-25%)	99	712	31%
PBS/(iso/APP 3/1) 70/30	369 (+31%)	73 (-24%)	51	402	11%
PBS/(iso/APP 1/1) 70/30	274 (-3%)	67 (-25%)	81	432	17%
PBS/(iso/APP 1/3) 70/30	251 (-11%)	68 (-25%)	70	510	23%



Figure 64: MLC Residual char of PBS/(isosorbide/APP 1/3) 70/30

III.2.2 Isosorbide based polymer as carbonization agent

It has been presented that some of the polymers can be used as carbonization agent in an intumescent fire retardant system. Conventional bisphenol-A based polycarbonate has a charring effect upon heating. Thus the isosorbide based polycarbonate (poly isosorbide carbonate (PIC)) can be a potential carbonization agent in an intumescent fire retardant system.

MLC tests of PBS based formulations containing PIC used as carbonization agent are presented in **Figure 65** and **Table 9**. The additives were incorporated at a loading of 30 wt% in PBS. The determination of the best formulation is carried out by changing the ratio of PIC/APP of 3/1, 1/1, 1/3. The addition of PIC as carbonization agent shows direct influence of the decreasing of pHRR and THR. The best result is obtained when the ratio of PIC/APP is at 1/3. With this ratio, pHRR is decreased by 24 %, the THR is decreased by 48 % and the char yield can reach 44 %. Compared to the formulation without the carbonization agent, the formulation PBS/PIC/APP exhibits an enhanced performance for the main parameters measured at MLC. The formation of the char in this formulation may be the key point of the success. The residual char of PBS/APP 70/30 had obvious cracks and holes on the surface (**Figure 66**). Whereas the char of PBS/PIC/APP exhibits only small holes (**Figure 66**).

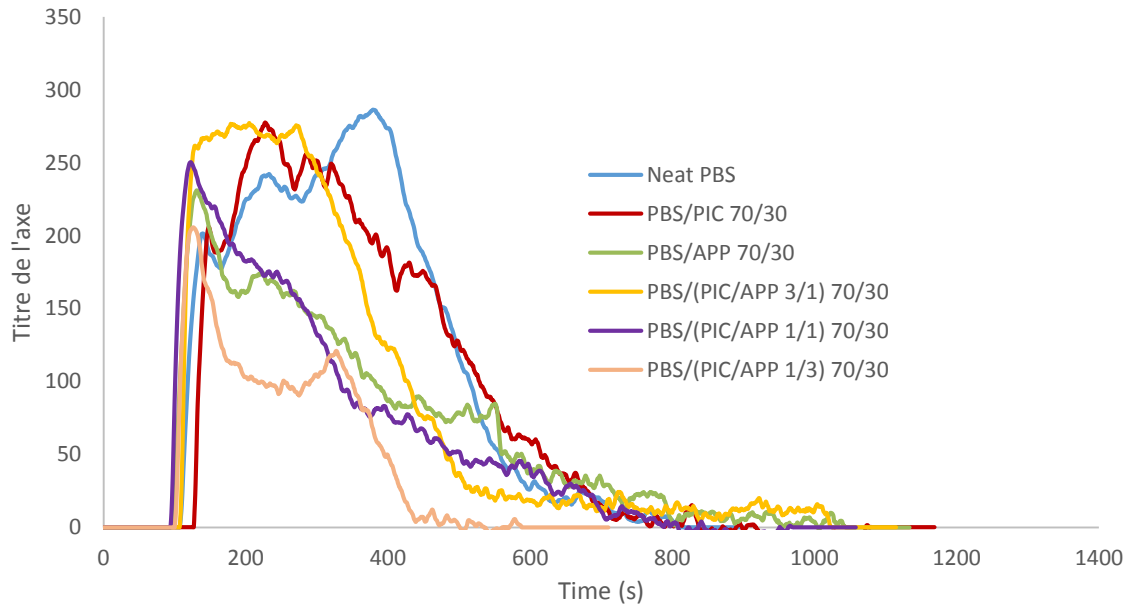


Figure 65: MLC tests of PBS with PIC and APP ($50 \times 50 \times 3 \text{ mm}^3$, 35 kW/m^2 , 25 mm)

Table 9: Results of MLC tests of PBS with PIC and APP

Ratio [wt.%]	pHRR [kW/m ²]	THR [MJ/m ²]	t _{ignition} [s]	t _{flameout} [s]	residue
Neat PBS	283	91	110	605	2%
PBS/PIC 70/30	275 (-2%)	88	126	767	1%
PBS/APP 70/30	231 (-19%)	67 (-25%)	99	712	23%
PBS/(PIC/APP 3/1) 70/30	277 (-2%)	84 (-8%)	110	490	9%
PBS/(PIC/APP 1/1) 70/30	250 (-11%)	61 (-33%)	112	766	18%
PBS/(PIC/APP 1/3) 70/30	216 (-24%)	47 (-48%)	105	484	44%

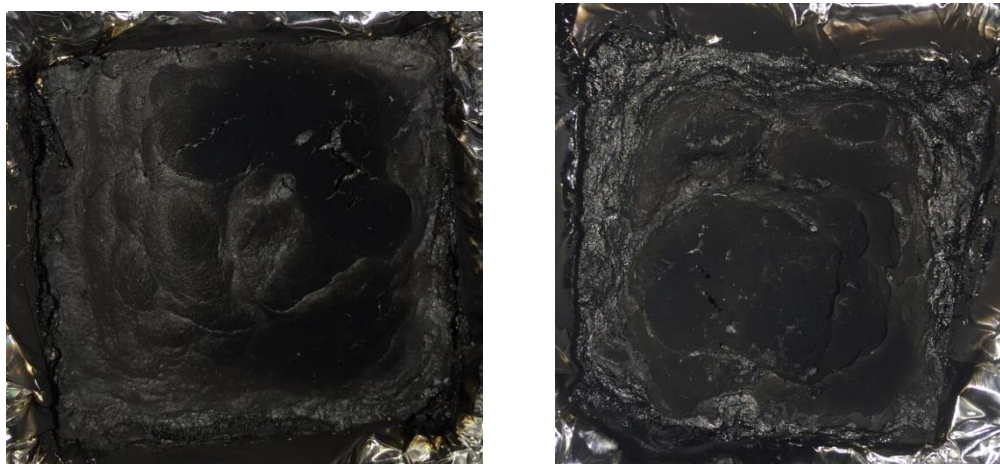


Figure 66: MLC residual char of PBS/APP 70/30 (left) and PBS/(PIC/APP 1/3) 70/30 (right)

III.2.3 Conclusion

Isosorbide or PIC, as bio-based compounds, when incorporated in PBS can improve the content of bio-based components. It is an extra benefit if the formulation keeps (or improves) its flame retardant effect. Isosorbide showed no significant improvement in the fire test. Whereas PIC is quite efficient in terms of char forming agent in MLC scenario. The effect of PIC occurs in improving the char yield and hence, a significant decrease of pHRR and THR. For this reason, the mechanism of this formulation is worth deeply being investigated (see chapter V).

III.3 Formulation based on DOPO or DOPO with conventional FRs for PBS

In this part, un-modified DOPO and DOPO derivatives are firstly discussed. Then the DOPOs are formulated with phosphorus based non-intumescent FRs, carbon nanotube, metal hydroxides and metal carbonate salts to flame retard PBS.

III.3.1 Formulation of neat DOPO with PBS

In the state of the art (chapter I), a brief introduction of DOPO and its derivatives indicate that they mainly act in the gaseous phase to poison the flame by quenching the free radicals of high energy. DOPO and its derivatives are mainly used for the flame retardancy of epoxy resin used for the applications of adhesives, composites and printed wiring boards etc. However, the un-modified DOPO has not been used to flame retard PBS due to his low decomposition temperature. Hence in our study, the effects of DOPO will be discussed.

Figure 67 shows that DOPO start to decompose/sublimate at 160°C (at 10°C/min) and PBS starts to decompose at 335°C. Thus DOPO is acceptable for the processing of PBS (processing of PBS is at 140°C).

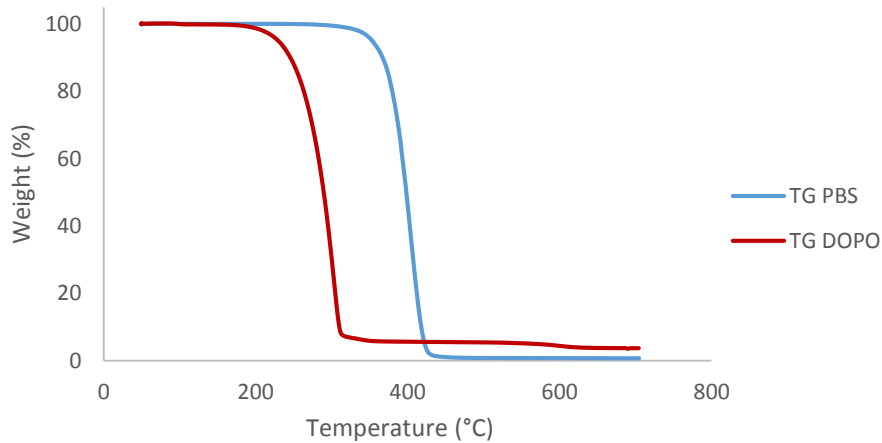


Figure 67: Thermal stability of PBS and DOPO (10°C/min, under N₂)

DOPO is incorporated in PBS at a loading of 10 wt%. The results of MLC test are presented in **Figure 68** and **Table 10**. It shows that DOPO increased a lot the TTI i.e. from 119 s to 410 s. The pHRR is increased by 10 % when DOPO was added in PBS, whereas the THR is decreased by 27 %. Flame extinguishing phenomenon is observed before ignition when DOPO was incorporated in PBS.

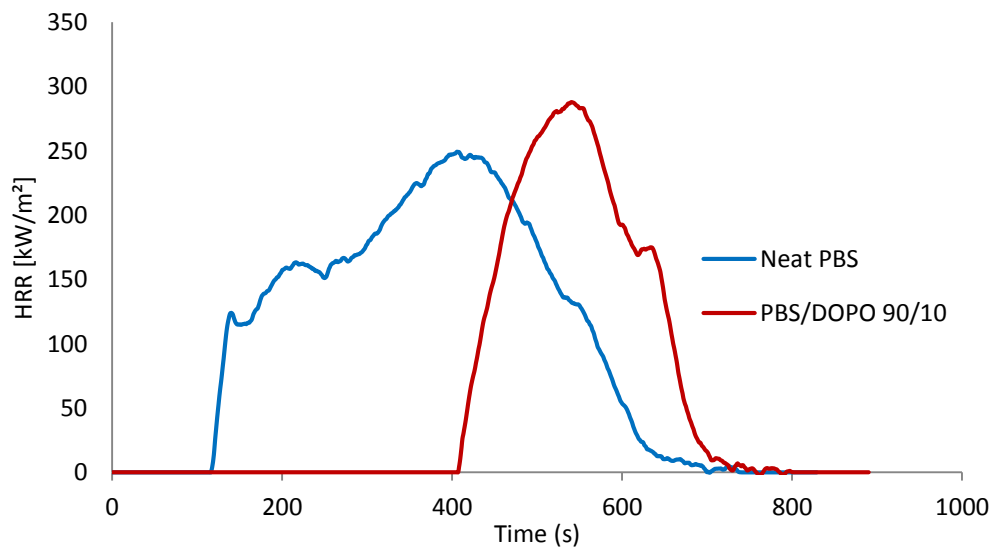


Figure 68: MLC test of PBS and PBS/DOPO (50 x 50 x 3 mm³, 35 kW/m², 25 mm)

Table 10: Results of MLC test of PBS and PBS/DOPO

Ratio [wt.%]	pHRR [kW/m ²]	THR [MJ/m ²]	t _{ignition} [s]	t _{flameout} [s]	residue	UL-94 (3.2 mm)	Dripping
Neat PBS	249	84	119	620	3%	NC	yes
PBS/DOPO 90/10	287 (+10%)	61 (-27%)	410 (+291s)	669	2%	V-0	yes

Then results of UL-94 (3.2 mm) is presented in **Table 10**. Neat PBS needs only once ignition to burn up to the clamp, it drips a lot and no classification is achieved. V-0 rating and no visible burning are observed in the case of PBS/DOPO 90/10. Drippings are observed but with no ignition of the cotton.

The great improvement of the ignition time suggests an action of the DOPO in the gas phase. With this phenomenon, it is also interesting to test the efficiency of some DOPO derivatives in PBS. These results will be presented in the next part. Furthermore, in order to combine a gas phase action and a condensed phase one, DOPO was combined with additives which work in condensed phase such as conventional phosphorus and nitrogen based intumescent FRs, hydroxide and carbonate metal salts and carbon nanotubes. These combinations and their associated results are presented in the following sections.

III.3.2 Formulation of DOPO derivatives with PBS

As DOPO works well in the gaseous phase, it is also interesting to evaluate the performances of DOPO derivatives, more particularly, some having also effect in the condensed phase. It is known that the environment of the phosphorus atom influences the performance in a fire scenario, thus compounds containing P-C, P-N, P-O bonds are chosen to be compared with neat DOPO which has a P-H structure. Chemical structures of DOPO-3-propanamide (DOPO-ACA), DOPO-1-oxyphospha-4-hydroxymethyl-2,6,7-trioxabicyclo[2,2,2]octane (DOPO-PEPA), DOPO-ethane-1,2-diylbis(azanediyl) (DOPO-EDA) are presented in **Figure 69**.

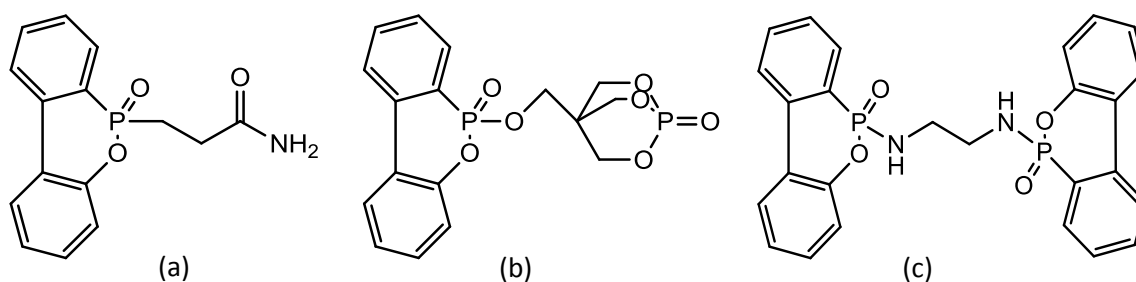


Figure 69: Chemical structures of a) DOPO-3-propanamide (DOPO-ACA) b) DOPO-1-oxyphospha-4-hydroxymethyl-2,6,7-trioxabicyclo[2,2,2]octane (DOPO-PEPA) c) DOPO-ethane-1,2-diylbis(azanediyl) (DOPO-EDA)

The loading of derivatives is based on the same content of the DOPO pattern as un-modified DOPO (11.6 mmol). MLC tests are presented in **Figure 70** and **Table 11**. It shows that the pHRR is increased and the THR is decreased for all the DOPO derivatives. Concerning the TTI, it shows that the DOPO-ACA which has a P-C bond increased the ignition time to 201 s, and the DOPO-PEPA which has a P-O bond increased the ignition time to 169 s, whereas the DOPO-EDA which has a P-N bond had no improvement of the TTI. The derivatives showed also the flame extinguishing phenomenon in the MLC test, but they are less effective than the un-modified DOPO.

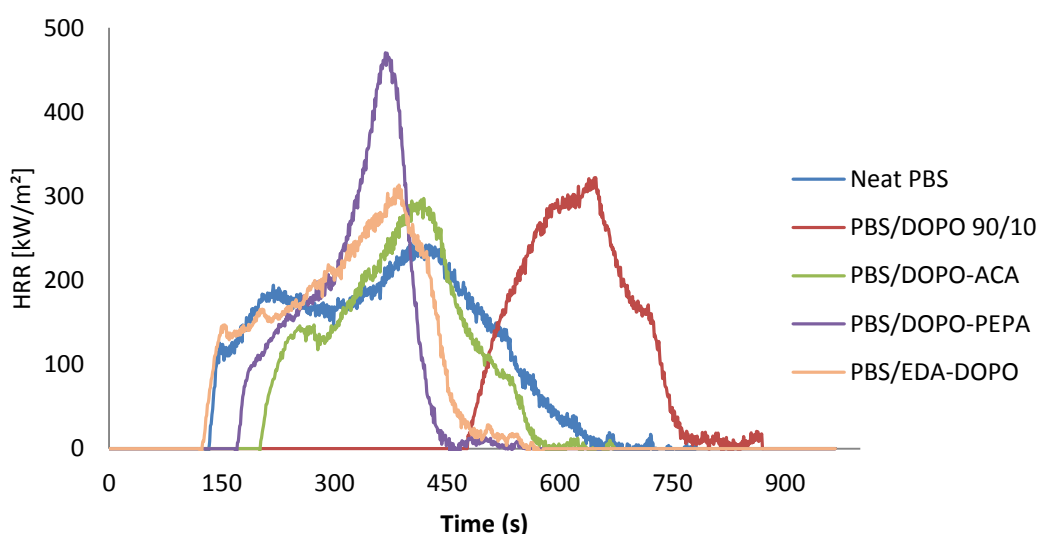


Figure 70: MLC tests of PBS with DOPO derivatives ($50 \times 50 \times 3 \text{ mm}^3$, 35 kW/m^2 , 25 mm)

Table 11: Results of MLC tests of PBS with DOPO derivatives

Ratio [wt.%]	pHRR [kW/m ²]	THR [MJ/m ²]	t _{ignition} [s]	t _{flameout} [s]	residue
Neat PBS	236	76	130	662	1%
PBS/DOPO 90/10	316 (+33%)	56 (-26%)	478	743	2%
PBS/DOPO-ACA 90/10	291 (+23%)	58 (-25%)	201	554	4%
PBS/DOPO-PEPA 90/10	464 (+97%)	58 (-25%)	169	432	9%
PBS/DOPO-EDA 90/10	304 (+29%)	65 (-14%)	122	457	3%

III.3.3 Formulation of DOPO and intumescent FRs with PBS

APP and melamine polyphosphate (MPP) are used as intumescent FRs to flame retard PBS. The degradation temperature of APP is 290°C under air at 10°C/min whereas in the same conditions MPP degrades at 350°C (**Figure 71**). Since PBS starts to decompose at 335°C, the degradation temperatures of APP and MPP are close to that of neat PBS.

The APP and MPP (20 wt%) are combined with 10 wt% of DOPO in PBS and are compared with formulations only based on APP and MPP (30 wt%). The results of the MLC tests are presented in **Figure 72** and **Table 12**. It showed that the addition of APP or MPP had some positive effect in MLC test: the pHRR is decreased by 18 % for APP and 9 % for MPP, and THR is decreased by 26 % for APP and 16 % for MPP. The char yield of these two formulations increased to 30 % and 18 % respectively. When DOPO is blended with APP, the TTI is slightly increased from 110 s to 150 s, whereas the pHRR is increased by 12 %. When MPP is blended with DOPO, TTI is similar as that of neat PBS and pHRR and THR remain unmodified compared to neat PBS. Thus, these formulations cannot combine the advantages of the gas phase action of DOPO with the advantages of the condensed phase action brought by APP or MPP.

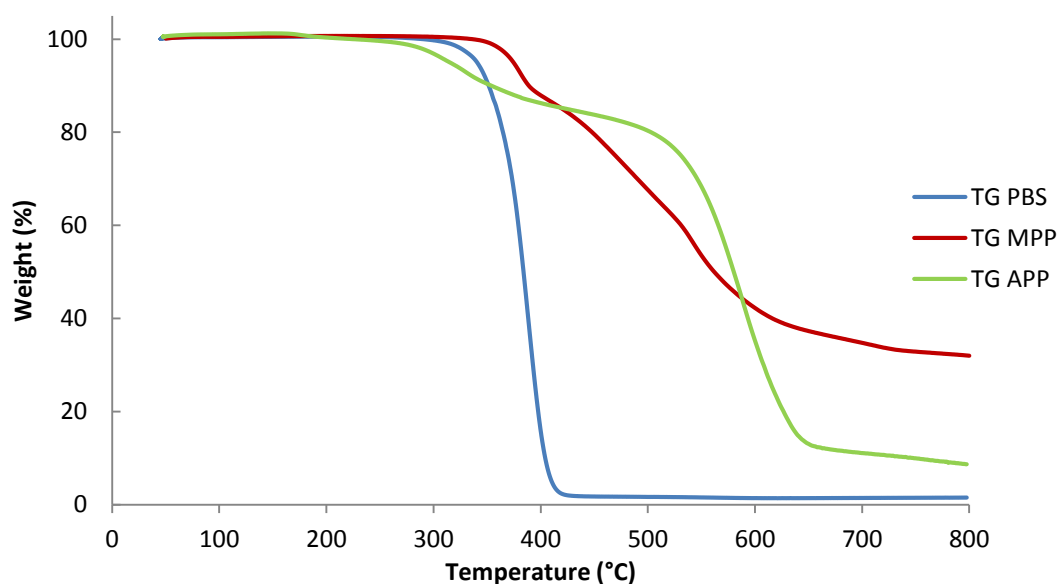


Figure 71: Thermal stability of neat PBS, APP and MPP (10°C/min under air)

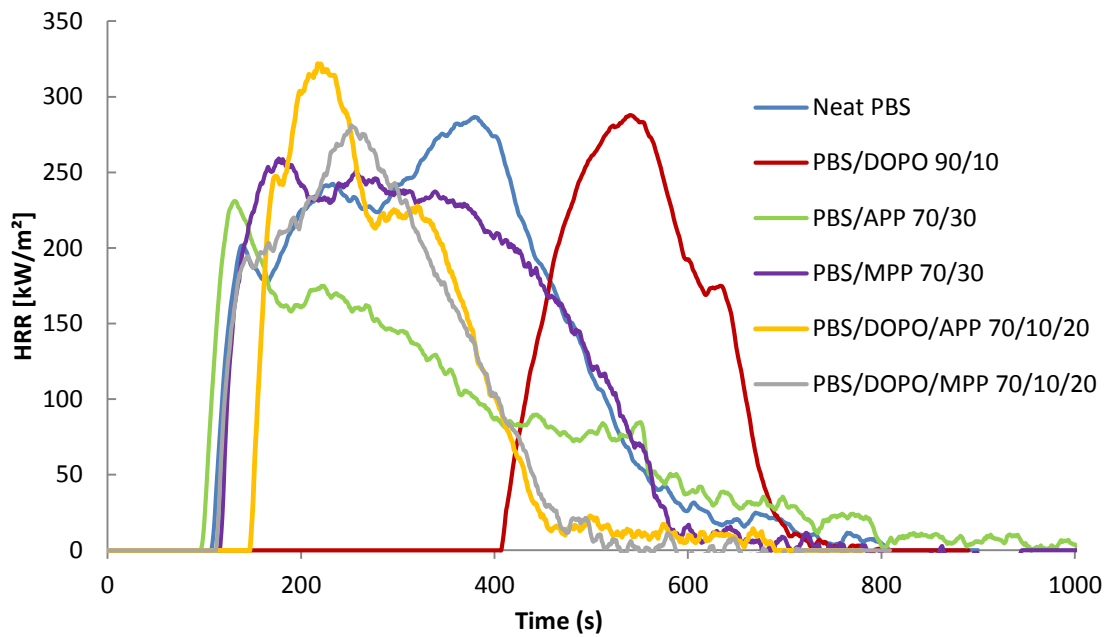


Figure 72: MLC tests of PBS with APP, MPP and DOPO ($50 \times 50 \times 3 \text{ mm}^3$, 35 kW/m^2 , 25 mm)

Table 12: Results of MLC test of PBS with APP, MPP and DOPO

Ratio [wt.%]	pHRR [kW/m ²]	THR [MJ/m ²]	t _{ignition} [s]	t _{flameout} [s]	residue
Neat PBS	283	91	110	605	2%
PBS/DOPO 90/10	287 (+1%)	65 (-27%)	410 (+291s)	669	2%
PBS/APP 70/30	231 (-18%)	67 (-26%)	99	712	30%
PBS/MPP 70/30	258 (-9%)	76 (-16%)	114	594	18%
PBS/DOPO/APP 70/10/20	321 (+12%)	62 (-28%)	150	453	20%
PBS/DOPO/MPP 70/10/20	281(-1%)	63 (-28%)	115	454	11%

It is well known that APP and MPP release ammonia that might disturb the gaseous phase action of DOPO. Therefore, in the next part, components that release low reactive gases such as CO₂ and H₂O are combined with DOPO.

III.3.4 Formulation of DOPO and metal hydroxides and metal carbonate salts with PBS

Metal hydroxides and metal carbonate can release H₂O or CO₂ upon heating. Thus this part discusses the combination of these salts with DOPO.

The selected hydroxide and carbonate salts are based on their decomposition temperature. Aluminum trihydroxide ($\text{Al}(\text{OH})_3$, ATH) and Magnesium dihydroxide ($\text{Mg}(\text{OH})_2$, MDH) have a dehydration temperature of 266°C and 353°C respectively. Magnesium carbonate (MgCO_3) and calcium carbonate (CaCO_3) have decarbonation temperature of 380°C and 681°C respectively. ATH was chosen due to lower degradation temperature than that of PBS, it was supposed to be active with DOPO before the ignition of PBS. Dehydration of MDH and decarbonation of MgCO_3 have close temperature to the degradation temperature of PBS, they are supposed to act when PBS start decomposing. Whereas CaCO_3 has much higher decarbonation temperature, it was supposed to be effective when DOPO had no effect in the gaseous phase and when PBS start to burn.

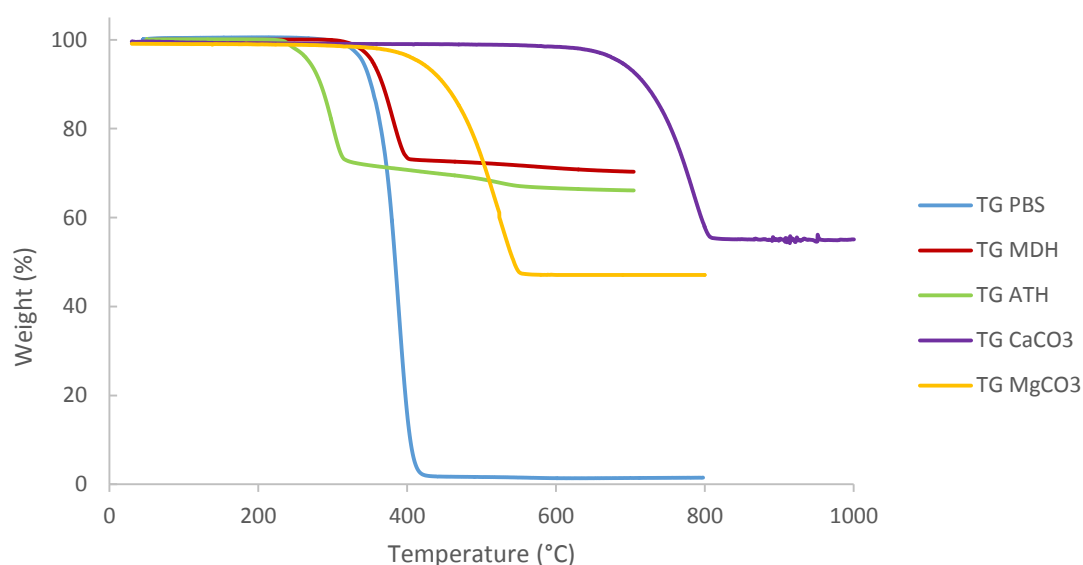


Figure 73: Thermal stability of ATH, MDH, MgCO_3 and CaCO_3 ($10^\circ\text{C}/\text{min}$ under N_2)

MLC tests of MDH and ATH based formulations are presented in **Figure 74** and **Table 13**. MDH and ATH showed good performances acting in the condensed phase: at 20 wt% loading of MDH and ATH, pHRR is decreased by 33 % and 10 % respectively, THR is decreased by 50 % and 5 % respectively. The theoretical residue of these two formulations are based on the hypothesis that the MDH and ATH are completely dehydrated into MgO and Al_2O_3 and no interaction occurred between the additives and the polymer matrix: so the calculated residue of these two formulations are 14 % and 13 %. In the real test, the residue yield increased to 38 % in the case of MDH which is much higher than the theoretical value, and it was 16 % in the case of ATH which is almost the same as the theoretical value. It shows that ATH is less

effective than MDH in the condensed phase. However, when DOPO was blended with MDH, pHRR, THR as well as TTI had no significant improvement compared to PBS/MDH. It shows that the action of DOPO in the gaseous phase is stopped. As for ATH, even though the pHRR had no decreasing, the TTI had improved from 110 s to 243 s, and the THR decreased by 35 %.

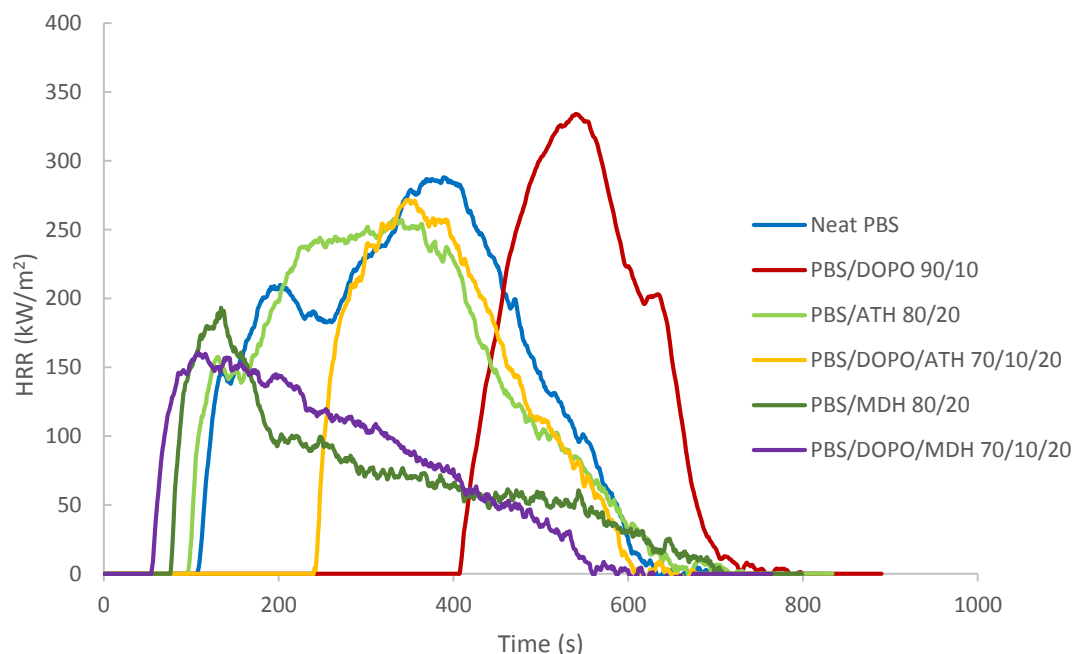


Figure 74: MLC tests of PBS with metal hydroxides and DOPO ($50 \times 50 \times 3 \text{ mm}^3$, 35 kW/m^2 , 25 mm)

Table 13: Results of MLC tests of PBS with metal hydroxides and DOPO

Ratio [wt.%]	pHRR [kW/m ²]	THR [MJ/m ²]	t _{ignition} [s]	t _{flameout} [s]	residue	Residue Calculated
Neat PBS	283	91	110	605	2%	/
PBS/DOPO 90/10	315 (+10%)	61 (-33%)	416	669	2%	/
PBS/ATH 80/20	258 (-10%)	87 (-5%)	99	623	16%	13%
PBS/DOPO/ATH 70/10/20	271 (-6%)	59 (-35%)	243	609	19%	13%
PBS/MDH 80/20	191 (-33%)	45 (-50%)	79	671	37%	14%
PBS/DOPO/MDH 70/10/20	160 (-44%)	48 (-48%)	57	553	38%	14%

MLC tests of PBS based formulations containing MgCO₃ and CaCO₃ are presented in **Figure 75** and **Table 14**. Like MDH and ATH, the incorporation of MgCO₃ and CaCO₃ in PBS permits to get good performances i.e. when 30 % of MgCO₃ and CaCO₃ are incorporated in PBS, pHRR is decreased by 52 % and 36 % respectively, THR is decreased by 29 % and 51 % respectively,

and the char yield increased to 38 % and to 32 % respectively. However, when DOPO is added to the formulation, there is no improvement of the TTI for MgCO₃, the pHRR and THR are even increased. For the combination DOPO/CaCO₃, the TTI is increased from 99 s to 206 s, whereas the pHRR and THR are increased.

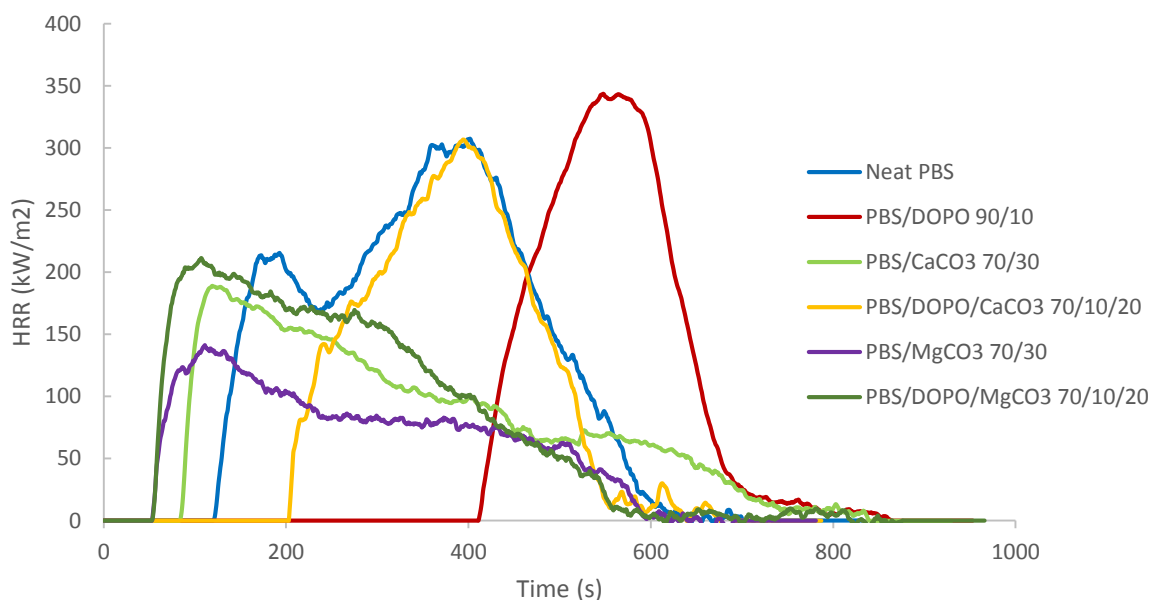


Figure 75: MLC test of PBS with carbonate salts and DOPO (50 x 50 x 3 mm³, 35 kW/m², 25 mm)

Table 14: Results of MLC tests of PBS with carbonate salts and DOPO

Ratio [wt.%]	pHRR [kW/m ²]	THR [MJ/m ²]	t _{ignition} [s]	t _{flameout} [s]	residue	Residue Calculated
Neat PBS	299	90	124	641	1%	/
PBS/DOPO 90/10	343 (+14%)	62 (-30%)	410	737	1%	/
PBS/CaCO ₃ 70/30	188 (-36%)	63 (-29%)	99	739	32%	16%
PBS/DOPO/CaCO ₃ 70/10/20	306 (+2%)	66 (-28%)	206	553	21%	11%
PBS/MgCO ₃ 70/30	140 (-52%)	44 (-51%)	56	577	38%	11%
PBS/DOPO/MgCO ₃ 70/10/20	211 (-29%)	66 (-28%)	55	738	19%	7%

It shows that metal hydroxides and metal carbonates may have good flame retardant effect in the condensed phase when singly incorporated in PBS. However, when they were blended with DOPO, the action in the gaseous phase and in the condensed phase can only partially

works: in some cases the TTI increased but the pHRR also increased, and in some other cases, both the pHRR and the THR are decreased but the TTI had no change.

The next part discusses the formulation of carbon nanotube and DOPO in PBS. Indeed, carbon nanotubes exhibit an action in the condensed phase, and it has no release of gases during a fire scenario.

III.3.5 Formulation of DOPO with carbon nanotubes with PBS

Carbon nanotubes (Cnano) do not evolve gas during the combustion, and it has been proven to be effective when incorporated in ABS,¹⁵⁶ PMMA¹⁵⁷ and PA¹⁵⁸ etc. They can often create protective barrier to flame retard polymers. As the action of carbon nanotubes occur in the condensed phase (accumulation of tubes at the surface and forming a protective layer), they were chosen to be formulate with DOPO in order to combine both actions.

Results of the MLC test are presented in **Figure 76** and **Table 15**. It shows that incorporation of 1 wt% carbon nanotube increased the pHRR by 8 % and the THR is decreased by 5 %. When DOPO was added, neither the TTI, nor the pHRR and the THR had significant improvement. Thus the combination of carbon nanotube with DOPO cannot work in the gaseous phase and in the condensed phase. The carbon nanotube is a nanoparticle which can have a barrier effect to prevent the action in the gaseous phase, and it can explain why the DOPO lost its effect in the gaseous phase.

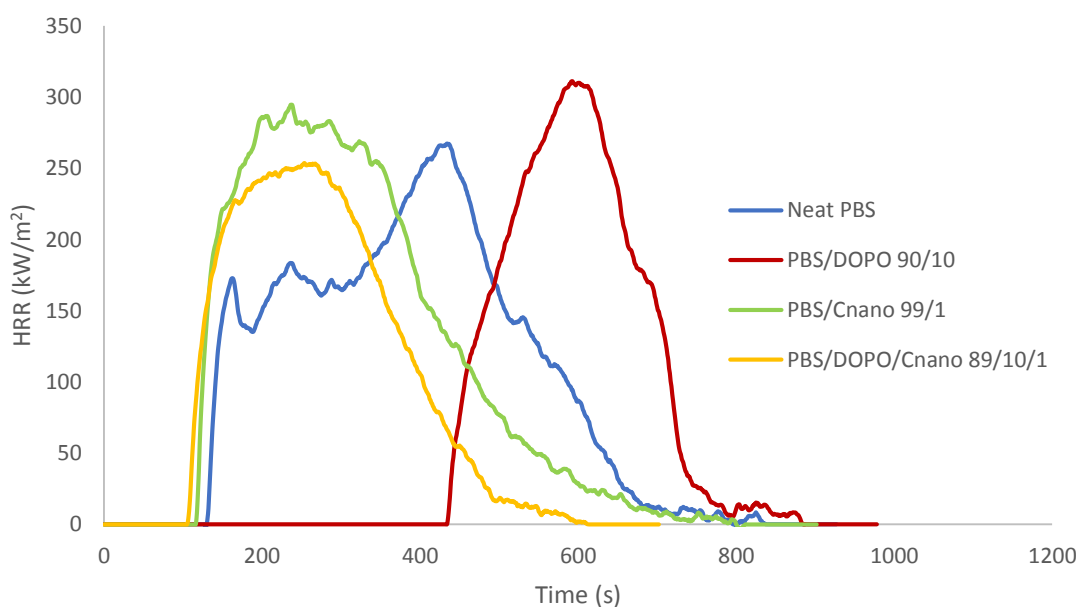


Figure 76: MLC tests of PBS with carbon nanotube and DOPO (50 x 50 x 3 mm³, 35 kW/m², 25 mm)

Table 15: Results of MLC tests of PBS with carbon nanotube and DOPO

Ratio [wt.%]	pHRR [kW/m ²]	THR [MJ/m ²]	t _{ignition} [s]	t _{flameout} [s]	residue
Neat PBS	271	84	122	581	1%
PBS/DOPO 90/10	311 (+15%)	62 (-26%)	437	723	1%
PBS/Cnano 99/1	294 (+8%)	88 (+5%)	119	689	3%
PBS/DOPO/Cnano 89/10/1	253 (-7%)	65 (-23%)	108	488	3%

III.3.6 Conclusion

In this part, conventional FRs were incorporated in PBS, the performance of these formulations in fire testing was presented. When un-modified DOPO was incorporated in PBS, a huge increase of the TTI was observed, which suggests a strong effect in the gaseous phase. Therefore, it is worth digging more information of the effect of DOPO in PBS. Additives working in the condensed phase were also tested, and some of them showed alone good performance such as MDH, MgCO₃ and CaCO₃ etc. Unfortunately, when these compounds were blended with DOPO, the expected 'double' flame retardant action in gaseous phase and in condensed phase was not as high as expected or the FR effect was lost.

III.4 Conclusion

This chapter described the three different approaches to flame retard PBS. Different additives and their performances in different fire scenario were presented. Isosorbide based FRs were synthesized and their thermo-stability of the synthesized FRs were commented. It was found that the phosphorus isosorbide based flame retardants shows often good performance in UL-94 test. In the MLC test, most of them showed no decrease of the THR and pHRR, whereas the TTI has increased when phosphorus based FRs with low degree of oxidation were incorporated in the PBS. Moreover, isosorbide and PIC were used as carbonization agent in intumescent FR system. Isosorbide showed no positive improvement in the MLC test, whereas PIC showed good performance compared to the formulation without carbonization agent. Then in the conventional FRs, DOPO shows dramatic performance in the gaseous phase. However, the combination of the gaseous phase and condensed phase action by using DOPO and various FRs was not successful.

The incorporation of un-modified DOPO is rarely reported in the literature. DOPO is mostly used in epoxy resin due to its low degradation/sublimation temperature. Our study shows that DOPO works efficiently in gaseous phase when incorporated in PBS. Thus, it is interesting to deeply seek the mechanism of DOPO during a fire scenario. More details of this research will be discussed in the next chapter.

PIC acting as carbonization agent to improve the flame retardancy of PBS shows some significant improvement especially the increasing of forming residual char. However, the reason why the different results were obtained when incorporated only 7 wt% of PIC into PBS is still unknown. Thus it is important to deeply understand the mechanism of this formulation during a fire scenario, and it will be reported in the chapter V.

Chapter IV - Investigation of the mode of action of DOPO in PBS

IV Investigation of the mode of action of DOPO in PBS

This chapter is dedicated to the investigation of the mode of action of DOPO in PBS according to different fire testing. The PBS/DOPO has showed huge performance in terms of improvement of TTI in MLC test and V-0 classification at the UL-94 test (3.2 mm). The first main part of this chapter is devoted to the mechanism of DOPO when PBS/DOPO is submitted to MLC test. In the first section, the performance of the formulation under different heat fluxes is firstly presented. Secondly, the thermal decomposition of the formulation is investigated. Thirdly the mode of action of PBS/DOPO is investigated by various techniques. The second main part presents the investigation of the dripping parameters of the formulations in a UL-94 test via an optimized UL-94 instrumentation. An original method for measuring the emissivity of the formulations is presented. Then the temperature evolution of the drops during a UL-94 test is investigated. Finally, the influence of the addition of DOPO in PBS is investigated by capturing the IR images and the measurement of the viscosity. A general discussion is made in the last section.

IV.1 Investigation of the mechanism of PBS/DOPO in MLC test

It was showed in the material screening chapter (Chapter III) that when DOPO was incorporated at 10 wt% loading in PBS, the TTI was increased from 119 s to 410 s under a heat flux of 35 kW/m². During the test and before ignition, a flame extinguishing phenomenon was observed. Deeply investigations of this formulation is made in this section in order to understand the mode of action of DOPO in PBS during MLC test.

IV.1.1 Investigation of the fire behavior of PBS/DOPO under different heat fluxes

Schartel et al. showed that the effect of FR usually exhibits significant changes as a function of the external heat flux.¹⁵⁹ The influence of the heat flux on behavior of PBS/DOPO is studied hereafter. The MLC curve at different heat flux (25, 35, 42.5 and 50 kW/m²) of neat PBS and PBS/DOPO is showed in **Figure 77** and more details are presented in **Table 16**.

For neat PBS, when heat flux was increased from 25 kW/m² to 50 kW/m², the TTI was decreased rapidly from 172 s to 43 s. However, the TTI of PBS/DOPO was decreased even more dramatically than that of neat PBS. Its TTI at 25 kW/m² is over 2200s, whereas at 50 kW/m² the TTI was decreased to only 70s. Nevertheless, it is revealed that DOPO has always a positive

effect in TTI whatever the heat flux applied but the effect of DOPO is less at higher heat flux. It is noteworthy that the flash extinguishing phenomenon is observed whatever the heat flux. It is also found that the higher heat flux, the higher pHRR is obtained. Particularly, the shape of the peak is changed with the variation of the external heat flux. These changes are observed in PBS and PBS/DOPO, whereas it is more pronounced for neat PBS. Hence, it is discussed in the case of neat PBS. The HHR curves which are close to the extinction or the flame out show the most interesting feature. With high heat flux 50 kW/m^2 or 42.5 kW/m^2 , a narrow peak is observed and the total burning time is only 400 s and 470 s respectively. When 35 kW/m^2 was applied on PBS, this peak became wider and the burning time increased to 530 s. With only 25 kW/m^2 , the peak flattened out which formed almost a plateau, and the burning time increased to 680 s. It should also be mentioned that the THR of PBS and PBS/DOPO has no significant change with different heat flux.

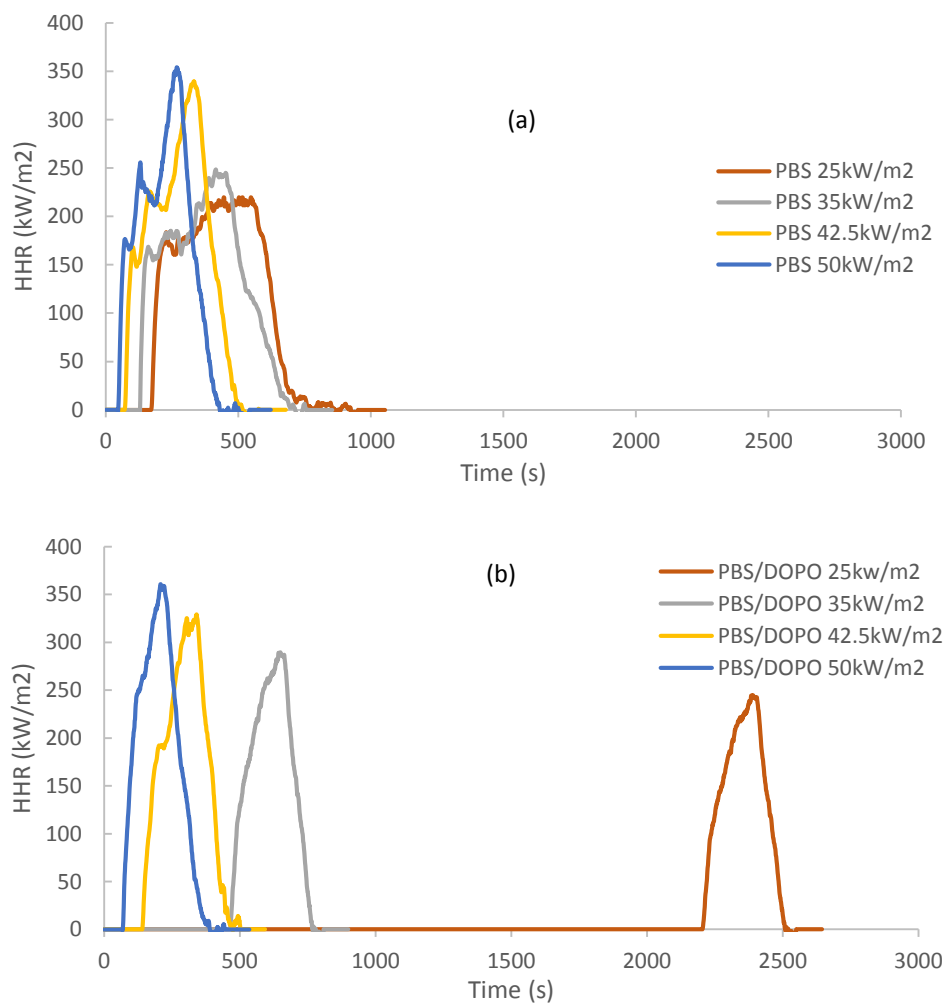


Figure 77: Fire behavior of a) PBS and b) PBS/DOPO in MLC test with different heat flux

Table 16: Results of MLC test of PBS and PBS/DOPO with different heat flux

Formulation	Heat flux (kW/m ²)	pHRR (kW/m ²)	THR (MJ/m ²)	t _{ignition} (s)	t _{flameout} (s)
Neat PBS	25 kW/m ²	219	77	172	854
	35 kW/m ²	248	85	119	658
	42.5 kW/m ²	339	82	76	539
	50 kW/m ²	353	84	43	458
PBS/DOPO 90/10	25 kW/m ²	244	52	2206	2459
	35 kW/m ²	289	54	467	762
	42.5 kW/m ²	327	61	144	483
	50 kW/m ²	361	63	70	388

With the great performance of PBS/DOPO under lower heat flux, it is interesting to estimate the critical heat flux (CHF) of ignition when 10 wt% DOPO is incorporated in PBS. The ignition theory indicates that the critical heat flux can be estimated by plotting $t_{ig}^{(-1/2)}$ as function of heat flux in hypothesis of thermally thick material or $t_{ig}^{(-1)}$ as function of heat flux in hypothesis of thermally thin material. Thus, for PBS/DOPO, the calculated CHF is 29.8 kW/m² while a thermally thin material is considered and 21.1 kW/m² for a considered thermally thick material (**Figure 78**). It was demonstrated by Gong et al.¹⁶⁰ that in the case of PMMA, if it is thinner than 2 mm it can be considered as thermally thin material and if it is thicker than 2 cm it can be considered as thermally thick material. Our plaques for the MLC test have 3 mm of thickness, which may be considered as a material between these two cases. The lowest heat flux used in our test is 25 kW/m², with TTI over than 2200 s, it can be considered that PBS/DOPO is almost impossible to be ignited at this heat flux. Therefore in our case, 25 kW/m² is between the CHF calculated with the hypothesis of thermally thin material and thermally thick material. It evidences the reliability of our calculation and suggests our material exhibits a behavior between thermally thin and thermally thick.

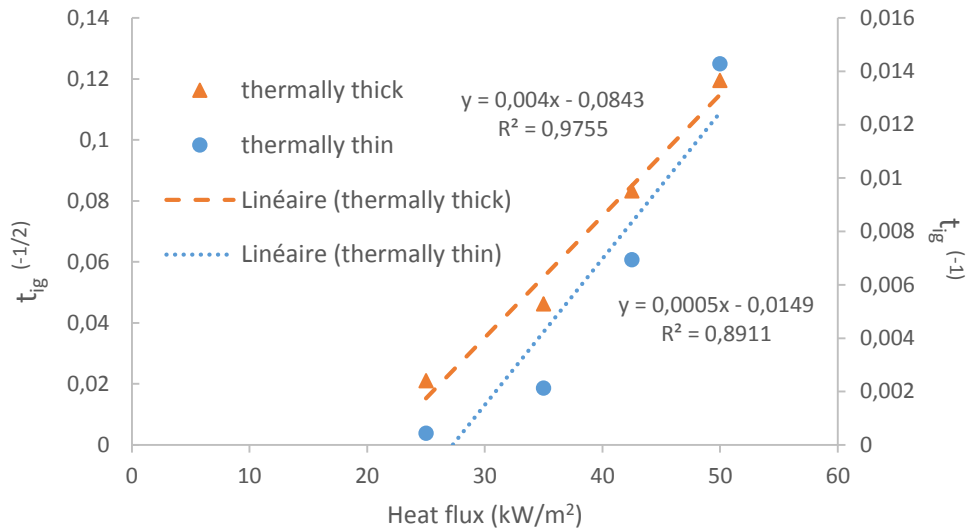


Figure 78: Estimation of critical heat flux of PBS/DOPO in the case of thermally thick or thermally thin material

Despite the improvement of ignition time and the decrease of THR, pHRR is a little bit increased when DOPO is incorporated in PBS. It is believed that these three factors have the biggest influence on fire hazard. Petrella et al. suggested an assessment of full-scale fire hazard by tracing the THR as function of $\text{pHRR}/t_{\text{ig}}$.¹⁶¹ Here THR is considered as heat evolved in the test and $\text{pHRR}/t_{\text{ig}}$ is considered as the fire growth index. Thus in our case, an overview of efficiency of DOPO in PBS is presented by tracing the Petrella plots (**Figure 79**) over a range of applied heat flux. It is evidenced that neat PBS and PBS/DOPO have higher fire hazard when higher heat flux is applied (higher fire growth index). It is also obvious that both the THR and the fire growth rate were decreased when DOPO was added in PBS. Thus, DOPO has flame retardancy effect for PBS whatever the heat flux.

Comprehension of the thermal decomposition of PBS and DOPO should give an explanation of the great performance of PBS/DOPO in MLC test, thus the next part will be focused on this point.

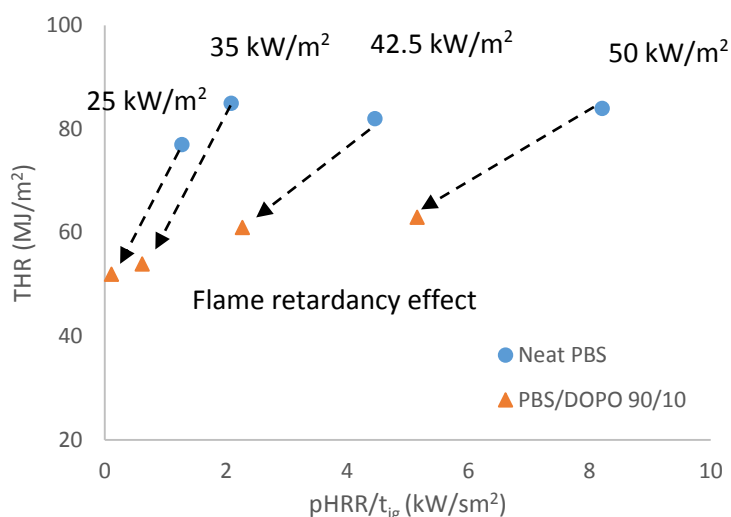


Figure 79: Petrella plots traced in an applied range of heat flux for PBS and PBS/DOPO

IV.1.2 Comprehension of the thermal decomposition of PBS/DOPO

To understand the mechanism of PBS/DOPO in MLC test, it is necessary to investigate its thermal degradation behavior. Thus, thermogravimetric analysis (TGA) and Pyrolysis - Gas Chromatography/Mass Spectrometry analysis (py-GC/MS) are presented to analyze the degradation behavior of PBS/DOPO and the composition of evolved gases under pyrolytic condition.

IV.1.2.1 Thermogravimetric analysis (TGA)

The thermo-oxidative decomposition of PBS, DOPO and PBS/DOPO at a constant heating rate (10°C/min) is presented in **Figure 80**. TG curve shows that the PBS degrades in two steps, the first degradation is the main degradation (335°C - 430°C). It can be assigned to the depolymerization of the chain of PBS. The second step (430°C - 480°C) is assigned to the formation of an intermediate char, which then degrades at a higher temperature (oxidation of the char). DOPO has also two degradation/sublimation steps, the first step starts from T2% of 205°C until 300°C with 36 % mass loss. Afterward the second degradation step is from 300°C to 440°C with 60 % of mass loss. Differential TG curve of PBS/DOPO shows that incorporation of DOPO in PBS exhibits significant destabilization between 300°C and 420°C. It reveals that DOPO can interact with the PBS matrix in this range of temperature, and the temperature range of this interaction suggests that DOPO may induce the depolymerization of PBS. DOPO

decomposes at a lower temperature than PBS, thus, phosphorus decomposed components are released before the decomposition of PBS.

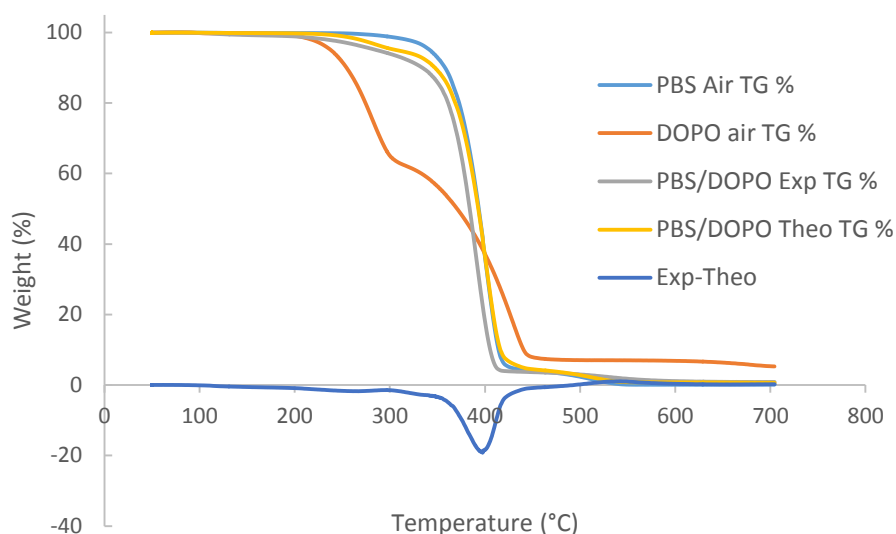


Figure 80: Mass loss of PBS and PBS/DOPO under air at 10°C/min

The decomposition of PBS, DOPO and PBS/DOPO under pyrolytic condition at a constant heating rate is presented in **Figure 81**. Unlike the decomposition under thermo-oxidative condition, PBS and DOPO exhibit only one decomposition step. Meanwhile, the decomposition temperatures of these two components are higher than those in air: 350°C under N₂ vs 335°C under air for neat PBS, 209°C under N₂ vs 205°C under air for DOPO. From the differential TG curve, an obvious destabilization when DOPO was added in PBS was also found between 340°C to 430°C. To understand the exact structure of the decomposition products of PBS and PBS/DOPO under pyrolytic condition, the results of pyrolyzer-Gas chromatography/Mass spectrometer (py-GC/MS) are presented in the next part.

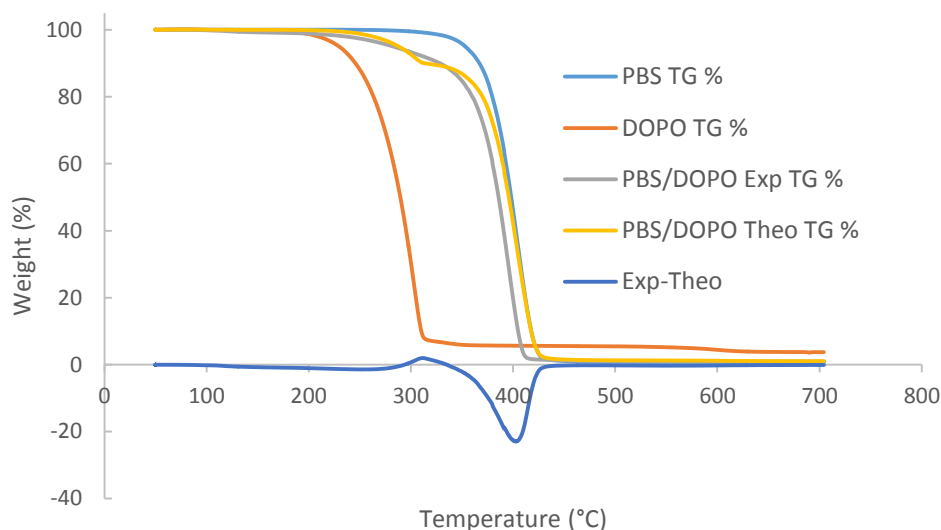


Figure 81: Mass loss of PBS and PBS/DOPO under N₂ at 10°C/min

IV.1.2.2 Pyrolysis - Gas Chromatography/Mass Spectrometry analysis (py-GC/MS)

The structure of the degradation products under pyrolytic conditions is investigated using a py-GC/MS. The pyrolytic products of neat PBS was investigated in the literature.³³ In our study, most of the pyrolytic products of neat PBS are also observed for PBS/DOPO. They are mainly small molecules deriving from the monomers i.e. 1,4-butanediol and succinic acid and also fragments of PBS chains (**Figure 82**). Possible chemical structure of these degradation products of PBS/DOPO are presented in **Table 17**. They include units that come from 1,4-butanediol (B) and succinic acid (S): low weight molecules like tetrahydrofuran (1), 1, 4-butanediol (2), and succinic anhydride (3); cyclized products with different size (5, 13); fragments with -OH or/and -COOH groups at chain end (4, 7, 8, 9, 12) and chains of esters and alkenes (4, 5, 7, 8, 9, 10, 12, 13). Possible mechanism of the formation of the degradation products can be suggested: i) formation of carboxylic acid and alkene is explained by de-esterification of the polymer chain, ii) cyclized products are produced by intramolecular esterification, iii) decarboxylation of the chains containing carboxylic acid group occurred at the chain end to form the structure as (4). Though the degradation products showed a similarity between PBS and PBS/DOPO, it is still found some differences. Firstly, degradation products of DOPO (6) and sublimated DOPO (11) are found in the PBS/DOPO formulation. Secondly, as the py-GC/MS is a semi-quantitative method to characterize the released gases,

by using the same quantity of products (200 μg) for the experiment, the comparison of neat PBS and PBS/DOPO shows that the addition of DOPO in PBS generates more THF and more succinic anhydride than neat PBS.

The decomposition of PBS/DOPO is now elucidated. It is linked with the temperature of the material upon testing and so, the surface temperature of a material will be evaluated in the next section.

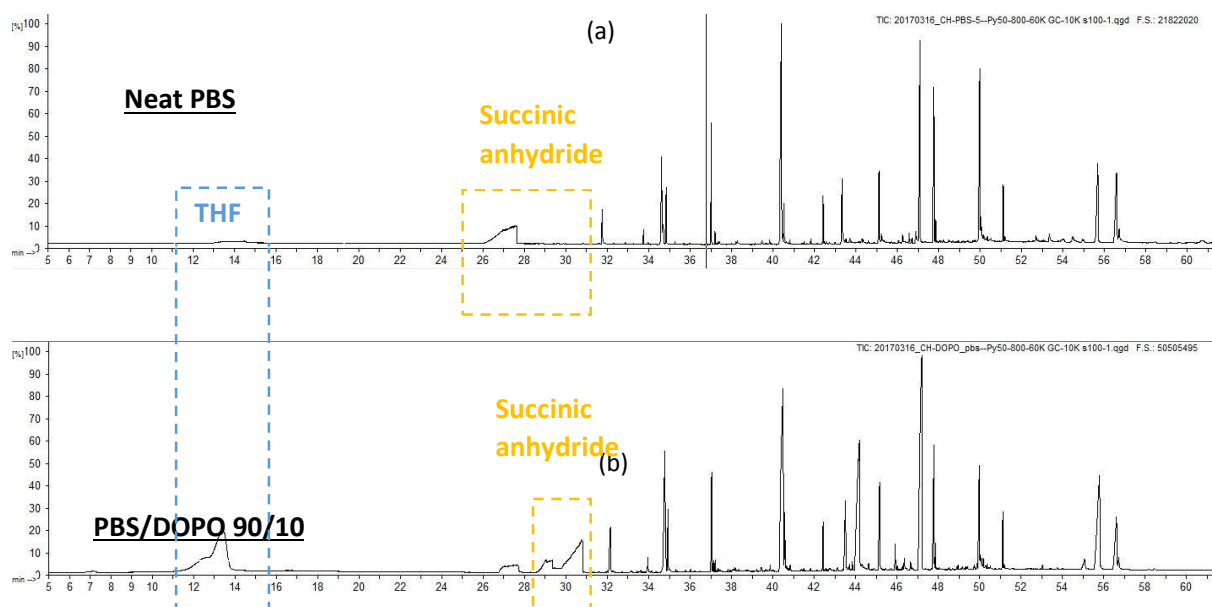
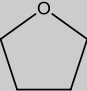
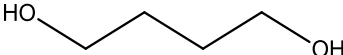
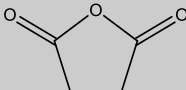
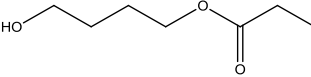
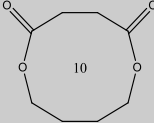
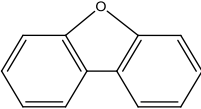
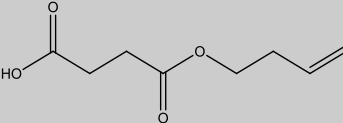
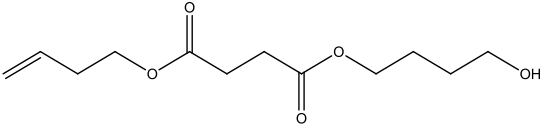
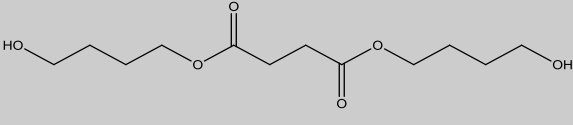
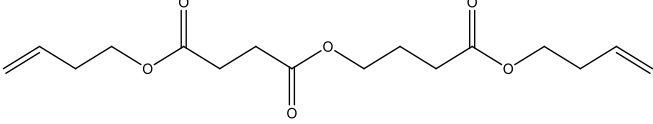
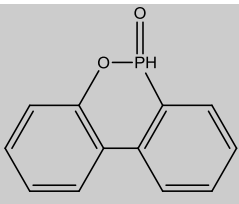
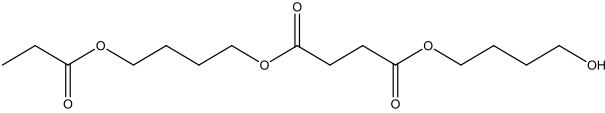
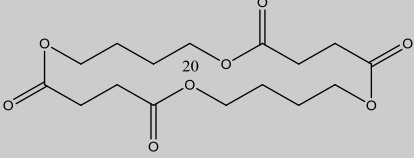


Figure 82: Pyrogramme of a) neat PBS and b) PBS/DOPO

Table 17: Degradation products of PBS/DOPO analyzed by GC/MS

N°	Time of retention (min)	Molecule	Blocks	Molar mass	Fitting (%)	Data Base
1	11-14		B	72	96	NIST
2	27-28		B	90	98	F-search
3	29-31		S	100	93	NIST
4	32.2		B + S	146	97	F-search
5	35.3		B + S	172	94	F-search
6	37.1		DOPO	168	99	F-search
7	37.2		B + S	172	92	F-search

8	40.2		2B + S	244	97	F-search
9	40.3		2B + S	262	98	F-search
10	42.4		2B + 2S	356	93	F-search
11	44.0		DOPO	216	96	NIST
12	45.0		2B + 2S	318	98	F-search
13	47.1		2B + 2S	344	97	F-search

IV.1.3 Surface temperature evolution measured by thermocouples

A hypothesis on the long TTI of PBS/DOPO in MLC test is that DOPO could modify the thermo-physical/optical properties of PBS/DOPO material compared to neat PBS. The surface temperature of neat PBS and PBS/DOPO were measured as a function of time during MLC test (**Figure 83**). It is observed that the surface temperature reaches about $300 \pm 25^\circ\text{C}$ before the ignition (119 s) in both cases and the heating rate before the ignition is also the same estimated at $180^\circ\text{C}/\text{min}$ from the curves of **Figure 83**. The heating source (heat radiation) is the same for PBS and PBS/DOPO and it suggests that DOPO should not change a lot the thermo-physical properties of PBS. Therefore, this cannot explain the long TTI of PBS/DOPO. The surface temperature of PBS/DOPO presents a plateau of approximatively at 300°C between 119s and its ignition. Small peaks are observed which may correspond to the flash of flame appeared in the experiment.

The interesting feature of the measurement of the surface temperature of PBS/DOPO indicates that changes occur on the surface. In this case, it is necessary to identify the released gases for PBS/DOPO upon heating and during the fire testing. Therefore in the next part, the released gases will be analyzed using an FTIR on top of the MLC chimney.

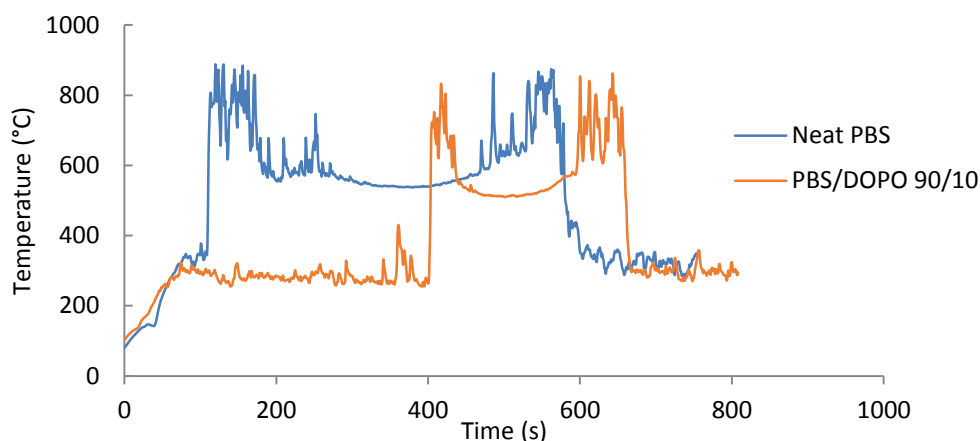


Figure 83: Temperature measured during MLC by thermocouple embedded in plaques of PBS and PBS/DOPO (35kW/m^2)

IV.1.4 Investigation of released gases of PBS/DOPO upon heating

With the measurement of the surface temperature, it was found that a change occurred on the surface of the sample. The incorporation of DOPO in PBS has good performance in the gaseous phase which leads to a huge improvement of TTI. The mode of action of PBS/DOPO in the gaseous phase is not clear. Thus in this section, how DOPO influences the evolved gases and why TTI is increased are discussed by using a thermogravimetric analysis (TGA) linked with a Fourier transform infrared spectrometer (FTIR) and a mass loss cone calorimeter (MLC) linked to a FTIR.

IV.1.4.1 Thermogravimetric analysis - Fourier transform infrared spectrometer (TGA-FTIR)

TGA coupled with the FTIR is used to analyze the decomposition products of neat PBS and PBS/DOPO. In order to mimic the experimental condition of the MLC test for PBS/DOPO, the heating rate was set to $180^\circ\text{C}/\text{min}$ from 50°C to 300°C for the first step, then followed by a isotherm of 300°C for 30 min.

PBS and PBS/DOPO exhibit small mass loss in the first 1 min 30 s during the heating step. When the temperature reaches 300°C, PBS/DOPO loses 10 % of mass in just 8 min, whereas neat PBS lose 10 % of mass in 16 min. The mass loss becomes the same after 30 min (**Figure 84**).

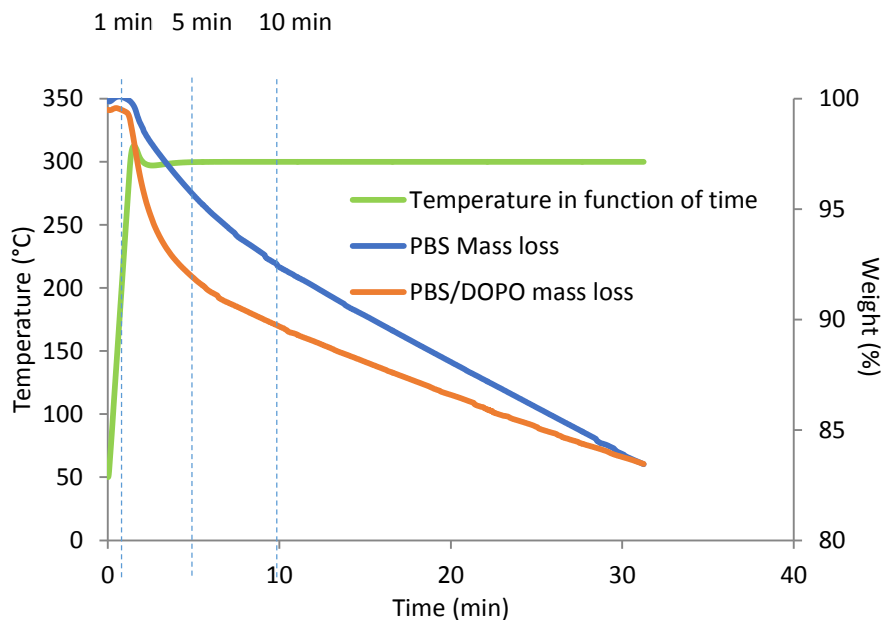


Figure 84: Mass loss of PBS and PBS/DOPO as function of time with similar heating rate to MLC test

FTIR spectra of the released gases at 1 min, 5 min and 10 min of PBS and PBS/DOPO are presented in **Figure 85**. Degradation of PBS released mainly CO₂, H₂O, THF (2981 cm⁻¹, C-H stretching) and succinic anhydride (1811 cm⁻¹, C=O stretching). It shows that at 1 min, both of the formulations have almost no release of THF and succinic anhydride. Furthermore, it can be seen that there is the release of THF and succinic anhydride at 5 min in the case of PBS/DOPO which is barely found for neat PBS at 5 min. It should be mentioned that the largest difference of mass loss occurs at 5 min (9 % mass loss for PBS/DOPO vs. 4 % mass loss for neat PBS), that explains the difference on FTIR spectra. At 10 min, there is 8 % mass loss for neat PBS, and THF and succinic anhydride can be clearly identified on the FTIR spectra.

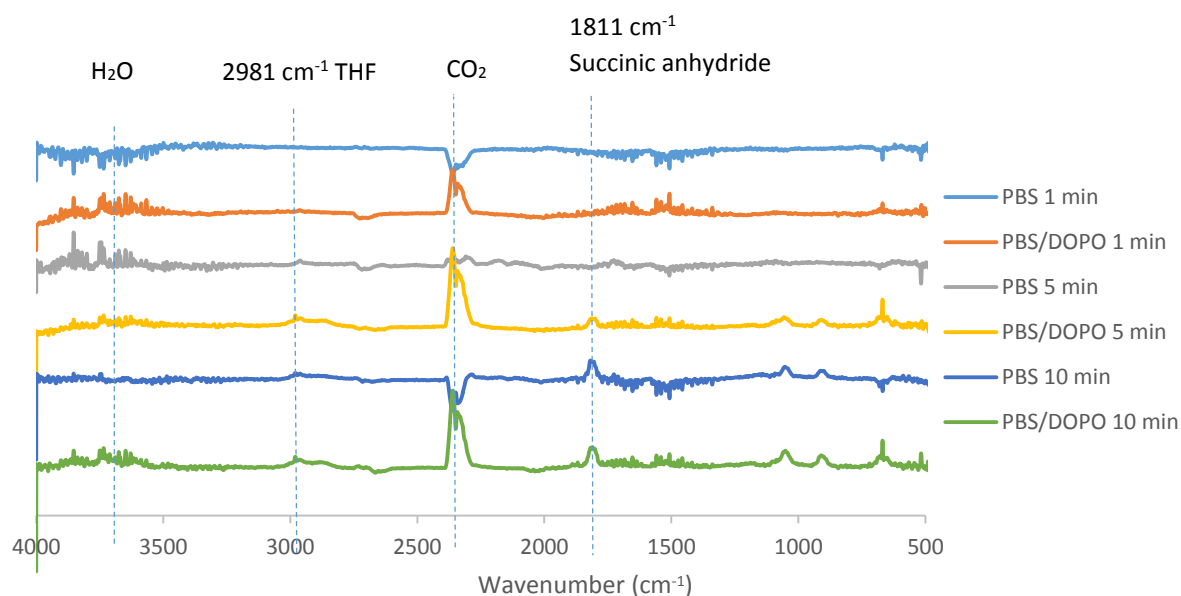


Figure 85: FTIR spectra of degradation products of PBS and PBS/DOPO at different time

IV.1.4.2 Mass loss cone calorimeter - Fourier transform infra-red spectrometer

To understand the intrinsic mechanism of the action of DOPO in the whole process of MLC test, the released gases during the combustion of neat PBS and PBS/DOPO were then further studied with MLC-FTIR. FTIR spectra of released gas before ignition of PBS (119 s) and PBS/DOPO (410 s) is showed in **Figure 86**. FTIR spectra reveals that CO, CO₂, H₂O, THF and succinic anhydride are the main degradation products before ignition. It is found that before ignition of these two formulations, the intensity of THF and succinic anhydride for PBS/DOPO is much more intense than that for PBS. Particularly the characteristic peak of THF at 2981 cm⁻¹ (C-H stretching) and the characteristic one of succinic anhydride at 1811 cm⁻¹ (C=O stretching) (**Figure 86**). By plotting the intensity evolution of these two characteristic peaks (2981 cm⁻¹ and 1811 cm⁻¹), the intensity evolution of evolved THF and succinic anhydride is presented in **Figure 87**. Before the ignition of PBS (119 s), small amount of THF and succinic anhydride are released. After 119 s, once the neat PBS started to burn, both of these two flammable gases, THF and succinic anhydride, are rapidly consumed and the major products released are CO₂ and H₂O. Ignition of a material involves several different aspects such as the pressure, temperature and the concentration of the combustible gases. It indicates that small quantity of the combustible gases is sufficient for the ignition of neat PBS at the current pressure and temperature condition. Whereas for PBS/DOPO, intensity of THF and succinic anhydride are

detected to be more and more intense until the ignition (410 s). The peaks of THF and succinic anhydride in PBS/DOPO is 6.5 times more intense than the peaks obtained in PBS. Like the neat PBS, THF and succinic anhydride are totally and rapidly consumed, which confirms that the concentration of these two flammable gases is the key element of the ignition of these two formulations. Evolution of these two products follow the same trend in each formulation: the peak of THF and succinic anhydride occurred at the ignition in the test (119 s for neat PBS, 410 s for PBS/DOPO). It should be mentioned that during the test, caused by the low quantity of DOPO (only 10 %), and also the bands of phosphorus compounds presented in the region ($600 - 1300 \text{ cm}^{-1}$) that can be mixed with other components, thus the phosphorus were not identified on the IR spectra.

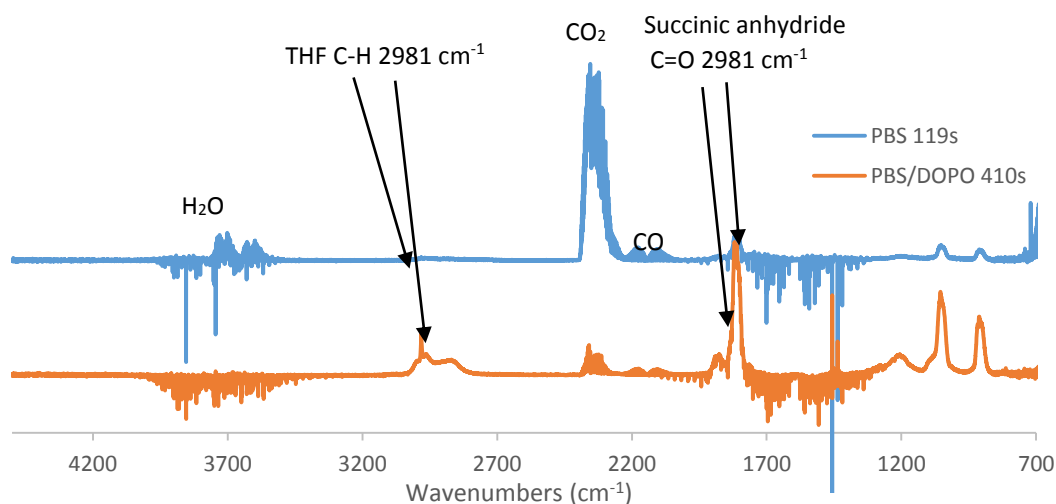


Figure 86: FTIR spectra of released gases at 119s for neat PBS and 410s for PBS/DOPO (35 kW/m^2)

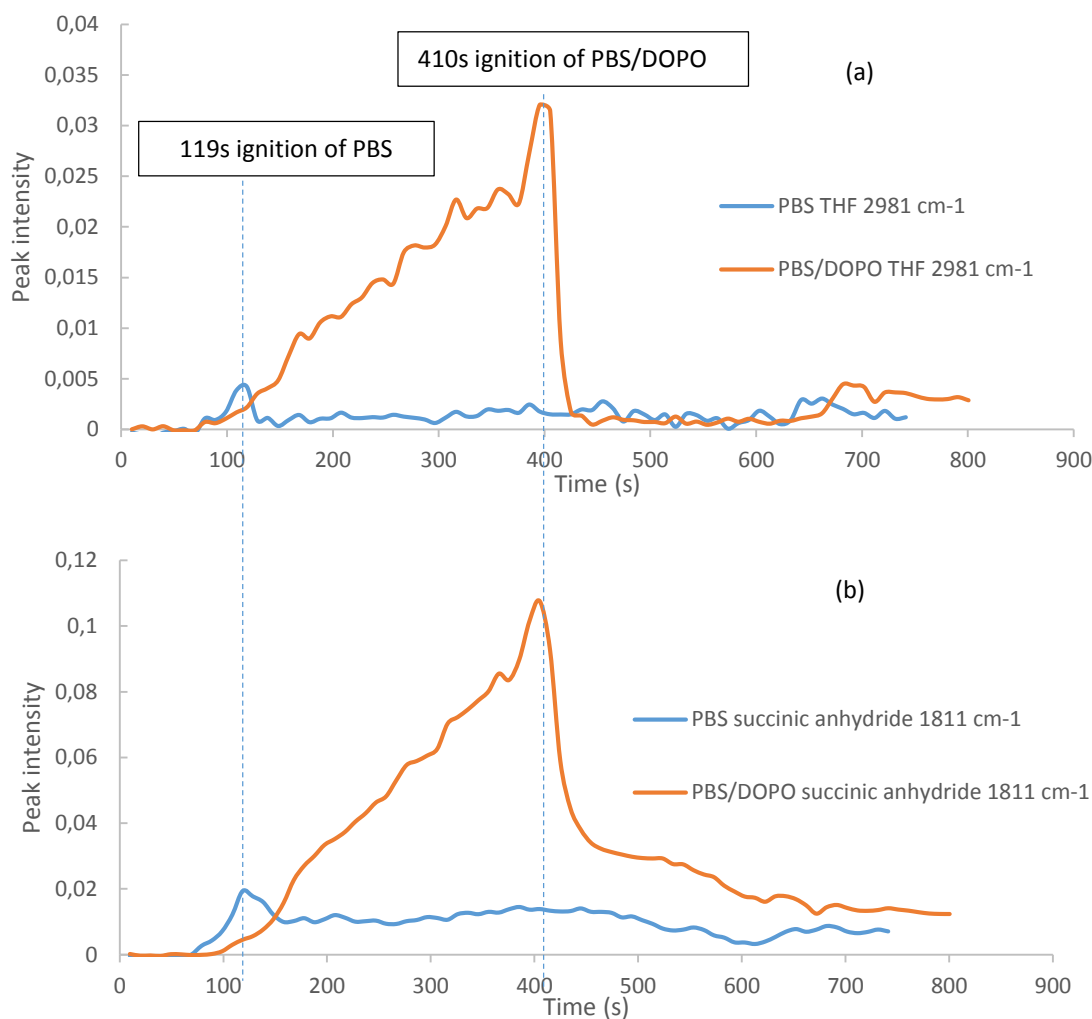


Figure 87: Intensity evolution of a) THF (2981 cm⁻¹) and b) succinic anhydride (1811 cm⁻¹) as function of time during MLC (35 kW/m²)

To further understand the mode of action of DOPO, quantification of the gases is carried out. Our device is calibrated for several different gases (CO₂, H₂O, CO etc.) but not calibrated for the THF and succinic anhydride, thus this test was a semi-quantified experiment for measuring the evolved gases in our study. For this reason, exact quantification of THF and succinic anhydride has not been carried out.

Figure 88 a) shows the MLC curve of PBS and PBS/DOPO, and the quantification of released CO₂, H₂O and CO are presented in **Figure 88 b)**. For PBS and PBS/DOPO, the released CO₂ and H₂O exhibit the same shape of their HRR curves during the whole test. It makes sense that CO₂ and H₂O are released during the combustion. Before ignition, the temperature of the material is lower than 300°C, only small amount of CO₂, H₂O and CO are released, because of the low degradation rate at the beginning of the experiment of the material. After the ignition, CO₂

and H₂O are released in large quantity, indicating they are the major combustion products when it starts to burn. Little quantity of CO is detected during the combustion, for neat PBS the ratio of released CO₂/CO is 254 and for PBS/DOPO the ratio of released CO₂/CO is 42, which shows that the burning of PBS is quite complete in the case of neat PBS and less complete in the case of PBS/DOPO.

Figure 88 c) shows the intensity of total released gases (Gram-Schmidt) of PBS and PBS/DOPO during the MLC test. In the Gram-Schmidt, the curve of neat PBS follows the same shape of its HRR curve, and only small quantity of gases are released before the ignition. In the case of PBS/DOPO, the intensity of released gases increased continuously until the ignition, and this curve does not follow the shape of the MLC curve. As mentioned above, the CO₂, CO and H₂O are found before the ignition at a very low quantity, but the highest concentration of the gases released are THF and succinic anhydride. THF and succinic anhydride are known to be flammable, however the presence of DOPO and/or of its degradation products (phosphorus-based molecules) quench the high energy free radicals in the gaseous phase which prevent the further oxidation of THF and succinic anhydride. Thus the flame poisoning effect of DOPO in the gaseous phase is the reason why for several times the flashing flame appeared and is quickly extinguished: it explains the long ignition time. After the ignition, the Gram-Schmidt curve of PBS/DOPO shows the same shape as the curve of CO₂ and H₂O, which can be explained by the fact that the combustion products of THF and succinic anhydride are majorly CO₂ and H₂O.

To understand why the DOPO acts well in the gaseous phase before the ignition and why no more flame extinguishing effect at the point of ignition and the formulation started to burn, two hypotheses can be suggested: i) DOPO had been totally consumed in the condensed phase to supply the flame extinguishing effect; ii) The concentration of combustible gases are high enough even though the DOPO still exists in the condensed phase. Elemental analysis in the next section will be described in order to investigate these two hypothesis.

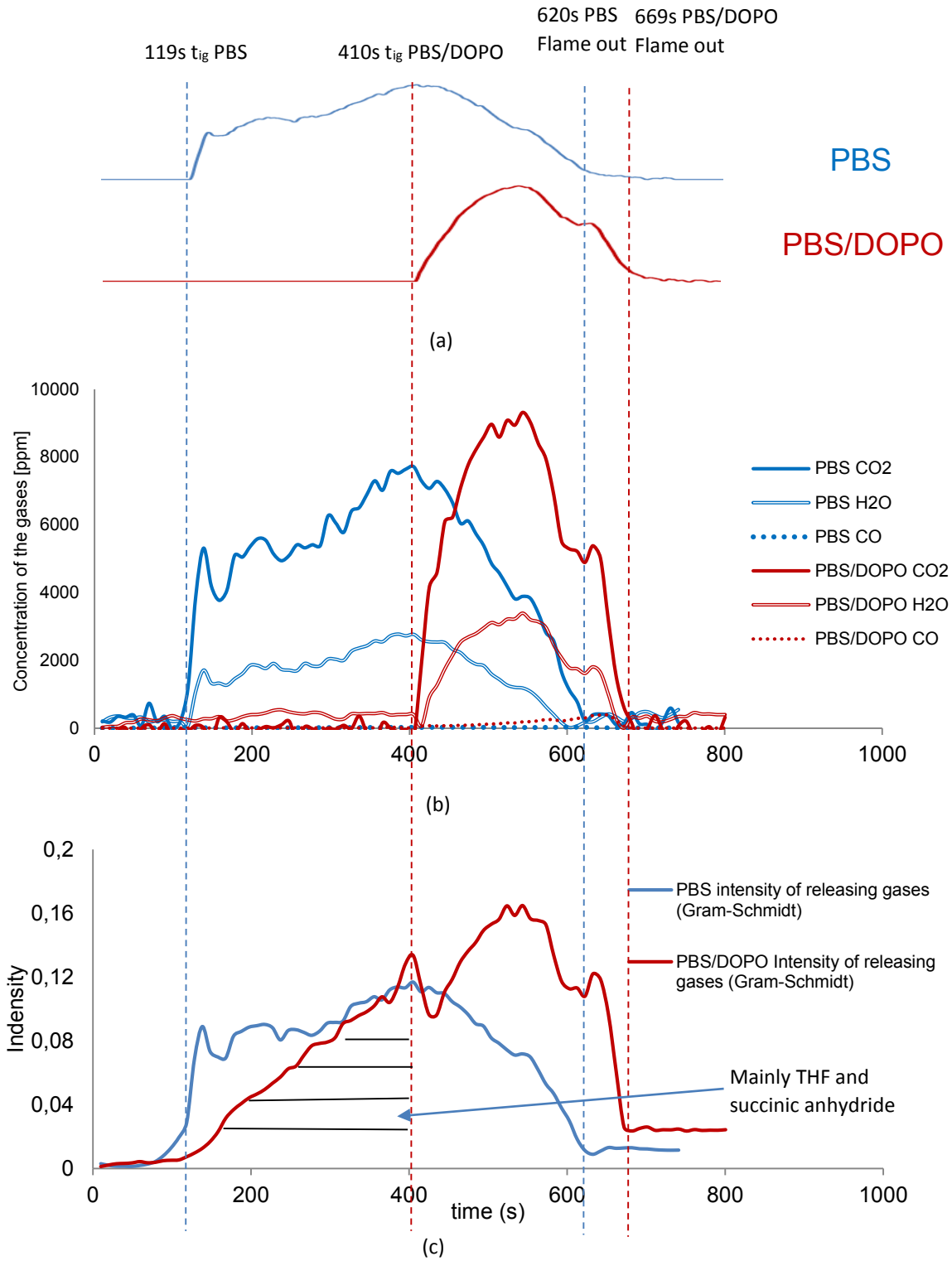


Figure 88: a) MLC curve of PBS and PBS/DOPO, b) quantification of released CO, CO₂ and H₂O, c) intensity of total gases release (Gram-Schmidt)

IV.1.4.3 Elemental analysis

Elemental analysis were carried out on Carbon, Hydrogen, Oxygen and Phosphorus (only for DOPO based formulation). The residues were analyzed at different MLC times: before the ignition, at ignition and at pHRR. The time are 60 s, 119 s and 415 s for neat PBS and 200 s, 410 s, and 550 s for PBS/DOPO. The concentration of each elements are presented in **Table 18** for neat PBS and in **Table 19** for PBS/DOPO.

Table 18: Elemental analysis of PBS at different stage of MLC test

PBS	C (wt %)	H (wt %)	O (wt %)
60 s	55.51	7.05	37.38
119 s	56.04	7.20	36.55
415 s	57.08	7.31	35.29

Table 19: Elemental analysis of PBS/DOPO at different stage of MLC test

PBS/DOPO 90/10	C (wt %)	H (wt %)	O (wt %)	P (wt %)
60 s	56.98	6.69	34.75	1.195
119 s	56.79	6.84	34.99	1.177
415 s	57.88	6.96	32.22	2.136

For neat PBS and PBS/DOPO the composition of C and H slightly increased when exposed under heat and after burning, whereas oxygen decreased in these two cases. For PBS/DOPO, phosphorus had no significant change before the burning. However, the ratio phosphorus/carbon increased after burning, which is reasonable that the carbon were released under form of CO₂, CO and combustible gases. It indicates that phosphorus compounds still exists in the condensed phase after the ignition. Hence, it can be deduced that in the MLC test, when the concentration of combustible gases become high enough, the ignition occurs.

IV.1.5 Proposed mechanism of PBS/DOPO during MLC test

With the evidences provided above, the mechanism of action of DOPO can be determined (**Figure 89**). At the beginning of the test (before 300 s), PBS started to melt and decompose.

Combustible gases were released, which mainly contains THF and succinic anhydride. Meanwhile, DOPO decomposed/sublimated, and phosphorus-based species were released. These released P-containing components are able to quench the high energy free radicals to poison the flame. Hence in this stage of the test, no ignition was observed. In the second stage (300 s to 410 s), the concentration of combustible gases increased. Flame appeared and was rapidly extinguished. The concentration of combustible gases (THF and succinic anhydride) increased until the time where the ratio of combustible gases to the phosphorus components reached a critical value, the plaque started to burn. The third stage is after the ignition, THF and succinic anhydride were rapidly consumed. Large quantity of H₂O and CO₂ were released until the plaque was totally burned out.

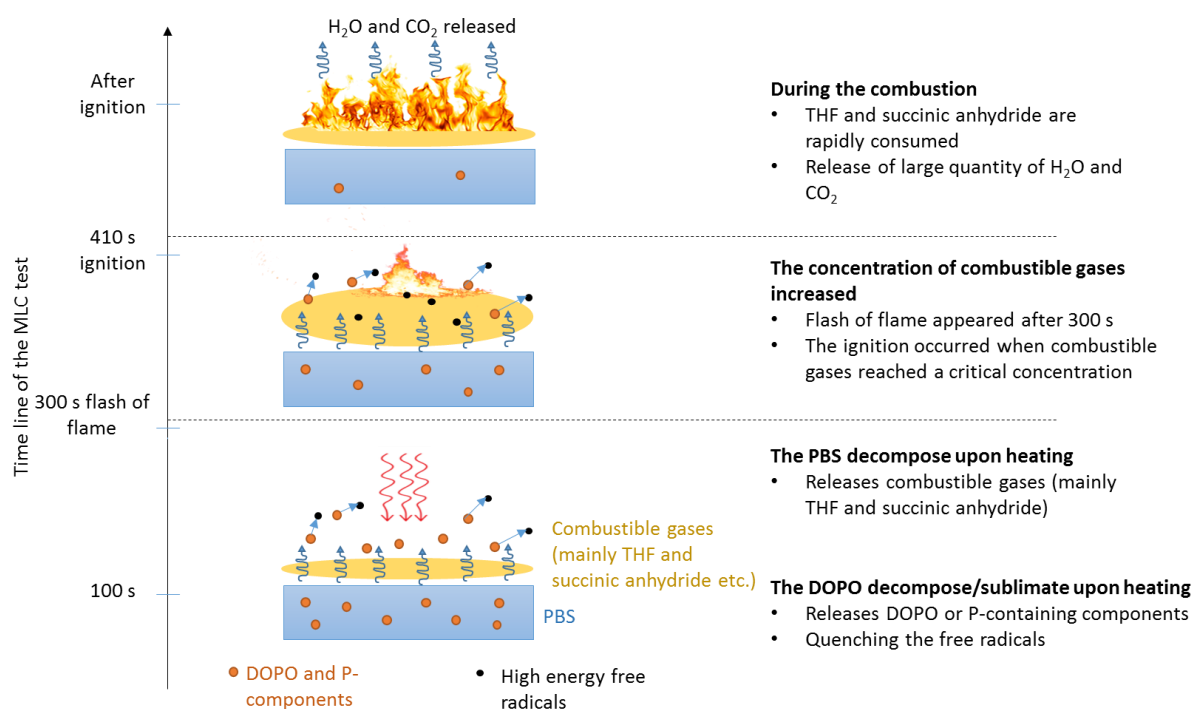


Figure 89: Mechanism of PBS/DOPO during a MLC test

IV.1.6 Conclusion

The mode of action of PBS/DOPO in the MLC test was deeply investigated in this section. A complete study of the degradation behavior of PBS and PBS/DOPO shows clearly their degradation route under thermo-oxidative and pyrolytic conditions. Identification and quantification of the released gases in MLC test reveal that the presence of decomposition/sublimation products of DOPO have a strong flame poisoning effect. Especially

when low heat flux applied on the PBS/DOPO, the performance has increased dramatically. These results have proven our hypothesis that the DOPO acts in the gaseous phase when incorporated in PBS.

IV.2 Investigation of dripping parameters of PBS/DOPO by UL-94 instrumentation

The results of neat PBS and PBS/DOPO in UL-94 test have been presented in the material screening chapter (Chapter III). No classification and V-0 rating were achieved for neat PBS and PBS/DOPO respectively (**Figure 90**). Dripping occurred in the two cases. The interesting feature is that the drops of PBS ignites the cotton while it is not the case for PBS/DOPO. It can be then assumed that the parameters governing the dripping should be the major cause of the two different results at UL-94.



Figure 90: Residual Bars of PBS (left) and PBS/DOPO (right) after the UL-94 testing (3.2 mm).

Except the classification and whether the drops can ignite the cotton or not, the original UL-94 test does not provide scientific parameters such as the measurement of temperature in the bars, the mass flow of the condensed matter (mass of the drops) and of the evolved gases (mass loss). In order to provide a scientific way to use UL-94 in addition of a simple classification, recent work has been reported in the literature. Kandola et al. have proposed a method to quantify dripping by exposing the materials to a known temperature.¹⁶² Based on this previous work, they also measured the temperature of the melting drops in an electric furnace to predict the degree of degradation.¹⁶³ Then Dupretz et al. have embedded the thermocouples in the polymers to measure the temperature gradient in the bar during the UL-94 test.¹⁶⁴ Furthermore, combined with a system of balances, they have successfully quantified the melting drops and the gases evolved during a UL-94 test. However, the evolution of a single drop (shape and temperature) during the UL-94 is still unknown. Some

papers report that the drops formed in a UL-94 test is one of the most important factors to influence the classification of a polymer.^{165,166} It makes sense because the forming drops can take away the heat from the materials but at the same time, the falling drop can ignite the cotton. So, a polymeric material can generate melting drops which do not ignite the cotton and hence it can achieve a good classification in UL-94 test. For these reasons, it is very important to understand the evolution of a single drop during a UL-94 test. Two major challenges prevent researchers to achieve this measurement: (i) a drop could be surrounded by flame, so it is almost impossible to visualize its surface and to measure its surface temperature with a traditional IR camera; (ii) the emissivity of a polymer/charred material as a function of temperature is usually unknown and measurement done by IR thermography could not be accurate. The two issues mentioned above in measuring the evolution of a single melting drop are addressed and are considered designing an optimized UL-94 instrumentation. Based on the instrumentation developed in the lab, we used an IR camera which is equipped with a specific filter that can visualize the surface of a flaming material (emitted IR wavelength corresponding to the flame is blocked) to characterize the surface properties of the drops. To achieve the measurement, this section is divided into three parts. The determination of the emissivity of a material is the key point to measure the temperature, so the first part describes how the emissivity can be estimated from the UL-94 instrumentation and the determination of the emissivity by integrating sphere apparatus. The second part focused on the temperature evolution of the drops during the fire testing. The third part describes the influence of incorporation of DOPO on physico-mechanical properties of PBS.

IV.2.1 Emissivity measurement of the drops

This section uses two methods to determine the emissivity of the PBS/DOPO. In order to estimate the emissivity via the UL-94 instrumentation, the temperature gradient inside the bar was studied. (The instrumentation can be found in **Figure 44**, Chapter II, page 63)

Temperature gradient inside the bar

The temperatures measurement of PBS and PBS/DOPO samples evaluated by the thermocouples embedded in the materials are presented in **Figure 91**. When a thermocouple is no more completely embedded in the bar, the temperature is not taken into account.

In the case of neat PBS, at the end of the first ignition (10 s), the thermocouples T1 to T5 can reach respectively temperatures of 453°C, 214°C, 159°C, 138°C and 127°C. Temperature difference between T1 and T2 is 236°C, however the difference between T4 and T5 is only 11°C (**Table 20**).

In the case of PBS/DOPO, at the end of the first ignition (10 s), the temperatures measured by T1 to T5 reach respectively temperatures of 403°C, 208°C, 153°C, 112°C and 102°C. The PBS/DOPO showed also its own temperature distribution as a function of distance: the temperature difference between T1 and T2 is at 195°C, whereas the temperature difference between T4 and T5 is only 10°C **Table 20**. All these measured temperatures were lower than those obtained in neat PBS. Between the first and the second ignition, a decrease of temperature at around 51°C/s was observed for T1 when the burner was removed. It is noteworthy that during the whole test, the temperatures measured in PBS/DOPO are always lower than those of neat PBS even though the PBS/DOPO has two ignitions. Unlike the neat PBS that have all five thermocouples in the air at the end of the experiment, T4 and T5 remains embedded in the bar in the case of PBS/DOPO after two ignitions. As the PBS/DOPO has no visible burning, the temperature evolution measured by the thermocouples followed the presence of burner which can be clearly identified in **Figure 91**.

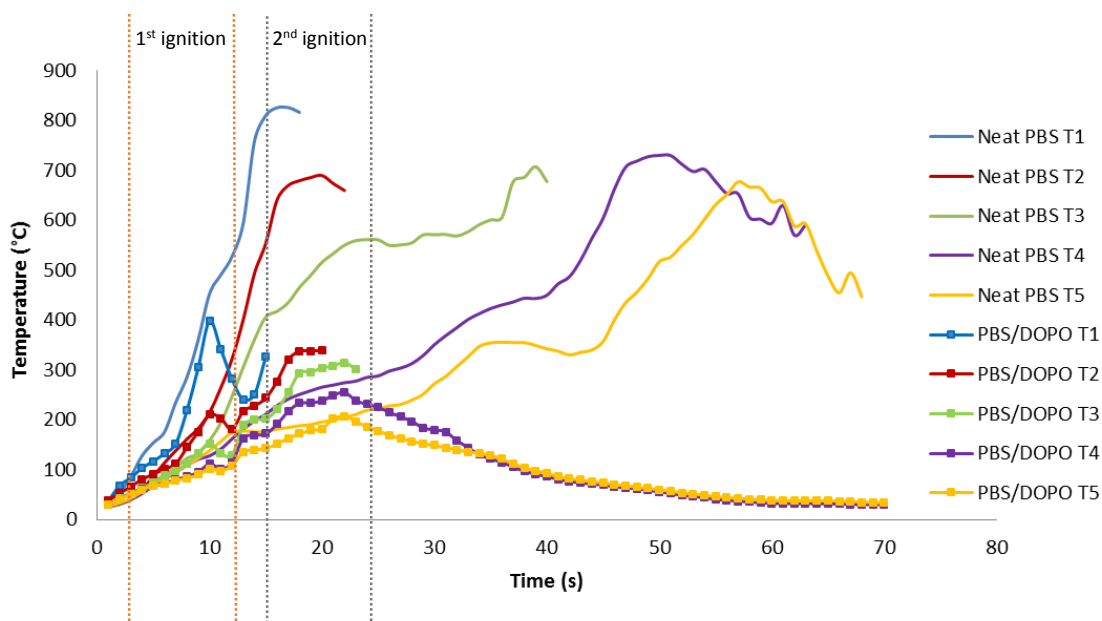


Figure 91: Results of the thermocouples of PBS and PBS/DOPO during UL-94 testing.

Table 20: Temperature gradient inside the bar of PBS and PBS/DOPO at the end of first ignition

	T1	T2	ΔT_{1-T2}	T3	ΔT_{2-T3}	T4	ΔT_{3-T4}	T5	ΔT_{4-T5}
	(°C)	(°C)	(°C)	(°C)	(°C)	(°C)	(°C)	(°C)	(°C)
PBS 1st ignition	453	214	236	159	55	138	21	127	11
PBS/DOPO 1st ignition	403	208	195	153	55	112	41	102	10

IV.2.1.2 Emissivity measurement by UL-94 instrumentation and integrating sphere

The emissivity measurement of the drops is achieved by two methods. The first one is to measure the temperature of the drop with the thermocouple embedded in the bar (here it is assumed that the thermal gradient is negligible) and to adjust the emissivity of the IR camera to match with the measured temperature. The second one is the direct measurement by integrating sphere at room temperature with a solid state of the drops.

In the case of UL-94 instrumentation, the first thermocouple embedded in the bar is very close to the edge (2 mm), so it is reasonable to assume that the temperature measured by the thermocouple is the temperature of the first drop detaching the bar. Therefore the emissivity of PBS and PBS/DOPO can be estimated (see above).

To avoid the influence of burner on the temperature of bar and drops, the drops' temperature are measured when the burner was removed (the end of the first ignition and the end of the second ignition). In the case of neat PBS, as only one ignition is applied, only the drops of the end of the first ignition are measured. According to the results of T1, the temperature of the first drop was formed at $453 \pm 10^\circ\text{C}$. To get the same temperature with the IR camera, emissivity has to be set at 0.91 (**Figure 92**). The same work is carried out for PBS/DOPO, the temperature of T1 is $403 \pm 10^\circ\text{C}$ when the first drop formed. The estimated emissivity is also estimated at 0.91 (**Figure 92**). It should be mentioned that the flame extinguishing action by DOPO is very rapid (no visible burning is observed). Those results indicate that the incorporation of DOPO into PBS has no significant influence on its emissivity. In order to

confirm these results, the drops of the experiment are collected to be analyzed by integrating sphere for measuring the emissivity at room temperature.

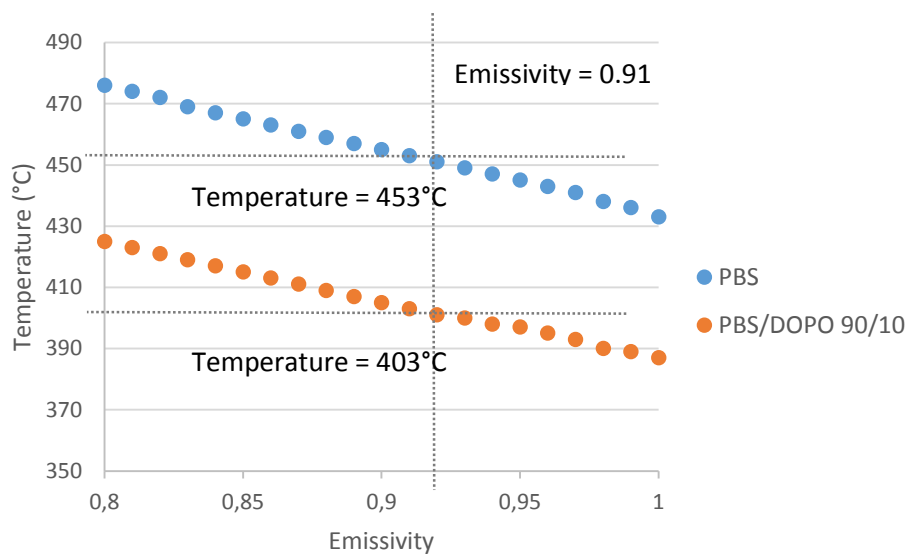


Figure 92: Temperature evolution as a function of the emissivity set to the IR camera

The results obtained using the integrating sphere give emissivity of 0.946 ± 0.005 for neat PBS and of 0.951 ± 0.005 for PBS/DOPO respectively. The values are similar for the two formulations and it shows that the incorporation of DOPO into PBS has no significant change on the emissivity, which is consistent with the measurements made with the thermocouple. The measured emissivity is very close to the value estimated by the UL-94 instrumentation (0.91 for PBS and PBS/DOPO).

Even though a good correlation of the emissivity is measured by the two different methods, a slight difference (around 0.05) is obtained. That can be explained by the following facts: i) emissivity measured by the integrating sphere is a real value, but the UL-94 instrumentation is an estimation according to the temperature measured by the thermocouples which can be less accurate, and ii) between the measured emissivity and the estimated one, the experimental condition is different: the temperature of the melting drops is over 400°C , whereas the emissivity measurement of the drops from the UL-94 experiment is achieved at room temperature.

IV.2.2 Temperature evolution of the drops

Based on the estimated emissivity obtained (0.91 for PBS and PBS/DOPO), temperature changes of the falling drops can be estimated with the IR camera. (Images of the drops are in **Figure 46**, Chapter II, page 64)

For neat PBS, only the drop of the end of first ignition was evaluated. Five experiments are carried out to study its repeatability. The evolution of the temperature of drops shows a good repeatability with an error margin within $\pm 10^{\circ}\text{C}$ (**Figure 93**). It is observed that the temperature decreases fast when the drop detaches from the bar, which took only 4cm from $453 \pm 10^{\circ}\text{C}$ to $440 \pm 10^{\circ}\text{C}$. Afterward the temperature does not change significantly for the next 12 cm which is only 6°C .

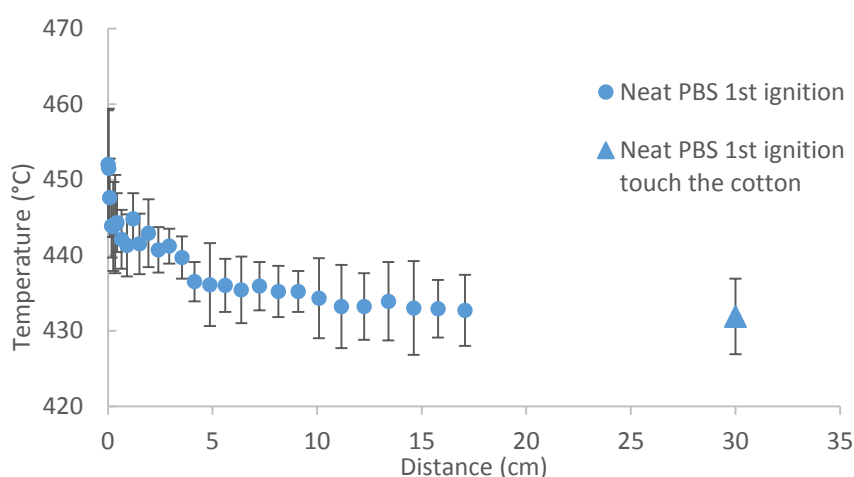


Figure 93: Temperature evolution of a single drop of neat PBS at the end of ignition

For PBS/DOPO, the drop at the end of the first ignition is firstly evaluated. Four experiments are carried out to study the repeatability. An error margin within $\pm 10^{\circ}\text{C}$ is obtained. Like the neat PBS, the surface temperature of the drop of PBS/DOPO decreases faster at the beginning when it detaches the bar, it takes only 4cm from $403 \pm 10^{\circ}\text{C}$ to $394 \pm 10^{\circ}\text{C}$ (**Figure 94 a**). Then the temperature reaches a pseudo steady state in temperature as for neat PBS (over 12cm the temperature decreases only by 3°C). The drop of the second ignition is also evaluated. In this case, an error margin within $\pm 15^{\circ}\text{C}$ is estimated. The temperature evolution was similar to that of neat PBS and the drop of end of first ignition of PBS/DOPO: the temperature decreased from $313^{\circ}\text{C} \pm 15^{\circ}\text{C}$ to $301 \pm 15^{\circ}\text{C}$ $^{\circ}\text{C}$ takes only 4cm, and it does not change significantly for the next 12cm which decreases only by 5°C (**Figure 94 b**).

The temperature of the drops when they detach from the bar is presented in **Figure 95** for both PBS and PBS/DOPO. In the case of neat PBS, the temperature of all the drops is almost the same (453°C). Therefore, once the bar starts to burn, the released heat can continuously supply the further combustion of the bar and the formation of drops. This phenomenon can explain why the neat PBS needs only one ignition to burn up to the clamp. For PBS/DOPO, the drops' temperature is at least 50°C lower than that of neat PBS at any moment of the experiment. Once the burner is removed, the temperature of drops decreases rapidly. Considering the cooling of the drops, when the burner is removed after the second ignition, the decreasing speed is at around 40°C/s. It shows also clearly that in PBS/DOPO, even though there is no visible burning in first and second ignition, the performances of the drops are different: the first ignition generates only 2 to 3 drops, however the second ignition generates much more drops than first ignition. This phenomenon can be explained by: i) the first ignition is applied to the cold bar, it takes time to spread the heat into the bar, ii) the bar starts to melt and decompose, so the drops form only at the end of the first ignition, iii) after the first ignition, the structure of the bar has been partially modified and part of the bar pre-melt, iv) when the burner is applied for the second ignition, there is already an accumulation of heat, and it becomes easier to form a drop at a relatively low temperature (faster melting of the materials), so the second ignition is capable to generate more drops than the first ignition.

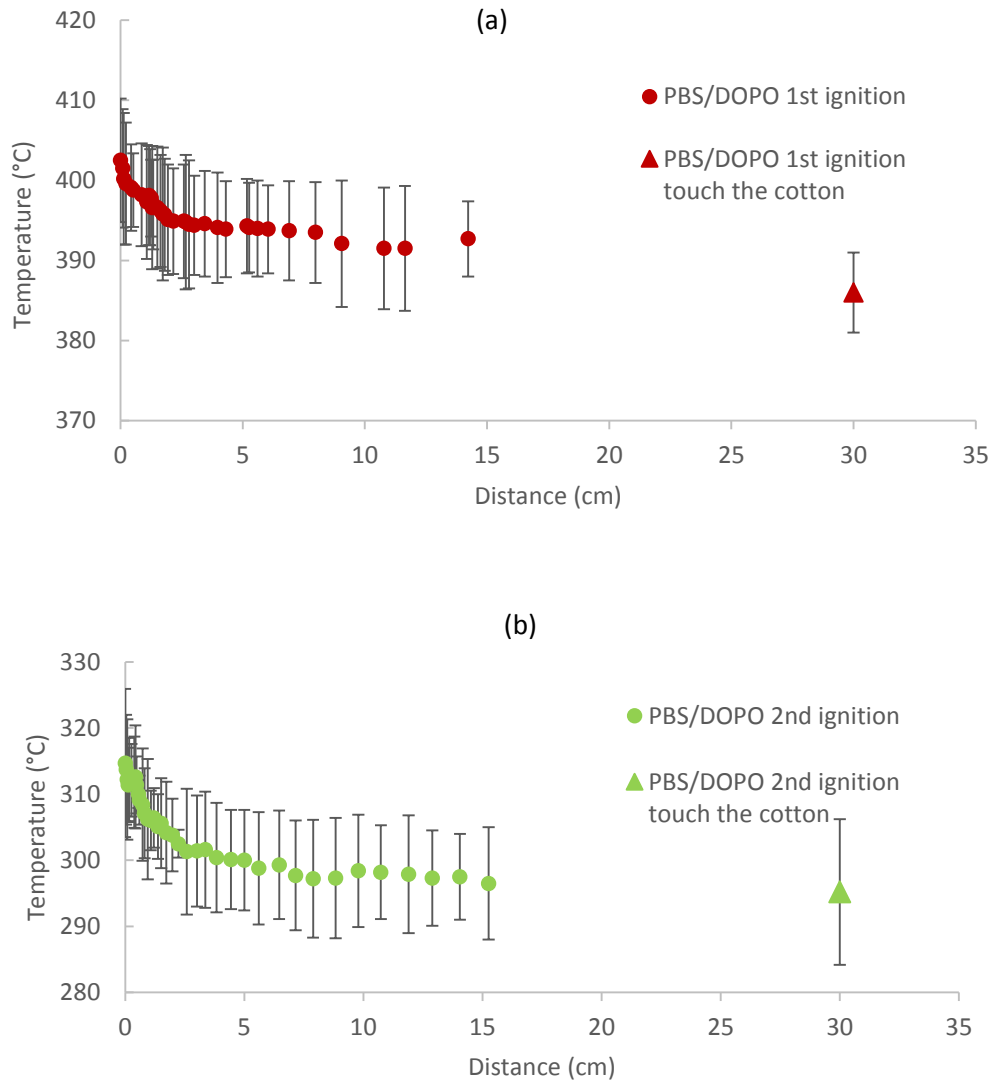


Figure 94: a) Temperature evolution of a single drop of PBS/DOPO at the end of first ignition b) Temperature evolution of a single drop of PBS/DOPO at the end of second ignition

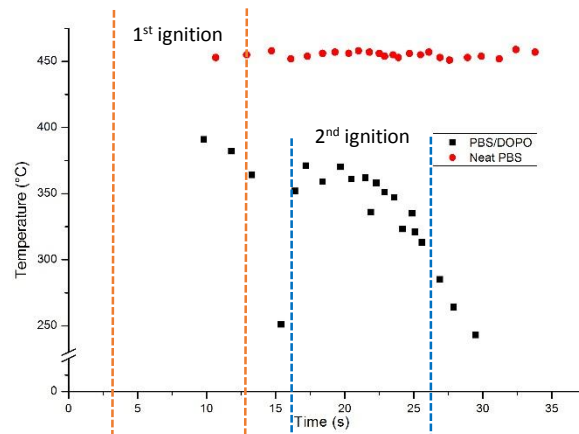


Figure 95: temperature of the drops detaching the bar

Another interesting feature found in this experiment is that the temperature of the surface of the bars has significantly changed when the drops detach from the bar (**Table 21**). For the neat PBS, the temperature of bars is around $453 \pm 10^\circ\text{C}$ when the drops start to form, then the surface of bars decreases by 15°C when the drop detaches from the bar. Afterward, the temperature of the bar slowly reaches $453 \pm 10^\circ\text{C}$ again until the forming of the next drop. For PBS/DOPO, the temperature of bars is about $403 \pm 10^\circ\text{C}$ at the end of the first ignition, and it had a decreasing of 17°C when the drop fell. At the end of second ignition, it shows also a decreasing of 17°C when the drops detach the bar. Those results show directly that the forming drops can take away heat and material from the bar.

The temperature of drops falling on the cotton has been evaluated (**Table 21**). For the neat PBS, the temperature of all the drops hitting the cotton is at $435 \pm 5^\circ\text{C}$ during the whole experiment. On the other hand, drop of PBS/DOPO exhibits very different values when hitting the cotton. At the end of the first ignition, the drops have a temperature of $385 \pm 10^\circ\text{C}$. At the end of second ignition, the drop temperature hitting the cotton is only $295 \pm 15^\circ\text{C}$. All these temperatures are around 18°C lower than those of drops detaching from the bar. Obviously, the temperature of neat PBS is at least 50°C higher than the temperature of PBS/DOPO when they touch the cotton. It was reported that the cotton's maximum degradation rate occurs at 377°C .¹⁶⁷ All the drops of PBS/DOPO have lower temperature than 377°C when hitting the cotton, whereas the drops of neat PBS have much higher temperature than 377°C . Thus it can explain why the drops of neat PBS can ignite the cotton and those of PBS/DOPO cannot. Particularly, the temperature of drops hitting the cotton matches perfectly with the curves plotted previously of the temperature evolution of drops (**Figure 93**, **Figure 94 a** and **Figure 94 b**). It evidences that the drop temperature tends to stabilize when they fall more than 4 cm from the bar until the moment they hit the cotton. Combining with the measurement of temperature when drops detach the bar, it can be concluded that the drops have a heat removal effect when they fall. That is why in certain cases, the UL-94 test can be achieved with a good classification by producing the drops but no success in some other fire tests, such as MLC, glow wire and limiting oxygen index etc.

Table 21: temperature measured by IR camera with an estimated emissivity when drops detach the bar and when they touch the cotton

	Neat PBS end of 1 st ignition (°C)	PBS/DOPO end of 1 st ignition (°C)	PBS/DOPO end of 2 nd ignition (°C)
Bar	438±10	386±10	296±15
Drop	453±10	403±10	313±15
$T_{\text{drop}} - T_{\text{bar}}$	15	17	17
Drop on the cotton	435±5	385±10	295±15

IV.2.3 Influence of DOPO on physico-mechanical properties

It is found that the physical properties might be changed when DOPO is incorporated into PBS. Visually, this phenomenon can be observed on the IR images: for neat PBS, only when a drop reaches a temperature over 450°C, it detaches from the bar (**Figure 96 a**) and the drops keep always their own drop-shape, whereas the bar of PBS/DOPO lengthens and makes line-shape edge when the temperature is over 400°C for the end of the first ignition and 300°C for the end of the second ignition (**Figure 96 b**). Viscosity measurement of PBS and PBS/DOPO between 120°C to 250°C is shown on **Figure 97**. PBS and PBS/DOPO show both low viscosity at high temperature. The viscosity of PBS is 307 Pa.s at 120°C and it decreases to 36 Pa.s at 250°C. Viscosity of PBS/DOPO is between 0.5 to 1.5 Pa.s when the temperature is over 125°C, which is close to castor or olive oil at room temperature. The different viscosity explains why the different phenomenon observed on the images captured by IR camera. It also demonstrates that the drops can be formed at a lower temperature for PBS/DOPO than neat PBS.

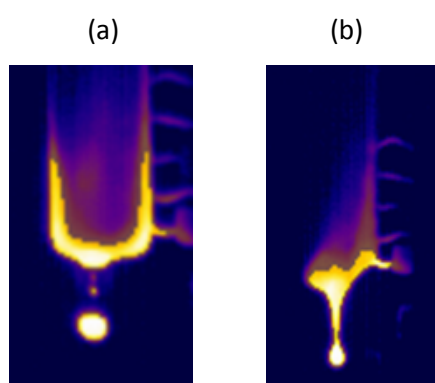


Figure 96: Images of the drops detaching from the bar captured by IR camera a) Neat PBS b) PBS/DOPO

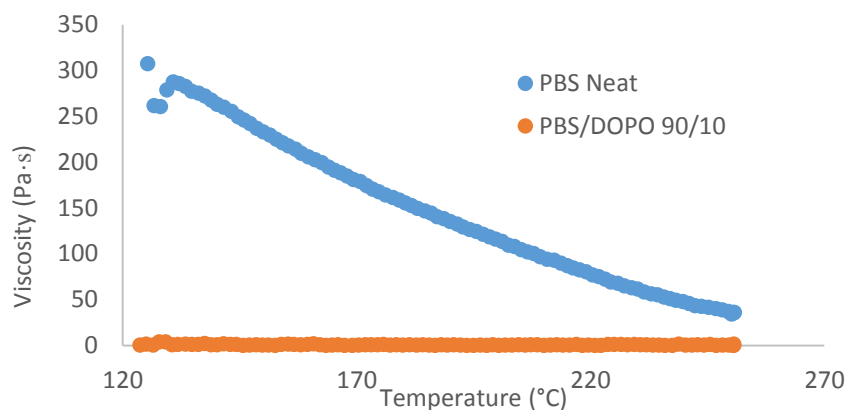


Figure 97: Viscosity as function of temperature of PBS and PBS/DOPO

IV.2.4 Conclusion

In this part, an optimized UL-94 instrumentation has been developed to understand the evolution of a single drop during the UL-94 test. This UL-94 instrumentation which contains an IR camera equipped with a specific filter and the thermocouples embedded in the bar permit to estimate the emissivity of materials during UL-94 test. The temperature evolution inside bars and on the surface of drops was measured in situ and in dynamic during UL-94 test. The temperature propagation of PBS/DOPO inside the bar and also the shape and temperature evolution of the drops were clearly captured. Then with that information, it was demonstrated that the different classification of neat PBS and PBS/DOPO in UL-94 was governed by the temperature of the drops. Meanwhile, good repeatability and good agreement of the results between thermocouple and the IR camera obtained with neat PBS and PBS/DOPO confirmed the reliability of this UL-94 instrumentation.

IV.3 Conclusion

In this chapter, a comprehensive study of the mode of action of PBS/DOPO in different fire testing was made.

In the first section, the degradation route and the behavior in MLC test of PBS/DOPO have been completely investigated. It shows that un-modified DOPO is capable to be effective in an aliphatic polyester. Especially the great effect of DOPO acting in the gaseous phase provides researchers more ideas of using DOPO and its derivatives to flame retard (bio-based) polyesters with low processing temperature.

In the second section, the use of the special IR camera and evaluating the emissivity to measure the drops temperature is an original method for the study of the material's behavior in UL-94 test. With this novel approach, it was evidenced that the drops' temperature of neat PBS and PBS/DOPO governed their classification in the test. Furthermore, with the advantages mentioned in this paper, this instrumentation can be used for understanding the mechanism of some other types of polymers and their additives, especially when drops are generated, and therefore to provide researchers new method to design a better flame retardant system.

Chapter V - Investigation of the mechanism of the flame retardancy of PBS/PIC/APP

V Investigation of the mechanism of the flame retardancy of PBS/PIC/APP

In the chapter of material screening (Chapter III), it was shown that the poly(isosorbide carbonate) (PIC) can act as a carbonization agent in an intumescent flame retardant system to flame retard PBS. The purpose of this chapter is therefore to fully understand the mode of action of this formulation, particularly the role of PIC during a fire scenario. To achieve this goal, in the first part different approaches are used to understand the evolution of the mass loss and the temperature in the formulation. Then the chemical composition of the char during the MLC test is investigated. In the third part, thermal decomposition behavior of PBS/PIC/APP is described. The fourth part is dedicated to the investigation of the gases released during the decomposition. The fifth and the sixth parts are dedicated to char morphology and mechanical properties respectively. In the final part, a general conclusion is given.

V.1 Investigation of the mass and temperature evolution during MLC test

The results of MLC test are presented in **Figure 98 a**). When 30 wt% of APP was incorporated in PBS, the pHRR was decreased by 19 % and the THR was decreased by 25 % with 23 % of residue remained. The formulation PBS/(PIC/APP 1/3) 70/30 exhibits even better performance according to the MLC test with 24 % decreasing of pHRR and 48 % decreasing of THR. In addition to this, a good yield of residual char was obtained (44 %).

The mass loss during the MLC test was presented in **Figure 98 b**). From the beginning of the experiment to the ignition (110 s for neat PBS, 99 s for PBS/APP and 100 s for PBS/PIC/APP), the materials softened and melted, but there was no significant mass loss during this stage. From the ignition to 200 s, the char can be visually observed in the formulation of PBS/APP and PBS/PIC/APP. Neat PBS had 6 % of mass loss, and it started to degrade with a high mass loss rate (0.25 %/s) until the matter had almost totally burned out. However, PBS/APP and PBS/PIC/APP kept a low mass loss rate during the formation of the char, which had only 1 % of mass loss. From 200 s to 330 s, visual observation indicates that the char of PBS/APP and PBS/PIC/APP kept a stable state at the beginning (200 s to 270 s), then it cracked a little (270 s to 330 s) according to the MLC curve. The mass loss rate of PBS/APP starts to increase to

0.17 %/s at 200 s, and PBS/PIC/APP reaches a similar mass loss rate at 230 s. After 300 s, PBS/APP kept the same mass loss rate (0.17 %/s) up to 600 s, but the mass loss rate of PBS/PIC/APP decreased continuously to only 0.03 %/s at 600 s. The final residue of neat PBS was almost 0 %, that of PBS/APP was 23 % and that of PBS/PIC/APP was 44 %.

The efficiency of the formed char acting as heat barrier was evaluated by thermocouples embedded in the plaques. The position of the thermocouples are presented in **Figure 99**. The first thermocouple (T1) was placed under the plaques in order to measure the temperature of the bottom, whereas the second thermocouple was placed on the surface of the plaque through a drilled hole (T2) to measure the surface temperature of the plaque. It is noteworthy that T2 remains always 3 mm height above the bottom. Therefore, in the case of neat PBS, T2 measures the surface temperature of the material until the thermocouple is no longer embedded in the matter (after the ignition). In the case of PBS/APP and PBS/PIC/APP, T2 measures the surface temperature before the ignition and also after the ignition because of the formation of the intumescent char. T2 remains embedded in the char and heat gradient can be measured between T1 and T2.

Temperature measured by thermocouples are presented in **Figure 98 c)**. It shows that before ignition, the surface of all three materials have similar heating rate (about 180°C/min). At ignition the surface temperature (T2) of PBS (110 s), PBS/APP (99 s) and PBS/PIC/APP (100 s) is 330°C, 296°C and 291°C respectively. The similar heating rate and surface temperature suggests that the incorporation of the additives does not modify significantly the thermo-physical properties of PBS. On the bottom of the plaques (T1), the temperature of PBS is 83°C lower than that of the surface, while for PBS/APP and PBS/PIC/APP the temperatures are 72°C and 69°C lower than the surface temperatures respectively.

From the ignition (110 s) to 200 s, the heating rate of T1 for neat PBS is quite high and estimated at 80°C/min, and the temperature of T1 increased continuously up to 465°C until the thermocouple is no longer embedded in the matter (about 400 s). For PBS/APP, there is char formation and visually it is formed between 100 s to 200 s. T1 and T2 curves of PBS/APP exhibit similar evolution and are parallel during this stage. The heating rate (measured via T1 or T2) is estimated at 40°C/min (100 s to 200 s) and is twice lower than that of neat PBS. For PBS/PIC/APP, the char formation was also visually observed between 100 s to 200 s. During its formation, T1 of PBS/PIC/APP exhibits similar temperature of that of PBS/APP, but T2 is

20°C lower than that of PBS/APP. It is noteworthy that the heating rate of T2 is about 24°C/min and is significantly lower than that of PBS/APP. It can explain at least partially why the HRR of PBS/PIC/APP is 51 kW/m² lower than that of PBS/APP at 200 s.

From 200 s to 330 s, T1 and T2 of PBS/APP measure the same heating rate (40°C/min), and the bottom temperature (T1) of PBS/APP shows that a temperature gradient between T1 and T2 is over than 70°C. Whereas for PBS/PIC/APP, T1 and T2 reach a stable plateau (steady state) after the formation of the char (200 s) until the end of the test (583 s, T2 - T1 = 45°C).

After 330 s, T1 and T2 of PBS/APP increased up to 372°C (485 s) and 471°C (485 s) respectively. T1 and T2 of PBS/APP always had an increase of temperature from 100 s to 485 s even after the formation of the char. This indicates that the char cannot act perfectly as heat barrier. Afterward, T1 and T2 decrease and reach a steady state at 370°C and 410°C respectively. The temperature gradient between T1 and T2 at this steady state is only 40°C. As for PBS/PIC/APP, the temperature gradient between T1 and T2 at the steady state is 45°C. Moreover, these two plateaus obtained with PBS/PIC/APP have always lower temperatures than those measured in the case of PBS/APP: PBS/PIC/APP T1 equals 315°C vs PBS/APP T1 equals 370°C and PBS/PIC/APP T2 equals 360°C vs PBS/APP T1 equals 410°C.

These results evidence that the char of PBS/PIC/APP are more efficient than that of PBS/APP in term of heat barrier. Its relatively low heating rate under the char leads to a lower decomposition rate of the polymer, which can explain the low pHRR and THR. The formation of char is related to a series of chemical reactions and so, it is important to know the different chemical composition of the char to understand the mechanism of these two formulations. Therefore the next part focuses on the nature of the char at different stage of the MLC test.

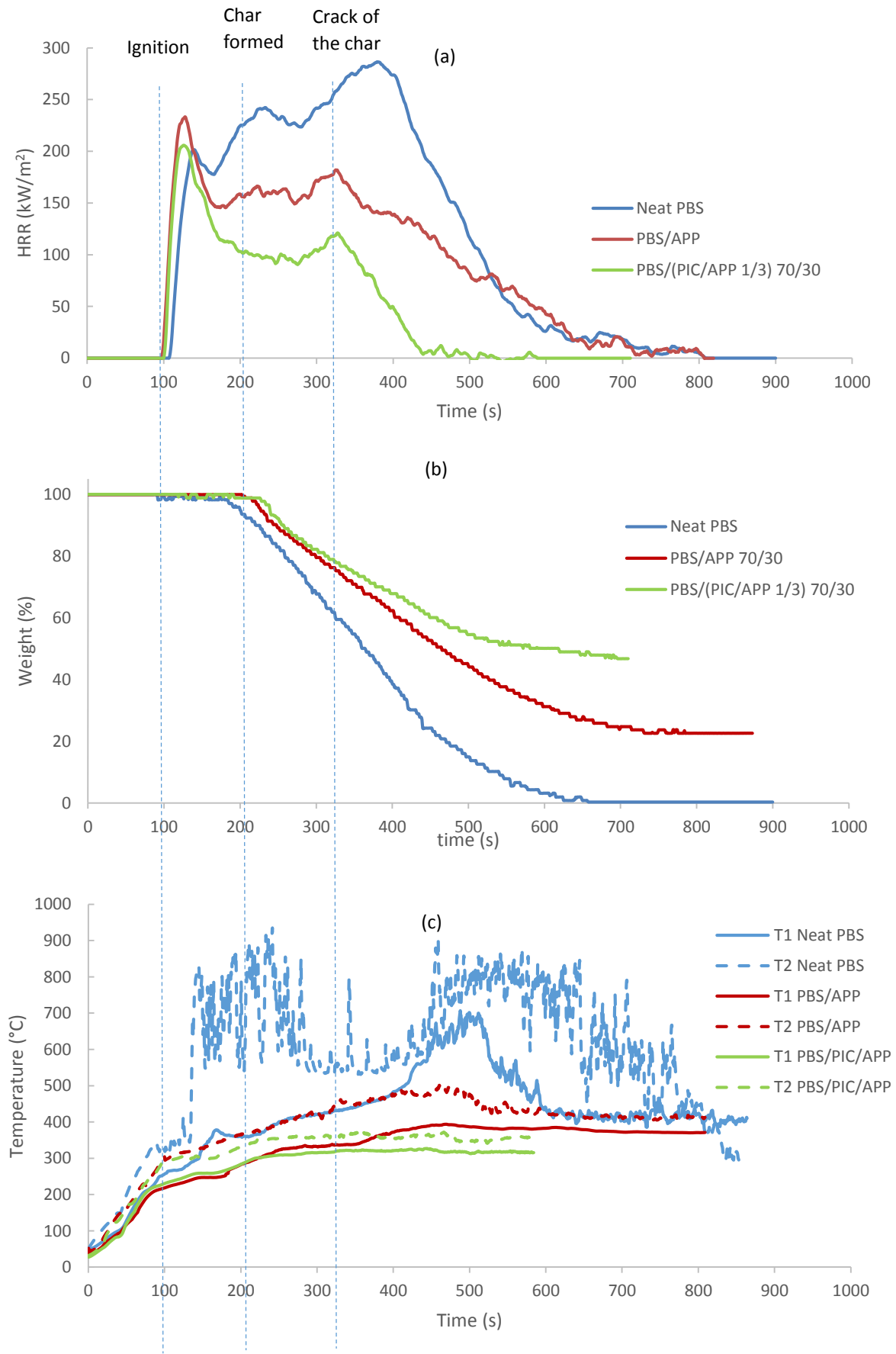


Figure 98: a) MLC test of PBS, PBS/APP and PBS/PIC/APP, b) mass loss during the MLC test, c) temperature measured by the thermocouples

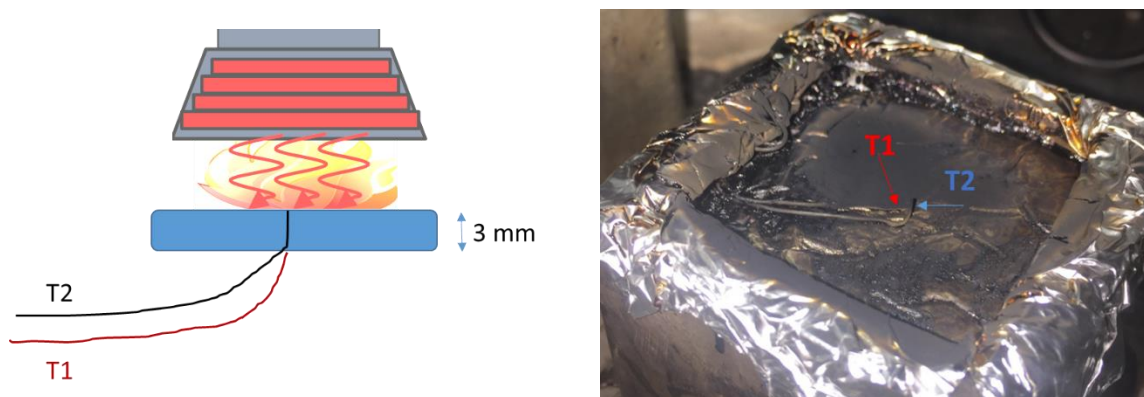


Figure 99: Position of the thermocouples (left), in real situation (right)

V.2 Investigation of the chemical composition of the forming char by solid state NMR

Chemical composition of the residual char at different stage during MLC test was investigated using solid state NMR. The considered nuclei are ^{31}P and ^{13}C . The residual chars were collected at three different stages during the MLC test: the first stage was at 120 s where the char started to form; the second stage was at 250 s where the formed char stabilized; the third stage was at 420 s where the heat release rate decreased.

V.2.1 Characterization of ^{31}P NMR

The magic angle spinning (MAS) ^{31}P spectra of PBS/APP 70/30 and PBS/(PIC/APP 1/3) 70/30 are presented in **Figure 100** and **Figure 101**. It was found that during the experiment of solid state NMR, the presence of phosphoric acid may cause explosion of the rotor during the rotation in the probe, which may cause severe damage to the probe (viscous phosphate trapped in the char creates a pressure on the rotor cap which is ejected). The chars were then washed with water to eliminate viscous phosphate. The chars were dried under 90°C for 24 h before the analysis. Only two samples (PBS/APP stage 1 and PBS/APP stage 2) were analyzed without washing and thus can be compared with the samples after the washing (**Figure 100**).

Before the MLC test, the MAS ^{31}P NMR of the un-burned PBS/APP and PBS/PIC/APP showed a doublet at -21.5 ppm and -22.5 ppm, which are assigned to P-O in the APP.^{168,169} The same chemical shift of the phosphorus for neat APP is observed indicating that PBS and PIC had no chemical reaction with APP during the processing (extrusion and compressing molding). For

the washed samples, at the stage 1 (120 s), PBS/APP and PBS/PIC/APP show a broad band centered at 0.5 ppm. This band can be assigned to orthophosphate which linked with aliphatic groups and/or orthophosphoric acid.^{168,169,170} The shape and the width of the band indicates a disordered structure suggesting a glass-type behavior. At the stage 2 (250 s), for PBS/APP, besides the band at 0 ppm, a narrow sharp band was found at 2.3 ppm, which can be assigned to the P-O-C group (might be orthophosphate linked with ester groups).^{171,172} PBS/PIC/APP exhibits similar two bands at 0 ppm and 2.3 ppm, but the band at 0 ppm shows a flattened feature, which indicates that the orthophosphates may be less ordered than those of PBS/APP. At the stage 3 (420 s), for PBS/APP, the two bands at 0 ppm and 2.3 ppm are still observed but unlike the stage 2, the ratio between the band at 2.3 ppm and the band at 0 ppm changed from 1 : 1.2 (stage 2) to 1 : 3.9 (stage 3). For PBS/PIC/APP, the band at 0 ppm shows a more flattened feature. The final chars of these two formulations present only a broad band at 0 ppm suggesting a disordered structure like a glass-type structure.

Un-treated samples showed different behavior than washed samples in MAS ³¹P spectra (**Figure 100**). For un-treated char of PBS/APP at stage 1 and stage 2, three bands were presented at 0 ppm, -12.1 ppm and -25.3 ppm. Like the washed samples, the band at 0 ppm can be assigned to the orthophosphoric acid and/or orthophosphate groups which linked to the aliphatic groups. Then the band at -12.1 ppm may possibly be assigned to the pyrophosphate groups and/or orthophosphate linked to the aromatic groups (di-phenylorthophosphate and tri-phenylorthophosphate).^{169, 173} It was found that after the washing with water, this band (-12.1 ppm) disappeared, which reveals that only the free pyrophosphate groups that without chemical bond with the phenyl groups were produced, and these free pyrophosphate groups were trapped in the char. To attribute the band at -25.3 ppm, the phosphates that contain a single PO₄ or multiple PO₄ that linked with each others are noted as follows (**Figure 102**): i) Q₀, phosphate that has a single PO₄, ii) Q₁, phosphate that contains one bridged oxygen, iii) Q₂, phosphate that has two bridged oxygen and iv) Q₃, phosphate that has a ramified structure which contains three bridged oxygen. Thus the band at -25.3 ppm can be assigned to the phosphate in a Q₂ structure.¹⁷⁴ It is noteworthy that this band is broad which indicates the structure of these phosphates are disordered.

With the information provided above, the evolution of phosphorus in PBS/APP and PBS/PIC/APP during MLC test can be concluded. The decomposition of the matter formed Q₀

structure orthophosphates which link with the aliphatic groups, Q_1 structure pyrophosphates that do not link with aromatic groups and Q_2 structure phosphates. Then the Q_1 structure orthophosphates that contained a P-O-C structure was formed. Specially, at this stage, the band of the orthophosphates linked with the aliphatic groups of PBS/PIC/APP is broader and more flattened than that of PBS/APP, which shows that the incorporation of PIC increased the disorder of the phosphate species. This disordered structure indicates the formation of a glass-type structure, which can be a reason that the PBS/PIC/APP has better performance than PBS/APP in MLC test. Finally, only the orthophosphates that linked with the aliphatic groups are found in the final char.

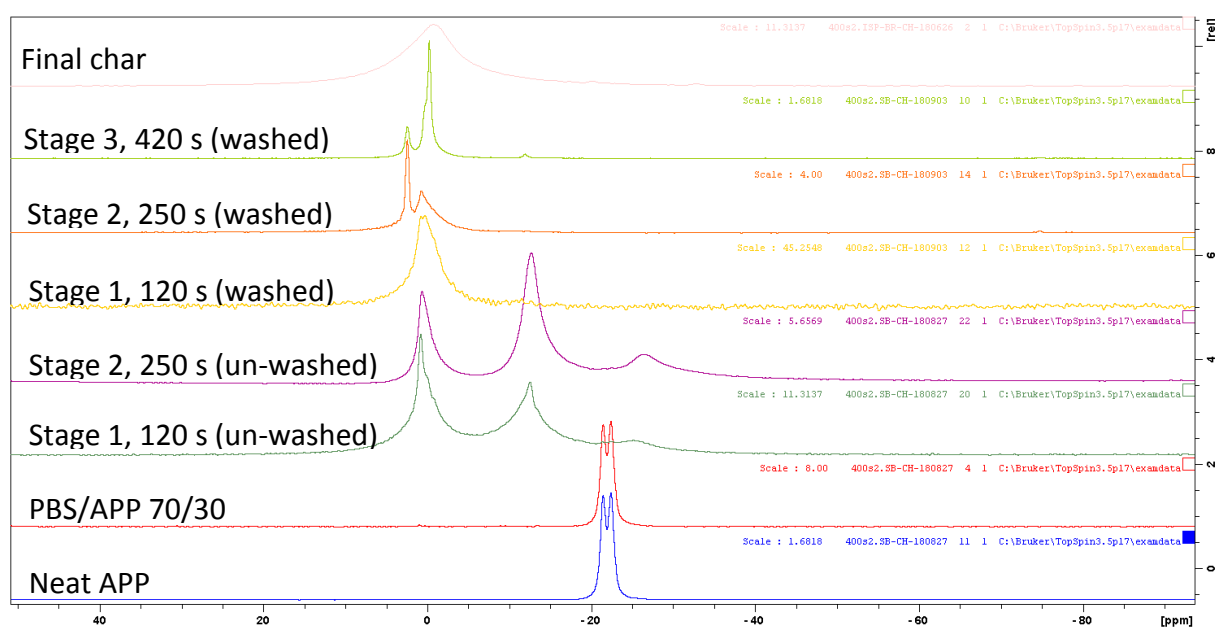


Figure 100: Solid state NMR MAS ^{31}P spectra of PBS/APP at different stage

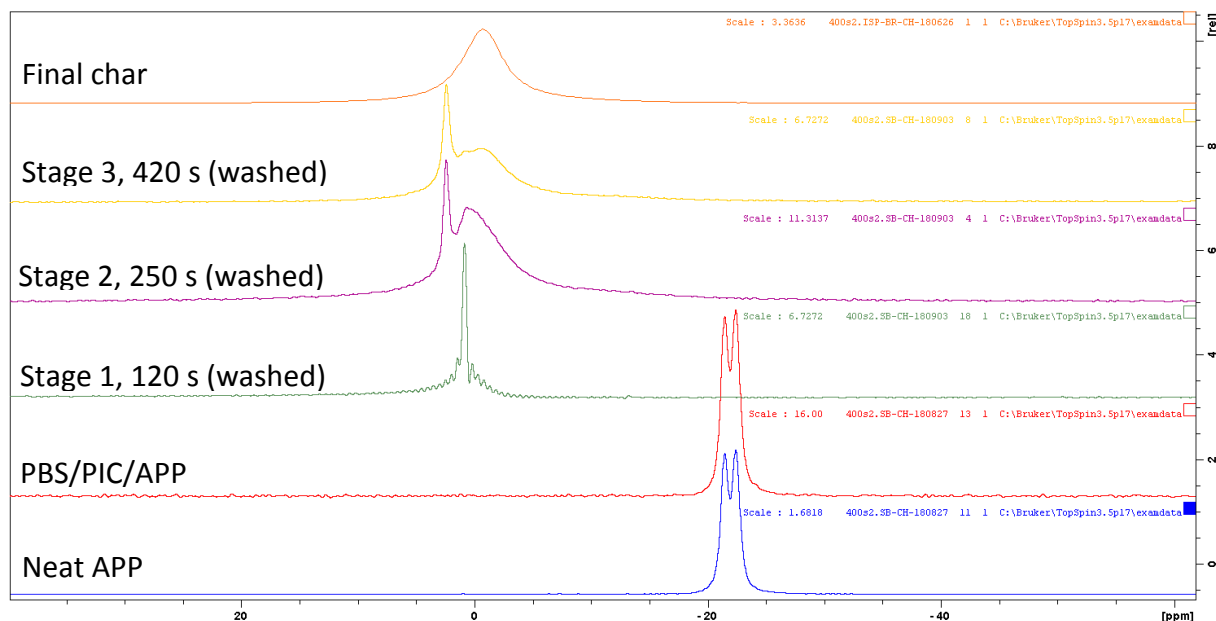


Figure 101: Solid state NMR MAS ^{31}P spectra of PBS/PIC/APP at different stage

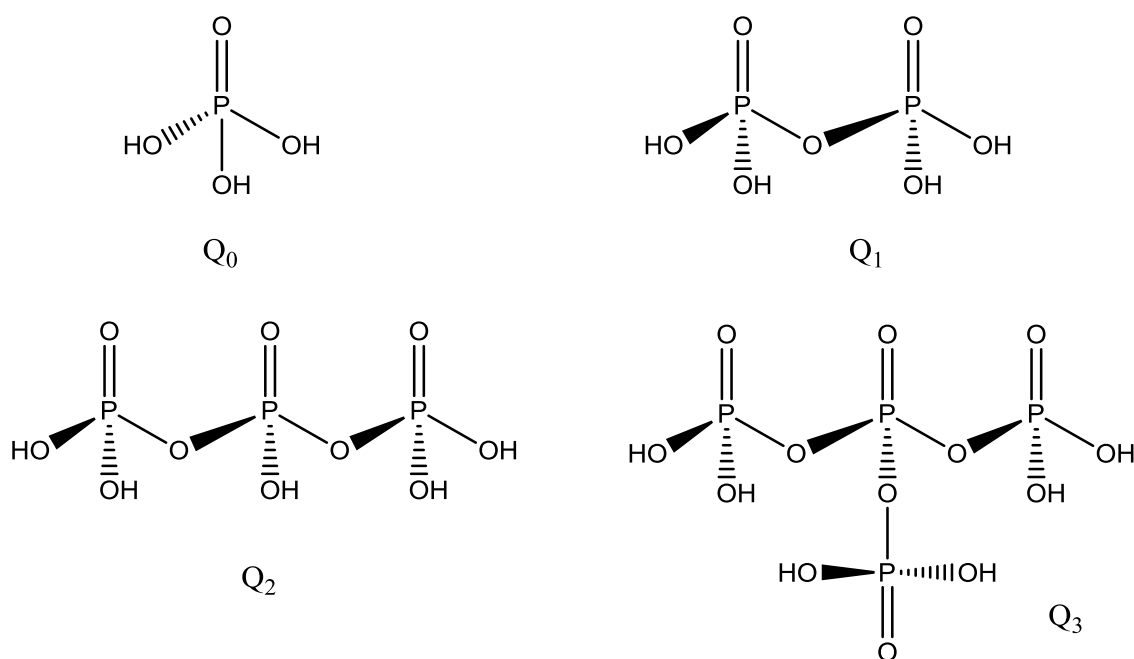


Figure 102: Nomenclature of the different types of phosphate

V.2.2 Characterization of ^{13}C NMR

The magic angle spinning (MAS) ^{13}C spectra of PBS/APP 70/30 and PBS/(PIC/APP 1/3) 70/30 are presented in **Figure 103** and **Figure 104**.

Before the fire test, neat PBS exhibit four bands at 25.6 ppm, 29.1 ppm, 64.3 ppm and 172.6 ppm. The band at 25.6 ppm is assigned to the $-\text{CH}_2-$ in the butanol which is not linked with the oxygen. The band at 29.1 ppm is assigned to the $-\text{CH}_2-$ in the succinate that is not linked with

the oxygen. The band at 64.3 ppm is assigned to the O-CH₂ in the butanol, and the band at 172.4 ppm is assigned to the carbon of the carbonyl group.^{175,176} When PBS was blend with APP and PIC, these four bands showed the same chemical shift as neat PBS, hence it confirms that there is no chemical interaction during the processing. Neat PIC presents an obvious band at 155.3 ppm which can be assigned to the carbonate group.¹⁷⁷

For the samples at 120 s, 250 s, 420 s and the final char, there is a broad band at 130 ppm. It can be assigned to unsaturated carbon (C=C, aromatic and polyaromatic species).^{178,179} This band became more and more intense with the evolution of the time, which indicate that an aromatization occurring during the formation of the char. A broad band was also found at about 30 ppm which can be assigned to the aliphatic carbons.^{178,180} For PBS/APP and PBS/PIC/APP, they showed similar ¹³C NMR spectra, which indicates that the incorporation of PIC had no significant change on the chemical composition of the char.

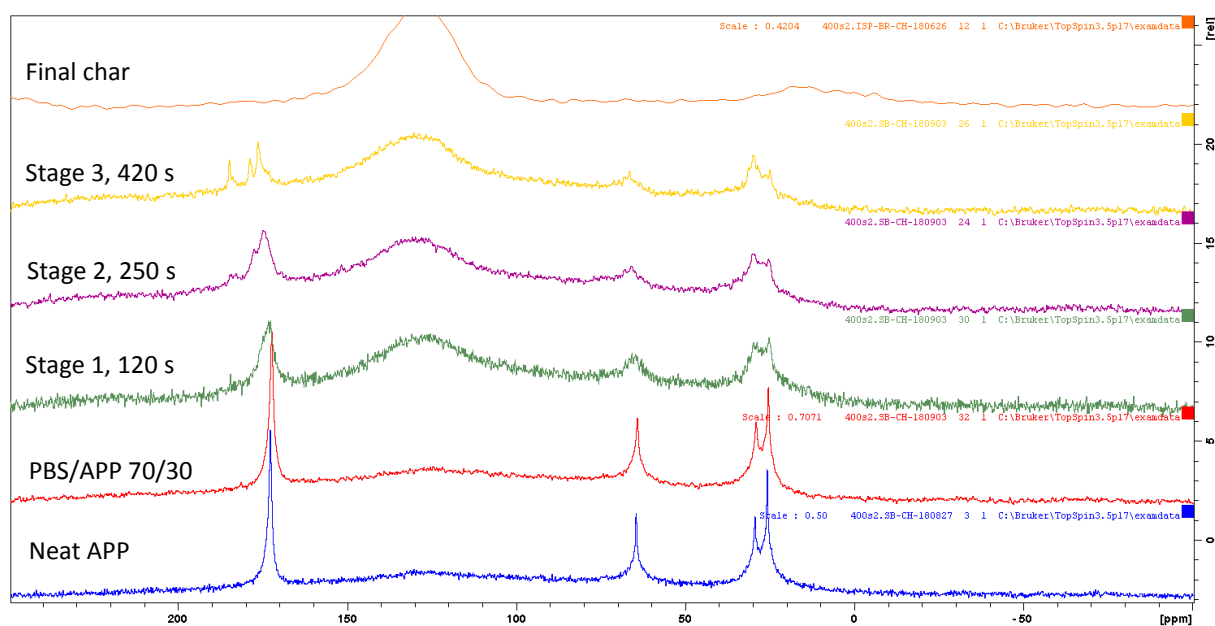


Figure 103: Solid state NMR MAS ¹³C spectra of PBS/APP at different stage

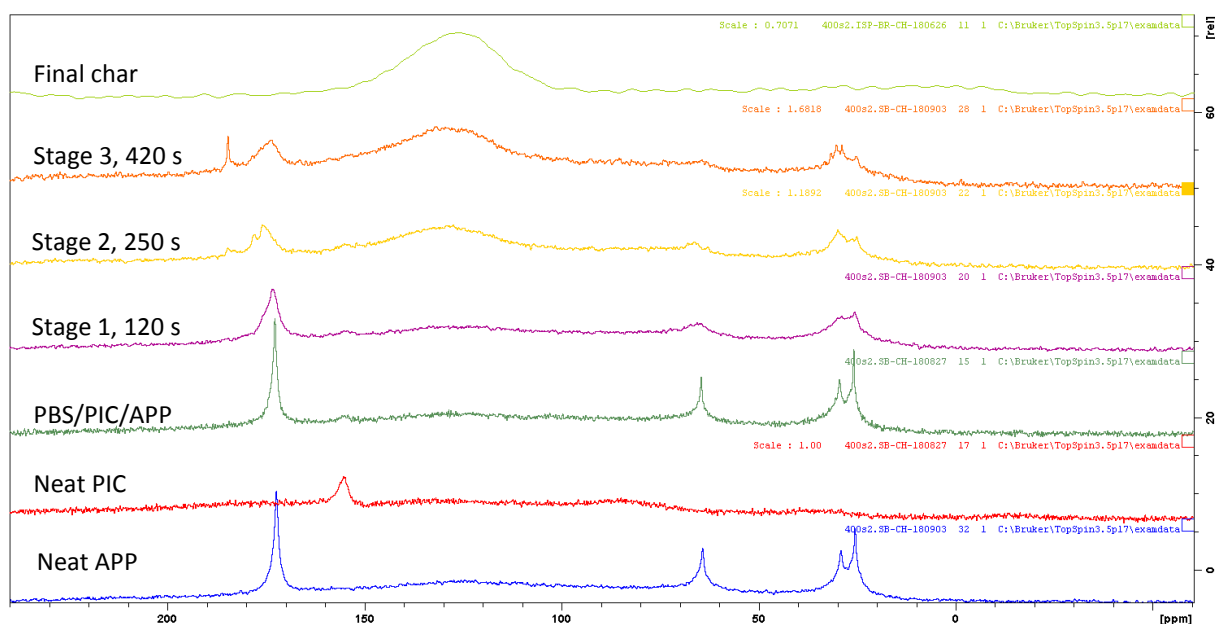


Figure 104: Solid state NMR MAS ^{13}C spectra of PBS/PIC/APP at different stage

V.3 Thermal stability analysis

To understand the decomposition behavior of the different formulations and the formation of residual char, thermal stability of PBS/APP 70/30 and PBS/(PIC/APP 1/3) 70/30 are analyzed under thermo-oxidative condition.

The thermal stability of neat PBS and the formulations with additives under thermo-oxidative conditions was investigated by TGA (**Figure 105**). APP exhibits a two-step decomposition process. The first step ranges from 250°C to 450°C with a mass loss of 18 %, and this mass loss corresponds to the release of water and ammonia.⁶² Meanwhile, a cross linked P-O-P structure formed by elimination of H₂O between P-OH groups which were released by the evolution of NH₃. The second step range from 450°C to 650°C with a mass loss of 59 % can be assigned to the release of phosphoric acid.^{181,182} It is noteworthy that the residue of APP has low stability at high temperature. The residue mass decreases continuously from 23.6 % at 650°C to 12.5 % at 800°C.

The decomposition of PBS involves two steps of process. The first step ranges from 335°C to 430 °C with a mass loss of 94.3 %. This step is attributed to depolymerization of the PBS.²⁶ The second step, from 430°C to 520°C, is the formation and the degradation of a transient char. PIC exhibits also two steps decomposition process, the first degradation ranges from 308°C to 383°C which is assigned to the depolymerization of PIC.¹⁸³ The second step was from 383°C to

530°C which is assigned to the formation and degradation of a transient char. PBS and PIC exhibit no residual char after the experiment.

When APP was incorporated into PBS, there are two steps of decomposition process. In the first step, incorporation of APP accelerates the beginning of the degradation, ($T_2\%$ is lowered by 26 °C in comparison to neat PBS). The first step has 72 % of mass loss which can be assigned to the decomposition of the APP and the depolymerization of PBS. The second step was between 350°C to 570°C and is assigned to the formation and the degradation of transient char. It should be mentioned that after 570°C, the residual char of PBS/APP was not stable, and the mass of the residue continuously decreases from 12.8 % at 570°C to only 3.7 % at 800°C. When PIC is incorporated into PBS and APP, there are still two steps of decomposition steps. The $T_2\%$ (306°C) is not modified compared to that of PBS/APP (309°C). However, the mass loss of the first step is 78 % which is 6 % more than that obtained with PBS/APP. Furthermore, during the second step, the residual mass of PBS/PIC/APP is 6 % lower than that of PBS/APP at the same stage of the experiment. This result shows that the char yield of PBS/APP is higher than that of PBS/PIC/APP during the formation of char. An interesting feature is observed at 587°C where the curve of PBS/PIC/APP crossed with the curve of PBS/APP. It reveals that the char of PBS/PIC/APP is more resistant at high temperature i.e. over than 530°C. The curve of PBS/PIC/APP formed a steady plateau with 8.9 % of residue from 600°C to 800°C. To understand the role of PIC in the intumescent formulation, PIC/APP with a ratio of 1/3 was also investigated. PIC/APP exhibit two decomposition steps. The first step starts from 286°C ($T_2\%$) to 350°C with only 31 % of mass loss. Then the second steps was from 350°C to 600°C with 41 % of mass loss which can be assigned to the formation and degradation of transient char. The residual mass reaches 12.5 %.

Differential TG curves (which is the result of the difference between the experimental TG curve and the calculated one) were plotted for PBS/APP, PIC/APP and PBS/PIC/APP. This permits to investigate potential interactions between PBS, PIC and APP (**Figure 106**). PBS/APP and PBS/PIC/APP exhibits a significant destabilization between 320 and 420°C. This strong destabilization indicates that APP promotes the decomposition of PBS. As for PIC/APP, it exhibits also a destabilization at this range of temperature but with much less intensity. A second destabilization was observed from 500°C to 600°C for these three formulations, which can be assigned to the degradation of the transient char. A slight stabilization (7.9 % for

PIC/APP and 5.7 % for PBS/PIC/APP) was found after 600°C for the formulations containing PIC (PBS/PIC/APP and PIC/APP).

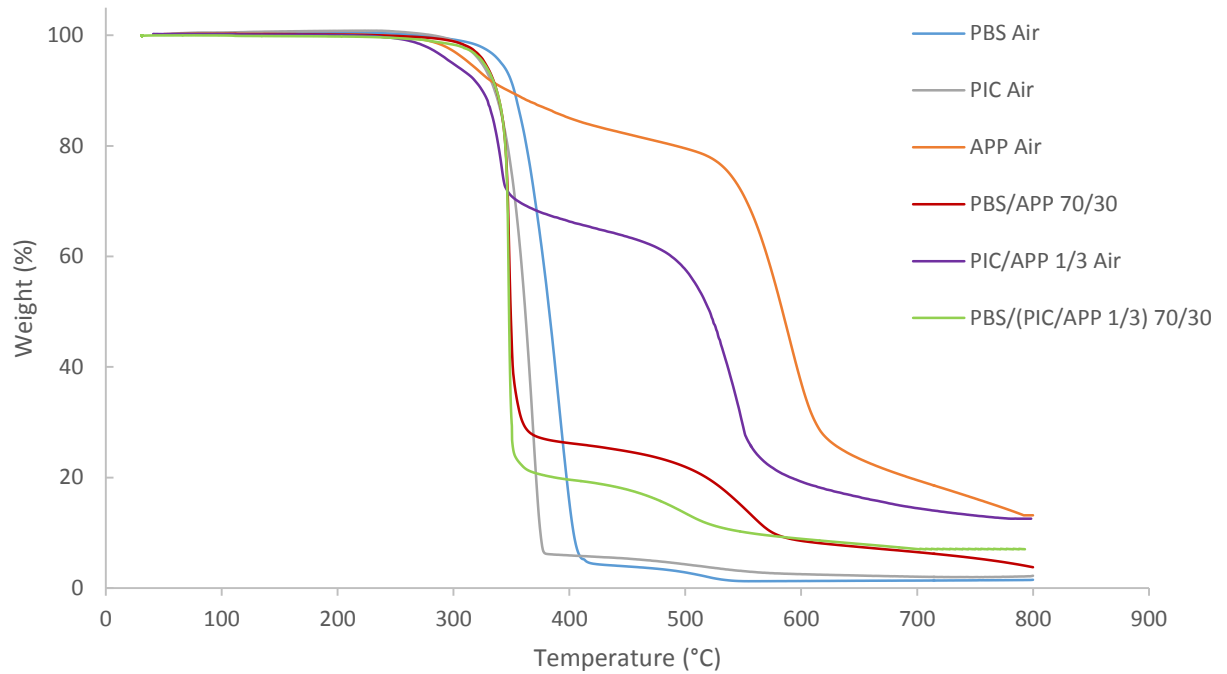


Figure 105: Thermal degradation of PBS with the additives under thermo-oxidative condition (10°C/min, Air)

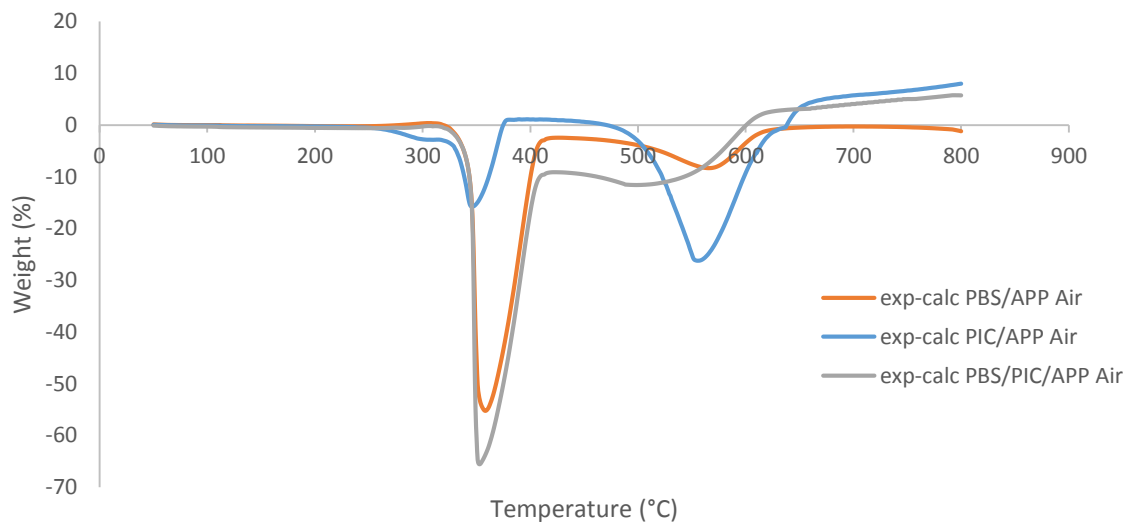


Figure 106: Differential TGA of PBS/APP, PIC/APP and PBS/PIC/APP under thermo-oxidative condition (10°C/min, Air)

V.4 Analyses of the released gases by TGA-FTIR

Although it was shown that the mechanism involved mainly a condensed phase process, it is still unknown whether a mode of gas could be also involved. Thus, the evolved gases released during the decomposition was analyzed by TGA linked with a Fourier transform infrared spectrometer (FTIR).

The mass loss of PBS/APP and PBS/PIC/APP was plotted as function of time in **Figure 107**. **Figure 108** shows the chemigram of these two formulations during the decomposition. These two formulations decompose at almost the same time. The formation and degradation of the transient char is observed between 31 min to 50 min. Infrared spectra at 31 min for the two formulations is presented in **Figure 109**. The composition of the released gases is similar. The detected gases are mainly THF (2981 cm^{-1} C-H), succinic anhydride (1811 cm^{-1} C=O), H_2O and CO_2 . The identical composition of the released gases indicates that the decomposition pathway is not significantly modified and confirms the flame retardant action occurred mainly in the condensed phase via the formation of char.

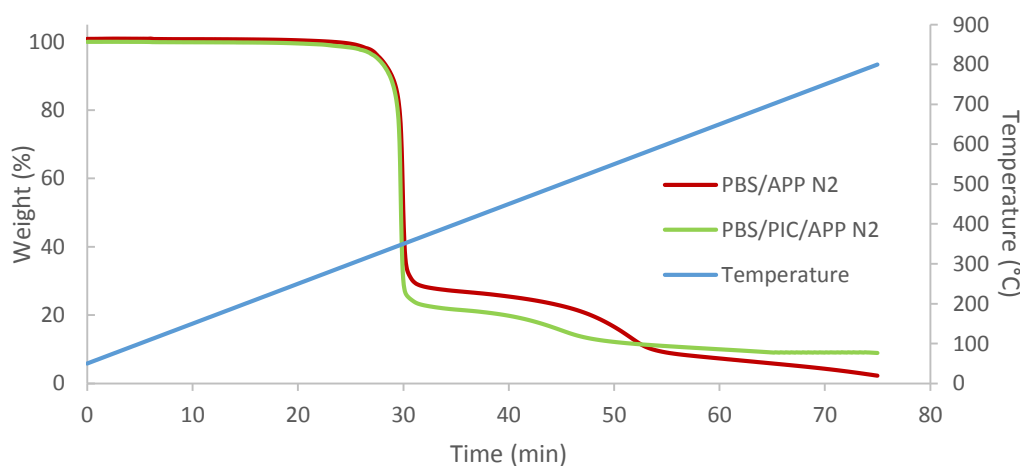


Figure 107 : Mass loss of PBS/APP and PBS/PIC/APP as function of time ($10^\circ\text{C}/\text{min}$, N_2)

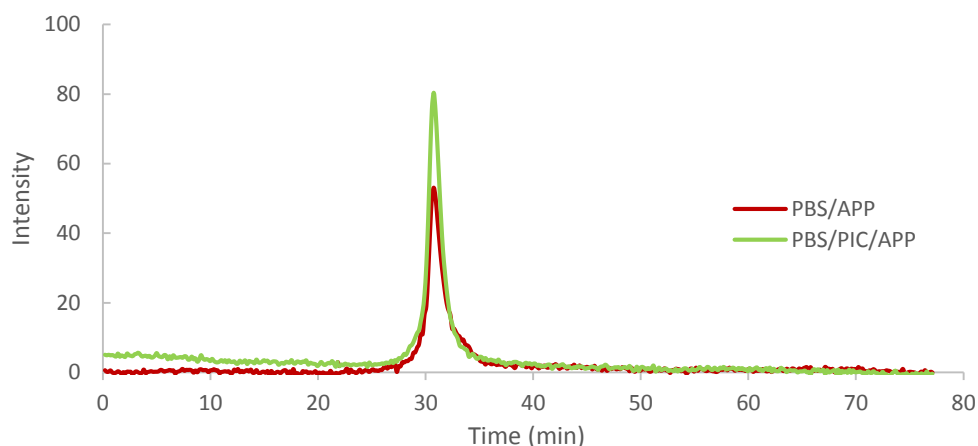


Figure 108: Chemigram of PBS/APP and PBS/PIC/APP during the TGA

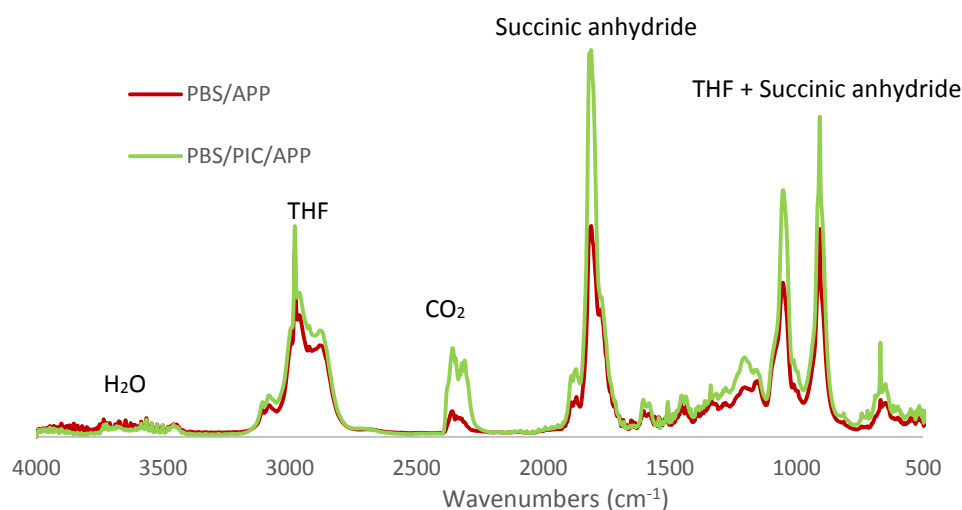


Figure 109: Infrared spectra of the decomposition products of PBS/APP and PBS/PIC/APP at 31 min

V.5 Investigation of char morphology

The morphology of the char is investigated at multi-scale using optical microscopy (mm scale) and scanning electron microscopy (SEM) (μm scale), then by using electron probe micro analysis (EPMA) (chemical composition at μm scale), the distribution of the phosphorus which can be involved in the mechanism of action is presented.

V.5.1 Char morphology investigated by optical microscope

The char residues of PBS/APP and PBS/PIC/APP were collected and cut on the side face. The flank side of out layer of the char is presented in **Figure 110 a)** for PBS/APP and **Figure 110 b)** for PBS/PIC/APP. The layer of the char of PBS/APP has 2.8 to 3.5 mm of thickness, whereas

the layer of the char of PBS/PIC/APP has only 1.0 to 1.4 mm of thickness. The outside of the char showed no significant difference between these two formulations (so the photo is not presented) on optical microscope. Then the inner side of these two chars layer are presented in **Figure 110 c)** for PBS/APP and **Figure 110 d)** for PBS/PIC/APP. The inner side of PBS/APP is porous with numerous holes of different sizes. However, PBS/APP/PIC has smaller and less holes on inner side of its char. The obvious differences of the chars between these two formulations may explain the different performance in the MLC test. Indeed, the char with less holes reduce the supply of the fuel (combustible gases that come from the decomposition of PBS) to the flame, which slowed down the burning process. Particularly, the mass loss curve **Figure 98 b)** measured during the MLC test evidences difference between PBS/APP and PBS/PIC/APP: the mass loss rate between 250 s to 500 s decreased from 0.17 %/s for PBS/APP to 0.13 %/s for PBS/PIC/APP.

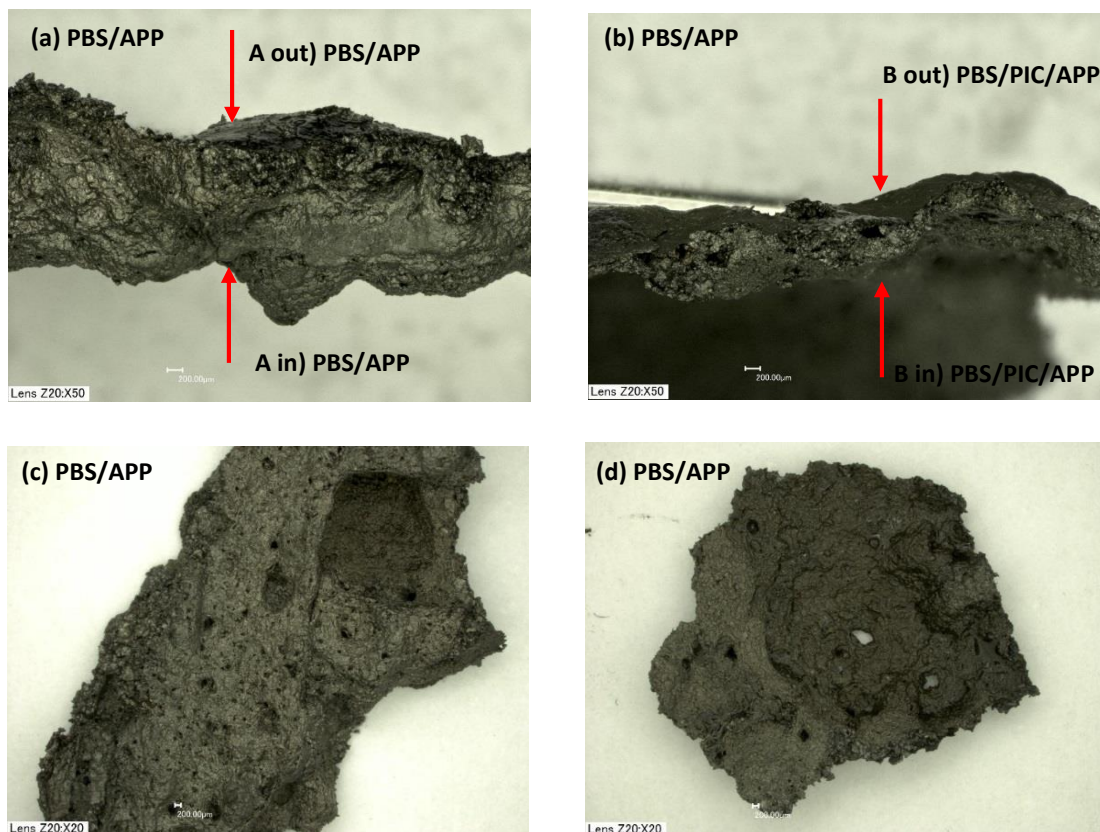


Figure 110: Observation of the residual char by optical microscope: a) flank of residual char layer of PBS/APP, b) flank of residual char layer of PBS/PIC/APP, c) inner surface of the char layer of PBS/APP, d) inner surface of the char layer of PBS/PIC/APP

V.5.2 Char morphology investigated by SEM and EPMA

Although the outside of the char layers showed no significant difference between PBS/APP and PBS/PIC/APP with optical microscope, they are now investigated by SEM (**Figure 111**) on a μm scale. On the exterior side, the surface of the char layer of PBS/PIC/APP is homogenous and no significant defect can be distinguished. Whereas, the surface of the char of PBS/APP has cracks and small holes.

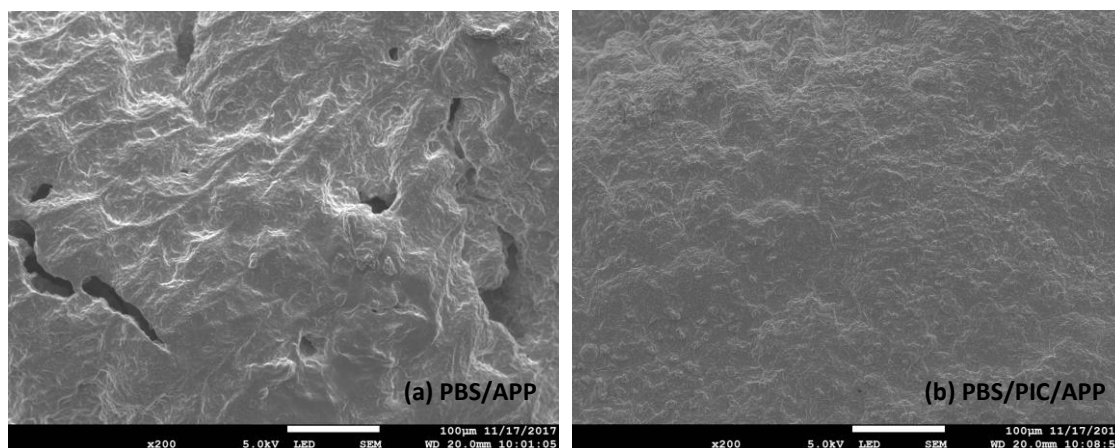
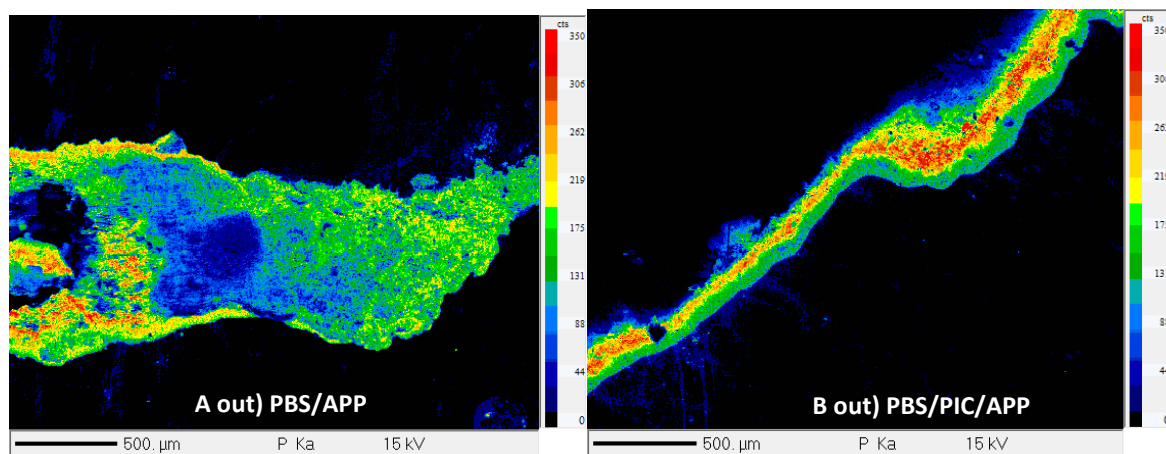


Figure 111: Observation of the residual char by SEM: a) surface of residual char of PBS/APP, b) surface of residual char of PBS/PIC/APP

At the same time of analysis of SEM, the phosphorus distribution is measured by EPMA. As presented in **Figure 110**, the outside of the char layer [A out) PBS/APP and B out) PBS/PIC/APP] and inner side of the char layer [A in) PBS/APP and B in) PBS/PIC/APP] were prepared to be analyzed. The exterior side of the char of PBS/PIC/APP shows that the phosphorus is mainly located on a very thin layer **Figure 112 B out**), which is 50-150 μm thick in size. Despite the low thickness of this layer, there is almost no defect and the phosphorus is highly concentrated on this thin layer. In the case of PBS/APP, on the exterior char, the distribution of phosphorus is on a thick layer of 500 to 1000 μm **Figure 112 A out**). The distribution of the phosphorus is not homogenous and zone without P in this layer can be distinguished. Note that the concentration of the phosphorus is lower than that found in the case of PBS/PIC/APP. The inner side of the char shows different behaviors for the two formulations as well. For PBS/PIC/APP, the distribution of the phosphorus shows the presence of cavity of different size **Figure 112 B in**). A mechanism of the formation of this cavity can be proposed: i) combustible gases were released during the decomposition of the polymer, and these gases diffuse to the surface of the char; ii) the char layer of PBS/PIC/APP which had some permeability cannot

perfectly isolate these gases from the flame, however it keeps still an internal pressure which reduce the diffusion speed of the combustible gases, and it can be confirmed by the mass loss curve (PBS/PIC/APP has less mass loss rate than PBS/APP); iii) thus the char of PBS/PIC/APP may have a lower permeability than PBS/APP and the combustible gases have a lower diffusion speed, hence the combustible gases formed cavity structure instead of creating 'tunnel' like passage in the char. Moreover, the concentration of the phosphorus is relatively low compared to the distribution of phosphorus on the exterior char, which reveals that phosphorus in the char is concentrated at the surface. In the case of PBS/APP, on the inner side of the char shows no cavity structure (close to a 'tunnel' like structure), and the concentration of the phosphorus is higher than that obtained in PBS/PIC/APP **Figure 112 A in**).

In conclusion, significant differences of the P distribution of the inner side and exterior side of the char layer can explain why smaller and less holes were observed on the surface of PBS/PIC/APP. Furthermore, the cavity structure in PBS/PIC/APP reveals a slower diffusion of the combustible gases in the char which can reduce the supply of 'fuel' in MLC test, thus lower pHRR and THR were obtained in the case of PBS/PIC/APP.



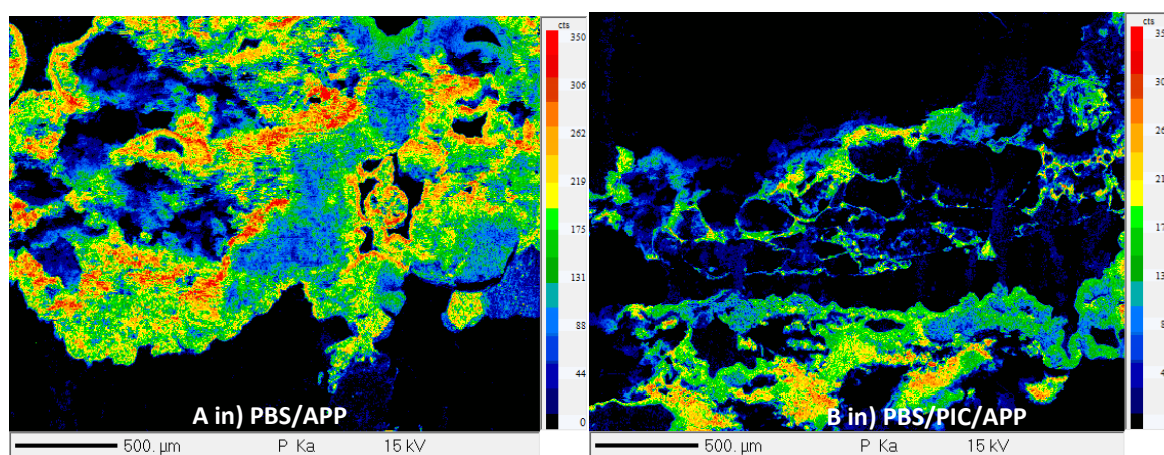


Figure 112: Phosphorus distribution of the residual char on the flank side: A out) out side of the char layer of PBS/APP, B out) out side of the char layer of PBS/PIC/APP, A in) inner side of the char layer of PBS/APP, B in) inner side of the char layer of PBS/PIC/APP

V.6 Mechanical analysis of the char

V.6.1 Measurement of viscosity

Rheology analysis of the char as a function of temperature is used to assess the expansion of the char in a polymeric material and its mechanical strength. In the last part, the distribution of the phosphorus on the char's layer of PBS/PIC/APP was observed to be formed differently than that of PBS/APP after MLC test. Thus, the measurement of the viscosity was undertaken to evaluate how the incorporation of PIC influences the charring process.

The viscosity of PBS/APP and PBS/PIC/APP are tested from 25 to 500°C with a heating rate of 10°C/min (**Figure 113**). The viscosity started to decrease at 115°C which corresponds to the melting temperature of PBS. The increase of the viscosity at 324°C for PBS/APP and PBS/PIC/APP is assigned to the formation of char. Note that PBS/APP and PBS/PIC/APP exhibit the same temperature of char formation. The experiment was done under thermo-oxidative condition and hence, the formation of char can be related to the formation of a transient char observed at 365°C in TG under air. Similar viscosities are measured indicating the charring is similar in terms of rheology whereas it is different in terms of chemical composition. Another parameter of the char, char resistance, can be a factor that impact the performance in fire test, and it is discussed in the next part.

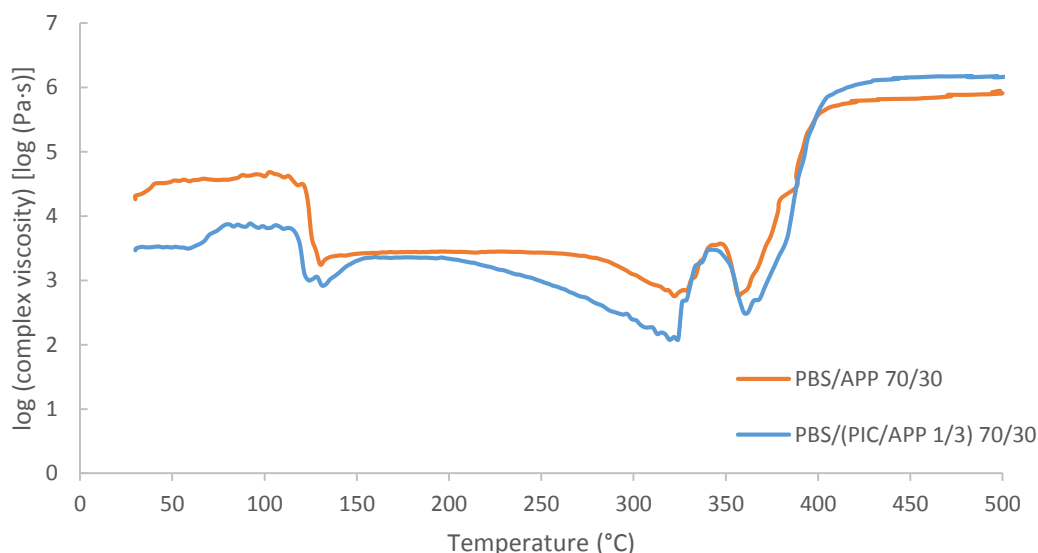


Figure 113: Viscosity of PBS/APP and PBS/PIC/APP (25-500°C, 10°C/min, under air)

V.6.2 Measurement of the char resistance

In the formulation PBS/PIC/APP, one reason that PBS/PIC/APP generates more residual char and lower THR, pHRR than PBS/APP in MLC test may be due to a better char resistance. The resistance of char is an important property which can govern (at least partially) the performance of a formulation acting in the condensed phase via a charring mechanism. The resistance of the char was measured by tracing the force applied on the char as function of the gap between the samples holder and the top plate in the rheometer. The char of PBS/APP and PBS/PIC/APP have steady viscosity at 500°C and it was shown the char was generated from 360 to 500°C. The temperature of this measurement was then maintained at 500°C during the test.

The char resistance results are presented in **Figure 114**. It can be seen from the curve that the force starts to increase (when the top plate starts touching the char) when the gap is 2 mm for PBS/PIC/APP and 2.3 mm for PBS/APP. The thickness of the sample was 1 mm before the experiment, hence it indicates that the char generated in the experiment is 2 times thicker than the original sample (the difference between 2 and 2.3 mm for the formulations is not significant) in our experimental conditions. The slope of the curves are traced, which shows that PBS/APP and PBS/PIC/APP have similar char resistance (5034 g/mm). Combining the results obtained with the measurement of the viscosity, it indicates that the chars formed by PBS/APP and PBS/PIC/APP have no significant differences of mechanical properties.

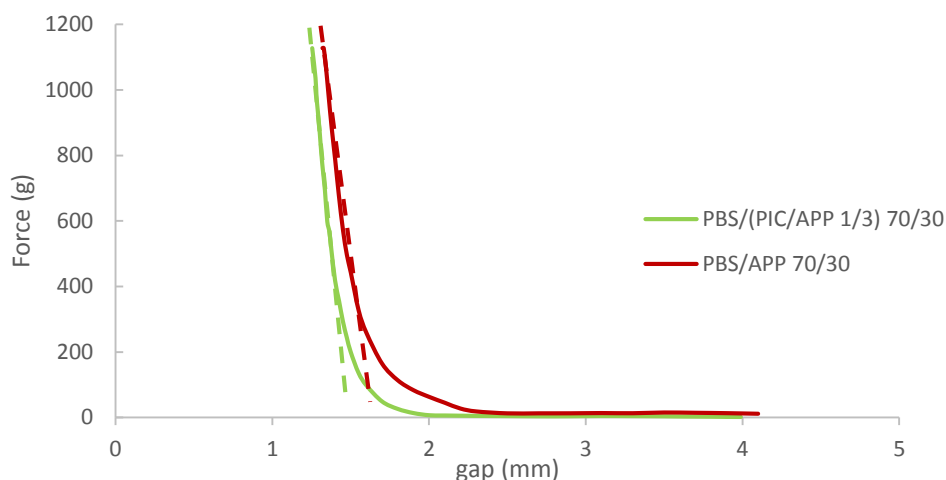


Figure 114: Char resistance of PBS/APP and PBS/PIC/APP

V.7 Proposed mechanism of PBS/PIC/APP during MLC test

With the evidences provided above, the mechanism of PBS/PIC/APP was determined (**Figure 115**). At the beginning of the test (before 100 s), PBS and PIC starts to melt and decompose releasing combustible gases (majorly THF and succinic anhydride). Meanwhile, APP decompose and release H₂O and NH₃. Then PBS/APP and PBS/PIC/APP start to burn at almost the same moment (100 s). Between 100 s to 450 s, intumescent char which is mainly consisted of orthophosphates, pyrophosphate, aliphatic and aromatic groups are formed. The char of PBS/PIC/APP showed a glass-type structure, and the phosphates concentrate on the surface of the char layer leading to lower mass loss rate, heat release rate than PBS/APP. After the combustion, cavity structure was found in the char of PBS/PIC/APP, whereas ‘tunnel’ type structure was found in the char of PBS/APP, which indicate a lower diffusion speed of the combustible gases presented in the char of PBS/PIC/APP. Therefore, PBS/PIC/APP has lower THR and pHRR than PBS/APP.

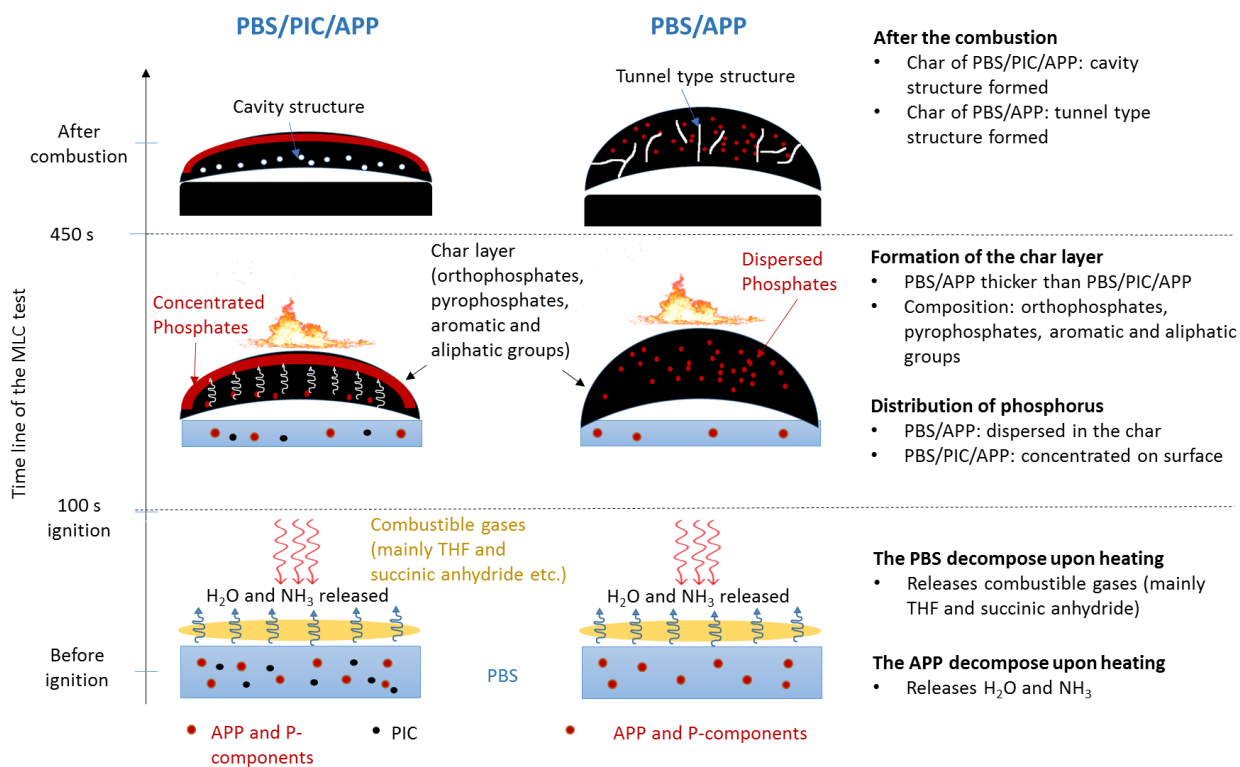


Figure 115: Proposed mechanism of PBS/PIC/APP and PBS/APP

V.8 Conclusion

This chapter discussed the investigation of the mode of action of a formulation PBS/(PIC/APP 1/3) 70/30, which showed good performance in the MLC test.

It was firstly showed that during the MLC test, the intumescent char formed by PBS/PIC/APP has better heating-rate-decreasing effect than that of PBS/APP. Secondly, the morphology of the char after the fire test showed the incorporation of PIC changed the distribution of the phosphorus in the char, which influences the performance of the formulations. Thirdly, when PIC was incorporated, the mechanical properties of the char were not significantly modified whereas the stability of the char at a high temperature was significantly improved. Finally, it was shown that the incorporation of PIC has no influence on the composition of the released gases during the decomposition, but it created a glass type char. Furthermore, according to the mass loss measured in the MLC test, the char of PBS/PIC/APP may slow down the diffusion of the combustible gases which caused smaller and less hole than PBS/APP and the cavity structure in the char. It confirms that the performance of the char is the major factor to influence the MLC results.

In conclusion, the addition of only 2.5 wt% of PIC in PBS/APP enhanced the performance of the system in MLC test. It evidences that isosorbide-based compounds can act as carbonization agent in an intumescent FR system. Moreover, the application of PIC improves the ratio of bio-based components and the flame retardancy of PBS/APP, the double benefits lead to more ideas of using the bio-based components to flame retard polymeric materials.

Nevertheless, it is still unknown if this formulation can be used to flame retard some other types of polymers and there are still some understanding of the formulation are not clear. Combining with the questions left in the understanding of action of DOPO, further studies need to be carried out to the full comprehension of different formulations to flame retard PBS. In this context, a general conclusion and a proposition of the outlook of this study are presented in the next parts.

General Conclusion

This study was dedicated to the development of flame retarded polybutylene succinate (PBS), a bio-based polymer, which possess good mechanical properties and biodegradability, by various different approaches. In this context, modifications of isosorbide were achieved. Then isosorbide and poly(isosorbide) carbonate (PIC) were blended with PBS and APP to form intumescent flame retardant system acting as carbonization agent. DOPO was incorporated in PBS as well.

The incorporation of DOPO in PBS had a significant improvement of the ignition time in MLC test especially under a relatively low heat flux (25 kW/m^2). In UL-94 test, the classification was also improved up to V-0 rating. The mechanism of DOPO was successfully investigated, which indicates that the phosphorus species (degradation products and/or sublimated DOPO) quench the high energy free radicals in the gaseous phase to poison the flame. Furthermore, an original test method permits the measurement of the surface temperature of the melting drop in UL-94 test, which shows that the lower temperature of drops in PBS/DOPO than that of neat PBS governed their different classification.

As for investigation of the mode of action of PIC in an intumescent flame retardant system, a better charring effect of PIC/APP than PBS/APP leads to the formation of a better char layer. This char layer of PBS/PIC/APP contains a higher concentration of phosphorus than that of PBS/APP. Obviously, this char layer decreased the mass loss rate and the diffusion speed of the combustible gases (feeding to the flame), and thus lower temperature under the char layer is observed as well. Therefore the decreasing of pHRR and THR in MLC test can be attributed to these improvement brought by the incorporation of PIC.

As a conclusion, our study provides multiple methods to improve the flame retardancy of PBS: i) isosorbide modification confirmed the possibility of using synthesized bio-based flame retardants for PBS, ii) un-modified DOPO permits a flame retardant action for PBS mainly in the gaseous phase, iii) incorporation of PIC in PBS/APP provides a flame retardant action in the condensed phase by using a bio-based polymer as charring agent. Furthermore, we have achieved not only the development of new flame retarded PBS formulations, but also the design of the new characterization methods for understanding the mode of action. The

success of using un-modified DOPO indicates the possibility of its application for other polymers that possess low processing temperature, and the use of PIC as carbonization agents increased our knowledge of using bio-based compounds as carbonization agent in an intumescent flame retardant system. The information provided in this thesis can therefore be used as reference for the future studies.

Outlook

The work of this PhD has provided multiple approaches to flame retard PBS, particularly the mode of action of un-modified DOPO and PIC were deeply investigated. However, there are still some understandings which are not clear and which need to be furtherly studied.

For the formulation of PBS/DOPO, it was assumed that the flame retardant action occurred in the gaseous phase was led by a free radical quenching process, which was not directly observed in our study. It is well known that the free radicals after thermal decomposition could be investigated by electron paramagnetic resonance as mentioned in literatures,^{184,185,186} hence the free radical produced in PBS/DOPO should be detected with this technique to prove our assumption. Moreover, caused by the low decomposition/sublimation temperature and the high reactivity of DOPO, un-modified DOPO was barely applied for polymers other than epoxy resin. The dramatical extension of the ignition time found in PBS/DOPO reveals that the un-modified DOPO has the potential to be applied for some other polymers which possess low processing temperature (e.g. polycaprolactone). It should be also mentioned that efforts has been undertaken to combine the formulation of PBS/DOPO with additives which can be effective in the condensed phase, but the 'double' effects that act in the gaseous phase and condensed phase were not appeared as expected. Investigation of the chemical composition of the condensed phase and the gaseous phase may provide a better understanding of this point.

For the formulation of PBS/PIC/APP, the deceasing of diffusion rate of the combustible gases (bubbles) was conjectured according to the decreasing of mass loss rate. However, our study had no direct evidence of this conclusion. Modeling of the growth rate, migration, and thermal effects of the bubbles in intumescence was presented by Butler et al.,¹⁸⁷ a similar study which correspond to our experimental condition can be a solution to explain the behavior of the intumescence of PBS/PIC/APP. In the literature, synergists such as POSS, organo-nanoclay and graphene that works in the intumescent flame retardant system has been described to flame retard PBS.^{188,189,190} Thus, it is interesting to investigate if these synergists can/cannot enhance the formulation PBS/PIC/APP. Besides polycarbonate, polyamide¹⁹¹ and polyurethane¹⁹² can also act as carbonization agent in an intumescent flame retardant system. Thus, isosorbide

based polyamide¹⁹³ and polyurethane¹⁹⁴ may act as the charring agent in PBS/APP as well. This study permits to compare the charring effect of different types of isosorbide based polymers.

Considering the modification of isosorbide, the secondary hydroxyl groups is not reactive enough to react with some desired functional groups. Amination^{116,117,118} and epoxidation^{109,110} of isosorbide acting as intermediates may provide more possibility of the modification of the isosorbide.

List of Figures and Tables

Figure 1: Global polymer market share in %	15
Figure 2: Number of publications and patents containing 'polybutylene succinate' and 'polybutylen succinate + flame retardancy' (scifinder march 2018).	16
Figure 3: Two steps synthesis route of PBS	21
Figure 4: Two synthesis routes of succinic acid	22
Figure 5: Relationship with molecular weight, melt flow rate (MFR) and processing methods of PBS and PBSA.....	24
Figure 6: Degradation of PBS in moisture soil	24
Figure 7: Derivative mass loss (DTG) of 1) polybutylene succinate 2) polyethylene succinate (10°C/min N ₂).....	25
Figure 8: Formation of alkene and carboxylic groups at the chain end	26
Figure 9: Decarboxylation at the end of chains	26
Figure 10: Formation of cyclic compounds	26
Figure 11: General aspects of fire showed on 'Fire Triangle'	27
Figure 12: Global FRs share by type in 2016.....	28
Figure 13: Mechanism of radical quenching by halogenated FRs, X = F, Cl, Br and I, R = organic group	29
Figure 14: Fire retardant action of triphenylphosphine oxide and triphenyl phosphate in gaseous phase (M is a third body species)	30
Figure 15: Commercially available aluminium phosphinates (Exolit OP 930/935)	31
Figure 16: Aromatic phosphates	31
Figure 17: 9,10-dihydro-9-oxa-10-phosphaphenanthrene-10-oxide (DOPO).....	31
Figure 18: Degradation of Magnesium hydroxide and aluminum hydroxide.....	33
Figure 19: structure of polydimethylsiloxane (PDMS)	34
Figure 20: Structure of montmorillonite	35
Figure 21: Structure of graphene	36
Figure 22: Structure of POSS	36
Figure 23: Synthesis route of isosorbide	37
Figure 24: Isosorbide and its isomers	37
Figure 25: Isosorbide based polymers and aminated, diisocyanated isosorbide	39
Figure 26: Phosphorus ester starting from a combination of isosorbide and 10-undecenoic acid	41
Figure 27: Chemical structure of isosorbide based fire retardants proposed by BASF Company	42
Figure 28: Isosorbide based bis-phosphorus ester	43
Figure 29: polymer based on isosorbide and phosphorus compound.....	43
Figure 30: Chemical structure of APP	44
Figure 31: Chemical structure of MP, MPi, MHP	45
Figure 32: Synthesis of copolyester based on monomers modified by DOPO	46
Figure 33: modification of isosorbide with sulfur, silicon and phosphorus compounds	54
Figure 34: chemical structure of Di-tosyl-isosorbide (Dti)	55
Figure 35: Chemical structure of Polydimethylsiloxane isosorbide (PDMSi)	55
Figure 36: Chemical structure of Polymethylphenylsiloxane isosorbide (PMPSi).....	56
Figure 37: Chemical structure of Polyphenylphosphate isosorbide (PPPAI).....	57
Figure 38: Chemical structure of polyphenylphosphonate isosorbide (PPPI).....	58
Figure 39: Chemical structure of Diphenylphosphinate isosorbide (DPPII)	58
Figure 40: Chemical structure of Diphenylphosphate isosorbide (DPPI)	59

Figure 41: Chemical structure of Di-DOPO-isosorbide (DDi).....	59
Figure 42: DSM micro extruder.....	60
Figure 43: The experimental set-up for the UL-94 test.....	62
Figure 44: a) Instrumentation of UL-94 b) Position of thermocouple embedded in the bar	63
Figure 45: Repeatability study of temperature measured by Thermocouple (T1)	63
Figure 46: different results obtained with (a) conventional IR camera and (b) IR camera with a specific filter	64
Figure 47: configuration of the mass loss cone	65
Figure 48: rheometer ARES 20A and the parameter recorded	66
Figure 49: Schematic presentation of the Py-GCMS device.....	71
Figure 50: Synthesis of Di-tosyl-isosorbide (Dti)	78
Figure 51: Thermal stability of Di-tosyl-isosorbide (Dti) (10°C/min under air).....	79
Figure 52: MLC test of PBS and PBS/Dti (50 x 50 x 3 mm ³ , 35 kW/m ² , 25 mm).....	79
Figure 53: Synthesis of 1) polydimethylsiloxane isosorbide (PDMSi) and 2) polymethylphenylsiloxane isosorbide PMPSi	80
Figure 54: Thermal stability of polydimethylsiloxane isosorbide (PDMSi) and polymethylphenylsiloxane isosorbide (PMPSi) (10°C/min under air).....	81
Figure 55: MLC tests of PBS with PDMSi, PMPSi (50 x 50 x 3 mm ³ , 35 kW/m ² , 25 mm).....	82
Figure 56: MLC tests of PBS with PDMSi, PMPSi and APP (50 x 50 x 3 mm ³ , 35 kW/m ² , 25 mm)	82
Figure 57: MLC residual char of PBS/PDMSi/APP 70/10/20 (left) and PBS/PMPSi/APP 70/10/20 (right)	83
Figure 58: MLC results of PC and PC/PMPSi 90/10 (50 x 50 x 3 mm ³ , 50 kW/m ² , 25 mm)	84
Figure 59: MLC Residual char of PC/PMPSi	84
Figure 60: Synthesis of (1) polyphenylphosphate isosorbide (PPPAI), (2) polyphenylphosphonate isosorbide (PPPI), (3) Di-DOPO-isosorbide (DDi), (4) diphenylphosphinate isosorbide (DPPII), (5) diphenylphosphate isosorbide (DPPI).....	85
Figure 61: Thermal stability of PPPAI, PPPI, DPPI, DPPII and DDi under a) Air and b) N ₂ (10°C/min) ...	87
Figure 62: MLC test of PBS with PPPI, PPPAI, DPPII, DPPI and DDI (50 x 50 x 3 mm ³ , 35 kW/m ² , 25 mm)	88
Figure 63: MLC tests of PBS with APP and isosorbide (50 x 50 x 3 mm ³ , 35 kW/m ² , 25 mm)	90
Figure 64: MLC Residual char of PBS/(isosorbide/APP 1/3) 70/30.....	91
Figure 65: MLC tests of PBS with PIC and APP (50 x 50 x 3 mm ³ , 35 kW/m ² , 25 mm)	92
Figure 66: MLC residual char of PBS/APP (left) and PBS/(PIC/APP 1/3) 70/30 (right)	93
Figure 67: Thermal stability of PBS and DOPO (10°C/min, under N ₂)	94
Figure 68: MLC test of PBS and PBS/DOPO (50 x 50 x 3 mm ³ , 35 kW/m ² , 25 mm)	94
Figure 69: Chemical structures of a) DOPO-3-propanamide (DOPO-ACA) b) DOPO-1-oxophospha-4-hydroxymethyl-2,6,7-trioxabicyclo[2,2,2]octane (DOPO-PEPA) c) DOPO-ethane-1,2-diylbis(azanediyl) (DOPO-EDA).....	95
Figure 70: MLC tests of PBS with DOPO derivatives (50 x 50 x 3 mm ³ , 35 kW/m ² , 25 mm).....	96
Figure 71: Thermal stability of neat PBS, APP and MPP (10°C/min under air).....	97
Figure 72: MLC tests of PBS with APP, MPP and DOPO (50 x 50 x 3 mm ³ , 35 kW/m ² , 25 mm)	98
Figure 73: Thermal stability of ATH, MDH, MgCO ₃ and CaCO ₃ (10°C/min under N ₂)	99
Figure 74: MLC tests of PBS with metal hydroxides and DOPO (50 x 50 x 3 mm ³ , 35 kW/m ² , 25 mm)	100
Figure 75: MLC test of PBS with carbonate salts and DOPO (50 x 50 x 3 mm ³ , 35 kW/m ² , 25 mm)...	101
Figure 76: MLC tests of PBS with carbon nanotube and DOPO (50 x 50 x 3 mm ³ , 35 kW/m ² , 25 mm)	102
Figure 77: Fire behavior of a) PBS and b) PBS/DOPO in MLC test with different heat flux	108

Figure 78: Estimation of critical heat flux of PBS/DOPO in the case of thermally thick or thermally thin material	110
Figure 79: Petrella plots traced in an applied range of heat flux for PBS and PBS/DOPO	111
Figure 80: Mass loss of PBS and PBS/DOPO under air at 10°C/min	112
Figure 81: Mass loss of PBS and PBS/DOPO under N ₂ at 10°C/min	113
Figure 82: Pyrogramme of a) neat PBS and b) PBS/DOPO	115
Figure 83: Temperature measured during MLC by thermocouple embedded in plaques of PBS and PBS/DOPO (35kW/m ²).....	117
Figure 84: Mass loss of PBS and PBS/DOPO as function of time with similar heating rate to MLC test	118
Figure 85: FTIR spectra of degradation products of PBS and PBS/DOPO at different time	119
Figure 86: FTIR spectra of released gases at 119s for neat PBS and 410s for PBS/DOPO (35 kW/m ²).....	120
Figure 87: Intensity evolution of a) THF (2981 cm ⁻¹) and b) succinic anhydride (1811 cm ⁻¹) as function of time during MLC (35 kW/m ²)	121
Figure 88:a) MLC curve of PBS and PBS/DOPO, b) quantification of released CO, CO ₂ and H ₂ O, c) intensity of total gases release (Gram-Schmidt)	123
Figure 89: Mechanism of PBS/DOPO during a MLC test	125
Figure 90: Residual Bars of PBS (left) and PBS/DOPO (right) after the UL-94 testing (3.2 mm).	126
Figure 91: Results of the thermocouples of PBS and PBS/DOPO during UL-94 testing.	128
Figure 92: Temperature evolution as a function of the emissivity set to the IR camera	130
Figure 93: Temperature evolution of a single drop of neat PBS at the end of ignition	131
Figure 94: a) Temperature evolution of a single drop of PBS/DOPO at the end of first ignition b) Temperature evolution of a single drop of PBS/DOPO at the end of second ignition	133
Figure 95: temperature of the drops detaching the bar.....	133
Figure 96: Images of the drops detaching from the bar captured by IR camera a) Neat PBS b) PBS/DOPO.....	135
Figure 97: Viscosity as function of temperature of PBS and PBS/DOPO	136
Figure 98: a) MLC test of PBS, PBS/APP and PBS/PIC/APP, b) mass loss during the MLC test, c) temperature measured by the thermocouples.....	144
Figure 99: Position of the thermocouples (left), in real situation (right).....	145
Figure 100: Solid state NMR MAS ³¹ P spectra of PBS/APP at different stage	147
Figure 101: Solid state NMR MAS ³¹ P spectra of PBS/PIC/APP at different stage.....	148
Figure 102: Nomenclature of the different types of phosphate	148
Figure 103: Solid state NMR MAS ¹³ C spectra of PBS/APP at different stage	149
Figure 104: Solid state NMR MAS ¹³ C spectra of PBS/PIC/APP at different stage	150
Figure 105: Thermal degradation of PBS with the additives under thermo-oxidative condition (10°C/min, Air).....	152
Figure 106: Differential TGA of PBS/APP, PIC/APP and PBS/PIC/APP under thermo-oxidative condition (10°C/min, Air).....	152
Figure 107 : Mass loss of PBS/APP and PBS/PIC/APP as function of time (10°C/min, N ₂)	153
Figure 108: Chemigram of PBS/APP and PBS/PIC/APP during the TGA	154
Figure 109: Infrared spectra of the decomposition products of PBS/APP and PBS/PIC/APP at 31 min	154
Figure 110: Observation of the residual char by optical microscope: a) flank of residual char layer of PBS/APP, b) flank of residual char layer of PBS/PIC/APP, c) inner surface of the char layer of PBS/APP, d) inner surface of the char layer of PBS/PIC/APP.....	155
Figure 111: Observation of the residual char by SEM: a) surface of residual char of PBS/APP, b) surface of residual char of PBS/PIC/APP	156

Figure 112: Phosphorus distribution of the residual char on the flank side: A out) out side of the char layer of PBS/APP, B out) out side of the char layer of PBS/PIC/APP, A in) inner side of the char layer of PBS/APP, B in) inner side of the char layer of PBS/PIC/APP 158

Figure 113: Viscosity of PBS/APP and PBS/PIC/APP (25-500°C, 10°C/min, under air) 159

Figure 114: Char resistance of PBS/APP and PBS/PIC/APP 160

Figure 115: Proposed mechanism of PBS/PIC/APP and PBS/APP 161

<i>Table 1: Mechanical properties of PBS, LDPE, HDPE and PP</i>	23
<i>Table 2: The different criteria for the classifications of UL-94 test</i>	62
<i>Table 3: Results of MLC tests for PBS and PBS/Dti</i>	79
<i>Table 4: Results of MLC tests of PBS with PDMSi, PMPSi and APP</i>	82
<i>Table 5: Results of MLC test of PC and PC/PMPSi</i>	84
<i>Table 6: Thermal stability and residues of phosphorus modified isosorbide</i>	87
<i>Table 7: Results of MLC test of PBS with PPPI, PPPAI, Di-DOPO-isosorbide, DPPII and DPPI</i>	88
<i>Table 8: Results of MLC tests of PBS with APP and isosorbide</i>	90
<i>Table 9: Results of MLC tests of PBS with PIC and APP</i>	92
<i>Table 10: Results of MLC test of PBS and PBS/DOPO</i>	94
<i>Table 11: Results of MLC tests of PBS with DOPO derivatives</i>	96
<i>Table 12: Results of MLC test of PBS with APP, MPP and DOPO</i>	98
<i>Table 13: Results of MLC tests of PBS with metal hydroxides and DOPO</i>	100
<i>Table 14: Results of MLC tests of PBS with carbonate salts and DOPO</i>	101
<i>Table 15: Results of MLC tests of PBS with carbon nanotube and DOPO</i>	103
<i>Table 16: Results of MLC test of PBS and PBS/DOPO with different heat flux</i>	109
<i>Table 17: Degradation products of PBS/DOPO analyzed by GC/MS</i>	115
<i>Table 18: Elemental analysis of PBS at different stage of MLC test</i>	124
<i>Table 19: Elemental analysis of PBS/DOPO at different stage of MLC test</i>	124
<i>Table 20: Temperature gradient inside the bar of PBS and PBS/DOPO at the end of first ignition</i>	129
<i>Table 21: temperature measured by IR camera with an estimated emissivity when drops detach the bar and when they touch the cotton</i>	135

Appendix

Grades

1000 SERIES (PBS) AND 3000 SERIES (PBSA)

	MFR (g/10min)	Grade	Process
Bionolle™ 1000 series polybutylene succinate (PBS) -O-(CH ₂) ₄ -O-CO-(CH ₂) ₂ -CO-	1-3	1001 MD 3001 MD	Blown film extrusion Extrusion blow molding
Bionolle™ 3000 series polybutylene succinate adipate (PBSA) -O-(CH ₂) ₄ -O-CO-(CH ₂) _{2,4} -CO-	4-9 20-34	1903 MD 1020 MD, 3020 MD	Foam extrusion Injection molding

Two different grades of Bionolle™ grades are commercially available. Polybutylene succinate (PBS), known as the 1000 series, and polybutylene succinate/adipate (PBSA), the 3000 series. High modulus and slow biodegradability can be seen in the 1000 series whereas the 3000 series exhibits low modulus and fast biodegradability. With specific formulations, rigidity and speed of biodegradation can be controlled.

	Bionolle™		Conventional Plastics		
	1000 series	3000 series	PP	HDPE	LDPE
Density (g/cm ³)	1.26	1.23	0.9	0.95	0.92
Heat of Combustion (kJ/g)	23.6	23.9	43.9	46	46
HDT at 0.45MPa (°C)	97	69	145	110	88
Degree of Crystallinity (%)	35-45	20-35	56	69	49
Melting Point (°C)	114	94	164	130	108
Glass Transition Temperature (°C)	-32	-45	5	-120	-120

Typical properties; not to be construed as guaranteed values.

Mechanical Properties

HIGH QUALITY PRODUCT

Bionolle™ 1001 MD and 3001 MD have a MFR of less than 3 g/10 min. This makes these grades suitable for blown-film extrusion and facilitates the production of thin, high quality film by using conventional blown film extruders. Film made of Bionolle™ shows excellent mechanical properties similar to film made of LLDPE.

			Bionolle™		LLDPE
			1001 MD	3001 MD	
Tensile Stress at Yield (MPa)	ISO 527-3	MD	31	18	13
		TD	31	18	11
Tensile Stress at Break (MPa)	ISO 527-3	MD	62	40	43
		TD	59	45	22
Tensile Elongation at Break (%)	ISO 527-3	MD	660	780	370
		TD	710	970	420
Young's Modulus (MPa)	ISO 527-3	MD	470	320	330
		TD	540	340	370
Tear Strength (N/mm)	ISO 6383-2	MD	3.6	4.4	10
		TD	11	23	200
Impact Strength (kJ/m)	ASTM D3420		24	29	22
Heat Seal Strength (N)	SDK method ^{*)}		3.5	1.5	1.2
Haze (%)	ISO 13468-1		42	20	7

^{*)} 120 °C, 0,2 MPa, 1 sec., 15 mm in width

Typical properties; not to be construed as guaranteed values.

Appendix 1: Properties of the used PBS in this work

References

- ¹ Plastics - the Facts 2017 - An analysis of European plastics production, demand and waste data, PlasticsEurope, 2017.
- ² Fire in the United States 2006-2015 (19th Edition), U.S. fire administration, 2017.
- ³ Ishioka R, Kitakuni E, Ichikawa Y (2002) Aliphatic polyesters: "Bionolle". In: Doi Y, Steinbüchel A (eds) Biopolymers, vol. 4, Polyesters III Applications and commercial products. Wiley-VCH, Weinheim, 275
- ⁴ T. Fujimaki, Processability and properties of aliphatic polyesters, 'BIONOLLE', synthesized by polycondensation reaction, *Polymer Degradation and Stability*, 1998, 59, 209
- ⁵ Market Research Store, march 2018, <http://www.marketresearchstore.com/news/global-isosorbide-market-176>
- ⁶ Roquette, activity and sustainable development report 2015, March 2018, https://www.roquette.com/-/media/corporate/embrace-today/embrace-today-_downloads/roquette-annual-report-2015-en-accessible-bd.pdf?la=en.
- ⁷ J. Xu, B. H. Guo, Microbial succinic acid, its polymer poly(butylene succinate), and applications. In: Chen, G. Q.(Ed.), *Plastics from Bacteria: Natural Functions and Applications*, Microbiology Monographs, Vol. 14, Springer-Verlag, Berlin, Heidelberg 2010, 347
- ⁸ N. Jacquel, F. Freyermouth, F. Fenouillot, A. Rousseau, J. P. Pascault, P. Fuertes, R. Saint-Loup, Synthesis and Properties of Poly(butylene succinate): Efficiency of Different Transesterification Catalysts, *Journal of Polymer Science Part A: Polymer Chemistry*, 2011, 49, 5301
- ⁹ L. P. Ferreira, A. N. Moreira, J. Carlos Pinto, F. G. de Souza, Synthesis of Poly(butylene succinate) Using Metal Catalysts, *Polymer Engineering and Science*, 2015, 3, 1889
- ¹⁰ Novament, march 2018, <http://www.novamont.com/eng/read-press-release/mater-biotech/>
- ¹¹ Marketsandmarkets, march 2018, <https://www.marketsandmarkets.com/Market-Reports/succinic-acid-market-402.html>
- ¹² Transparency Market Research, march 2018, <https://www.transparencymarketresearch.com/bio-succinic-acid.html>
- ¹³ H. Song, S. Y. Lee, Production of succinic acid by bacterial fermentation, *Enzyme and Microbial Technology*, 2006, 39, 352
- ¹⁴ L. Dammer, M. Carus, A. Raschka, L. Scholz, Market Developments of and Opportunities for bio-based products and chemicals, 2013, reference number 52202, nova-Institute for Ecology and Innovation
- ¹⁵ Y. Yasuda and E. Takiyama, Polyester injection-molded articles with good biodegradability and heat stability, US Patent, 5391644, 1995
- ¹⁶ M. Imaizumi, M. Kotani, R. Kamei and E. Takiyama, US Patent 5658627, 1997.
- ¹⁷ T. Taka, Y. Yasukawa and E. Takiyama, Heat-stable and biodegradable polyester films, US Patent 5324794, 1994
- ¹⁸ A. Nakamura, R. Kamei, T. Takahashi, S. Terazono and E. Takiyama, Polyester flat and split yarn, US Patent 5348700, 1994.
- ¹⁹ T. Takahashi, H. Uda, A. Nakamura, R. Kamei, and E. Takiyama, Biodegradable aliphatic polyester fibers, US Patent 5349028, 1994
- ²⁰ J. H. Zhao, X. Q. Wang, J. Zeng, G. Yang, F. H. Shi, Q. Yan, Biodegradation of Poly(Butylene Succinate) in Compost, *Journal of Applied Polymer Science*, 2005, 97, 2273
- ²¹ M.L. Tansengco and Y. Tokiwa, Comparative population study of aliphatic polyesters-degrading microorganisms at 50°C, *Chemistry Letters*, 1998, 10, 1043

References

- ²² M. Nishioka, T. Tuzuki, Y. Wanajyo, H. Oonami, and T. Horiuchi, Biodegradation of BIONOLLE, in *Biodegradable Plastics and Polymers*, Vol. 12(3), ed. Y. Doi and K. Fukuda. Elsevier, Amsterdam, 1994, 584.
- ²³ Y. J. Phua, W. S. Chow, Z. A. Mohd Ishak, The hydrolytic effect of moisture and hygrothermal aging on poly(butylene succinate)/organo-montmorillonite nanocomposites, *Polymer Degradation and Stability*, 2011, *96*, 1194
- ²⁴ W. K. Lee and J. A. Gardella, Hydrolytic Kinetics of Biodegradable Polyester Monolayers, *Langmuir*, 2000, *16*, 3401
- ²⁵ H. Elwathig, W. You, J. He, M. H. Yu, Dynamic Mechanical Properties and Thermal Stability of Poly(lactic acid) and Poly(butylene succinate) Blends Composites, *Journal of Fiber Bioengineering and Informatics*, 2013, *6*, 85
- ²⁶ K. Chrissafis, K.M. Paraskevopoulos and D.N. Bikiaris, Thermal degradation mechanism of poly(ethylene succinate) and poly(butylene succinate): comparative study, *Thermochimica Acta*, 2005, *435*, 14
- ²⁷ X.S. Wang, X.G. Li and D. Yan, High-resolution thermogravimetric analysis of poly(trimethylene terephthalate) with different molecular weights, *Polymer Testing*, 2000, *20*, 491
- ²⁸ H. Ohtani, T. Kimura, K. Okamoto and S. Tsuge, CHARACTERIZATION OF POLYURETHANES BY HIGH-RESOLUTION PYROLYSIS-CAPILLARY GAS CHROMATOGRAPHY, *Journal of Analytical and Applied Pyrolysis*, 1987, *12*, 115
- ²⁹ O. Persenaire, M. Alexandre, P. Degee and P. Dubois, Mechanisms and Kinetics of Thermal Degradation of Poly(E-caprolactone), *Biomacromolecules*, 2001, *2*, 288
- ³⁰ F.D. Kopinke, M. Remmler, K. Mackenzie, K. Möder and O. Wachsen, Thermal decomposition of biodegradable polyesters. II. Poly(lactic acid), *Polymer Degradation and Stability*, 1996, *53*, 329
- ³¹ F.D. Kopinke, M. Remmler and K. Mackenzie, Thermal decomposition of biodegradable polyesters. I: poly(β -hydroxybutyric acid), *Polymer Degradation and Stability*, 1996, *52*, 25
- ³² H. Sato, M. Furuhashi, D. Yang, H. Ohtani, S. Tsuge, M. Okada, K. Tsunoda and K. Aoi, A novel evaluation method for biodegradability of poly(butylene succinate-co-butylene adipate) by pyrolysis-gas chromatography, *Polymer Degradation and Stability*, 2001, *73*, 327
- ³³ Y.F. Shih, Thermal Degradation and Kinetic Analysis of Biodegradable PBS/Multiwalled Carbon Nanotube Nanocomposites, *Journal of Polymer Science: Part B: Polymer Physics*, 2009, *47*, 1231
- ³⁴ G. L. Nelson, A. B. Morgan, and C. A. Wilkie, Fire retardancy in 2009, *ACS symposium series*, 2009, *1013*, 1
- ³⁵ D. Price, G. Anthony, and P. Carty, *Fire Retardant Materials*, ed. Woodhead publishing Ltd., 2001
- ³⁶ Wakeupuk, march 2018, <http://wakeupuk.org/flame-retardant-chemicals-market-2016-industry-size-growth-analysis-2020/>
- ³⁷ Flameretardants-online, march 2018, <https://www.flameretardants-online.com/flame-retardants/market>
- ³⁸ S. Bocchini and G. Camino, Hlogen-Containing Flame Retardants, In *Fire Retardancy of Polymeric Materials*, J. Green, A. F. Grand, Wilkie, C.A., Eds., CRC Press: FL, USA, 2000, 75.
- ³⁹ M. J. Day, D. V. Stamp, K. Thompson and G. Dixon-lewis, Inhibition of hydrogen-air and hydrogen-nitrous oxide flame by halogen compounds, Thirteenth Symposium (International) on Combustion, the Combustion Institute, Pittsburgh. PA, 1971, 705
- ⁴⁰ J. Green, A Review of Phosphorus- Containing Flame Retardants, *Journal of Fire Sciences*, 1996, *14*, 353
- ⁴¹ B. Perret, B. Scharrel, K. Stoss, M. Ciesielski, J. Diederichs and M. Döring, Novel DOPO-based flame retardants in high-performance carbon fibre epoxy composites for aviation, *European Polymer Journal*, 2011, *47*, 1081
- ⁴² X. Wang, Y. Hu, L. Song, W. Y. Xing, H. D. Lu and P. Lv, Flame retardancy and thermal degradation mechanism of epoxy resin composites based on a DOPO substituted organophosphorus oligomer, *Polymer* 2010, *51*, 2435
- ⁴³ J. W. Gu, G. C. Zhang, S. L. Dong, Q. Y. Zhang and J. Kong, Study on preparation and fire retardant mechanism analysis of intumescent flame-retardant coatings, *Surface and Coatings Technology*, 2007, *201*, 7835

References

- ⁴⁴ S.R. Sandler, Polyester resins flame retarded by poly(metal phosphinate)s, Pennwalt, U.S. Patent 4,180,495, 1979.
- ⁴⁵ H.J. Kleiner and W. Budzinsky, Flameproofed polyester molding composition, Ticona, U.S. Patent 5,780,534, 1998.
- ⁴⁶ H.J. Kleiner and W.K. Budzinsky, C. Flame retardant polyester moulding composition, Ticona, European Patent 0941996, 1999.
- ⁴⁷ W. Herwig, H.J. Kleiner and H.D. Sabel, Flame-retarding agents and their use in the preparation of fire-proof thermoplastic polymers, Hoechst, European Patent 0006568, 1980.
- ⁴⁸ S. Hoerold, Flame-retarding thermosetting compositions Clariant, U.S. Patent 6,420,459, 2002.
- ⁴⁹ U. Braun and B. Schartel, Flame Retardancy Mechanisms of Aluminium Phosphinate in Combination with Melamine Cyanurate in Glass-Fibre, Reinforced Poly(1,4-butylene terephthalate). *Macromolecular Materials and Engineering*, 2008, *293*, 206
- ⁵⁰ S.V. Levchik and E.D. Weil, Overview of recent developments in the flame retardancy of polycarbonates, *Polymer International*, 2005, *54*, 981
- ⁵¹ S.V. Levchik and E.D. Weil, A review of recent progress in phosphorus-based flame retardants, *Journal of Fire Science*, 2006, *24*, 345
- ⁵² T. Saito, Cyclic organophosphorus compounds, Patent US 3702878, 1972
- ⁵³ J. Stawinski and A. Kraszewski, How to get the most out of two phosphorus chemistries, *Studies on H-phosphonates. Accounts of Chemical Research*, 2002, *35*, 952
- ⁵⁴ K. A. Salmeia and S. Gaan, An overview of some recent advances in DOPO-derivatives: Chemistry and flame retardant applications, *Polymer Degradation and Stability*, 2015, *113*, 119
- ⁵⁵ J. Artner, M. Ciesielski, O. Walter, M. Döring, R. M. Perez and J. K. W. Sandler, A novel DOPO-based diamine as hardener and flame retardant for epoxy resin systems, *Macromolecular Materials and Engineering*, 2008, *293*, 503
- ⁵⁶ M. Ciesielski, A. Schäfer and M. Döring. Novel efficient DOPO-based flame-retardants for PWB relevant epoxy resins with high glass transition temperatures, *Polymers for Advanced Technologies*, 2008, *19*, 507
- ⁵⁷ B. Perret, B. Schartel, K. Stöss, M. Ciesielski, J. Diederichs and M. Döring, Novel DOPO-based flame retardants in high-performance carbon fibre epoxy composites for aviation. *European Polymer Journal*, 2011, *47*, 1081
- ⁵⁸ E. D. Weil, Mechanisms and Modes of Action in Flame Retardancy of Polymers, In *Proceedings of the Conference on Recent Advances in Flame Retardancy of Polymeric Materials*, Stamford, CT, USA, 22-24 May 2000
- ⁵⁹ S. V. Levchik, G. F. Levchik, A. I. Balanovich, G. Camino and L. Coast, Mechanistic study of combustion performance and thermal decomposition behavior of nylon 6 with added halogen-free fire retardants, *Polymer Degradation and Stability*, 1996, *54*, 217
- ⁶⁰ H.L. Vandersall, Intumescent coating systems, their development and chemistry, *Journal of Fire Flammability*, 1971, *2*, 97
- ⁶¹ S. Bourbigot and S. Duquesne, Fire retardant polymers: Recent developments and opportunities, *Journal of Materials Chemistry*, 2007, *17*, 2283
- ⁶² G. Camino, L. Costa and L. Trossarelli, Study of the Mechanism of Intumescence in Fire Retardant Polymers: Part V--Mechanism of Formation of Gaseous Products in the Thermal Degradation of Ammonium Polyphosphate, *Polymer Degradation and Stability*, 1985, *12*, 203
- ⁶³ F. Laoutid, L. Bonnaud, M. Alexandre, J.M. Lopez-Cuesta and P. Dubois, New prospects in flame retardant polymer materials: From fundamentals to nanocomposites, *Materials Science and Engineering: R: Reports*, 2009, *63*, 100
- ⁶⁴ S. Bourbigot, M. Le Bras, R. Leeuwendal, K. K. Shen, D. Schubert, Recent advances in the use of zinc borates in flame retardancy of EVA, *Polymer Degradation and Stability*, 1999, *64*, 419

References

- ⁶⁵ M. Rakotomalala, S. Wagner and M. Döring, Recent Developments in Halogen Free Flame Retardants for Epoxy Resins for Electrical and Electronic Applications, *Materials*, 2010, **3**, 4300
- ⁶⁶ S. Bourbigot, C. Hoffendahl, G. Fontaine and S. Duquesne, Recent advances in fire retardancy of EVA, *Proceedings of the Annual Conference on Recent Advances in Flame Retardancy of Polymeric Materials*, 2016, **26**, 267
- ⁶⁷ Z.D. Han, Y.L. Wang, W.Z. Dong and P. Wang, Enhanced fire retardancy of polyethylene/alumina trihydrate composites by graphene nanoplatelets, *Materials Letters*, 2014, **128**, 275
- ⁶⁸ C. Formicola, A. De Fenzo, M. Zarrelli, A. Frache, M. Giordano and G. Camino, Synergistic effects of zinc borate and aluminium trihydroxide on flammability behaviour of aerospace epoxy system, *EXPRESS Polymer Letters*, 2009, **3**, 376
- ⁶⁹ R. Bagheri, M. Liauw and S. N. Allen, Factors effecting the performance of montmorillonite/magnesium hydroxide/poly(propylene) ternary composites, 1. Flame retardation and thermal stability, *Macromolecular Materials and Engineering*, 2008, **293**, 114
- ⁷⁰ M. Casetta, G. Michaux, B. Ohl, S. Duquesne and S. Bourbigot, Key role of magnesium hydroxide surface treatment in the flame retardancy of glass fiber-reinforced polyamide 6, *Polymer Degradation and Stability*, 2018, **148**, 95
- ⁷¹ P.R. Hornsby and C.L. Watson, A study of the mechanism of flame retardance and smoke suppression in polymers filled with magnesium hydroxide, *Polymer Degradation and Stability*, 1990, **30**, 73
- ⁷² T. Kashwagi, T. G. Cleary, G. C. Davis and J. H. Lupinski, A non-halogenated, flame flame retarded polycarbonate, *Conference of Advanced Fire Resistance Aircraft Interior Materials*, Atlantic City, NJ, February 9-11, 1993, 175
- ⁷³ R. Benrashid and G. L. Nelson, Flammability improvement of polyurethanes by incorporation of a silicon moiety into the structure of block copolymers, in *Fire and Polymers ACS Symposium, Series 599*, American Chemical Society, Washinton D. C., 1995, 127
- ⁷⁴ A. Hermansson, T. Hjertberg and B .A. Sultan, The flame retardant mechanism of polyolefins modified with chalk and silicone elastomer, *Fire Materials*, 2003, **27**, 51
- ⁷⁵ L. A. Mercado, J. A. Reina and M. Galia, Flame retardant epoxy resins based on diglycidylmethoxyphenylsilane, *Journal of Polymer Science: Polymer chemistry*, 2006, **44**, 5580
- ⁷⁶ J. R. Ebdon, B. J. Hunt and P. Joseph, Thermal degradation and flammability characteristics of some polystyrenes and poly(methylmethacrylate)s chemically modified with silicon-containing group, *Polymer Degradation and Stability*, 2004, **83**, 181
- ⁷⁷ T. Kashiwagi, J. W. Gilman, K. M. Butler, R. H. Harris, J. R. Shields and A. Asano, Flame retardant mechanism of silica gel/silica, *Fire and Materials*, 2000, **24**, 277
- ⁷⁸ T. Kashiwagi, J.R. Shields, H.R. Harris and D.R. Davis, Flame-retardant mechanism of silica: effects of resin molecular weight, *Journal of Applied Polymer Science*, 2003, **87**, 1541
- ⁷⁹ M.Z. Fu, and B.J. Qu, Synergistic flame retardant mechanism of fumed silica in ethylene-vinyl acetate /magnesium hydroxide blends, *Polymer Degradation and Stability*, 2004, **85**, 633
- ⁸⁰ E. P. Giannelis, polymer layered silicate nanocomposites, *Advanced Materials*, 1996, **8**, 29
- ⁸¹ J.U. Ha and M. Xanthos, Functionalization of nanoclays with ionic liquids for polypropylene composites. *Polymer Composites*, 2009, **30**, 534
- ⁸² K.K. Shen and E. Olson, Borates as fire retardants in halogen-free polymers, *Proceedings of the Conference on Recent Advances in Flame Retardancy of Polymeric Materials*, 2004, **15**, 128
- ⁸³ C. Kaynak, H.O. Gunduz and N.A. Isitman, Use of nanoclay as an environmentally friendly flame retardant synergist in polyamide-6, *Journal of Nanoscience and Nanotechnology*, 2010, **10**, 7374
- ⁸⁴ S. Zhang, R.A. Horrocks, R. Hull and B.K. Kandola, Flammability, degradation and structural characterization of fibre-forming polypropylene containing nanoclay-flame retardant combinations, *Polymer Degradation and Stability*, 2006, **91**, 719

References

- ⁸⁵ R.S. Sinha and M. Okamoto, Polymer/layered silicate nanocomposites: a review from preparation to processing, *Progress in Polymer Science*, 2003, *28*, 1539
- ⁸⁶ R.M. Reilly, Carbon Nanotubes: Potential Benefits and Risks of Nanotechnology in Nuclear Medicine, *Journal of Nuclear Medicine*, 2007, *48*, 1039
- ⁸⁷ K. S. Novoselov, A. K. Geim, S. V. Morozov, D. Jiang, Y. Zhang, S. V. Dubonos, I. V. Grigorieva and A. A. Firsov, Electric field effect in atomically thin carbon films, *Science*, 2004, *306*, 666
- ⁸⁸ X. B. Fan, W. C. Peng, Y. Li, X. Y. Li, S. L. Wang, G. L. Zhang and F. B. Zhang, Deoxygenation of exfoliated graphite oxide under alkaline conditions: a green route to graphene preparation, *Advanced Materials*, 2008, *20*, 4490
- ⁸⁹ S.J. Wang, F. Xin, Y. Chen, L.J. Qian and Y.J. Chen, Phosphorus-nitrogen containing polymer wrapped carbon nanotubes and their flame-retardant effect on epoxy resin *Polymer Degradation and Stability*, 2016, *129*, 133
- ⁹⁰ S. Bourbigot, G. Fontaine, A. Gallos, C. Gerard and S. Bellayer, Functionalized-carbon multiwall nanotube as flame retardant for polylactic acid, *ACS Symposium Series*, 2009, 1013(Fire and Polymers V), 25
- ⁹¹ B. Schartel, P. Pötschke, U. Knoll and M. Abdel-Goad, Fire behaviour of polyamide 6/multiwall carbon nanotube nanocomposites, *European Polymer Journal*, 2005, *41*, 1061
- ⁹² B. Sang, Z.W. Li, X.H. Li, L.G. Yu, and Z.J. Zhang, Graphene-based flame retardants: a review, *Journal of Materials Science*, 2016, *51*, 8271
- ⁹³ D. W. Scott, Thermal rearrangement of branched-chain methylpolysiloxanes, *Journal of the American Chemical Society*, 1946, *8*, 1250
- ⁹⁴ A. Vannier, S. Duquesne, S. Bourbigot, A. Castrovinci, G. Camino and R. Delobel, The use of POSS as synergist in intumescent recycled poly(ethylene terephthalate), *Polymer Degradation and Stability*, 2008, *93*, 818
- ⁹⁵ X. Wang, Y. Hu, L. Song, W.Y. Xing and H.D. Lu, Thermal degradation behaviors of epoxy resin/POSS hybrids and phosphorus–silicon synergism of flame retardancy, *Journal of Polymer Science Part B: Polymer Physics*, 2010, *48*, 693
- ⁹⁶ L. Costes, F. Laoutid, S. Brohez and P. Dubois, Bio-based flame retardants: When nature meets fire protection, *Materials Science and Engineering R*, 2017, *117*, 1
- ⁹⁷ R. Rinaldi and F. Schüth, Acid Hydrolysis of Cellulose as the Entry Point into Biorefinery Schemes, *ChemSusChem*, 2009, *2*, 1096
- ⁹⁸ G. Flèche and M. Huchette, Isosorbide. Preparation, properties and chemistry, *Starch/Staerke*, 1986, *38*, 26
- ⁹⁹ P. Stoss and R. Hemmer, 1,4:3,6-dianhydrohexitols, *Advances in Carbohydrate Chemistry and Biochemistry*, 1991, *49*, 93
- ¹⁰⁰ R. U. Lemieux and A. G. McInnes, THE PREFERENTIAL TOSYLATION OF THE ENDO-5-HYDROXYL GROUP OF 1,4:3,6-DIANHYDRO-D-GLUCITOL, *Canadian Journal of Chemistry*, 1960, *38*, 136
- ¹⁰¹ J. S. Brimacombe, A. B. Foster, M. Stacey and D. H. Whiffen, Aspects of stereochemistry—I: Properties and reactions of some diols, *Tetrahedron*, 1958, *4*, 351
- ¹⁰² K. W. Buck, A. B. Foster, A. R. Perry and J. M. Webber, 789. Aspects of stereochemistry. Part XV. Influence of intramolecular hydrogen bonding on the rates of esterification of some derivatives of 5-hydroxy-1,3-dioxan and of 1,4:3,6-dianhydro-D-glucitol, *Journal of the Chemical Society*, 1963, 4171
- ¹⁰³ C. Giuseppe, J. Paul and I. Hans-Ulrich, Use of nitrates in ischemic heart disease, *Expert Opinion on Pharmacotherapy*, 2015, *16*, 1567
- ¹⁰⁴ J. R. Collins, Polyesters. GB patent 1,079,686, Courtaulds Ltd., 1967.
- ¹⁰⁵ H. Medem, M. Schreckenber, R. Dhein, W. Nouvertne and H. Rudolph, Thermoplastic polycarbonates, their preparation and their use as shaped articles and films, US patent 4,506,066, Bayer A.G. (Germany), 1985.
- ¹⁰⁶ S. Chatti, G. Schwarz and H. G. Kricheldorf, Cyclic and noncyclic polycarbonates of isosorbide (1,4:3,6-dianhydro-d-glucitol), *Macromolecules*, 2006, *39*, 9064
- ¹⁰⁷ O. Betiku, M. Jenni, K. Ludescher, E. Meierdierks, J. Lunt and J. Schroeder, Synthesis and characterization of isosorbide carbonate:lactide copolymers, *Polymer Preprints*, 2007, *48*, 802

References

-
- ¹⁰⁸ C. H. Lee, H. Takagi, Y. Katagiri and M. Kato, Polycarbonate and method for producing the same, EP patent 2,143,751, Toyota (Japan), 2011
- ¹⁰⁹ J. G. Morrison, Polyglycidyl ethers of cyclic anhydro hexitols and their aqueous solutions, US patent 3,041,300, Martin-Marietta Corp., 1962.
- ¹¹⁰ J. D. Zech and J. W. L. Maistre, Diglycidyl ethers of isohexides. US patent 3,272,845, Atlas Chemical Industries, Inc., 1966.
- ¹¹¹ D. Achet, M. Delmas, A. Gaset, Biomass as a source of chemicals. VI. Synthesis of new polyfunctional ethers of isosorbide in solid-liquid heterogeneous mixtures, *Biomass*, 1986, 9, 247
- ¹¹² J. Thiem and H. Lueders, Synthesis and directed polycondensation of starch-derived anhydroalditol building blocks, *Starch/Staerke* 1984, 36, 170
- ¹¹³ J. Thiem and H. Lueders, Synthesis of polyterephthalates derived from dianhydrohexitols, *Polymer Bulletin*, 1984, 11, 365
- ¹¹⁴ R. Storbeck, M. Rehahn and M. Ballauff, Synthesis and properties of highmolecular-weight polyesters based on 1,4:3,6-dianhydrohexitols and terephthalic acid, *Makromolekulare Chemie*, 1993, 194, 53
- ¹¹⁵ L. F. Charbonneau, R. E. Johnson, H. B. Witteler and G. Khanarian, Polyesters including isosorbide as a comonomer and methods for their production, US patent 5,959,066, HNA Holdings Inc. (USA), 1999.
- ¹¹⁶ S. Imm, S. Bähn, M. Zhang, L. Neubert, H. Neumann, F. Klasovsky, J. Pfeffer, T. Haas and M. Beller, Improved Ruthenium-Catalyzed Amination of Alcohols with Ammonia: Synthesis of Diamines and Amino Esters, *Angewandte Chemie International Edition*, 2011, 50, 7599
- ¹¹⁷ A. Caouthar, P. Roger, M. Tessier, S. Chatti, J. C. Blais and M. Bortolussi, Synthesis and Characterization of New Polyamides Based on Diphenylaminoisosorbide, *Journal of Polymer Science Part A: Polymer Chemistry*, 2005, 43, 6480
- ¹¹⁸ A. Caouthar, A. Loupy, M. Bortolussi, J.-C. Blais, L. Dubreucq and A. Meddour, Synthesis and characterization of new polyamides derived from di(4-cyanophenyl)isosorbide, *European Polymer Journal*, 2007, 43, 220
- ¹¹⁹ F. Bachmann, J. Reimer, M. Ruppenstein and J. Thiem, Synthesis of Novel Polyurethanes and Polyureas by Polyaddition Reactions of Dianhydrohexitol Configured Diisocyanates, *Macromolecular Chemistry and Physics*, 2001, 202, 3410
- ¹²⁰ J. Thiem, Synthesis and properties of polyurethanes derived from diaminodianhydroalditols, *Macromolecular Chemistry*, 1986, 187, 2775
- ¹²¹ M. K. Grachev, K. L. Anfilov, A. K. Bekker and E. E. Nifant'ev, Phosphorylation of 1,4:3,6-dianhydro-D-mannitol, *Zhurnal Obshchei Khimii*, 1995, 65, 1946
- ¹²² K. A. Petrov, E. E. Nifant'ev, A. A. Shcheglov and N. A. Khudyntsev, Synthesis and chemical properties of phosphinites of 1,4:3,6-dianhydrohexitols, *Zhurnal Obshchei Khimii*, 1962, 32, 3074
- ¹²³ M. D. Chen, J. C. Yuan, Y. H. Zhang, S. J. Lu, W. Sun and L. L. Wang, Synthesis of new chiral carbohydrate bisphosphites and their applications in the asymmetric hydroesterification of styrene, *Fenzi Cuihua*, 2001, 15, 385
- ¹²⁴ M. T. Reetz and T. Neugebauer, New Diphosphite Ligands for Catalytic Asymmetric Hydrogenation: The Crucial Role of Conformationally Enantiomeric Diols, *Angewandte Chemie International Edition*, 1999, 38, 179
- ¹²⁵ B. Howell and Y. G. Daniel, Thermal degradation of phosphorus esters derived from isosorbide and 10-undecenoic acid, *Journal of Thermal Analysis and Calorimetry*, 2015, 121, 411
- ¹²⁶ C. Fleckenstein and H. Denecke, Fire Retardant, US patent 20120252911 A1, BASF SE (Germany), 2012
- ¹²⁷ C. Fleckenstein and H. Denecke, Verfahren zur Herstellung von Zucker(thio)phosphaten, EP patent 2,574,615 A1, BASF SE (Germany), 2013
- ¹²⁸ Y. G. Daniel and B. Howell, Flame retardant properties of isosorbide bis-phosphorus esters, *Polymer Degradation and Stability*, 2017, 140, 25

References

- ¹²⁹ T. C. Mauldin, M. Zammarano, J. W. Gilman, J. R. Shields and D. J. Boday, Synthesis and characterization of isosorbide-based polyphosphonates as biobased flame-retardants, *Polymer Chemistry*, 2014, 5, 5139.
- ¹³⁰ C. F. Kuan, H. C. Kuan, C. C. M. Ma, C. H. Chen, Flame Retardancy and Non dripping Properties of Ammonium Polyphosphate/Poly(butylene succinate) Composites Enhanced by Water Crosslinking, *Journal of Applied Polymer Science*, 2006, 102, 2935
- ¹³¹ Y. Chen, J. Zhan, P. Zhang, S. Nie, H. Lu, L. Song and Y. Hu, Preparation of Intumescent Flame Retardant Poly(butylene succinate) Using Fumed Silica as Synergistic Agent, *Industrial & Engineering Chemistry Research*, 2010, 49, 8200
- ¹³² Y. J. Liu, L. Mao and S. H. Fan, Preparation and Study of Intumescent Flame Retardant Poly(butylene succinate) Using MgAlZnFe-CO₃ Layered Double Hydroxide as a Synergistic Agent, *Journal of Applied Polymer Science*, 2014, 40736,1
- ¹³³ C. Nguyen, M. Lee, and J. Kim, Relationship between structures of phosphorus compounds and flame retardancy of the mixtures with acrylonitrile-butadiene-styrene and ethylene-vinyl acetate copolymer, *Polymers for Advanced Technologies*, 2009, 22, 512
- ¹³⁴ H. Y. Yang, L. Song, Q. L. Tai, X. Wang, B. Yu, Y. Yuan a, Y. Hua and R. K.K. Yuen, Comparative study on the flame retarded efficiency of melamine phosphate, melamine phosphite and melamine hypophosphite on poly(butylene succinate) composites, *Polymer Degradation and Stability*, 2014, 105, 248
- ¹³⁵ D. Pospiech, A. Korwitz, H. Komber, D. Jehnichen, L. Häußler, H. Scheibner, M. Liebmann, K. Jähnichen and B. Voit, Biobased Aliphatic Polyesters with DOPO Substituents for Enhanced Flame Retardancy, *Macromolecular Chemistry and Physics*, 2015, 216, 1447
- ¹³⁶ H. Chen, X. Wen, Y. Guan J. Min, Y. L. Wen, H. F. Yang and T. Tao, Effect of particle size on the flame retardancy of poly(butylene succinate)/Mg(OH)₂ composites, *Fire and Materials*, 2016, 40, 1090
- ¹³⁷ X. Wang, L. Song, H. Y. Yang, H. D. Lu and Y. Hu, Synergistic Effect of Graphene on Antidripping and Fire Resistance of Intumescent Flame Retardant Poly(butylene succinate) Composites, *Industrial & Engineering Chemistry Research*, 2011, 50, 5376
- ¹³⁸ X. Wang, Y. Hua, L. Song, H. Y. Yang, B. Yua, B. Kandolac and D. Deli, Comparative study on the synergistic effect of POSS and graphene with melamine phosphate on the flame retardancy of poly(butylene succinate), *Thermochimica Acta*, 2012, 543, 156
- ¹³⁹ G. Dorez, A. Taguet, L. Ferry and J. L. Cuesta, Phosphorous compounds as flame retardants for polybutylene succinate/flax biocomposite: Additive versus reactive route, *Polymer Degradation and Stability*, 2014, 102, 152
- ¹⁴⁰ S. Nie, X. Liu, G. Dai, S. Yuan, F. Cai, B. Li, and Y. Hu, Investigation on Flame Retardancy and Thermal Degradation of Flame Retardant Poly(butylene succinate)/Bamboo Fiber Biocomposites, *Journal of Applied Polymer Science*, 2012, 125, E485.
- ¹⁴¹ J. Zeng, L. Jiao, Y. D. Li, M. Srinivasan, T. Li and Y. Z. Wang, Bio-based blends of starch and poly(butylene succinate) with improved miscibility, mechanical properties, and reduced water absorption, *Carbohydrate Polymers*, 2011, 83, 762
- ¹⁴² T. Ohkita and S. H. Lee, Crystallization Behavior of Poly(butylene succinate)/Corn Starch Biodegradable Composite, *Journal of Applied Polymer Science*, 2005, 97, 1107
- ¹⁴³ N. Lin, D. K. Fan, P. R. Chang, J. H. Yu, X. C. Cheng and J. Huang, Structure and Properties of Poly(butylene succinate) Filled with Lignin: A Case of Lignosulfonate, *Journal of Applied Polymer Science*, 2011, 121, 1717
- ¹⁴⁴ B. Prieur, M. Meub, M. Wittemann, R. Klein, S. Bellayer, G. Fontaine and S. Bourbigot, Phosphorylation of lignin to flame retard acrylonitrile butadiene styrene (ABS), *Polymer Degradation and Stability*, 2016, 127, 32
- ¹⁴⁵ L. Costes, F. Laoutid, M. Aguedo, A. Richel, S. Brohez, C. Delvosalle and P. Dubois, Phosphorus and nitrogen derivatization as efficient route for improvement of lignin flame retardant action in PLA, *European Polymer Journal*, 2016, 84, 652
- ¹⁴⁶ B. Howell and C. Ahn, Lignin as a base for the generation of flame retardants, *Proceedings of the NATAS Annual Conference on Thermal Analysis and Applications*, 2004, 32, 159

References

- ¹⁴⁷ L. Ferry, G. Dorez, A. Taguet, B. Otazaghine and J.M. Lopez-Cuesta, Chemical modification of lignin by phosphorus molecules to improve the fire behavior of polybutylene succinate, *Polymer Degradation and Stability*, 2015, *113*, 135
- ¹⁴⁸ S.C. Jiang, Y.F. Yang, S.B. Ge, Z.F. Zhang and W.X. Peng, Preparation and properties of novel flame-retardant PBS wood-plastic composites, *Arabian Journal of Chemistry*, 2018, *11*, 844
- ¹⁴⁹ Wikipedia, Bamboo, march 2018, <https://en.wikipedia.org/wiki/Bamboo>
- ¹⁵⁰ M. Lewin, Flame Retarding of Polymers with Sulfamates. I. Sulfation of Cotton and Wool, *Journal of Fire Sciences*, 1997, *15*, 263
- ¹⁵¹ M. Lewin, J. Brozek and M.M. Martens, The system polyamide/sulfamate/dipentaerythritol: flame retardancy and chemical reactions, *Polymers for Advanced Technologies*, 2002, *13*, 1091
- ¹⁵² M. Lewin, Flame retardant polyamide compositions, US Patent 5,424,344, E. I. DuPont de Nemours and Company, 1995, United States.
- ¹⁵³ M. Lewin, Flame retarding polymer nanocomposites: Synergism, cooperation, antagonism, *Polymer Degradation and Stability*, 2011, *96*, 256
- ¹⁵⁴ Lewin M., Unsolved problems and unanswered questions in flame retardance of polymers. *Polymer Degradation and Stability*, 2005, *88*, 13
- ¹⁵⁵ J. Thiem, H. Lüders, Synthesis and properties of polyurethanes derived from diaminodihydroalditols, *Makromol. Chem.* 1986, *187*, 2775
- ¹⁵⁶ L.F. Tong, H.Y. Ma and Z.P. Fang, Thermal decomposition and flammability of acrylonitrile-butadiene-styrene /multi-walled carbon nanotubes composites, *Chinese Journal of Polymer Science* 2008, *26*, 331
- ¹⁵⁷ C.M. Costache, D.Y. Wang, M.J. Heidecker, E. Manias and C.A. Wilkie, The thermal degradation of poly(methyl methacrylate) nanocomposites with montmorillonite, layered double hydroxides and carbon nanotubes, *Polymers for Advanced Technologies*, 2006, *17*, 272
- ¹⁵⁸ B. Schartel, P. Poetschke, U. Knoll and M. Abdel-Goad, Fire behavior of polyamide 6/multiwall carbon nanotube nanocomposites, *European Polymer Journal*, 2005, *41*, 1061
- ¹⁵⁹ B. Schartel and T. R. Hull, Development of fire-retarded materials—Interpretation of cone calorimeter data, *Fire and Materials*, 2007, *31*, 327
- ¹⁶⁰ J. H. Gong, Y. B. Li, Y. X. Chen, J. Li, X. Wang, J. C. Jiang, Z. R. Wang and J. H. Wang, Approximate analytical solutions for transient mass flux and ignition time of solid combustibles exposed to time-varying heat flux, *Fuel*, 2018, *211*, 676
- ¹⁶¹ R. V. Petrella, The assessment of full-scale fire hazards from cone calorimeter data, *Journal of Fire Sciences* 1994, *12*, 14
- ¹⁶² B. K. Kandola, D. Price, G.J. Milnes and A. Da Silva, Development of a novel experimental technique for quantitative study of melt dripping of thermoplastic polymers, *Polymer Degradation and Stability*, 2013, *98*, 52
- ¹⁶³ B. K. Kandola, M. Ndiaye and D. Price, Quantification of polymer degradation during melt dripping of thermoplastic polymers, *Polymer Degradation and Stability*, 2014, *106*, 16
- ¹⁶⁴ R. Dupretz, G. Fontaine, S. Duquesne and S. Bourbigot, Instrumentation of UL-94 test: understanding of mechanisms involved in fire retardancy of polymers, *Polymers Advanced Technologies*, 2015, *26*, 865
- ¹⁶⁵ B. K. Kandola, D. Price, J. Milnes, A. Da Silva, F. Gao and R. Nigmatullin, Characterization of Melt Dripping Behavior of Flame Retarded Polypropylene Nanocomposites, *ACS symposium series*, 2012, *1118*, 311
- ¹⁶⁶ F. Kempel, B. Schartel, J. M. Marti, K. M. Butler, R. Rossi, S. R. Idelsohn, E. Onate and A. Hofmann, Modelling the vertical UL 94 test: competition and collaboration between melt dripping, gasification and combustion, *Fire and Materials*, 2015, *39*, 570
- ¹⁶⁷ C. Dong, Z. Lu, P. Wang, P. Zhu, X. Li, S. Sui, L. Zhang and J. Liu, Flammability and thermal properties of cotton fabrics modified with a novel flame retardant containing triazine and phosphorus components, *Textile Research Journal*, 2017, *87*, 1367

References

-
- ¹⁶⁸ J.R. Van Wazer, C.F. Callis, J.N. Shoolery and R.C. Jones, Principles of phosphorus chemistry. II. Nuclear magnetic resonance measurements, *Journal of the American Chemical Society*, 1956, *78*, 5715
- ¹⁶⁹ T.M. Duncan and D.C. Douglass, On the phosphorus-31 chemical shift anisotropy in condensed phosphates, *Chemical Physics*, 1984, *87*, 339
- ¹⁷⁰ S. Bourbigot, M. Le Bras, F. Dabrowski, J. W. Gilman and T. Kashiwagi, PA-6 Clay Nanocomposite Hybrid as Char Forming Agent in Intumescent Formulations, *Fire and Materials*, 2000, *24*, 201
- ¹⁷¹ I.V. Kovalev and N.O. Kovaleva, Organophosphates in agrogray soils with periodic water logging according to the data of ³¹P NMR spectroscopy, *Eurasian Soil Science*, 2011, *44*, 29
- ¹⁷² M.I. Makarov, L. Haumaier and W. Zech, The nature and origins of diester phosphates in soils: a ³¹P-NMR study, *Biology and Fertility of Soils*, 2002, *35*, 136
- ¹⁷³ S. Bourbigot, M. Le Bras, R. Delobel, R. Decressain and J. Amoureux, Synergistic effect of zeolite in an intumescence process: study of the carbonaceous structures using solid-state NMR, *Journal of the Chemical Society, Faraday Transactions*, 1996, *92*, 149
- ¹⁷⁴ G. Walter, U. Hoppe, J. Vogel, G. Carl, P. Hartmann, The structure of zinc polyphosphate glass studied by diffraction methods and ³¹P NMR, *Journal of Non-Crystalline Solids*, 2004, *333*, 252
- ¹⁷⁵ C. Ciulik, M. Safari, A. Ilarduyaa, J. Morales-Huerta, Amaia Iturrospe, Arantxa Arbe, A. J. Müller and S. Muñoz-Guerra, Poly(butylene succinate-ran-ε-caprolactone) copolyesters: Enzymatic synthesis and crystalline isodimorphic character, *European Polymer Journal*, 2017, *95*, 795
- ¹⁷⁶ T. Dong, Y. He, K. Shin and Y. Inoue, Formation and Characterization of Inclusion Complexes of Poly(butylene succinate) with α- and γ-Cyclodextrins, *Macromolecular Bioscience*, 2004, *4*, 1084
- ¹⁷⁷ Q. Li, W.X. Zhu, C.C. Li, G. H. Guan, D. Zhang, Y.N. Xiao and L.C. Zheng, A non-phosgene process to homopolycarbonate and copolycarbonates of isosorbide using dimethyl carbonate: Synthesis, characterization, and properties, *Journal of Polymer Science, Part A: Polymer Chemistry*, 2013, *51*, 1387
- ¹⁷⁸ G.E. Maciel, V.J. Bartuska and F.P. Miknis, Characterization of organic material in coal by proton-decoupled ¹³C nuclear magnetic resonance with magic-angle spinning, *Fuel*, 1979, *58*, 391
- ¹⁷⁹ G. Camino, L. Costa, G. Clouet, A. Chiotis, J. Brossas, M. Bert, A. Guyot, *Polymer Degradation and Stability*, 1984, *6*, 105
- ¹⁸⁰ G.E. Maciel, M.J. Sullivan, L. Petrakis and D.W. Grandy, ¹³C Nuclear magnetic resonance characterization of coal macerals by magic angle spinning *Fuel*, 1982, *61*, 411
- ¹⁸¹ G. Camino and M.P. Luda, Mechanistic study on intumescence, M. Le Bras, G. Camino, S. Bourbigot and R. Delobel (eds), *Pub. The Royal Society of Chemistry, Cambridge*, 1998, *224*, 48
- ¹⁸² H.L. Vandersall, Intumescent coating systems, their development and chemistry, *Journal of Fire and Flammability*, 1971, 97
- ¹⁸³ J.H. Park, M.S. Koo, S. H. Cho and M.Y. Lyu, Comparison of thermal and optical properties and flowability of fossil-based and bio-based polycarbonate, *Macromolecular Research*, 2011, *25*, 1135
- ¹⁸⁴ J. A. Franz, D. M. Camaioni, T. Autrey, J. C. Linehan and M.S. Alnajjar, Measurement of select radical processes in hydrocarbon pyrolysis, *Journal of Analytical and Applied Pyrolysis*, 2000, *54*, 37
- ¹⁸⁵ A.W. Pryor, S. K. Nuggehalli, K.V. Scherer and D.F. Church, An electron spin resonance study of the particles produced in the pyrolysis of perfluoro polymers, *Chemical Research in Toxicology*, 1990, *3*, 2
- ¹⁸⁶ S. Sarkar, Z. Gan, L.N. An and L. Zhai, Structural Evolution of Polymer-Derived Amorphous SiBCN Ceramics at High Temperature, *Journal of Physical Chemistry C*, 2011, *115*, 24993
- ¹⁸⁷ K.M. Butler, H.R. Baum and T. Kashiwagi, Three-dimensional modeling of intumescent behavior in fire, *Proceedings of the International Conference on Fire Research and Engineering, Orlando*, 1995, 261
- ¹⁸⁸ X. Wang, L. Song, H. Y. Yang, H. D. Lu and Y. Hu, Synergistic Effect of Graphene on Antidripping and Fire Resistance of Intumescent Flame Retardant Poly(butylene succinate) Composites, *Industrial & Engineering Chemistry Research*, 2011, *50*, 5376

References

- ¹⁸⁹ X. Wang, Y. Hua, L. Song, H. Y. Yang, B. Yua, B. Kandolac and D. Deli, Comparative study on the synergistic effect of POSS and graphene with melamine phosphate on the flame retardancy of poly(butylene succinate), *Thermochimica Acta*, 2012, *543*, 156
- ¹⁹⁰ Y. J. Liu, L. Mao and S. H. Fan, Preparation and Study of Intumescent Flame Retardant Poly(butylene succinate) Using MgAlZnFe-CO₃ Layered Double Hydroxide as a Synergistic Agent, *Journal of Applied Polymer Science*, 2014, *40736*,1
- ¹⁹¹ S. Bourbigot, M. Le Bras, F. Dabrowski, J. W. Gilman, and T. Kashiwagi, PA-6 Clay Nanocomposite Hybrid as Char Forming, *FIRE AND MATERIALS*, 2000, *24*, 201
- ¹⁹² M. Le Bras, M. Bugajny, J. Lefebvre and Serge Bourbigot, Use of polyurethanes as char-forming agents in polypropylene intumescent formulations, *Polymer International*, 2000, *49*, 1115
- ¹⁹³ J. Thiem and F. Bachmann, Synthesis and properties of polyamides derived from anhydro- and dianhydroalditols. *Makromol Chem*, 1991, *192*, 2163
- ¹⁹⁴ D. Braun and M. Bergmann, Polymers from 1,4:3,6-dianhydrosorbitol, *Journal fur praktische Chemie*, 1992, *334*, 298